Dissertation

submitted to the

Combined Faculties for the Natural Sciences and for Mathematics

of the Ruperto-Carola University of Heidelberg, Germany

for the degree of

Doctor of Natural Sciences

presented by

M.Sc.- Biochem. Bin She

born in ChengDu, China

oral examination:

Dynamic Modeling of the PI3K/Akt Signal Transduction Pathway to Dissect the Distinct Cell Fate Decisions Triggered by PI3K/Akt Signaling in Hematopoietic System

Referees: Prof. Dr. Ursula Klingmüller

Prof. Dr. Peter Lichter

Acknowledgements

Working as Ph.D. student in Ursula's group was an enjoyable and challenging experience to me. Here, I would like to express my deep and sincere gratitude to all the people who supported and contributed to my work.

First of all, I would like to thank my supervisor Prof. Dr. Ursula Klingmüller for introducing me to the world of systems biology and giving me the opportunity to work on this exciting interdisciplinary project. Without her valuable guidance and cheerful enthusiasm I could not have finished my Ph.D. successfully.

I would give my special thanks to Prof. Dr.Thomas Höfer for being a supportive collaboration partner on mathematical modeling and particularly for the critical and constructive discussions on the manuscript

I am very grateful to Prof. Dr. Peter Lichter and Prof. Dr Jens Timmer for their essential scientific supporting on my Ph.D. work as supervisors in my thesis advisory committee.

I am also thankful to PD Dr. Renate Voit for her valuable advice in improving the q-PCR measurement.

I am privileged for having Dr. Sandip Kar, Lu Wang and Dr. Carlos Salazar as the most dedicated modeling partners who have made essential scientific contributions to the project and to preparing the manuscript. In addition, I owe my gratitude to Dr. Schilling Marcel for his inspiring advice and discussion on both experimental and theoretical modeling areas from the very beginning of my study in Ursula's group.

I am also indebted to Dr. Seong-Hwan Rho for his scientific support on mathematical modeling as collaboration partner.

I am also very grateful for the fruitful collaboration with Maria Seile from Mannheim and Jie Bao, Dr. Hauker Busch from Freiburg in genomic Microarray performance and subsequently data analysis, respectively.

I would also like to convey my heartfelt thanks to all current and former members of Ursula's group for providing a good working atmosphere, in particular, Dr. Valentina Raia, Dr. Annette Schneide and Dr. Lorenza D'Alessandro for great accompany as friends for all those

years; Verana Becker and Agustin Rodriguez for recurring scientific support; Ute Bauman, Susan Lattermann and Sandra Manthey as well as Martina Kegel for the assistance in all aspects of the laboratory work. It will not be enough to express my gratitude in words to all my lovely colleagues man could wish for.

I also take this opportunity to express gratitude to the Chinese Evangelical Community Heidelberg for their care and assistance in all aspects of my stay in Heidelberg. Special thanks to Nuojia Wen, Dr. Shijun Wang and Dr. Junwie Li for their precious friendships.

Financial support has been provided by SBCancer of the Helmholtz Initiative on Systems Biology.

Finally, I am deeply grateful to my parents for their love and support in all my academic and professional achievements. Last but not less, I wish to express my endless gratitude to my husband Zheng Xu for his enduring love and support.

DEDICATED TO MY BELOVED MOTHER AND FATHER

Table of contents

Summary

A central issue in cell biology is how a particular signaling pathway can specifically trigger distinct cellular outcomes. The phosphatidylinositol 3-kinase (PI3K)/Akt pathway mediates the effects of a variety of extracellular signals in a number of cellular processes including cell cycle progression, cell growth, differentiation and survival. To explore how dinstinct cell fate decisions are determined by PI3K/Akt signaling, a data-based mathematical model of erythropoietin (Epo)-induced PI3K/Akt signaling pathway in primary erythroid progenitor (colony-forming unit erythroid stage, CFU-E) and the factor-dependent murine BaF3-EpoR cell line was established. The mathematical model was constrained by experimental measured concentrations of signaling components and calibrated by various Akt dynamics under different conditions. With this modeling approach, the different stoichiometries of components were identified as the major cause for cell type-specific Akt activation. Model analyses delineated the differential role of negative regulators PTEN and SHIP1 as well as scaffold protein Gab isoforms in shaping Akt activation in different hematopoietic cell types. The quantitative link of the cellular Akt response to cell proliferation revealed that Akt activation is necessary but not sufficient to predict cell proliferation in both cell types.

Further experiments revealed that Akt regulates cell growth and cell cycle progression in a context-dependent manner. Cell growth mediated by mTOR and GSK3 was Akt-dependent in CFU-E cells. However, in BaF3-EpoR cells the activation of mTOR pathway was only partially dependent on Akt while GSK3 phosphorylation was Akt-independent. Furthermore, the PI3K/Akt signaling pathway was identified as the major pathway regulating cell cycle progression in CFU-E cells, but not in BaF3-EpoR cells. In CFU-E cells, PTEN overexpression induced cell cycle arrest in the G1 phase, correlating with the increased mRNA levels of cell cycle inhibitors $p27^{kip1}$ and cyclinG2.

In conclusion, the dynamic modeling of PI3K/Akt pathway provided an insight of the quantitative mechanisms by which context-dependent PI3K/Akt signaling is linked to cell growth and cell cycle progression. The abundance of negative regulators PTEN and SHIP1 together with the isoform-specific Gab-mediated PI3K activation led to cell type-specific Akt activation. The tumor suppressor PTEN strongly suppressed cell proliferation in primary CFU-E cells, coordinating cell growth and cell cycle progression. In contrast, in BaF3-EpoR cells there was only a moderate suppression of cell growth mediated by PTEN, while cell cycle progression was PTEN/Akt-independent.

To date, a number of the components of the PI3K/Akt pathway have been found mutated or altered in abundance in a wide variety of human cancers highlighting the key role of this pathway in cellular transformation. This mathematical model will provide guidance for the rational design of effective therapeutic molecules and facilitate accurate predictions of the effect of existing drugs.

Zusammenfassung

Eine zentrale Frage in der Zellbiologie ist, wie eine bestimmte Signalkaskade unterschiedliche zelluläre Effekte auslösen kann. Der Phosphatidylinositol 3-Kinase (PI3K)/Akt Signalweg vermittelt die Wirkung einer Vielzahl extrazellulärer Signale, die in verschiedenen zellulären Prozessen wie Zellzyklusprogression, Zellwachstum, Zelldifferenzierung und Zellüberleben eine Rolle spielen. Um zu untersuchen, wie die Akt-Signalverarbeitung das Schicksal einer Zelle bestimmen kann, wurde ein datenbasiertes mathematisches Modell des Erythropoetin-induzierten PI3K/Akt Signalweges in primären erythroiden Vorläuferzellen (colony-forming unit erythroid stage, CFU-E) und in der murinen BaF3-EpoR Zelllinie etabliert. Die Modellparameter wurden durch experimentell gemessene Konzentrationen der Signalwegskomponenten festgelegt beziehungsweise mittels Daten über die Aktivierungsdynamik von Akt unter unterschiedlichen Bedingungen geschätzt. Mit Hilfe des mathematischen Modells wurde die Stöchiometrie der Signalwegskomponenten als die wesentliche Ursache für die Zelltyp-spezifische Aktivierung von Akt identifiziert. Modellanalysen machten deutlich, dass die negativen Regulatoren PTEN und SHIP1 sowie die Isoformen des Gerüstproteins Gab die Aktivierungskinetik von Akt in den untersuchten hematopoietischen Zelltypen unterschiedlich beeinflussen. Durch eine quantitative Verknüpfung des Akt-Signals mit der Zellvermehrung konnte gezeigt werden, dass Akt-Aktivierung notwendig, aber nicht ausreichend ist, um die Zellvermehrung in den beiden Zelltypen vorherzusagen.

Weitere Experimente verdeutlichten, dass Akt Zellwachstum und Zellzyklusprogression kontextspezifisch reguliert. In CFU-E-Zellen war das durch mTOR und GSK3 vermittelte Zellwachstum abhängig von Akt. In BaF3-EpoR-Zellen kontrollierte Akt die Aktivierung der mTOR-Kaskade jedoch nur teilweise, während die GSK3-Phosphorylierung unabhängig von Akt war. Zudem wurde der PI3K/Akt Signalweg als der Hauptweg für die Zellzyklusprogression in CFU-E-Zellen identifiziert, nicht jedoch in BaF3-EpoR-Zellen. In CFU-E-Zellen induzierte die Überexpression von PTEN einen Zellzyklus-Stopp in der G1-Phase, was mit erhöhten mRNA-Mengen der Zellzyklusinhibitoren $p27^{kip1}$ und CyclinG2 korrelierte.

Zusammenfassend ermöglichte die dynamische Modellierung des PI3K/Akt Signalweges einen Einblick in die quantitativen Mechanismen, durch welche die kontextabhängige Akt-Signaltransduktion mit Zellwachstum und Zellzyklusprogression gekoppelt sind. Die Menge der negativen Regulatoren PTEN und SHIP1 sowie die spezifische PI3K Aktivierung über die Gab-Isoformen führte zu einer Zelltyp-spezifischen Akt-Phosphorylierung. In primären CFU-E-Zellen unterdrückte der Tumorsupressor PTEN die Zellproliferation erheblich durch Koordination von Zellwachstum und Zellzyklus. In BaF3-EpoR-Zellen hingegen vermittelte

PTEN nur eine schwache Inhibition des Zellwachstums, während die Zellzyklusprogression sich PTEN/Akt-unabhängig zeigte.

Viele der Komponenten des PI3K/Akt Signalweges wurden mittlerweile in einer Vielzahl von humanen Krebsarten als mutiert oder in ihrer Menge verändert identifiziert, was die Schlüsselrolle dieses Signalweges in der zellulären Transformation verdeutlicht. Dieses mathematische Modell könnte eine Orientierung zur zielgerichteten Entwicklung effektiver therapeutischer Substanzen geben und genaue Vorhersagen über die Wirkung existierender Medikamente ermöglichen.

1. Introduction

1.1 The PI3K/Akt signaling pathway

The phosphatidylinositol 3-kinase (PI3K)/Akt pathway mediates the effects of a variety of extracellular signals in a number of cellular processes including cell growth, proliferation, and survival (Castaneda et al., 2010). Among several subtypes of PI3K, class I PI3Ks are best understood. Activation of Class I PI3Ks is facilitated by some receptors such as the erythropoietin receptor (EpoR), the platelet-derived growth factor (PDGF) through direct binding of PI3K to the tyrosin phosphorylated receptors (Damen et al., 1995; Rottapel et al., 1994). However, scaffolding adaptor proteins such as insulin receptor substrate (IRS) (Richmond et al., 2005), GRB2-associated-binding protein (Gab) (Wickrema et al., 1999) have been reported to induce PI3K activation by bringing PI3K to cell membrane in close proximity to its phospholipid substrates. To ensure that the activation of PI3K signaling is appropriately suppressed or terminated, the phosphatases PTEN (Hlobilkova et al., 2003) and SHIP (Kalesnikoff et al., 2003) counteract PI3K by dephosphorylation of PIP3. PIP3 at the cell membrane recruits protein kinases Akt and its kinase PDK1. Activated Akt mediates a large spectrum of cellular functions, ranging from control of cell proliferation and survival to modulation of intermediary metabolism and angiogenesis (Bellacosa et al., 2005).

1.1.1 Class IA PI3K

There are three classes of PI3K (class I, class II and class III) based on structural features and lipid substrate preference (Figure 1.1). Mammals have three classe I PI3K isoforms: PI3K-C2α (PI3KC2A), PI3K-C2β (PI3KC2B) and PI3K-C2γ (PI3KC2G). *In vitro*, they can convert phosphatidylinositols (PIs) and phosphatidylinositol-4-phosphate (PI4P) to the corresponding 3-phosphoinositide lipids (PI3P). The role of class II PI3Ks in mammals are still unknown (Vanhaesebroeck et al., 2010). Vacuolar protein sorting 34 (Vps34; known as PI3KC3) is the only class III PI3K. Vps34 has a lipid substrate specificity limited to PI, generating PI3P (Schu et al., 1993; Volinia et al., 1995). All known biological functions of Vps34 in mammals are related to the regulation of vesicle traffic, including autophagy, endocytosis and phagocytosis (Kihara et al., 2001). Class I PI3Ks are best understood. They are heterodimeric molecules composed of a regulatory and a catalytic subunit.

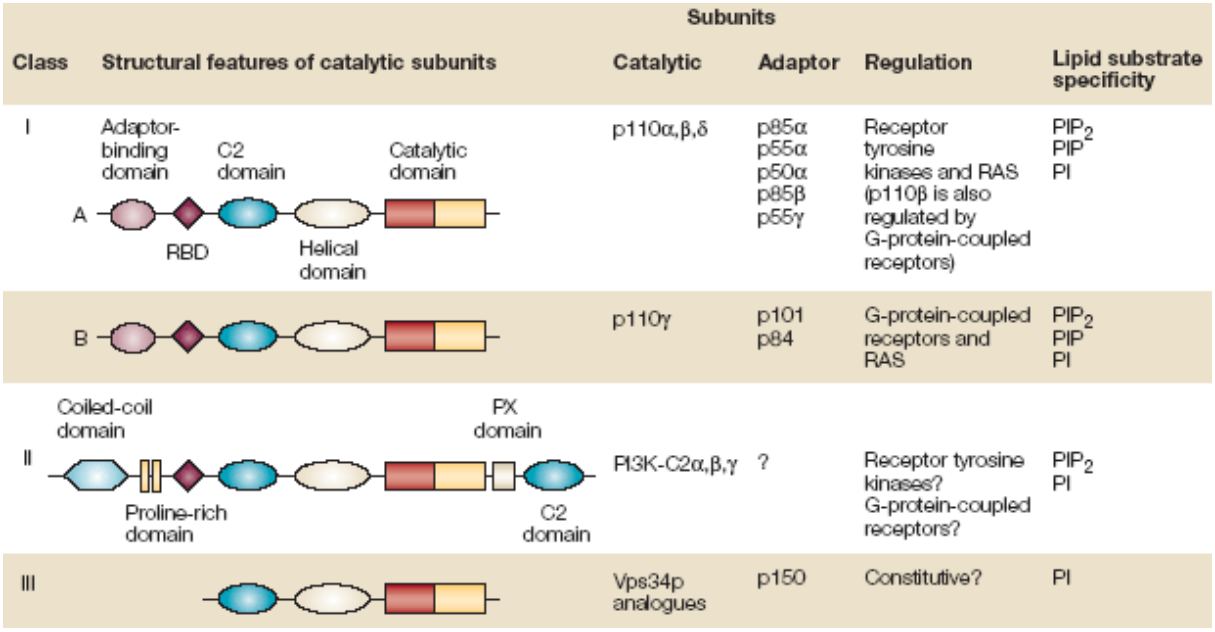

Figure 1.1 Classification of PI3K members and substrate preference. Adapted from (Bader et al., 2005).

Structure and function of PI3K regulatory subunit

Class I PI3Ks were originally classed into those that bind the regulatory subunit p85 (class IA, p110α,–β and –δ) and those that bind to one of the two regulatory subunits p101 and p84 (class IB, p110γ). Here, this study only focused on class IA PI3K mediated signaling.

To date, five isoforms of p85 have been identified and are encoded by either *PIK3R1* (p85α, p55α, p50α), *PI3KR2* (p85β) and *PI3KR3* (p55γ). All p85 isoforms have two Src homology2 (SH2) domains, which specifically bind to phosphorylated YXXM motifs of activated receptors and engage class IA PI3Ks with Tyr kinase signaling pathways (Backer et al., 1992). Between two SH2 domains, there is the inter-SH2 (IS) domain, which is capable of binding to p110 catalytic subunit (Panayotou et al., 1992). At the N-SH2 domain, all p85 isoforms have a proline-rich region, which may interact with the SH3 domain of the ubiquitous adaptor protein, such as Grb2 or Gab, facilitating the activation of PI3K (Wang et al., 1995). The isoforms p85α and p85β also contain an SH3 domain, a second proline-rich region and a BCA-homology GTPase activation domain (BH)-domain (Chamberlain et al., 2008; Vanhaesebroeck et al., 2010). However, the roles of individual p85 subunits are unknown. In summary, regulatory subunits p85 provide at least three functions to p110 proteins: (i) stabilization, (ii) blocking of their kinase activity in basal state and (iii) recruitment to pTyr residues in receptors and adaptor molecules (Vanhaesebroeck et al., 2010).

Structure and function of PI3K catalytic subunits

Mammals have three catalytic subunits of class IA PI3K, p110α, -β and –δ, which exhibit distinct and specific functions. The α and β isoforms have a broad tissue distribution; the expression of p110δ is more restricted and predominantly detected in leukocytes (Chantry et

al., 1997; Vanhaesebroeck et al., 1997). All three isoforms share a basic domain structure containing an adaptor binding domain to p85 in the N-terminal portion of the protein, a phospholipids binding C2, a helical domain and a kinase domain at the C-terminal (Vanhaesebroeck et al., 1997; Wymann et al., 2003). Experiments using gene-targeted mice and p110 isoform selective inhibitors have uncovered nonredundant physiological functions of the p110 isoforms. p110β and p110δ are the most prevalent catalytic subunits in non-leukocytes and untransformed leukocytes, respectively (Bilancio et al., 2006; Geering et al., 2007; Papakonstanti et al., 2008). However, p110δ shares its role with p110α in immortalized and transformed leukocytes (Papakonstanti et al., 2008). Indeed, p110 isoforms interact non-selectively with the different p85s, and have the same lipid substrate preference (Vanhaesebroeck et al., 1997). Using affinity and ion exchange chromatography and quantitative mass spectrometry, studies of Vanhaesebroeck's group further demonstrated that the p85 regulatory and p110 subunits of class IA PI3Ks are present in equimolar amount in mammalian cell lines and tissues and are assembled in obligate heterodimers (Geering et al., 2007). Their data argue against the ‘‘free p85’’ model, by which the p85 can compete with heterodimeric p85/p110 complexes for pTyr binding sites, thereby decreasing PI3K signaling (Luo and Cantley, 2005; Ueki et al., 2003). Tumor-specific (somatic) mutations only present in *PI3CA*, the gene encoding p110α (Samuels et al., 2004), mostly induce gain-of-function of p110α. The amplification of other PI3K isoforms in cancer is also documented (Kok et al., 2009).

Signal transmission from phosphoinositides

Under normal conditions, the level of the phosphoinositides is tightly regulated by a set of specific kinases and phosphatases, as indicated in Figure1.2.

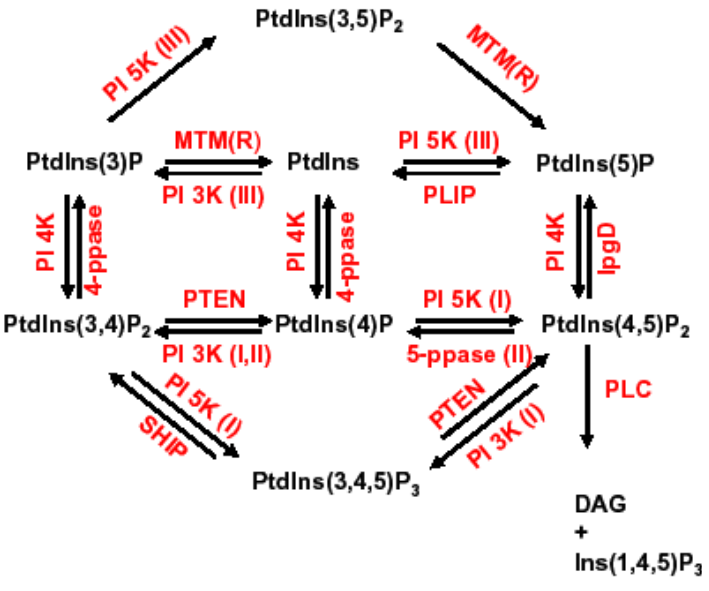

Figure 1.2 The metabolism of phosphoinositides.

PI3K: phosphatidylinositol 3-kinase, ***PI4K:*** phosphatidylinositol 4-kinase, ***PI5K:*** phosphatidylinositol 5-kinase, ***MTM:*** myotubularin, ***PTEN***: phosphatase and tensin homolog detected on chromosome 10, ***PLIP:*** PTEN-like phosphatases, ***SHIP:*** SH2-containing inositol polyphosphate 5-phosphatase. Adapted from (Blero et al., 2007).

Class I PI3Ks phosphorylates the 3-inositol position of PI (PtdIns), PI4P (PtdIns(4)P) and PI(4,5)P2 to produce PI3P (PtdIns3P), PI(3,4)P2 (PtdIns(3,4)P2) and PI(3,4,5)P3 (PtdIns(3,4,5)P3), which serve as membrane docking sites for multiple effector proteins containing phosphoinositide-binding domains, such as phox homology (PX) domain (Karathanassis et al., 2002), pleckstrin homology (PH) domains (Musacchio et al., 1993; Wang and Shaw, 1995) and cysteine-rich FYVE domains (Leevers et al., 1999). The preferred substrate of class IA PI3Ks is PI(4,5)P2. Its product PI(3,4,5)P3 regulates as an important second message the localization and function of Ser/Thr and Tyr protein kinases (such as Akt and BTK, respectively), adaptor proteins (such as Gab) and regulators of small GTPases (GAPs and GEFs) (Vanhaesebroeck et al., 2001). Inactivation of PI(3,4,5)P3 is quickly mediated by PI3- and PI5-phophatases, such as PTEN and SHIP. All PI3Ks are inhibited by the drugs wortmannin and LY294002. Furthermore, a number of pharmaceutical companies have been working on PI3K isoform specific inhibitors including the p110δ isoform specific inhibitors IC486068 and IC87114 (Lee et al., 2006). In addition to the lipid kinase activity, several PI3Ks also have protein kinase activity (Backer, 2005) but their physiological substrates remain unknown.

1.1.2 Scaffold adaptor protein Gab

The Grb2 associated binder (Gab) adaptor/scaffolding protein family comprises conserved proteins: mammalian Gab1, Gab2 and Gab3, Drosophila Dos and Caenorhabditis elegans Soc1 (Nishida and Hirano, 2003). Originally, Gab1 was identified as a binding protein for Grb2 (Holgado-Madruga et al., 1996). Both Gab1 and Gab2 are ubiquitously expressed, while Gab3 is highly expressed in lymphoid tissue (Gu et al., 1998; Nishida et al., 1999; Wolf et al., 2002). All three Gab proteins contain common domains: (i) a PH domain in the amino-terminal region, (ii) tyrosine-based motifs mediating the binding of Grb2, Crk, p85, and SHP2, (iii) proline-rich sequences (PXXP) and (iv) the c-Met binding domain (MBD) in the C-terminal region (Nishida and Hirano, 2003) (Figure 1.3). In hematppoietic systems, Gab isoforms are differentially expressed in various cell lines, while only Gab1 is expressed in primary hematopoietic progenitors (Bouscary et al., 2001; Wickrema et al., 1999). Various studies have demonstrated that Gab1 and Gab2 are tyrosine phosphorylated and associate with several signaling molecules including Grb2, Shc, SHP2 and PI3K in response to various cytokines and growth factors, such as insulin, epidermal growth factor, thrombopoietin (Tpo) and Epo (Bouscary et al., 2001; Takahashi-Tezuka et al., 1998; Wickrema et al., 1999). Gab1 and Gab2 have 15 conserved tyrosines, distinct phosphorylation patterns of Gab isoforms evoked by different ligands and receptors might be the molecular basis for signaling selectivity (Brummer et al., 2008; Gual et al., 2000; Lehr et al., 1999). Studies of Gab1 and Gab2 knockout mice have clearly indicated an important role for Gab proteins *in vivo*. Gab1-

deficient mice die as embryos with multiple defects in placental, heart, skin, and muscle development (Itoh et al., 2000). Gab2-deficient mice are viable, but have a defect in mast cell lineages and in allergic reactions (Nishida et al., 2002).

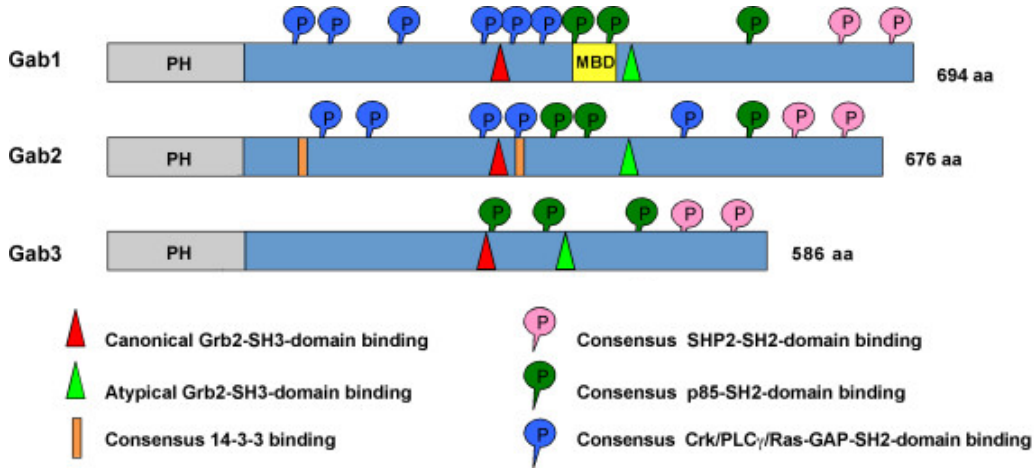

Figure 1.3 Conserved structural features of Gab proteins. Adapted from (Wohrle et al., 2009).

1.1.3 Phosphatases PTEN and SHIP1

To ensure that the activation of PI3K signaling is appropriately suppressed or terminated, PTEN and SHIP counteract PI3K activity by hydrolyzing PI(3,4,5)P3 at the 3- or 5-position of the inositol ring, yielding PI(4,5)P2 and PI(3,4)P2, respectively. Mouse knockout studies have suggested that PTEN and SHIP have profound different biological functions. Homozygous PTEN knockout is early embryonic lethal while heterozygous mice survive, but die from multiple sporadic tumors. On the other hand, mice heterozygous for SHIP loss are virtually normal (Helgason et al., 1998; Liu et al., 1999). Also the homozygous SHIP-null mice do not have an increased susceptibility to cancer; however, they have a myeloproliferative disorder resulting in a decreased life span which may preclude complete assessment of susceptibility changes to cancer in these animals (Rohrschneider et al., 2000).

PTEN

The 403-amino-acide protein PTEN is a dual protein/lipid phosphatase, which comprises an N-terminal phosphatase domain and a C2 domain both required for the enzymatic activity (Figure 1.4). The *Pten* gene shows high identity between human and mouse (Steck et al., 1997). In the majority of cell types PTEN is constitutively active thereby influence the basal PI(3,4,5)P3 level, maintaining it below the critical signaling threshold (Stambolic et al., 1998; Sun et al., 1999). Negative regulation of PTEN has been shown to occur via reactive oxygen species and Ser/Thr phosphorylation. PTEN undergoes reversible oxidation, forming a disulphide bond with a neighboring Cys in the catalytic active-site Cys residue. (Leslie et al., 2003). Studies on the oxidative inactivation of PTEN show that this physiological regulation mechanism may have significant implications for the regulation of apoptosis in macrophages

and other oxidant producing leukocytes (Cho et al., 2004; Leslie et al., 2003). On the other hand, there is increasing evidence that indicates the importance of the Ser/Thr phosphorylation in the regulation of PTEN function. The dephosphorylation of the C-terminal tail results in an open conformation in basic regions that can interact with anionic lipids, thus enhancing its association with the plasma membrane and orientating the active site towards its lipid substrates (Das et al., 2003; Tolkacheva et al., 2001). The constitutively active Ser/Thr casein kinase 2 (CK2) (Li et al., 2002), and other kinases, such as Ser/Thr kinase 11 (STK11/LKB1) (Mehenni et al., 2005), the microtubule associated kinase (MAST205) (Valiente et al., 2005) as well as GSK3β have been reported to phosphorylate PTEN at specific residues *in vitro* studies (Al-Khouri et al., 2005).

In many primary and metastatic human cancers, mutations, deletions or promoter methylation lead to an inactive PTEN (Blanco-Aparicio et al., 2007; Parsons et al., 2005). Beyond PTEN mutations, deregulation of the PTEN network also occurs through crosstalk with other tumorigenic signaling pathways, such as those involving Ras, p53, TOR (Cully et al., 2006).

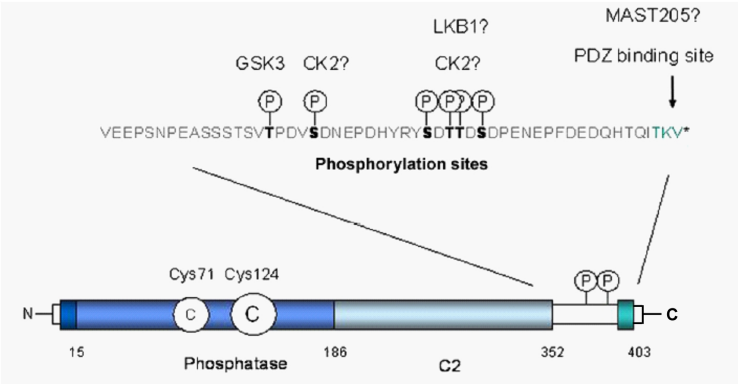

Figure 1.4 PTEN C-terminal tail phosphorylation sites and their protein kinase partners. The 403-amino-acid PTEN protein comprises an N-terminal phosphatase domain (amino acids 7–185) and a C2 domain (amino acids 186–351) that are both required for enzymatic activity. The catalytic cysteines Cys124 and Cys71 form a reversible disulphide bond upon oxidation. At the far end of the C-terminal tail a common protein-interaction PDZ binding sequence is present and within the C-terminal tail exist two PEST sequences, which are rich in proline (P), glutamic acid (E), serine (S), and threonine (T). The phosphorylation sites spanning a highly acidic stretch of the C-terminal tail and their proposed protein kinase partners are highlighted. Adapted from (Downes et al., 2007)

SHIP1

SHIP1 and SHIP2 are the products of two different genes and belong to the family of the inositol polyphosphate 5-phosphatases. Ten mammalian inositol 5-phosphatase isoenzymes have been reported. However, SHIP1 and SHIP2 have a strongly conserved domain architecture. They contain an N-terminal SH2 domain, two NPXY motifs interacting with PTB domains and a C-terminal proline-rich region (PxxP motifs) with consensus sites for SH3 domain interactions (Figure 1.5). The SH2 domain and NPXY sites mediate the binding of SHIP with a series of consensus motifs of adaptor proteins, such as Shc, Grb2, various Doks

and immunoreceptor signaling motifs (ITIM) (Pesesse et al., 2006). Knockout studies on SHIP1 and SHIP2 showed that these proteins are not redundant in function. SHIP2 is broadly expressed, while SHIP1 is specifically expressed in immune and hematopoietic cells. SHIP1 controls the levels of PI(3,4,5)P3 and is important in terminating signal transduction from cytokine-mediated signaling in hematopoietic systems. Recently, Mason *et al.* reported that SHIP1 binds to the EpoR in an SH2-dependent fashion through multiple pTyr residues, including Tyr401, Tyr429, and Tyr431, and that Epo stimulates the formation of a ternary complex consisting of SHIP1, Shc, and Grb2 (Mason et al., 2000).

As antagonist of PI3K, PTEN hydrolyzes PIP3 to PI(4,5)P2, while SHIP1 removes the PIP3 5-phosphate, generating PI(3,4)P2. A high binding affinity of Akt to PI(3,4)P2 has been reported *in vitro*, but the activation of Akt by PI(3,4)P2 *in vivo* is still under debate. A constitutively active SHIP1 protein in Jurkat cells caused increased PI(3,4)P2 level. However, the Akt phosphorylation was reduced in these cells (Isakoff et al., 1998; Lemmon and Ferguson, 2001). PI(3,4)P2 can interact with an array of protein effectors. Proteins such as DAPP1 (dual adaptor of phosphotyrosine and 3-phosphoinositides 1) and TAPP (tandem PH domain-containing protein) can selectively interact with PI(3,4)P2 (Lemmon and Ferguson, 2000). In addition, SHIP1 contains multiple structural domains, such as SH2-domains, C2 domains and NPXY motifs that allow SHIP1 to function as a scaffolding protein for facilitating protein-protein interactions (Rohrschneider et al., 2000; Sly et al., 2007). Hence, SHIP1 may alter the activities of a subset of PIP3 effectors, potentially redirect signaling rather than stop it (Harris et al., 2008).

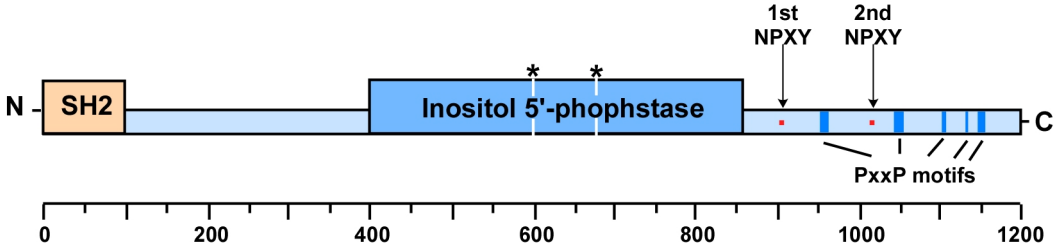

Figure 1.5 The domain structure of SHIP. Two asterisks above the central enzymatic domain mark the locations of homology regions with all 5-phosphatases. The scale below the SHIP domain structure designates its length in amino acids. Adapted from (Rohrschneider et al., 2000)

1.1.4 Akt

The AGC kinases (related to AMP/GMP kinase and protein kinase C) includes the Akt1, Akt2, and Akt3 kinases. They consist of an N-terminal PH domain, followed by a kinase domain and a C-terminal regulatory hydrophobic motif (Knighton et al., 1991; Thomas et al., 2002) (Figure 1.6). The specific or redundant functional roles of the three Akt isoforms are not clear. Activation of Akt involves its membrane translocation mediated by PIP3 and subsequently phosphorylation at both Ser473 and Thr308 sites (Vanhaesebroeck and Alessi, 2000). At the membrane, phosphorylation at Thr308 in the activation T-loop is mediated by

the 3-phosphoinositide-dependent kinase 1 (PDK1) (Alessi et al., 1997). However, the identity of the kinase(s) responsible for Ser473 phosphorylation in hydrophobic motif is quite controversial. Candidates include the integrin-linked kinase (ILK), MAPK2, mTORC2 and Akt, PDK1 themselves (Bellacosa et al., 2005; Chan and Tsichlis, 2001).

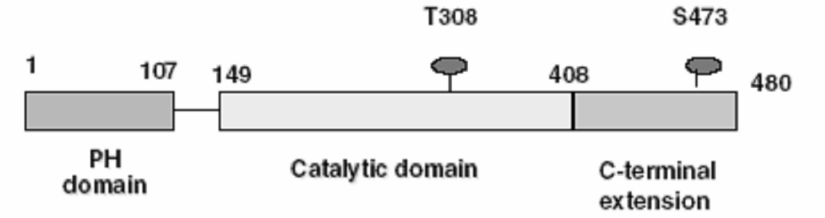

PAIR	*PH*	*LINK*	*CAT*	*EXT*
Akt1/Akt2	**80**	**46**	**90**	**66**
Akt1/Akt3	**84**	**40**	**88**	**76**
Akt2/Akt3	**76**	**17**	**87**	**70**

Figure 1.6 Pairwise % identity in Akt domains. Domain definitions using Akt1 residue numbers. ***PH****:* Pleckstrin Homology domain. ***LINK****:* Linker region, Akt 1(108–148), no significant homology to other proteins. ***CAT****:* Kinase Catalytic domain, homologous to all kinases, ~ 50% identical to the PKC, PKA, SGK and S6 families. ***EXT****:* C-terminal Extension, ~ 15% identical to the PKA family and ~35–40% identical to the rest of AGC family members. Adapted from (Kumar and Madison, 2005).

1.1.5 Akt mediated biological processes

Activated Akt mediates a large spectrum of cellular functions, ranging from control of cell proliferation and survival to modulation of intermediary metabolism and angiogenesis (Figure 1.7).

Cell proliferation

Phosphorylation of multiple substrates results in the proliferative effect of Akt: phosphorylation and consequent inhibition of GSK3 β prevents degradation of cyclin D1 (Diehl et al., 1998); translation of cyclin D1 and D3 transcripts is regulated by Akt/mTOR signaling (Muise-Helmericks et al., 1998); phosphorylation by Akt directly induces the cytoplasmic retention of cell cycle inhibitors, such as $p21^{WAF1}$ and $p27^{Kip1}$ (Testa and Bellacosa, 2001), the transcription of $p27^{Kip1}$ can be further suppressed through Akt/FoxO axis (Medema et al., 2000).

Cell survival

Akt has an effect on both the caspase cascade and the transcriptional control to provide survival signals and prevent apoptosis (Kim et al., 2001; Testa and Bellacosa, 2001). Akt directly inhibits the caspase cascade by phosphorylating the pro-apoptotic factor BAD (Creagh and Martin, 2001), procaspase-9 and astrocytic phosphoprotein PED/PEA15 (Trencia et al., 2003). In parallel, cytoplasmic retention of forkhead family factors prevents transcription of the pro-apoptotic genes Fas ligand, BIM, TRAIL, and TRADD (Basu et al., 2003; Datta et al., 1999). On the contrary, Akt promotes nuclear translocation of the nuclear

factor NF-κB, which transcribes the anti-apoptotic genes BFL1, cIAP1, and cIAP2 (Ouyang et al., 2006).

Cell growth

Akt also participates in the control of cell growth defined as an increase in cell size, not cell number, which is modulated by Akt/mTOR pathway. mTOR stimulates protein synthesis by phosphorylating two targets: ribosomal protein S6 kinase (p70 S6K) and eukaryotic initiation factor 4E binding protein 1, 2, and 3 (4E-BPs) (Gingras and Sonenberg, 1997; Kim and Sabatini, 2004).

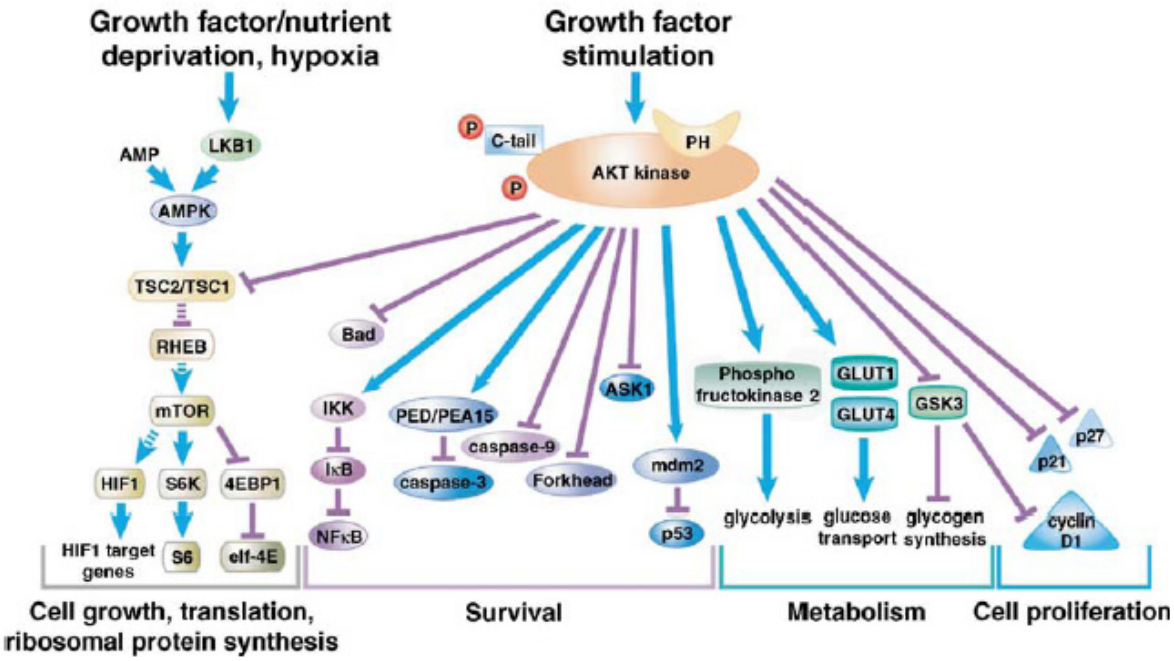

Figure 1.7 Downstream signaling: Akt substrates and their functions. Scheme depicting Akt substrates and associated cellular functions. Continuous lines imply direct phosphorylation by Akt, leading to activation (arrow end) or inhibition (blunt end). Broken lines indicate indirect or unknown mechanisms of activation/inhibition. Adapted from(Bellacosa et al., 2005).

1.1.6 Alterations of PI3K/Akt signaling in human cancers

Mounting evidence over the past dozen years indicates that PI3K/Akt alterations are common in many forms of human cancer. Hyperactivation of Akt is achieved in human cancer by an assortment of mechanisms, including amplification, overexpression, point mutation of the genes of Akt and of their upstream activators or by alteration of the downstream targets, and deletion or inactivation of pathway inhibitors (Bellacosa et al., 2005).

Upstream activators

There are several mechanisms leading to the alteration of downstream Akt activation in human cancers. Overexpression of growth factor HER-2/neu in breast cancer (Zhou and Hung, 2003), overexpression of epidermal growth factor (EGF) receptor in glioblastoma

multiforme (Schlegel et al., 2002), mutation in the EpoR gene in primary familial congenital polycythemia (PFCP) (Rives et al., 2007), amplification/upregulation of the *PIK3CA* gene (Shayesteh et al., 1999) and mutation of *PIK3CA* or *PIK3R1* (Philp et al., 2001; Samuels et al., 2004).

Akt

Akt2 is the predominant Akt family member broadly involved in cancers as shown in ovarian carcinoma (Cheng et al., 1992), primary pancreatic carcinomas and pancreatic cancer cell lines (Cheng et al., 1996; Miwa et al., 1996) as well as in hepatocellular carcinoma (Xu et al., 2004). Increased Akt1 kinase activity was reported in about 40% of breast and ovarian cancers and in more than 50% of prostate carcinomas (Sun et al., 2001). Akt3 enzymatic activity was found in estrogen receptor-deficient breast cancer and androgen-insensitive prostate cancer cell lines (Nakatani et al., 1999).

Deletion or inactivation of pathway inhibitors

Like p53, PTEN was recognized as one of the most highly mutated tumor-suppressor genes. Somatic deletions or mutations of this gene have been identified in a large fraction of tumors, including glioblastomas and endometrial and advanced prostate cancers (Di Cristofano and Pandolfi, 2000; Sansal and Sellers, 2004). SHIP mutations have also been detected in acute myelogenous leukemia (AML) (Di Cristofano and Pandolfi, 2000). Evidence indicates that the loss of function of SHIP could be involved in leukemogenesis (Sattler et al., 1999).

Downstream targets of Akt

As downstream effector of mTOR, the translation initiation factor eIF4E has been shown to cooperate with c-Myc in B-cell lymphomagenesis (Ruggero et al., 2004; Wendel et al., 2004). Akt directly regulates the retention of FoxO transcription factor in the cytosol via phosphorylation. Studies with the dominant–negative FoxO or the inducible FoxO3aA3 revealed the role of FoxO as putative tumor suppressor on Myc-driven lymphomagenesis (Bouchard et al., 2007).

1.2 Epo induced PI3K/Akt pathway

1.2.1 Erythropoiesis

Erythropoiesis is the development of mature red blood cells (erythrocytes), which is regulated by various extracellular stimuli including a network of hematopoietic cytokines that exert their biologic effects through specific interactions with their cognate cell surface receptors (Arcasoy and Karayal, 2005; Krantz, 1991). The key regulator of the erythroid lineage is a 30.4-kDa glycoprotein hormone named erythropoietin (Epo) (Papakonstanti et al.). Epo is the ligand for the erythropoietin receptor (EpoR) (Krantz and Goldwasser, 1984), a transmembrane cytokine receptor predominantly present on erythroid precursor cells. However, the expression of EpoR is not found on multipotential hematopoietic stem cells and

the early burst-forming units-erythroid (BFU-E). It begins to appear on the later BFU-E and is found in highest concentration on colony-forming units-erythroid (CFU-E), after which receptor numbers decline (Broudy et al., 1991). While BFU-Es are promoted by a large number of cytokines, such as stem cell factor (SCF), interleukin 3 (IL-3), interleukin 6 (IL-6) and transferrin, in addition to Epo, CFU-Es are highly dependent on Epo for proliferation and differentiation (Figure 1.8). Although the Epo–/– and EpoR–/– mice die at embryonic 12.5 (E12.5) day owing to severe anemia, fetal livers of these mice contain normal numbers of committed erythroid CFU-E and BFU-E progenitors (Wu et al., 1995; Yoshimura et al., 1990). These studies suggested that Epo signaling is not required for lineage determination, but is required for proliferation of progenitors and their differentiation into mature red blood cells (Constantinescu et al., 1999).

The studies of Jacobson et al. in 1957 established the kidney as the main source of circulating Epo in the adult (Jacobson et al., 1957). The other major site of Epo production in the adult is the liver, but hepatic production cannot compensate for loss of the kidneys in cases of chronic renal failure (Erslev et al., 1980). Besides, the expression of Epo has also been found in the brain (Masuda et al., 1994), the testis (Tan et al., 1992), and the placenta (Conrad et al., 1996). These studies also demonstrated that the local production of Epo could be required for a purpose other than erythropoiesis.

Regulation of the Epo gene expression occurs mainly at the transcriptional level. There is no intracellular storage of the hormone (Moritz et al., 1997). Epo production is primarily regulated by the oxygen supply to a sensor in the kidney relative to its oxygen requirements (Bunn and Poyton, 1996). The Epo gene is activated by a hypoxia-inducible factor (HIF) (Huang et al., 1997; Wang and Semenza, 1993), which binds to the hypoxia-sensitive region of the Epo gene to activate it. Although the ratio of oxygen delivery to oxygen requirements is the primary physiologic regulator of Epo production, there are also other regulation mechanisms. For instance, androgenic steroids (Huang et al., 1997; Mirand et al., 1965), anabolic steroids (Doane et al., 1975), and cobaltous chloride (Goldwasser et al., 1957) stimulate Epo production by an unknown mechanism.

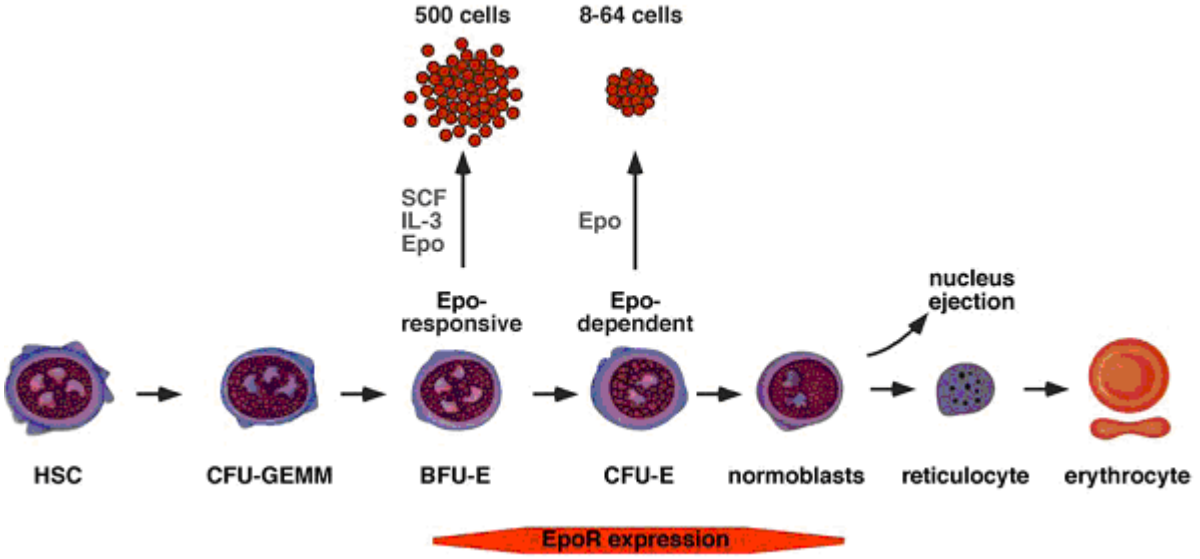

Figure 1.8 Schematic overview depicting the formation of erythrocytes from the Hematopoietic Stem Cell (HSC) during murine definitive erythropoiesis. The HSC gives rise to the multipotential progenitor cell CFU-GranulocyteErythrocyteMonocyteMegakaryocyte, which develops to the BFU-E after commitment to the erythroid lineage. Under the influence of SCF, IL-3, and Epo, the BFU-Es form burst-like colonies *in vitro* after 7-10 days. The CFU-E stage is strictly Epo-dependent and forms small colonies of about 8-64 cells after 2 days *in vitro*. The CFU-Es further develop into normoblasts under the tight control of Epo signaling. After ejection of the nucleus, the reticulocytes enter the blood stream and mature to erythrocytes. Adapted from (Becker, 2007).

1.2.2 Signaling through the erythropoietin receptor

In 1989 D'Andrea and coworkers successfully cloned the EpoR from murine erythroleukemia cells (D'Andrea et al., 1989). The EpoR is a member of the type I cytokine receptor family that includes receptors for various interleukins, granulocyte macrophage colony-stimulating factor (GM-CSF), granulocyte-colony stimulating factor (GCSF) and prolactin (Bazan, 1990; D'Andrea et al., 1990). The crystal structure analysis of EpoR revealed that the extracellular portion folds into two domains (D1 and D2), which form an L shape, with the long axis of each domain aligned at 90° to the other (Livnah et al., 1996). A common sequence motif, Trp-Ser-X-Trp-Ser (WSAWS), is highly conserved in the cytokine receptor superfamily. Most mutations in this motif abolish processing, ligand binding, and activation of the receptor (Yoshimura et al., 1992). EpoR exhibits no intrinsic tyrosine kinase enzymatic activity. Therefore, Epo/EpoR signaling is associated with the activation of the cytoplasmic Janus protein tyrosine kinase JAK2 (Witthuhn et al., 1993). The intracellular domain of EpoR contains two proline-rich motifs Box1 (residues 257–264) and Box2 (residues 303–313) and the region between Box1 and 2 (residues 265–302). These regions are implicated in the association of the EpoR with JAK2 (Huang et al., 2001; Miura et al., 1993) (Figure 1.9).

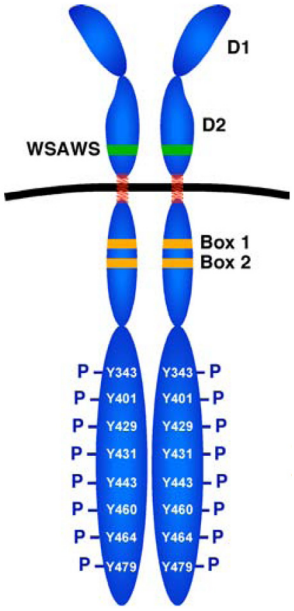

Figure 1.9 Schematic representation of conserved features and the domain structure of the EpoR. The cytokine receptor EpoR is a preformed homodimer consisting of an extracellular ligand-binding domain, a single transmembrane domain (indicated in red) as well as of a signal-transducing cytoplasmic domain. The extracellular domain displays two fibronectin type II domains (D1, D2), four characteristically spaced cysteine residues, as well as a membrane-proximal WSAWS motif (green bars). The cytoplasmic domain of the EpoR harbors two JAK2 binding sites, Box1 and Box2 (yellow bars) as well as eight Tyr residues that are phosphorylated by JAK2. Adapted from (Becker, 2007).

After ligand binding, EpoR undergoes a conformational change resulting in the rapid tyrosine phosphorylation of JAK2, which in turn phosphorylates the cytoplasmic Tyr residues of EpoR. The Tyr-phosphorylated EpoR then serves as a docking site for other Src Homology 2 (SH2) domains containing cellular proteins, initiating the subsequent signal transduction events including the phosphorylation and nuclear translocation of the signal transducer and activator of transcription 5 (STAT5), activation of phosphatidylinositol 3-kinase (PI3K), and the mitogen-activated protein kinase (MAPK) signaling pathway (Figure 1.10).

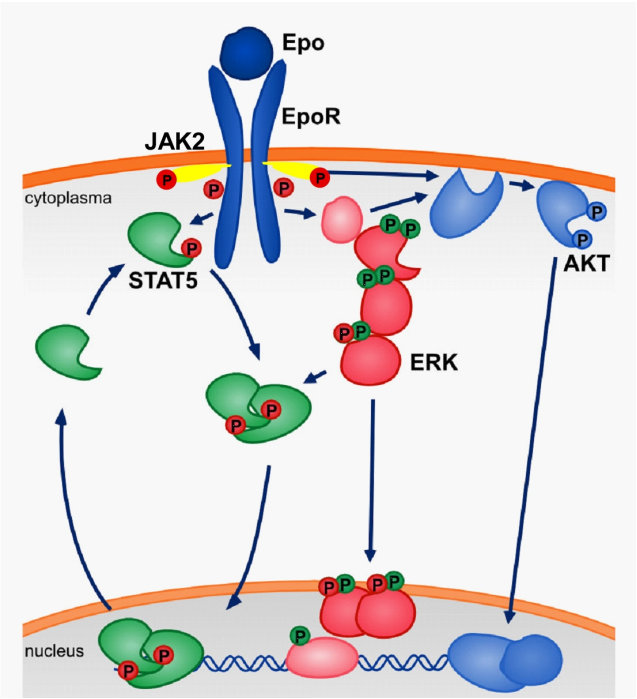

Figure 1.10 Signaling through the EpoR. The dimeric hematopoietic cytokine receptor EpoR with a single transmembrane domain is activated by Epo, which results in activation of the associated cytoplasmic tyrosine kinase JAK2. The latent transcription factor STAT5 is phosphorylated by JAK2 and translocates to the nucleus. EpoR phosphorylation also activates the PI3K pathway, leading to phosphorylation of the Ser/Thr kinase Akt. Activation of the MAPK cascade, an array of three kinases, leads to dual phosphorylation of Erk (Wymann and Marone, 2005).

JAK2

The Janus family of tyrosine kinases (JAK) includes JAK1, JAK2, JAK3 and Tyk2. They belong to a family of protein tyrosine kinases that couple to cytokine receptors. Upon ligand binding to cytokine receptors, JAKs phosphorylate themselves and their associated receptors. JAK2 is rapidly phosphorylated in response to Epo stimulation. A variety of studies have led to a model in which binding of Epo induces a conformational change in the cytoplasmic domain of the receptor and allows the juxtaposition of JAK2 molecules in a manner that facilitates their transphosphorylation within the activation loop, resulting in the activation of the kinase (de la Chapelle et al., 1993; Watowich et al., 1994). Mutation of JAK2 at Tyr1007 (Y1007F) can abolish the JAK2 activation (Feng et al., 1997). JAK2–/– mice die between day E13 and E15, with diminished number of fetal liver cells and erythroid progenitors. This suggested that JAK2 is required at an earlier stage of erythropoietic development compared to EpoR (Neubauer et al., 1998; Parganas et al., 1998).

STAT5

Studies of EpoR tyrosine-mutants concluded that either Tyr343 or Tyr401 is sufficient to mediate maximal activation of STAT5; Tyr 429 and Tyr 431 can partially activate STAT5 by association with its SH2 domain (Klingmuller et al., 1996). Ligand induced homodimerization of EpoR triggers the activation of JAK2. Following tyrosine phosphorylation by JAK2, STAT5 isoforms a and b either homo- (STAT5a/STAT5a or STAT5b/STAT5b) or heterodimerizes (STAT5a/STAT5b) translocate to the nucleus. STAT5 dimers bind to specific DNA binding sites and activate transcription in the nucleus (Meyer and Vinkemeier, 2004; Zeng et al., 2002). Some of the STAT5 targets identified are upregulated in several human cancers, suggesting that they might represent potential oncogenes in STAT5-associated malignancies (Chattopadhyay et al., 2007; Naka et al., 1997).

MAPK

Upon Epo binding, the growth factor receptor-bound protein 2 (GRB2) associated to the guanine nucleotide exchange factor (SOS) docks to the phosphorylated EpoR. Activated SOS switches the small GTPase protein Ras from the inactive (GDP-bound) to the active (GTP-bound) state (Zarich et al., 2006). Subsequently, Ras-activated factor (Raf) becomes activated when it binds to the active Ras. Raf activates the MAPK kinases (MEK)1/2, which in turn activate Erk 1/2 (Raman et al., 2007). Following the MAPK/Erk activation, a panoply of nuclear and cytoplasmic substrates becomes phosphorylated and activated, which are

involved in cell proliferation, survival, differentiation, motility and angiogenesis (Yoon and Seger, 2006). Hyperactivation of the MAPK pathway is frequently observed in human malignancies as a result of aberrant activation of receptor tyrosine kinases or gain-of-function mutations in Ras or Raf genes (Schubbert et al., 2007). Some studies have reported that the activation of PI3K by EpoR supports the activation of MAPK (Klingmuller et al., 1997). On the other hand, it has been reported that PI3K activity is not required for activation of MAPK by cytokines (Bouscary et al., 2003; Scheid and Duronio, 1996).

PI3K

Epo stimulation induces activation of PI3K through the direct association of PI3K with the last Tyr residue of the EpoR (Tyr479) (Damen et al., 1995; Gobert et al., 1995), or through recruitment with the Grb2-associated scaffold protein (Gab) via either Tyr343 or Tyr401 of the EpoR (Bouscary et al., 2003; Nishida et al., 1999). Some authors also reported the activation of the PI3K through the phosphorylation of the insulin receptor substrate 2 (IRS2) adaptor proteins (Bouscary et al., 2003). It has been previously proposed that IRS1 or IRS2 may play an essential role in Epo-regulated erythropoiesis (Richmond et al., 2005). However, it has been reported that mice lacking both IRS1 and IRS2 do not show defect in erythropoiesis (Pelletier et al., 2006). Activated PI3K phosphorylates phosphatidylinositol 4,5-bisphosphate (PI(4,5)P2) at the 3-position of the inositol ring, generating phosphatidylinositol 3,4,5-trisphosphate (PIP3), which, in turn, initiates a vast array of signaling events (Figure 1.11). Components of the PI3K pathway, including thymoma viral proto-oncogene (Akt), mammalian target of rapamycin (mTOR), glycogen synthase kinase 3 (GSK3) and the O subclass of the forkhead family of transcription factors (FoxO), are critical regulators of cell proliferation, survival, and motility (Bader et al., 2005; Cantley, 2002; Katso et al., 2001; Vivanco and Sawyers, 2002).

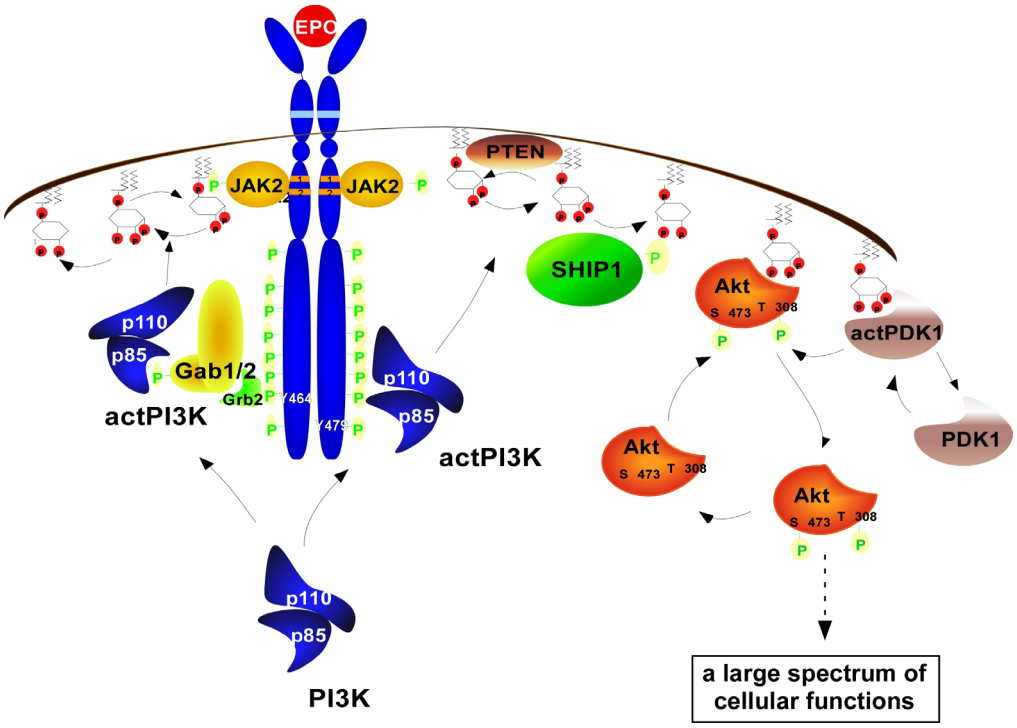

Figure 1.11 Graphical representation of the dynamic pathway model of Epo-induced PI3K pathway. In the hematopoietic system the PI3K can be activated through direct binding with the phosphorylated EpoR (pEpoR) at position Y479 or indirectly activated through the adaptor protein Gab1/2. Activated PI3K phosphorylates phosphatidylinositol 4,5-bisphosphate (PI(4,5)P2) at the 3-position of the inositol ring, generating phosphatidylinositol 3,4,5-trisphosphate (PIP3). PTEN and SHIP counteract PI3K activity by hydrolyzing PI(3,4,5)P3 at the 3- or 5-position of the inositol ring, yielding PI(4,5)P2 and PI(3,4)P2, respectively. PIP3 at the cell membrane recruits protein kinases Akt and its kinase PDK1. Akt is subsequently phosphorylated at both Ser473 and Thr308 sites and activated. Activated Akt mediates a large spectrum of cellular functions, ranging from control of cell proliferation and survival to modulation of intermediary metabolism and angiogenesis (Castaneda et al., 2010).

Termination of EpoR signal

The amplitude and duration of EpoR signaling are modulated by negative regulators. The cytokine-inducible SH2-containing protein (CIS) and the suppressor of cytokine signaling 3 (SOCS3) are members of the suppressors of cytokine signaling family binding EpoR, specifically on Tyr401 (Ketteler et al., 2003) and interfering with the receptor binding with STAT5. Additionally, CIS also mediates the ubiquitination and degradation of activated EpoR (Ungureanu et al., 2002). Phosphorylation of Tyr429 in the EpoR recruits the tyrosine phosphatase SHP1, which dephosphorylates and inactivates JAK2. Moreover, Epo binding promotes also endocytosis and degradation of the EpoR (Sawyer and Hankins, 1993; Walrafen et al., 2005).

1.3 Systems biology approach

"Systems biology...is about putting together rather than taking apart, integration rather than reduction. It requires that we develop ways of thinking about integration that are as rigorous

as our reductionist programmes, but different....It means changing our philosophy, in the full sense of the term" (Noble, 2006).

Systems biology integrates computational and theoretical methods with experimental efforts, to gain insight into the mechanisms and dynamics of biological systems on a system level (Friboulet and Thomas, 2005; Kitano, 2002). On one hand, the breakthrough in technical innovations in single-molecule measurements, nanotechnology and high-throughput measurements in molecular biology enable scientists to collect comprehensive data on system performance. On the other hand, a system with numerous components and interconnections or interactions gives rise to emergent properties that are not found in the individual components. In contrast to the traditional reductionistic approach, systems biology no longer focuses on the analysis of individual, isolated reactions, but on integrated networks. Therefore, with a systems biology approach it is possible to gain a deep insight into the complexity, robustness, modularity, feedback regulation and fragility of the complete system (Csete and Doyle, 2002). Moreover, a multi-scale systems-biology approach can span a wide range of spatial and temporal scales to understand, predict and control the properties of biological systems such as cells, organ, organism and ecosystem (Laubenbacher et al., 2009).

Mathematical modeling is an iterative process depicted in Figure 1.12 (Kitano, 2002; Kolch et al., 2005). A hypothesis-driven mathematical model is defined based on the established biological knowledge and available qualitative and quantitative experimental information. Of course, the decision which type of the model to choose and how detailed it should be depends on the biological question the model is supposed to answer. Models used for signaling pathway can be classified into different categories (Klipp and Liebermeister, 2006): (i) A deterministic process with defined future states is the counterpart to a stochastic process described through probability distribution. (ii) Continues models relied on finer timing and exact molecular concentrations are the counterpart to discrete models for representing data with a sequence of quantities. (iii) Models that may or may not describe the processes in space. Deterministic and continuous models are the common type of biological models and are represented by ordinary differential equations (ODE). ODE networks describe kinetics in a mass action approximation. Rates of a reaction i.e., d[Xi]/dt are proportional to the concentrations of the reacting species. When model structure and parameter values have been adjusted by implementing experimental data, further mathematical exploration and analysis can reveal underlying mechanisms beyond observations and examine complex biological interactions (Andrews and Arkin, 2006; Maiwald et al., 2007). Moreover, model simulation is powerful tool to guide new experiments, which in turn, can further improve the model (Becker, 2008).

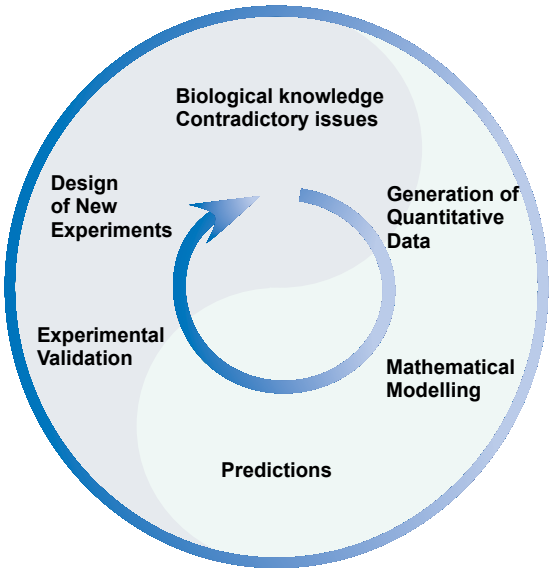

Figure 1.12 Iterative cycle between experiments and modeling in systems biology. In close collaboration between experimentalists and theoreticians, open biological questions are addressed in an iterative cycle approach of quantitative data generation, mathematical modeling, *in silico* predictions, experimental validation and design of new experiments. Adapted from (Kitano, 2002)

One of the particularly challenging tasks of systems biology is to understand the underlying structure of signaling networks and how changes in these networks can affect the transmission of information. In this respect, mathematical models representing the kinetic properties of a system have already proven to be predictive and useful tools in a number of cases. Examples of these are NGFR signaling (Qiu et al., 2004; Sasagawa et al., 2005), EGFR signaling (Schoeberl et al., 2002; Wiley et al., 2003), MAPK cascades (Kolch et al., 2005; Schilling et al., 2009), JAK-STAT signal transduction (Swameye et al., 2003; Yamada et al., 2003; Zi et al., 2005) and calcium signaling (Kummer et al., 2000). Recently, several integrative models have been used to examine the cross-talk of PI3K/Akt pathway and MAPK pathway by C. *et. al.* (C et al., 2008) and Wang *et.al*. (Wang et al., 2009). However, it is still required to develop computational models for a detailed description of the PI3K/Akt pathway structure and its dynamic in specific cell systems.

1.4 Objective

A central issue in cell biology is how a particular signaling pathway can specifically trigger distinct cellular outcomes. The specificity of response to one signaling cascade depends on diverse factors including the timing and strength of extracellular signals, the nature of protein isoforms, subcellular localization of signaling proteins, synergy and feedback controls, and quantitative differences in the expression of pathway constituents. How these regulating factors are integrated to determine the signaling output and what are their particular effects on fine-tuning the signal transduction still remain to be clarified. Moreover, how does the

pathway specify different biological output, leading to cell type-specific responses? It is a big challenge here for mathematical modeling.

In erythrogenesis, Epo induced PI3K/Akt pathway mediates a large spectrum of cellular functions of erythroid progenitor cells, ranging from control of cell survival, proliferation and differentiation. In order to closely representing PI3K/Akt signaling in an *in vivo* situation, primary erythroid progenitor cells at the CFU-E stage (CFU-E) were chosen as a cellular model system for our study. In addition, the factor-dependent murine pro-B cell line BaF3 exogenously expressing the murine EpoR is a well established system to study Epo-dependent signaling.

The goal of this work was to first establish an ODE model, representing the topology and dynamics of PI3K/Akt pathway in both systems based on stoichiometric analysis of the pathway components. The model was further calibrated by quantitative, time-resolved kinetic properties of the pathway. By applying mathematical approach, it was aimed to identify the crucial regulatory mechanisms, which determine the cell type-specific PI3K/Akt signaling in CFU-E and BaF3-EpoR cells, in particular, the PTEN and SHIP1 mediated negative regulations. Furthermore, the quantitative link of Akt activation to its downstream signaling as well as cellular decisions can help to understand how the PI3K/Akt pathway specifies different biological output, leading to context-dependent responses in different hematopoietic cells.

2. Results

2.1 Cell type-specific activation profile of Epo-induced PI3K/Akt signaling

2.1.1 Generation of time-course data in CFU-E and BaF3-EpoR cells

To explore the dynamic response of the pathway upon Epo stimulation, time courses of EpoR and Akt phosphorylation were performed by quantitative immunoblotting in CFU-E and BaF3-EpoR cells. A standardized protocol was established that optimizes the preparation, cultivation and stimulation of cells and ensures the reproducibility and comparability of experimental data. Preliminary tests and dose-response experiments revealed that a growth factor depletion time of 5 hours in BaF3-EpoR and 2 hours in CFU-E cells as well as a dose of 5 and 2.5 U/ml Epo, respectively, are appropriate for maximal signal activation within the linear range. Hence, these conditions were used in all time-course experiments. The experimental data demonstrated that in both cell types the initial phosphorylation of EpoR and Akt increased rapidly upon Epo stimulation, but their deactivation kinetics differed fundamentally (Figure 2.1 A, C). In CFU-E cells the phosphorylation of EpoR revealed a transient maximum approximately 10 min after Epo addition followed by a sharp decline, while the pAkt signal remained at a constant high level for at least 40 min. Interestingly, in contrast to the dynamics observed in primary cells, Akt phosphorylation in BaF3-EpoR cells returned to basal level after 30 min despite sustained pEpoR level over a one-hour observation period. Remarkably, it was found that not only the duration but also the magnitude of EpoR and Akt phosphorylation exhibited significant differences between these two cell types. Although the maximal amount of pEpoR measured in BaF3-EpoR cells was approximately 10-fold higher compared to CFU-E cells, the phosphorylation of Akt was considerably stronger (approximately 3-fold) in CFU-E cells (Figure 2.1 B, C).

Taken together, the observations reveal that Akt activation is more sustained and stronger in CFU-E cells than in BaF3-EpoR cells despite shorter and weaker EpoR activation (Figure 2.1.C). These striking discrepancies in the dynamic behavior of EpoR/PI3K/Akt signaling between CFU-E and BaF3-EpoR cells suggest that there are differences in the regulation of Akt activation and emphasized the importance of studies that compare the stoichiometry of pathway components and dissect potential positive and negative regulatory mechanisms of PI3K/Akt signaling in primary cells versus the cell line.

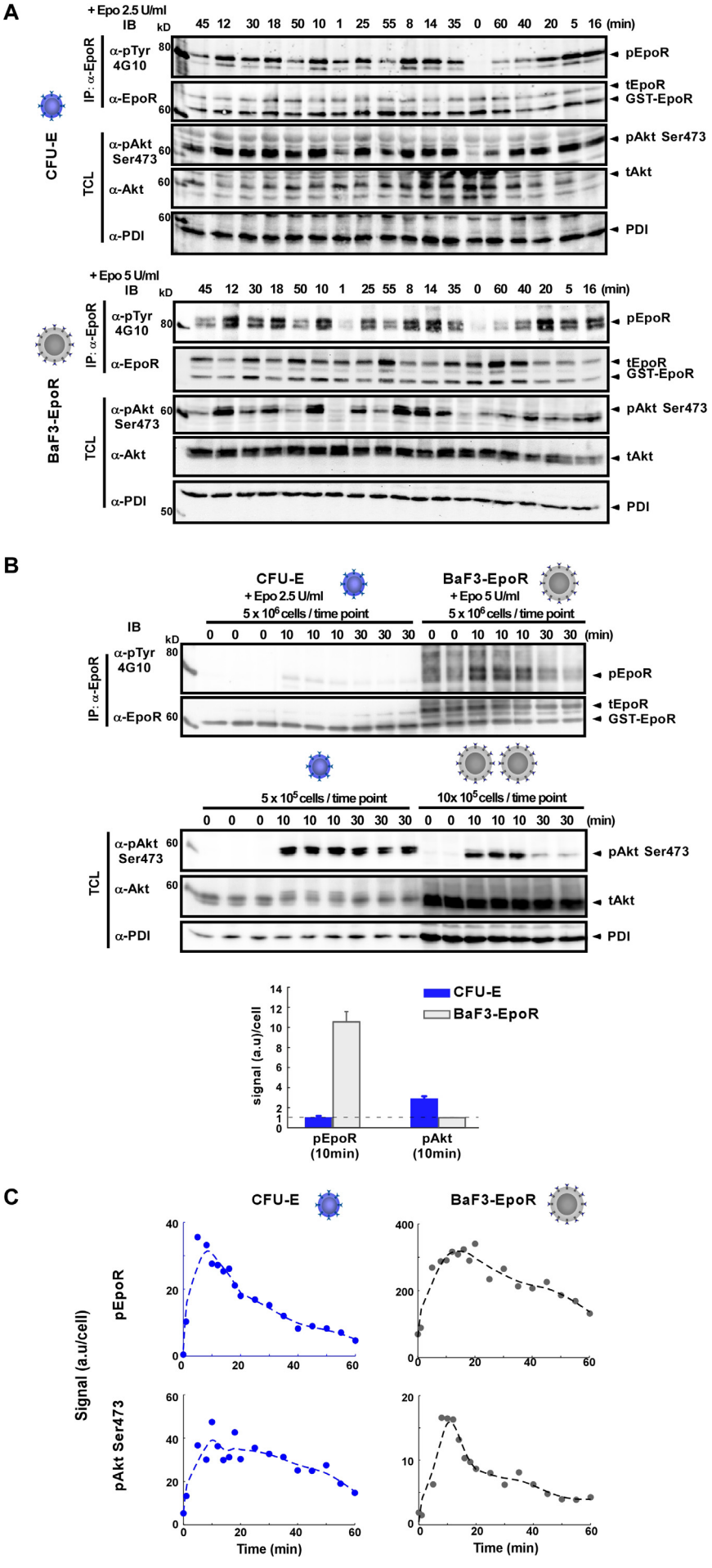
A
+ Epo 2.5 U/ml
IB
kD
45 12 30 18 50 10 1 25 55 8 14 35 0 60 40 20 5 16 (min)
IP: α-EpoR
α-pTyr 4G10
α-EpoR
pEpoR
tEpoR
GST-EpoR
CFU-E
TCL
α-pAkt Ser473
α-Akt
α-PDI
pAkt Ser473
tAkt
PDI
+ Epo 5 U/ml
BaF3-EpoR
B
CFU-E
+ Epo 2.5 U/ml
5 x 10^6 cells / time point
BaF3-EpoR
+ Epo 5 U/ml
5 x 10^6 cells / time point
0 0 0 10 10 10 30 30 30 0 0 10 10 10 30 30 (min)
5 x 10^5 cells / time point
10x 10^5 cells / time point
CFU-E
BaF3-EpoR
signal (a.u)/cell
pEpoR (10min)
pAkt (10min)
C
Signal (a.u/cell)
pEpoR
pAkt Ser473
Time (min)

Figure 2.1 Cell type-specific EpoR/PI3K/Akt signaling. Growth factor-depleted CFU-E cells ($2x10^7$ cells/ml) and BaF3-EpoR cells ($4x10^7$ cells/ml) were stimulated for the indicated times with 2.5 or 5 U/ml Epo, respectively. (**A**) Time courses of EpoR and Akt phosphorylation for 1h. EpoR was immunoprecipitated (IP) from total cytoplasmic lysates (TCL). Levels of phosphorylated and total EpoR as well as the calibrator GST-EpoR used for normalization of the IP were determined by subsequent quantitative immunoblotting (IB). TCL (100μg) were analyzed by immunoblotting with anti-phospho-Akt Ser473 (α-pAkt Ser473) and anti-Akt (α-Akt) antibodies. The endogenous level of PDI from TCL was quantified to normalize the phospho-Akt (pAkt) and total-Akt (tAkt) signals. (**B**) The magnitude of EpoR and Akt phosphorylation in CFU-E and BaF3-EpoR cells was compared by analyzing the samples on the same immunoblot. Bars represent the relative magnitudes of pEpoR and pAkt compared to each other in CFU-E and BaF3-EpoR cells after 10 min Epo stimulation. (**C**) To visualize the dynamics of experimentally measured EpoR and Akt phosphorylation in (A, B), smoothing splines (dashed lines) were calculated using the GelInspector software. Experimental data are depicted as solid circles (quantified data shown in Table 6.1, 6.2). Dashed lines represent the smooth splines. The experiment was repeated at least three times with similar results and representative blots are shown.

2.1.2 Quantification of PI3K/Akt pathway components

To quantify endogenous levels of pathway components, recombinant proteins were used in combination with quantitative immunoblotting. Recombinant proteins (calibrators) consisting of either the full-length protein of interest or a truncated version harboring the relevant epitopes for antibody binding were tagged with glutathione S-transferase (GST) or streptavidin binding-peptide (SBP) for purification and expressed in *E.coli*. The absolute concentrations of the calibrators were determined by means of a known BSA standard. To quantify endogenous protein levels, the respective calibrators were spiked into either cellular lysates or lysis buffer without cellular material in a dilution series prior to immunoprecipitation. After quantification of immunoblotting signals, endogenous protein concentrations could be estimated in absolute molecule numbers per cell based on the calculated calibration curves. The ratios of signaling components between CFU-E and BaF3-EpoR cells were further confirmed by directly comparing the immunoblotting signals of samples loaded on the same blot.

First, the endogenous levels of the negative regulators PTEN and SHIP1 were analyzed applying the calibrators SBP-PTEN and GST-SHIP1, respectively. Impressively, both PTEN and SHIP1 were found to be expressed almost 35-fold and 20-fold higher in BaF3-EpoR cells compared to their levels in CFU-E cells (Figure 2.2 A, B, F and Figure 2.3).

Next, other intracellular key components of PI3K/Akt signaling, PI3K, Akt as well as PDK1 were analyzed. The concentration of PI3K in cells was determined by detecting the protein level of p85 applying the calibrator SBP-p85. The endogenous levels of p85 were observed to be in the range of approximately 10,500 molecules per cell in BaF3-EpoR cells and 3,000 molecules per cell in CFU-E cells (Figure 2.2. C, F and Figure 2.3). The endogenous concentration of Akt in BaF3-EpoR cells was estimated to be in the range of 430,000 molecules per cell (Figure 2.2 E, F and Figure 2.3). By loading the samples on the same gel, the endogenous protein level of Akt in CFU-E cells was directly compared to its level in

BaF3-EpoR cells and determined to be in the range of 100,000 molecules per cell (Figure 2.2 F). For PDK1, we estimated a ratio of approximately 3:1 between BaF3-EpoR and CFU-E cells by directly comparing the immunoblotting signals of samples loaded on the same blot (Figure 2.2 F).

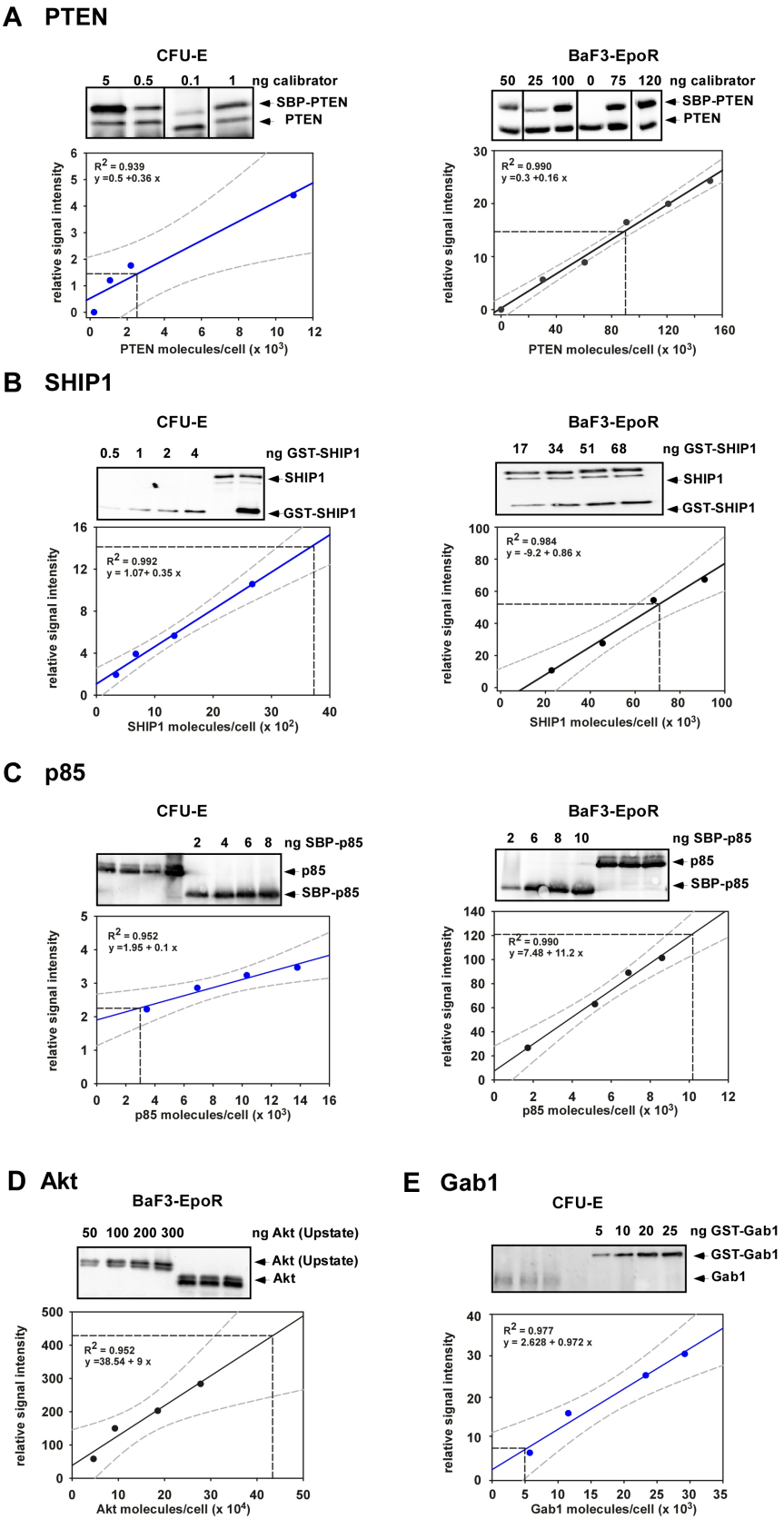

F

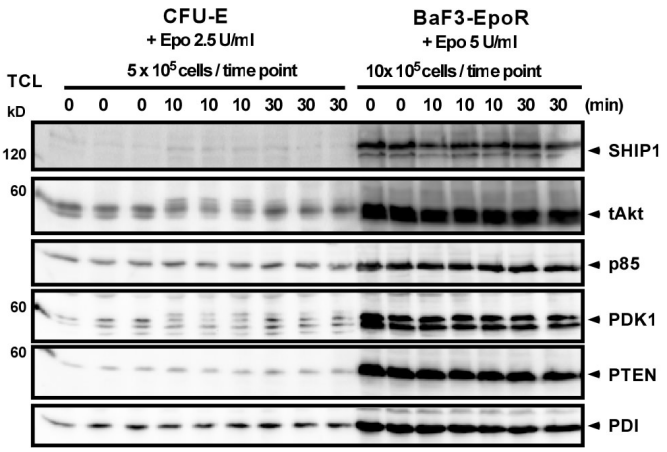

Figure 2.2 Quantification of molecule numbers per cell of PI3K/Akt pathway components. Endogenous protein levels of (**A**) PTEN, (**B**) SHIP1, (**C**) p85, (**D**) Akt and (**E**) Gab1 were estimated in cellular lysates of BaF3-EpoR and CFU-E cells using corresponding recombinant calibrator proteins. Non-stimulated 1×10^7 BaF3-EpoR cells or 5×10^6 CFU-E cells were lysed and proteins of interest including recombinant standards were immunoprecipitated and subsequently analyzed by quantitative immunoblotting. Dilution series of recombinant proteins were plotted with linear regression functions (solid lines), and 95% confidence intervals were defined (dashed lines). The levels of endogenous proteins are indicated by dashed drop lines. In (**F**), the ratios of PTEN, SHIP1, Akt, p85 and PDK1 between both cells were further confirmed by directly comparing the immunoblotting signals of samples loaded on the same blot.

The adaptor protein Gab that ispresent in different isoforms, i.e. Gab1 and Gab2, coordinates the assembly of the PI3K complex and thereby recruits and enhances the enzymatic activity of PI3K. In primary erythroid progenitors, EpoR utilizes Gab1, whereas Gab2 is dominantly present in BaF3-EpoR cells (Edmead et al., 2006; Miyakawa et al., 2001). In our study, we detected tyrosine phosphorylation of Gab1 and Gab2 in CFU-E and BaF3-EpoR cells respectively following exposure to Epo, see Figure 2.5. Furthermore, the endogenous level of Gab1 was determined in the range of 5,000 molecules per cell in CFU-E cells applying calibrator GST-Gab1 (Figure 2.2 E, F and Figure 2.3).

To consider the difference in cell size, the average cytoplasmic volumes of both cells were determined by confocal microscopy (experiment by Andrea C. Pfeifer, DKFZ Heidelberg). The quantification revealed that BaF3 cells have a cytoplasmic volume of 1400 μm^3, which is approximately 3 times larger compared to the cytoplasmic volume of CFU-E determined as 399 μm^3. This information was used to convert molecules/cell into concentration in nM. The number of EpoR on the cell surface of BaF3-EpoR cells was determined as 15,700 molecules per cell by a saturation-binding assay with [125I]-labeled Epo (Becker et al., 2010). Molecules per cell for EpoR on the surface of CFU-E cells was reported as 1,000 previously (D'Andrea and Zon, 1990). For an overview of the stoichiometry of pathway components see Figure 2.3.

Stoichiometry of PI3K Pathway Components

	CFU-E	BaF3-EpoR
cytoplasm volume (μm³)	399	1 400
cell surface area (μm²)	372	729
EpoR surface(molecules/μm²)	2.7	21.5
	molecules/cell (nM)	
Akt	97 700 (407)	430 000 (510)
PI3K	3 000 (12.5)	10 500 (12.5)
SHIP1	3 700 (15.4)	71 000 (84.2)
PTEN	2 500 (10.4)	90 500 (107.4)
Gab1	5 000 (20.8)	-
Gab2	-	+
PDK1(ratio)	1	1

Figure 2.3 Stoichiometric analysis of PI3K pathway components. See main text for detailed explanation of the quantification. '-' indicates the absence and '+' indicates the presence of protein in cells, for which quantitative information is not available.

In summary, the concentrations of pathway components Akt, PI3K and PDK1 were detected to be within the same range in both cell types. However, the density of EpoR on the cell surface and the endogenous levels of PTEN and SHIP1 were found to be profoundly higher in BaF3-EpoR cells. This is consistent with the kinetics of EpoR and Akt (Figure 2.1). Additionally, the expression of distinct Gab isoforms was observed in these two cell types. To address if the stoichiometry of different protein species participates in modulating the cell type-specific PI3K/Akt signaling in CFU-E and BaF3-EpoR cells, a mathematical modeling approach was applied, which can help to understand complex and highly dynamic interactions of PI3K/Akt pathway components beyond experimental observations.

2.2 Data-based mathematical model of EpoR/PI3K/Akt signaling

A mathematical modeling approach provides a useful tool to independently assess the effect of each core component during the complex and dynamic interactions in PI3K/Akt signaling. In essence, modeling analysis allows for examining various aspects associated with the dynamics of pathway components, yielding detailed information on reaction rates and fluxes, which are difficult to be investigated experimentally.

In collaboration with Sandip Kar, Lu Wang and Thomas Höfer (DKFZ, Heidelberg), an ODE-based mathematical model was developed for the Epo-induced EpoR/PI3K/Akt signal transduction in both CFU-E and BaF3-EpoR cell systems. The mathematical model incorporated protein-protein and protein-lipid interactions as well as enzymatic reactions without considering transient complex formation. As there is no feedback regulation from downstream components reaching the receptor, the receptor activation model could be separated from the core model of PI3K/Akt activation. In order to take into account the effect of the relative subcellular distribution of proteins on the reaction rates, cellular membrane

and cytoplasm were defined as distinct compartments. Based on the experimental measurements as well as on literature data, the concentrations of key reaction species in this pathway were fixed and rescaled to densities on the cellular membrane or to cytoplasmic concentrations (Table 6.10).

2.2.1 The receptor activation model

The receptor activation model was developed to capture signal initiation at the plasma membrane. Therefore, trafficking and multisite phosphorylation of EpoR were not considered and receptor down-regulation mechanisms such as receptor endocytosis as well as dephosphorylation were summarized in two negative feedback loops: (i) dephosphorylation of the receptor by phosphatase SHP1 (Klingmuller et al., 1995; Sharlow et al., 1997) and (ii) the signal suppression mediated by cytokine-inducible signaling suppressors, such as SOCS3, which inhibits the activity of upstream receptor kinase JAK2 (Marine et al., 1999). In addition, the depletion of extracellular ligand mediated by receptor endocytosis during the time of observation was detected by directly immunoprecipitating Epo from the medium. Experimental data showed that for BaF3-EpoR cells stimulated with 5 U/ml Epo, ligand depletion in the medium was rapid and could be described by an exponential decay function $y=5e^{-0.01732t}$ (Becker et al., 2010). Epo depletion in the medium of BaF3-EpoR cells was observed to be much slower at higher Epo concentrations due to the saturation of ligand-receptor binding (Becker, unpublished data). Moreover, data from that study allowed assuming a nearly constant ligand concentration for CFU-E cells stimulated with 2.5 U/ml Epo within one hour observation, which could be explained by an approximately 10-fold lower EpoR cell surface expression in primary cells compared to BaF3-EpoR cells. The established receptor activation model is schematically depicted in Figure 2.4, describing different Epo input functions in CFU-E and BaF3-EpoR cells, activation of EpoR upon Epo binding to the receptor and subsequent activation of two negative feedback loops.

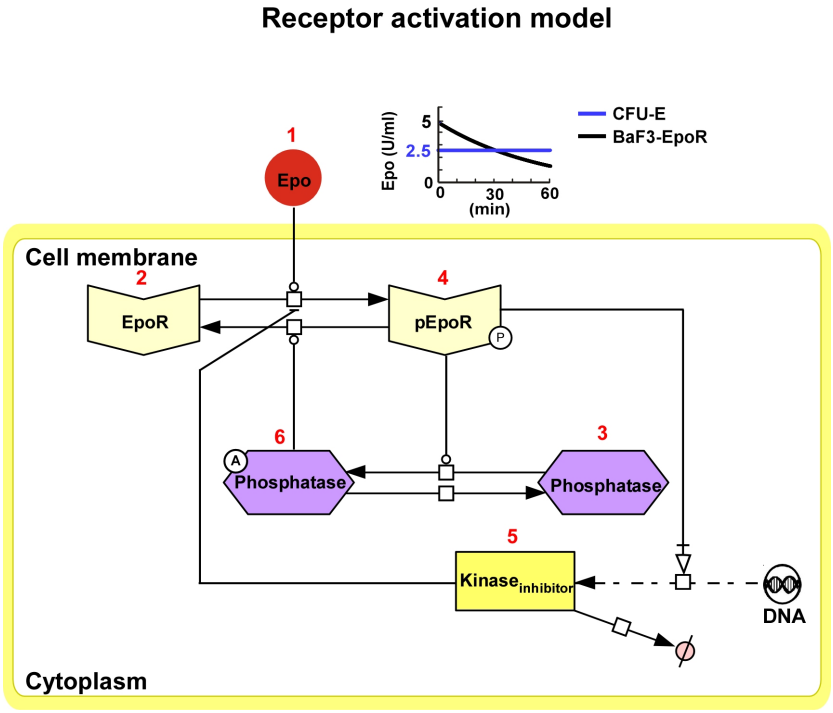

Figure 2.4 The receptor activation model. The receptor activation model includes different Epo input functions in CFU-E and BaF3-EpoR cells, activation of EpoR upon Epo binding to the receptor and subsequent activation of two negative feedback loops. The reaction steps of the model are numbered from 1 to 6 (red).The individual reactions and their parameters are listed in detail in *Appendix 6.3.*

2.2.2 The core model of PI3K/Akt activation

The core model is divided into three interconnected submodules describing *PI3K activation*, *PIP3 regulation* and *Akt activation*.

PI3K activation: was modeled through direct binding to phosphorylated EpoR (Miura et al., 1994) or via the scaffold protein Gab1/2 (Bouscary et al., 2003; Wojchowski et al., 1999). Although Gab1 and Gab2 seem to mediate overlapping biological signals in many cells, they may exert their functions by distinct mechanisms (Gu et al., 2000; Gu and Neel, 2003; Rodrigues et al., 2000). Results of a preliminary experiment using the PI3K inhibitor LY240002 show that Gab1 and Gab2 exhibited distinct activation kinetics: Gab1 phosphorylation was clearly reduced in the presence of LY240002 suggesting a PIP3-mediated positive feedback on Gab1 activation (Eulenfeld and Schaper, 2009; Itoh et al., 2000), whereas Gab2 phosphorylation was unaffected (Figure 2.5). Gab1, Gab2, and Gab3 were expressed in BaF3 cells, but the dominant isoform is Gab2 (Miyakawa et al., 2001). Therefore, isoform-specific parameters were assumed for the indirect PI3K activation mediated by Gab1 and Gab2 in CFU-E and BaF3-EpoR cells, respectively. Besides PI3K activation upon Epo stimulation, a cytosolic constitutive active PI3K was assumed in the model (Batty and Downes, 1996; Jia et al., 2008), which possesses a different catalytic activity than the complexes pEpoR-PI3K and pEpoR-Gab1/2-PI3K.

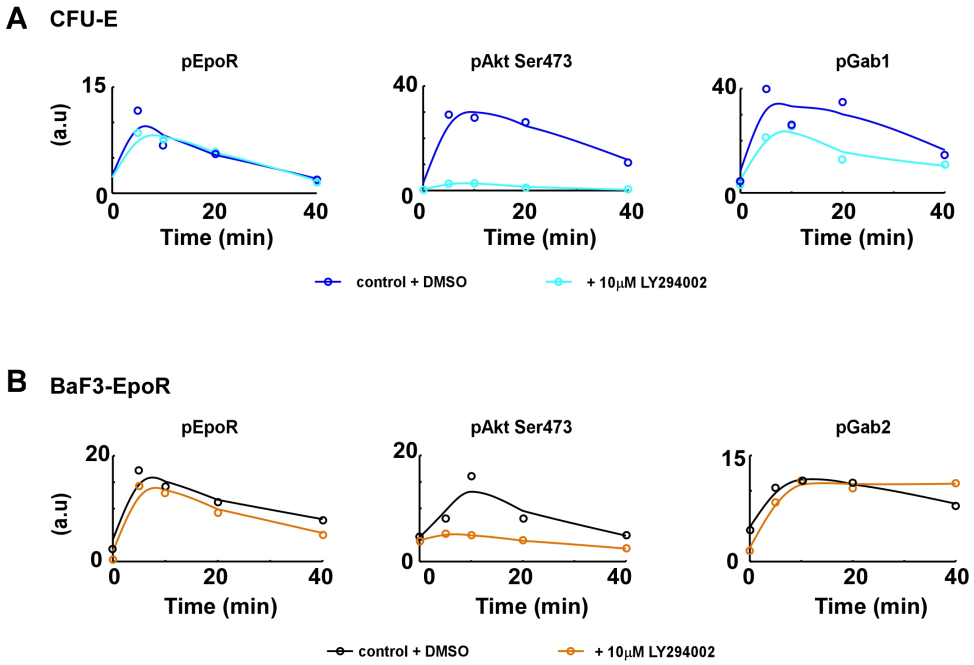

Figure 2.5 Distinct activation kinetics of Gab1 and Gab2. In a preliminary experiment, growth factor-depleted (**A**) CFU-E cells ($2x10^7$ cells/ml) or (**B**) BaF3-EpoR cells ($4x10^7$ cells/ml) were pre-incubated with 10 μM LY294002 for 30 min and then stimulated with 2.5 U/ml or 5 U/ml Epo respectively for the indicated times. As control, cells were treated with the same amount of DMSO and Epo. EpoR and Gab1/2 were immunoprecipitated from cellular lysates; phospho-EpoR (pEpoR) and phospho-Gab1/2 (pGab1/2) were detected by subsequent immunoblotting. pAkt Ser473 signals were detected from TCL. Pre-incubation with LY294002 for 30 min did not affect Epo-induced EpoR phosphorylation, but almost completely abolished Akt activation in both cell types. However, the phosphorylation of Gab1 in CFU-E cells was clearly reduced, whereas Gab2 phosphorylation was unaffected in BaF3-EpoR cells.

PIP3 regulation: Active PI3K phosphorylates PI(4,5)P2 generating PIP3 in the plasma membrane. It is well known that PTEN and SHIP1 share the property of negatively regulating PIP3 levels by hydrolyzing PI(3,4,5)P3. However, the mechanisms for their regulation remain elusive. Previous studies have indicated that in the majority of cell types PTEN is constitutively active, thereby influencing basal PI(3,4,5)P3 levels, maintaining it below a critical signaling threshold (Stambolic et al., 1998; Sun et al., 1999). In contrast, SHIP1 gets activated upon membrane recruitment mediated by its binding to the phosphorylated EpoR (Mason et al., 2000). These different activation mechanisms were implemented in the model, describing the regulation of PIP3 levels by PTEN and SHIP1.

Akt activation: PIP3, generated upon activation of PI3K, recruits Akt and its kinase PDK1 to the plasma membrane via their PH domain, facilitating PDK1 to phosphorylate Akt at Thr308 (Stokoe et al., 1997). Akt is also phosphorylated at Ser473 by other kinases to achieve its full activation (Shiota et al., 2006). A synchronized activation at both Thr308 and Ser473 of Akt in CFU-E cells was measured (Figure 2.6), while the phosphorylation at Thr308 was undetectable in BaF3-EpoR cells. Therefore, Akt double phosphorylation is summarized to one reaction catalyzed by membrane-recruited PDK1in the model. Activated Akt rapidly dissociates from the membrane and is dephosphorylated in the cytoplasm.

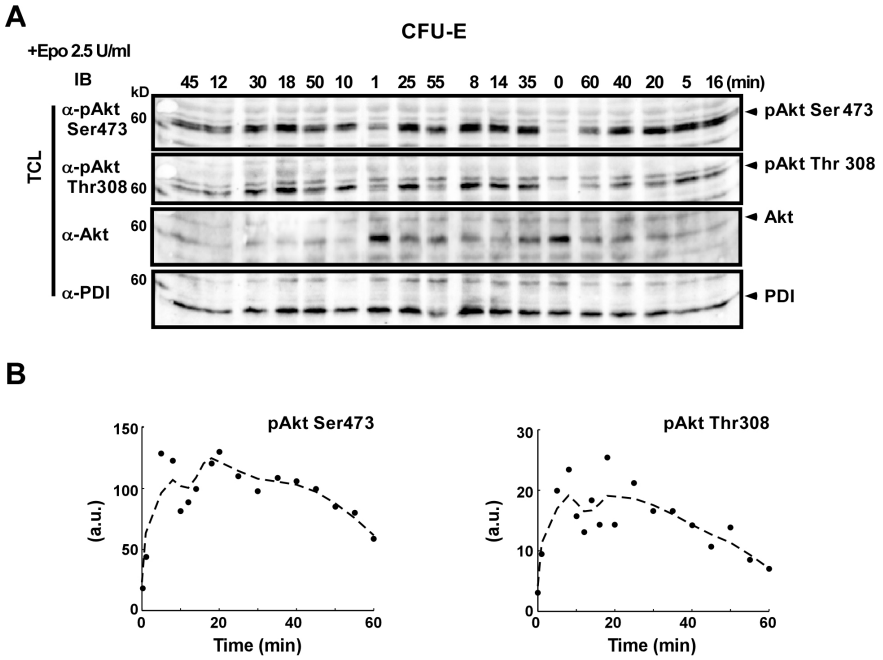

Figure 2.6 Synchronized activation of Akt at Ser473 and Thr308 in CFU-E cells. (**A**) Lysates of CFU-E cells treated with 2.5 U/ml Epo were collected at the time indicated and analyzed by immunoblotting with specific antibodies for pAkt Ser473, pAkt Thr308 and an antibody against total Akt. The endogenous level of PDI from TCL was quantified as normalizer. (**B**) Time courses of Akt phosphorylation at Ser473 and Thr308. Experimental data are depicted as dots. Dashed lines represent the smooth splines. The experiment was repeated at least three times with similar results and representative blots are shown.

To reduce model complexity, we condensed some sequential multi-step processes to a simplified one-step description without changing the network topology (Borisov et al., 2009). For instance, Gab cannot bind directly to Epo receptor. The activation of Gab requires an additional adaptor protein, Grb2, which mediates the recruitment of Gab to the pEpoR. Subsequently Gab is phosphorylated at multiple tyrosine residues (Borisov et al., 2009). Likewise, SHIP1 has been described to directly associate with EpoR in a SH2-dependent manner through multiple phosphotyrosine residues, including Tyr401, Tyr429, and Tyr431 (Mason et al, 2000) or to form a complex with Grb2 and Shc (Damen et al, 1996; Lioubin et al, 1996). As in those cases the key process is the membrane recruitment of Gab and SHIP1, all these simultaneously or sequential binding events should have a small effect on downstream signaling and can be described as one-step process.

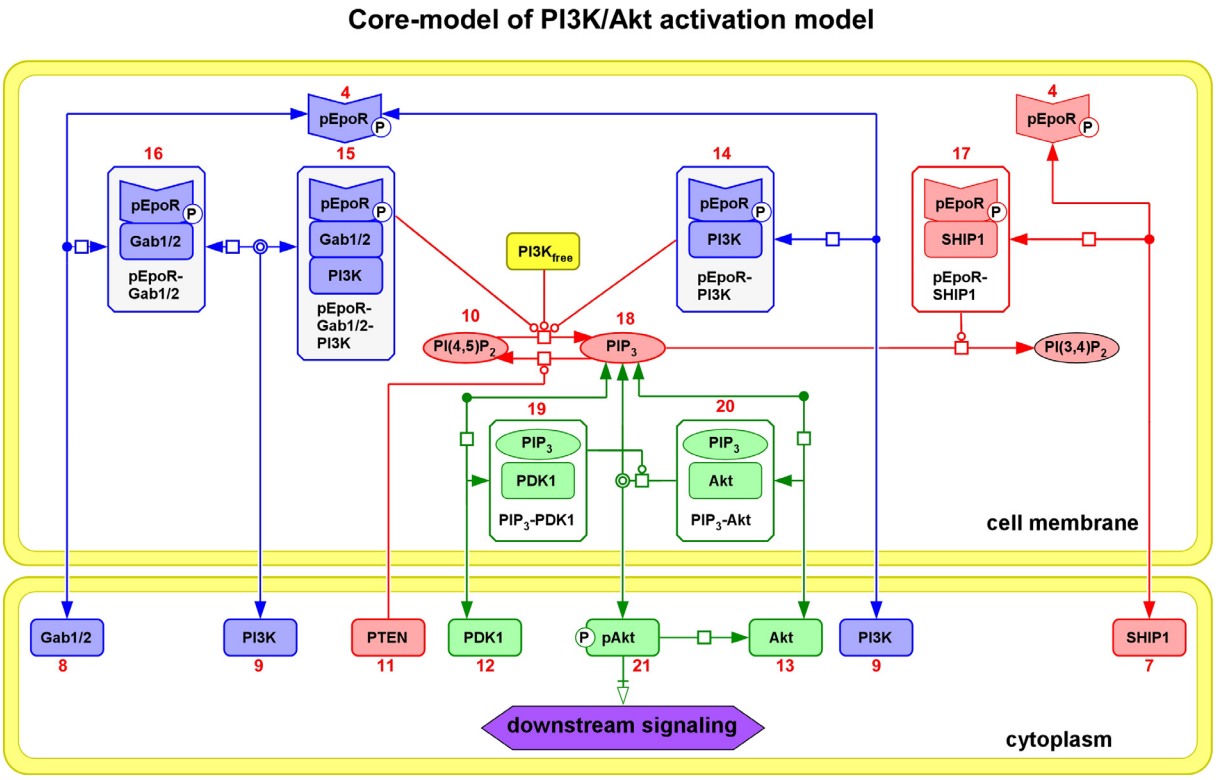

Figure 2.7 The core model of PI3K/Akt activation. The core-model of PI3K/Akt activation consists of three submodules: *activation of PI3K* (blue), *regulation of PIP3 level* at the plasma membrane (red), and *activation of Akt* (green). See text for a detailed explanation about the model modules. The reaction steps of the model are numbered from 1 to 21 (red). The individual reactions and their parameters are listed in detail in *Appendix 6.3.*

2.3 Model calibration using muti-experiment fitting

To determine the parameters of the EpoR/PI3K/Akt pathway model, time-resolved quantitative data of pathway activation were required to calibrate the models. The data sets were generated in CFU-E and BaF3-EpoR cells monitoring the kinetics of EpoR and Akt simultaneously by quantitative immunoblotting.

2.3.1 Epo ligand-receptor dynamics

To monitor ligand-receptor dynamics, EpoR phosphorylation in CFU-E and BaF3-EpoR cells was determined in a time-resolved manner in response to different doses of Epo within a range from 0.1 to 10 U/ml in CFU-E and 0.5 to 50 U/ml in BaF3-EpoR cells (Figure 2.8 A, B). In general, the receptor activation in primary cells was much weaker and more transient compared to BaF3-EpoR cells (see Figure 2.1 B). In both cells, a high dose of Epo prolonged the activation of receptor and shifted the activation peak to earlier time. Additionally, to accurately represent the dynamic behavior, time courses with more dense sampling were performed with an Epo stimulation of 2.5 U/ml in CFU-E cells and of 5 U/ml in BaF3-EpoR cells (see Figure 2.1).

For a quantitative modeling approach, information about the absolute concentration is particularly required for reliable parameter estimates. The relative signal intensities of

receptor phosphorylation between different doses of Epo as well as between CFU-E and BaF3-EpoR cells were experimentally determined. Quantification of the absolute amount of the phosphorylated receptor, however, is technically difficult. To define the absolute receptor phosphorylation level, it was assumed that the receptors on the CFU-E cell surface are maximally 75% phosphorylated (Figure 2.8 C, at 5 min stimulated with 10 U/ml Epo). In addition, a receptor phosphorylation level of 50% or 90% was also tested *in silico*, but this had no significant influence on the model behavior. Based on this assumption, experimental data were transformed into absolute concentrations in nM.

The receptor activation models were separately calculated to experimental data acquired in CFU-E and BaF3-EpoR cells, performing 1000 fits with random initial parameter guesses. The models were sufficient in representing both the dose response and particularly the densely sampled time course data in both cell types (Figure 2.8 C). The distribution of the calibrated parameter values of 10% of the best 1000 fits is plotted in Figure 2.9 A. Out of 7 parameters, only two were non-identifiable. These parameters were related to phosphokinase inhibitor and correlated with each other (Figure 2.9 B). The fixation of one of the two parameters led to the identification of all the parameters.

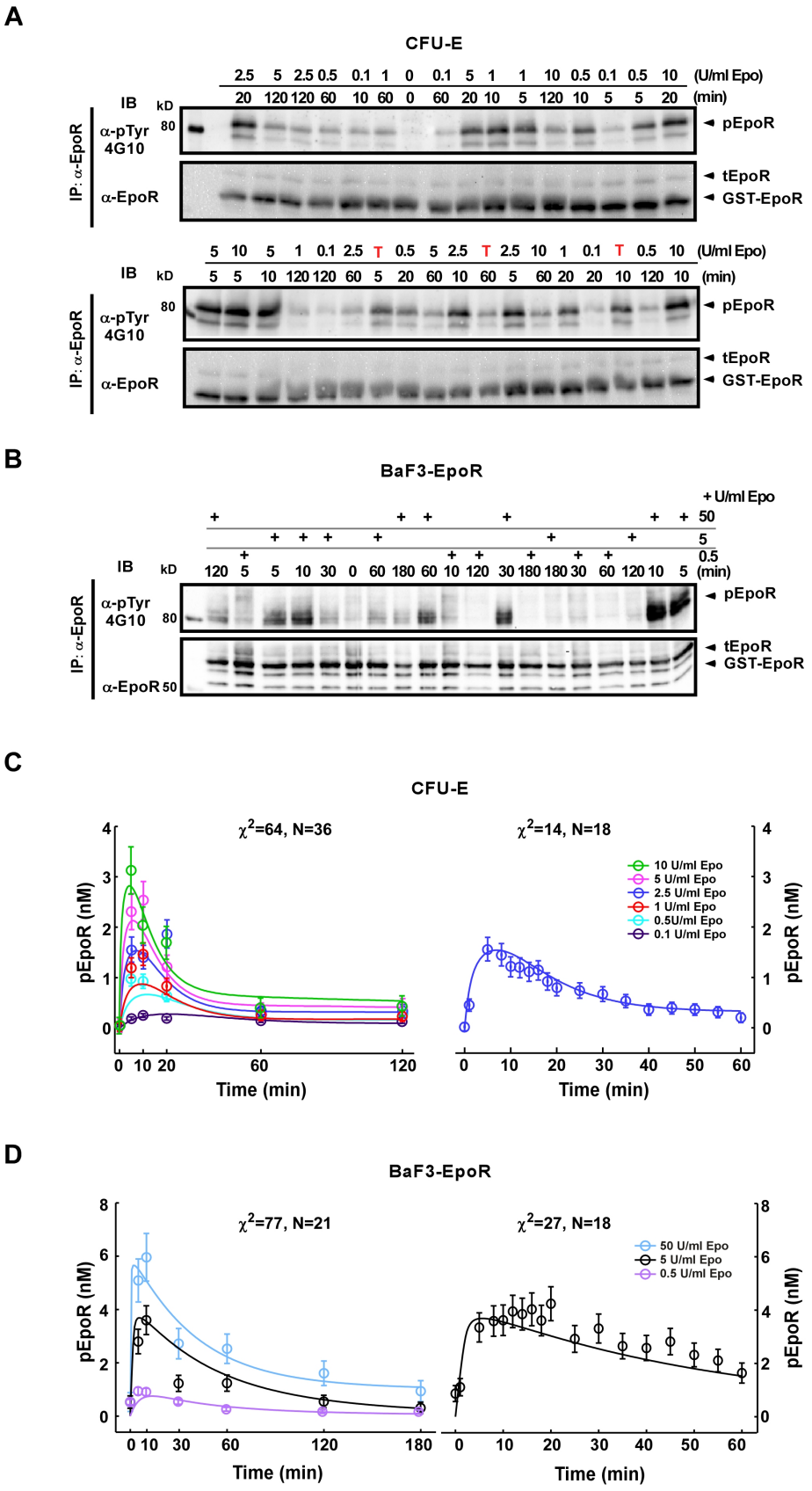
A
CFU-E
(U/ml Epo)
(min)
IB
kD
IP: α-EpoR
α-pTyr 4G10
α-EpoR
80
pEpoR
tEpoR
GST-EpoR
B
BaF3-EpoR
+ U/ml Epo
50
5
0.5
(min)
IP: α-EpoR
α-pTyr 4G10
α-EpoR
50
C
CFU-E
χ²=64, N=36
χ²=14, N=18
10 U/ml Epo
5 U/ml Epo
2.5 U/ml Epo
1 U/ml Epo
0.5U/ml Epo
0.1 U/ml Epo
pEpoR (nM)
Time (min)
D
BaF3-EpoR
χ²=77, N=21
χ²=27, N=18
50 U/ml Epo
5 U/ml Epo
0.5 U/ml Epo

Figure 2.8 Epo ligand-receptor dynamics. Immunoblotting analysis of EpoR phosphorylation in response to different Epo concentrations in (**A**) CFU-E and (**B**) BaF3-EpoR cells. T indicates samples generated in CFU-E cells transduced with the empty pMOWSnr vector as control for another independent experiment and those were excluded from the fitting. Model trajectories of the best fit are indicated by solid lines and experimental data are represented by circles with standard error for EpoR dose response (left) (quantified data shown in Table 6.3) and the densely sampled time courses (right) in (**C**) CFU-E and (**D**) BaF3-EpoR cells. Standard deviations of the measured data were estimated with a standard error model, considering contribution of relative errors E_{rel} (10% relative to measured value (Y)) and absolute errors E_{abs} (5% relative to max(Y) over all Y). The experiment was repeated two times with similar results and representative blots are shown.

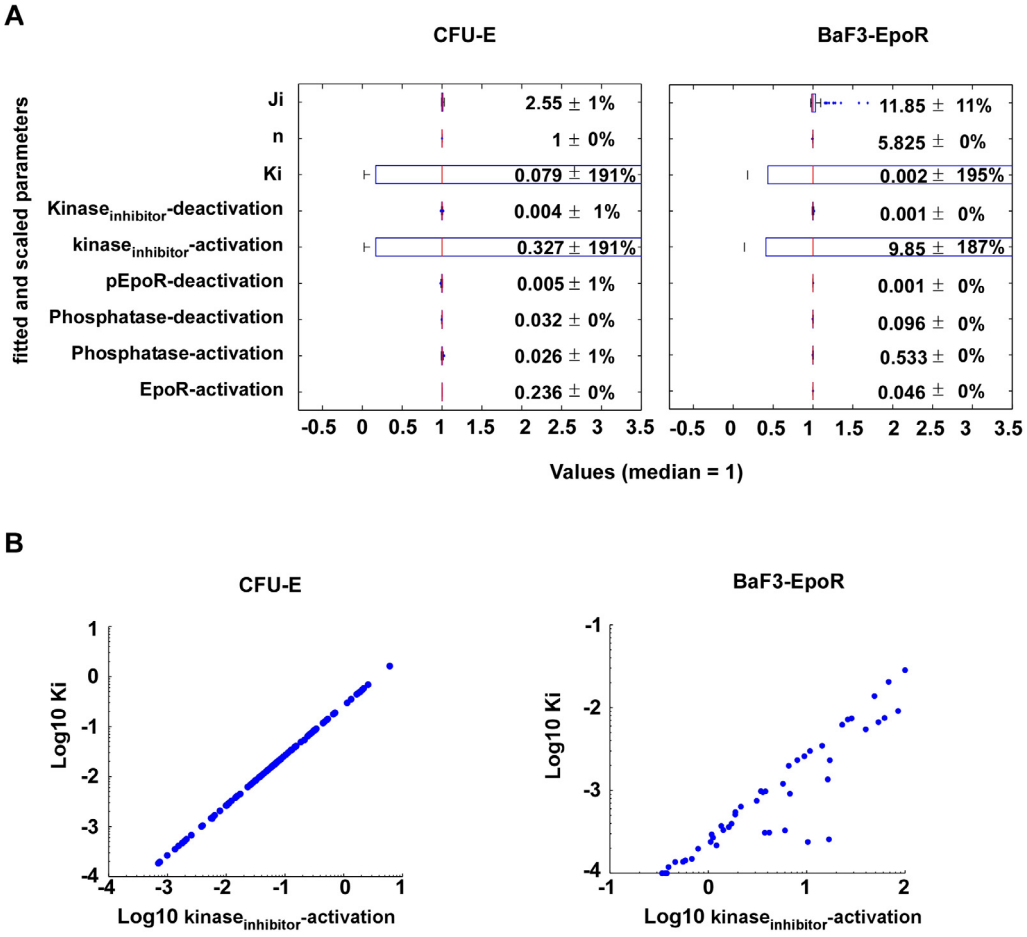

Figure 2.9 Parameter distribution analysis of the receptor activation model in CFU-E and BaF3-EpoR cells. (**A**) The distribution of the calibrated parameter values of 10% of the best 1000 fits, highlighting the non-identifiable parameters (blue boxes). **Ji:** EpoR occupying half of the binding sites, **n:** Hill coefficient, **Ki:** inhibition of EpoR activation by kinase inhibitor. (**B**) Dependency of the two non-identifiable phosphokinase inhibitor-associated parameters was identified with the mean optimal transformation approach (MOTA) (Hengl et al., 2007).

2.3.2 Core model calibration by muti-experiment fitting

Akt phosphorylation was measured as system's output signal in a time-resolved manner in both cells by quantitative immunoblotting (see Figure 2.1). To dissect the specific role of PTEN and SHIP1 in negative regulation, we overexpressed the two proteins individually in CFU-E cells and observed Akt activation as the response of the perturbed system. In order to perform time-course experiments in PTEN or SHIP1-overexpressing CFU-E cells, freshly isolated primary cells were retrovirally transduced. The transduction efficiency reached 10-

20%. Magnetic-activated cell sorting (MACS) with the low-affinity nerve growth factor receptor (LNGFR) surface marker enabled an efficient positive selection of transduced cells after 11-14 h transduction (see *Materials and methods 4.2.5*). PTEN was overexpressed on average 12-fold, while 11-fold increase on SHIP1 protein level was achieved (Figure 2.10 A, B). Overexpression of PTEN in CFU-E cells strongly abolished Akt phosphorylation, reducing the peak amplitude around 60%. SHIP1 overexpression only led to a reduction in pAkt signal duration. At 10 min, a reduction of 25 % was detected, while at 60 min a reduction of 60% was detected in SHIP1-overexpressing cells compared to control cells (Figure 2.10 A, C). Additionally, to accurately represent the pAkt dynamic, time course experiments with dense sampling were performed with an Epo stimulation of 2.5 U/ml in PTEN or SHIP1-overexpressing CFU-E cells (Figure 2.10 D).

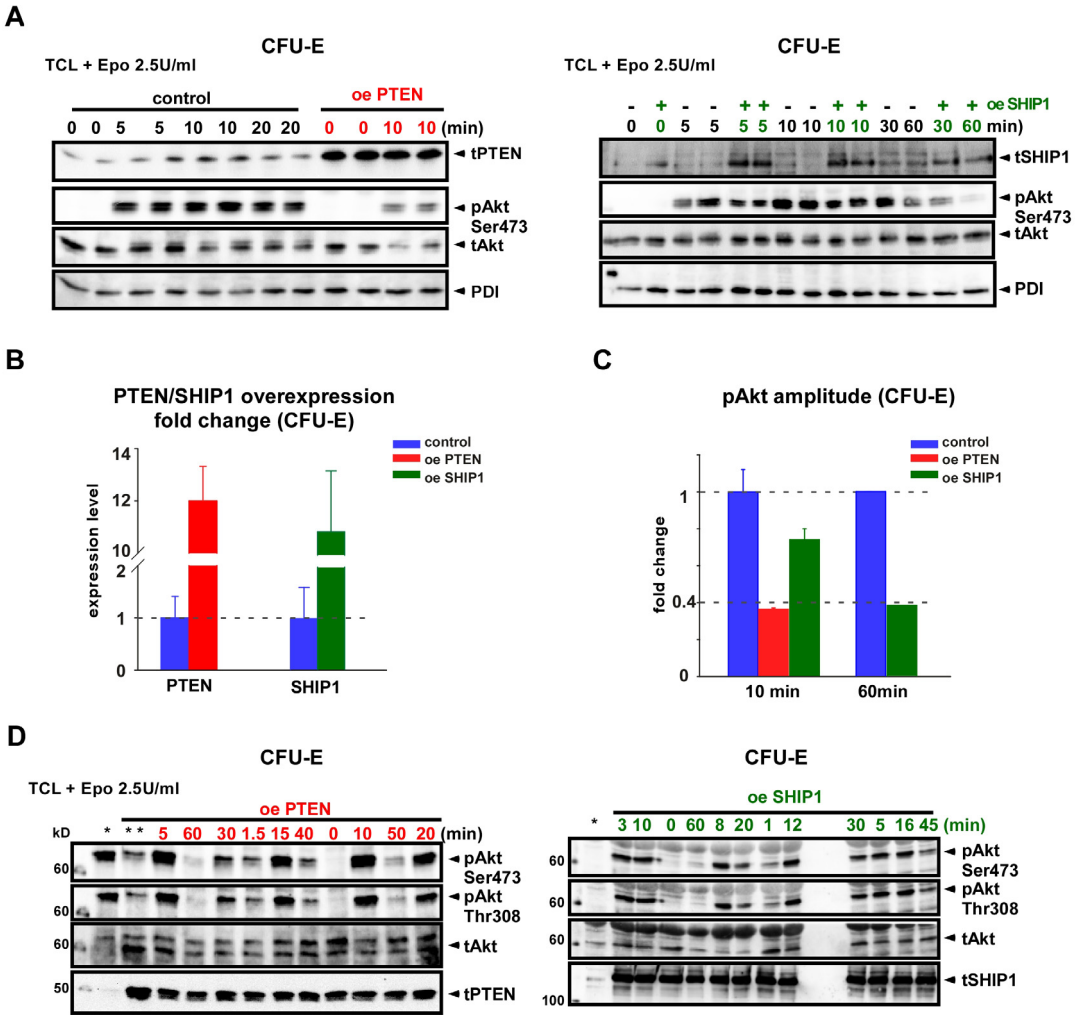

Figure 2.10 Overexpression of PTEN and SHIP1 in CFU-E cells. CFU-E cells retrovirally transduced with PTEN, SHIP1 or vector control were stimulated with 2.5 U/ml Epo for the indicated times and subjected to quantitative immunoblotting. (**A**) Immunoblotting data of TCL to determine the effects of PTEN and SHIP1 overexpression on Akt phosphorylation and the overexpression levels of PTEN and SHIP1. (**B**) The expression levels of PTEN and SHIP1. (**C**) The fold change of pAkt amplitude at 10 min and 60 min. (**D**) Time courses of pAkt Ser473 and Thr308 in PTEN or SHIP1-overexpressing CFU-E cells (quantified data shown in Table 6.5). (*) indicates a non-transduced sample as negative control and (**) indicates a PTEN-transduced sample from another independent experiment as positive control for transduction. The experiment was repeated at least three times with similar results and representative blots are shown.

Total protein levels remained constant during the time investigated, thus justifying application of mass conservation in the model. To define the absolute amount of phosphorylated Akt, a quantitative protein array was applied that combines in-spot normalization and binding model-based calibration. The maximal phosphorylation degree of Akt was determined to be 54% in CFU-E cells stimulated with 2.5 U/ml Epo at 10 min. Based on this information, all pAkt data in Figure 2.1 and Figure 2.10 were scaled to absolute concentrations in nM.

For the PI3K/Akt core model, the trajectory of receptor activation in each cell type based on the best parameter estimation served as input. The PI3K/Akt core model was simultaneously calibrated to multiple time-course data of Akt phosphorylation recorded in wild type CFU-E and BaF3-EpoR cells as well as in PTEN- or SHIP1-overexpressing CFU-E cells, performing 5000 fits with random initial parameter guesses. Standard deviations of the measured data were estimated with an error model, considering contribution of relative errors E_{rel} (10% relative to Y) and absolute errors E_{abs} (5% relative to max(Y) over all Y). For the best fit (Figure 2.11), the total χ^2 = 42.56, which is defined as the model deviation from the data normalized with the measurement error, indicates an accurate description of the data in respect to the total number of N = 58 data points.

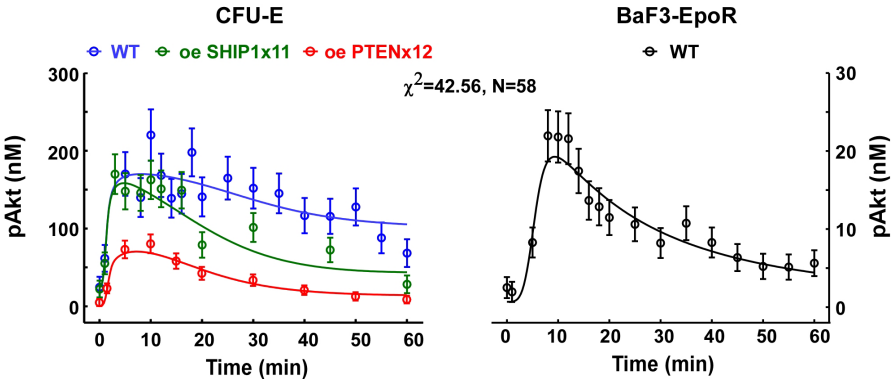

Figure 2.11 Muti-experiment fitting for the PI3K/Akt core model calibration. Trajectories of the best fit of the PI3K/Akt core model are indicated by solid lines and experimental data are represented by circles. Standard deviations of the measured data were estimated with the standard error model. Parameter estimation was performed to simultaneously fit the model to four different data sets (4 data sets) generated in wild type CFU-E (blue) and BaF3-EpoR (black) cells (data refer to Figure 2.1) as well as SHIP1 (green) and PTEN (red)-overexpressing CFU-E cells (data refer to Figure 2.10). χ^2-values comparable to N indicate accurate description of the data.

2.4 Model validation and control analysis of the PI3K/Akt pathway

2.4.1 Constrained model prediction of PTEN or SHIP1 overexpression in BaF3-EpoR cells

Having estimated the parameter sets of the kinetic model, the model quality was evaluated by deriving predictions from the model, which could then be tested experimentally. For a good accuracy of model simulations, the estimated parameters are required to be identifiable and display small confidence intervals. Thus, the calibrated core model parameter values of 1% of the best 5000 fits was plotted in Figure 2.12 A. Most of the parameters exhibited a large distribution of values indicating a non-identifiability. However, the rate constants of PIP3 turnover by PTEN (vPI45P2) and by SHIP1 (vPI34P2) as well as the two parameters directly related to Akt activation, namely the rate constants of Akt phosphorylation (vpAkt) and dephosphorylation (dpAkt), were well identified in a narrower relative distribution within 20% standard deviation. The response equation of pAkt that describes the phosphorylation level of Akt in steady state condition was solved as a function of PIP3 level (Figure 2.12 B). Since total levels of Akt and PDK1 are constant, the ability to predict Akt phosphorylation relies on the determination of PIP3 levels and the relevant correlations of dpAkt/vpAkt, lpAkt/kpAkt (dissociation / association rate constants of Akt to PIP3), lPDK1/kPDK1 (dissociation / association rate constants of PDK1 to PIP3) and dpAkt/kAkt. When PIP3 goes to infinity, pAkt only depends on dpAkt/vpAkt, indicating its decisive role in determining the Akt dynamics. The turnover of PIP3 level is strictly controlled by PTEN and SHIP1 activities, with the rate constants vPI45P2 and vPI34P2, respectively. A linear correlation between these two parameters was also identified.

Since each data set used for fitting contains information relevant for different parameters, the identifiability of the relevant parameter correlations was improved by fitting the core model to different data sets: these were two wild type BaF3-EpoR and CFU-E data sets (2 x WT) and three data sets including two wild type data and the overexpression of SHIP1 or PTEN in CFU-E cells (2 x WT + oe SHIP1 or 2 x WT + oe PTEN) and all data sets (4 data sets). The results show that the fitting to 4 data sets with the maximum amount of information constrains all the correlations in the best way (Figure 2.12 C). Remarkably, the high correlation between dpAkt and vpAkt was identified in all the cases, while the correlation between vPI45P2 and vPI34P2 was progressively increased by using the overexpression data in CFU-E cells, with PTEN having stronger effect in line with its more significant effects on Akt activation.

To examine the predictive power of the model for the effects of PTEN and SHIP1 overexpression on Akt activation in BaF3-EpoR cells, we first overexpressed PTEN or SHIP1 in BaF3-EpoR cells. The overexpression level of PTEN was 3-fold while a 4-fold increase was measured for SHIP1 compared to their endogenous protein levels by immunoblotting

(Figure 2.13 B). Overexpression of PTEN or SHIP1 reduced Akt phosphorylation in BaF3-EpoR cells, with PTEN having a stonger effect (Figure 2.13 B). As expected, the EpoR phosphorylation was not affected by overexpression (Figure 2.13 A). In line with the unchanged receptor levels, the activation of Erk1/2, the components of Epo-induced MAPK cascade, remained comparable between control cells and the cells-overexpressing PTEN or SHIP1.

Next, the model was employed to predict Akt phosphorylation in BaF3-EpoR with elevated PTEN or SHIP1 concentration, which was experimentally determined, as described above. Again, the model predictions were examined from the determined models fitted to different data sets. To verify the robustness of the predictions, the simulations were repeated with parameter sets obtained for 1% of the best 5000 fits of each determined model (Figure 2.13 C). Trajectories of pAkt in wild type BaF3-EpoR (black lines) and in PTEN (green lines) or SHIP1 (red lines)-overexpressing cells are converged tightly, which largely relies on the high correlation between dpAkt and vpAkt. The χ^2-values were calculated to determine the agreement between the overexpression data and the model predictions. The results show that the predictions derived from the models calibrated to PTEN data (2 x WT + oe PTEN and 4 data sets) were comparable and in good agreement with the experimental data, whereas the model calibrated to wild type data and SHIP1 data resulted in a much higher χ^2-value (Figure 2.14 B).

With this modeling approach, the correlation between dpAkt and vpAkt was identified as decisive factor to constrain the predicted pAkt behavior, while the correlation between vPI45P2 and vPI34P2 determined the differential effects of PTEN and SHIP1 on Akt activation. In the end, the best parameter set allowed to accurately predict pAkt dynamics after perturbation of PTEN and SHIP1 concentrations in BaF3-EpoR cells.

.

A

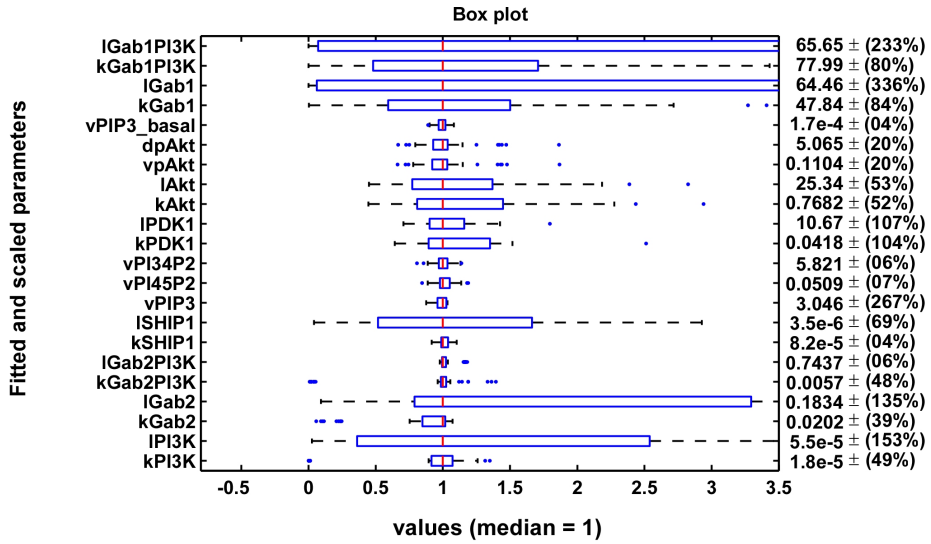

lGab1PI3K :	pEpoR_Gab1_PI3K dissociation	vPI34P2 :	PI34P2 generation by SHIP1
kGab1PI3K :	pEpoR_Gab1_PI3K assocoation	vPI45P2 :	PI45P2 generation by PTEN
lGab1 :	pEpoR_Gab1 dissociation	vPIP3 :	PIP3 generation by PI3K
kGab1 :	pEpoR_Gab1 association	lSHIP1 :	SHIP1 dictivation
vPIP3_basal :	PIP3_basal generation by free PI3K	kSHIP1 :	SHIP1 activation by pEpoR
dpAkt :	Akt phosphorylation by PDK_PIP3	lGab2PI3K :	pEpoR_Gab2_PI3K dissociation
vpAkt :	Akt dephosphorylation	kGab2PI3K :	pEpoR_Gab2_PI3K assocoation
lAkt :	Akt_PIP3 dissociation	lGab2 :	pEpoR_Gab2 dissociation
kAkt :	Akt_PIP3 association	kGab2 :	pEpoR_Gab2 association
lPDK1 :	PDK1_PIP3 dissociation	lPI3K :	PI3K deactivation
kPDK1 :	PDK1_PIP3 association	kPI3K :	PI3K activation

B

Response equations of pAkt steady state ($pAkt_s$)

$$pAkt_s = \frac{Akt_t * PDK1_t * PIP3^2}{\frac{dpAkt}{vpAkt}\left(\frac{lpAkt}{kpAkt} + PIP3\right)\left(\frac{lPDK1}{kPDK1} + PIP3\right) + PDK1_t * PIP3\left(\frac{dpAkt}{kAkt} + PIP3\right)}$$

when PIP3 → infinity (∞)

$$pAkt_s = \frac{Akt_t * PDK1_t}{\frac{dpAkt}{vpAkt} + PDK1_t}$$

C

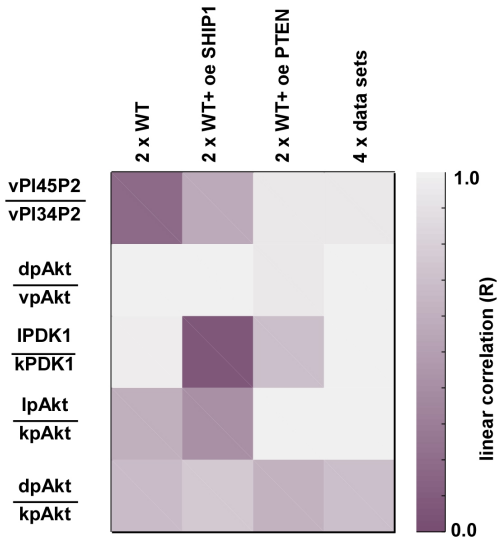

Figure 2.12 Parameter distribution analysis of the PI3K/Akt core model and data improved identifiability of the parameter correlations. (**A**) The distribution of the calibrated parameter values of 1% of the best 5000 fits, highlighting the non-identifiable parameters (blue boxes). The core model was calibrated to 4 data sets, refer to Figure 2.11. (**B**) Response equation of pAkt at steady state. (**C**) The relevant parameter correlations identified by fitting the core model to two wild type BaF3-EpoR and CFU-E data sets (2 x WT) to three data sets including two wild types and overexpression of SHIP1 or PTEN in CFU-E cells (2 x WT+ oe SHIP1 or 2 x WT + oe PTEN) and to 4 data sets.

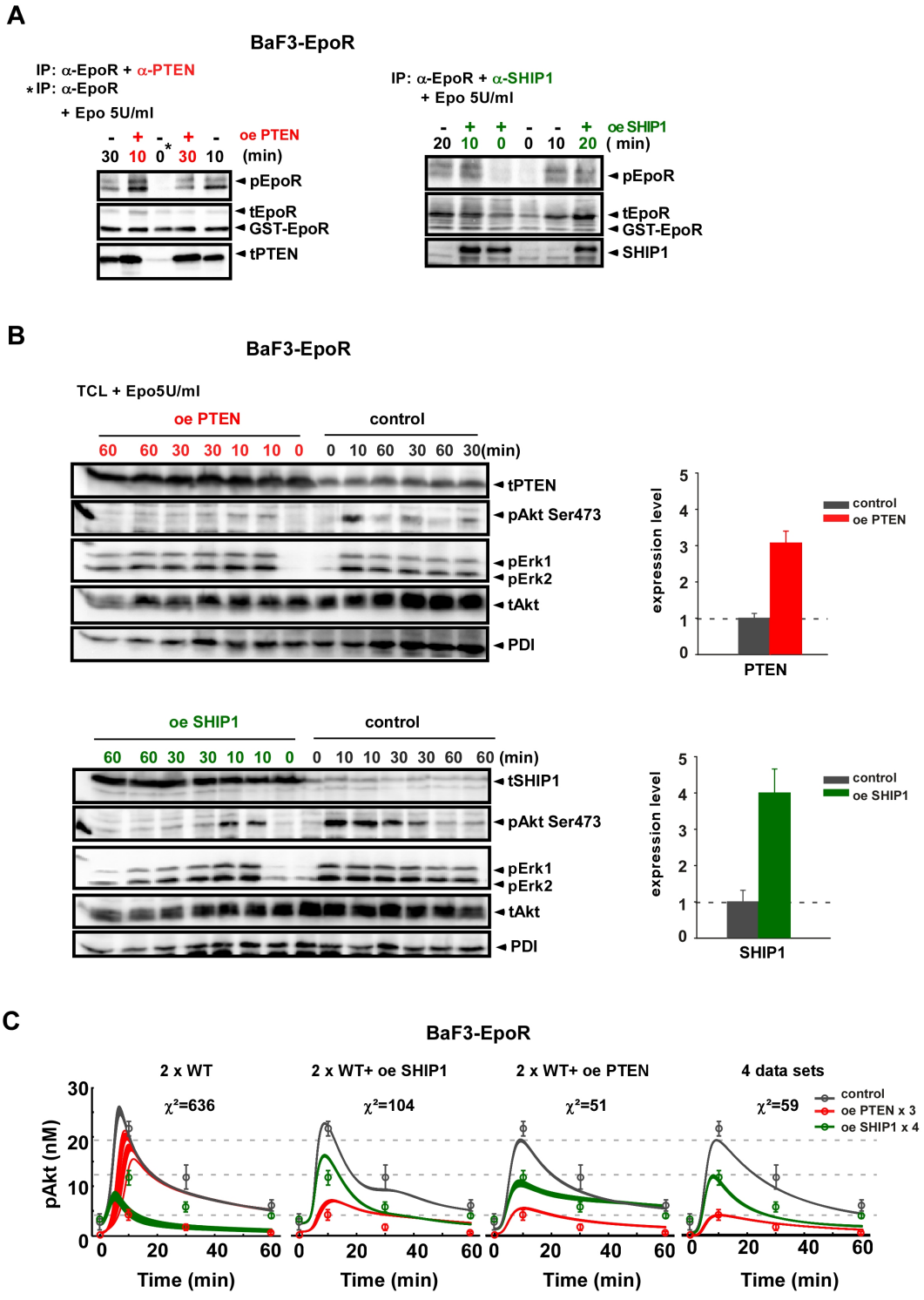

Figure 2.13 Experimental validation of model predictions: PTEN or SHIP1 overexpression in BaF3-EpoR cells. BaF3-EpoR cells retrovirally transduced with PTEN, SHIP1 or vector control were stimulated with 5 U/ml Epo for the indicated times and subjected to quantitative immunoblotting. (**A**) Comparable EpoR phosphorylation levels between PTEN or SHIP1-overexpressing and control BaF3-EpoR cells. Immunoprecipitations were performed with anti-EpoR together with anti-PTEN or anti-SHIP1. (**B**) Immunoblotting data of TCL to determine the effects of PTEN or SHIP1 overexpression on Akt and Erk phosphorylation. Expression levels of PTEN and SHIP1 were depicted as bar charts. (**C**) Simulation of the effects of PTEN (green lines) or SHIP1 (red lines) overexpression on Akt phosphorylation in BaF3-EpoR cells. Black lines represent the model trajectory of Akt phosphorylation in wild type cells. Red and green lines represent simulations of pAkt in PTEN or SHIP1-overexpressing cells, respectively, based on the best 1% of 5000 fits. Circles represent the experimental data with error bar based on biological replicates (quantified data shown in Table 6.6). The experiment was repeated at least three times with similar results and representative blots are shown.

2.4.2 Fine-tuned control of Akt activation by PTEN and SHIP1

A major focus of this study was to dissect the role of PTEN and SHIP1 in the regulation of Akt activation. The experimental model validation confirmed the initial assumption that PTEN is constitutively active while SHIP1 becomes activated upon binding to pEpoR. Next, to analyse the effects on pAkt dynamics, the calculated model was applied to simulate pAkt dynamics for different initial concentrations of PTEN or SHIP1 in CFU-E and BaF3-EpoR cells. In line with their activation mechanisms, in CFU-E cells PTEN strongly controled the initial level and amplitude (maximum activation) of pAkt, while SHIP1 had a major effect on the signal duration (time until signal drops down to 10% of its maximum activation) (Figure 2.14 A). In contrast, in BaF3-EpoR cells, the effects on pAkt were enhanced (Figure 2.14B), indicating that this cell type is more sensitive to changes in PTEN and SHIP1 levels. Particularly, SHIP1 strongly affected the amplitude of pAkt. Additionaly, it was explored how PTEN and SHIP1 affect the integral of pAkt activation (60 min) for different Epo concentrations ranging from 0.001 to 50 U/ml in both cell types (Figure 2.14 C, D). The results showed that constitutive active PTEN mainly contributed to regulate the PIP3 level at low levels of Epo. With increasing stimulus doses, more EpoR on the cell surface were getting phosphorylated, subsequently activating more SHIP1. Hence, in contrast to PTEN, SHIP1 played a crucial role in controlling the PIP3 levels at high levels of Epo.

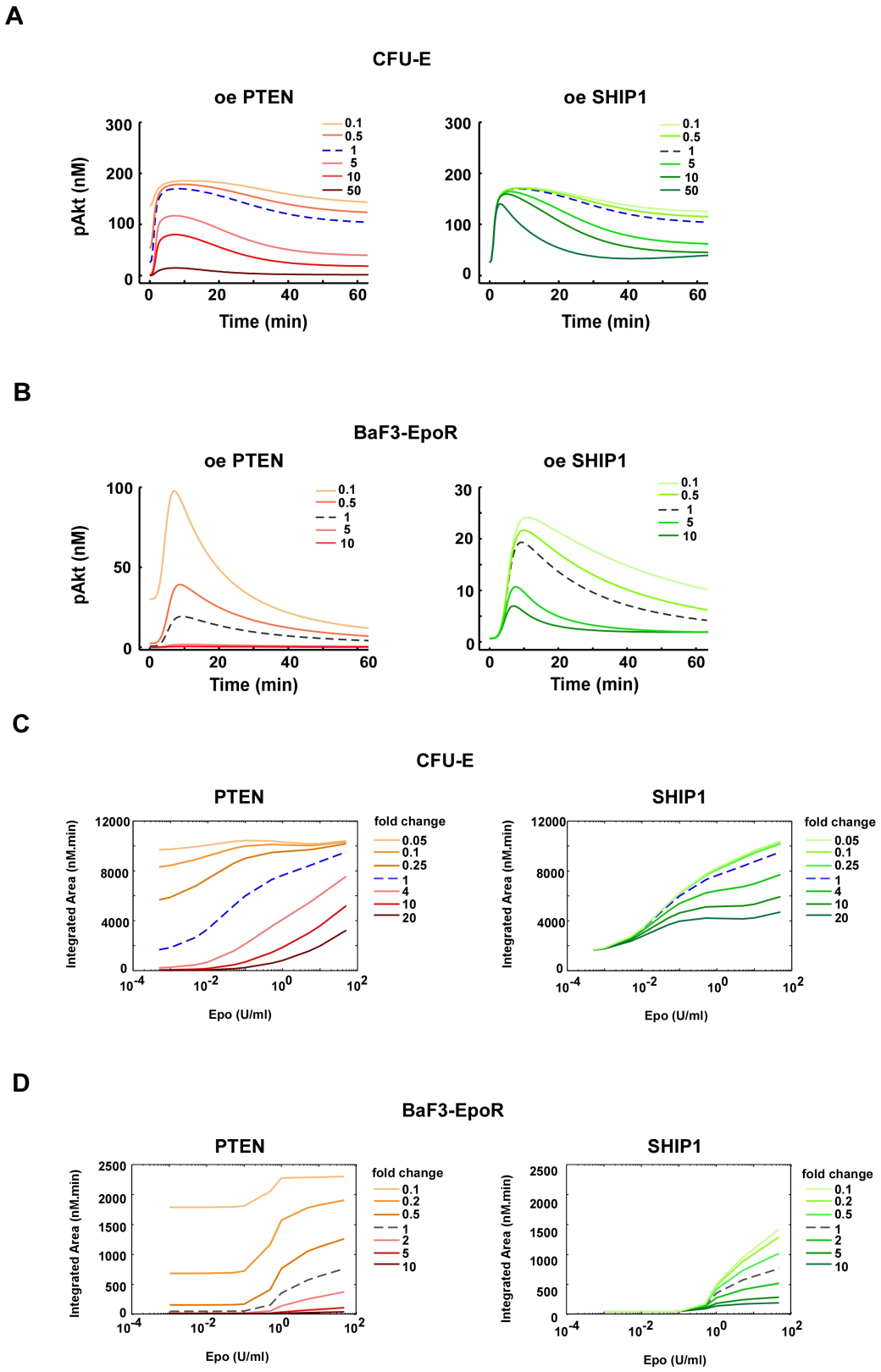

Figure 2.14 Fine-tuned control of Akt activation by PTEN and SHIP1. The calculated model was applied to simulate Akt dynamics for different initial concentrations of PTEN or SHIP1. Effect of relative changes in PTEN or SHIP1 concentration compared to the initial concentrations (dashed lines) on Akt dynamics in (**A**) CFU-E cells and (**B**) BaF3-EpoR cells and on the integral Akt activation (60 min) for different Epo concentrations in (**C**) CFU-E cells and (**D**) BaF3-EpoR cells.

2.4.3 Isoform-specific role of Gab1/2 on controlling PI3K/Akt signaling

Upon Epo stimulation, both Gab1 and Gab2 are phosphorylated at their tyrosine residues and associate with the Tyr-phosphorylated EpoR (pEpoR-pGab1/2 complex formation). The tyrosine motifs of Gab1/2 then mediate the engagement and activation of PI3K (pEpoR-pGab1/2-PI3K complex formation) (Wickrema et al., 1999). To dissect the dynamics of the Gab-mediated two-step activation of PI3K, the complex formations of pEpoR-pGab1/2 and pEpoR-pGab1/2-PI3K were stimulated (Figure 2.15 A, B). According to the model predictions, the activation of both pEpoR-pGab1/2 and pEpoR-pGab1/2-PI3K complexes would rapidly follow the EpoR phosphorylation, showing transient and sustained dynamics in CFU-E and BaF3-EpoR cells, respectively. Importantly, the ratio between the amplitude of pEpoR-pGab1/2-PI3K and pEpoR-pGab1/2 activation (indicated by arrows in Figure 2.15) indicates the activation efficiency of PI3K by pEpoR-pGab1/2. The model prediction:

$$\frac{\text{Amplitude}\,(\text{pEpoR - pGab1 - PI3K})}{\text{Amplitude}\,(\text{pEpoR - pGab1})} > \frac{\text{Amplitude}\,(\text{pEpoR - pGab2 - PI3K})}{\text{Amplitude}\,(\text{pEpoR - pGab2})}$$

indicates that pEpoR-pGab1 would activate PI3K with greater efficiency than pEpoR-Gab2, suggesting an isoform-specific role of Gab1/2 on Akt activation. Quantitative data on Gab1/2 phosphorylation was not used for model training and was now acquired experimentally to test the model predictions. The experimentally detectable total Gab1/2 phosphorylation constitutes the sum of the pEpoR-pGab1/2 and pEpoR-pGab1/2-PI3K fractions. Remarkably, the overlay of experimental data with the simulated total Gab1/2 phosphorylation dynamics were in good agreement (Figure 2.15), suggesting that our model can accurately describe the different kinetics of Gab1 in CFU-E cells and Gab2 in BaF3-EpoR cells.

To examine whether both Gab1 and Gab2 have decisive role on Akt activation, we reduced the core PI3K/Akt model by setting all Gab1 or Gab2 related parameters to 0 and calibrated them individually to 4 data sets, performing 5000 fits with random initial parameter guesses. The model without Gab1 failed to describe the data, in particular, the overexpression data in CFU-E cells, while the model without Gab2 was still sufficient in describing all the data, having a comparable χ^2-value to the core model (Figure 2.16 A). In addition, the model without Gab2 can also give correct predictions about the pAkt behavior in PTEN or SHIP1-overexpressing BaF3-EpoR cells. The likelihood-ratio test (LRT) further confirmed that only the model without Gab1 is not compliant with the data (goodness-of-fit: $p < 0.01$) (Maiwald and Timmer, 2008) (Figure 2.16 B). This model reduction approach reveals a vital role for Gab1 in CFU-E cells but a negligible role for Gab2 in BaF3-EpoR cells. Consistent with the approach above, the results demonstrate that besides the abundance of negative regulators, Gab-mediated isoform-specific PI3K activation is also important in determining the PI3K/Akt signaling in hematopoietic cells.

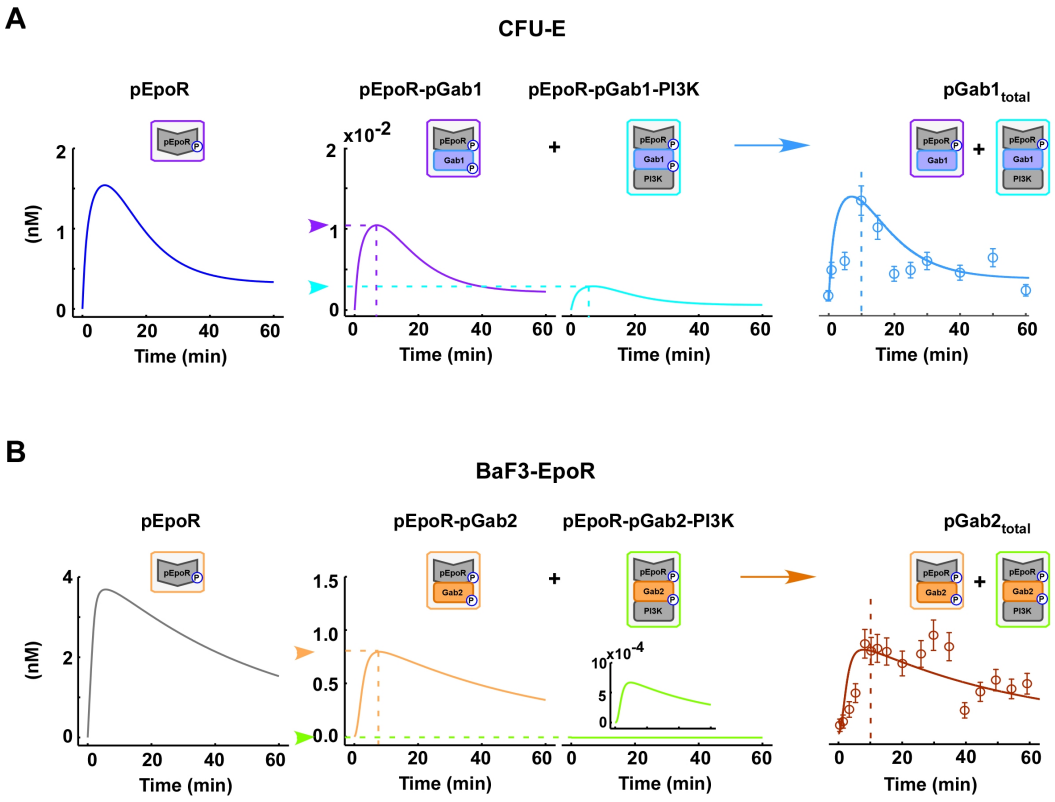

Figure 2.15 Experimental testing of the model predictions for Gab activation. Trajectories (solid lines) represent model predictions for EpoR phosphorylation and the complex formations of pEpoR-pGab1/2 and pEpoR-pGab1/2-PI3K. Experimental data are represented by circles with standard deviation in (**A**) CFU-E and (**B**) BaF3-EpoR cells. The amplitudes of pEpoR-pGab1/2 and pEpoR-pGab1/2-PI3K are indicated by dashed drop lines and arrows. The total phosphorylation levels of Gab1/2 ($pGab1/2_{total}$) are predicted by the model as the sum of the activation of pEpoR-pGab1/2 and pEpoR-pGab1/2-PI3K. Gab1 and Gab2 were immunoprecipitated with anti-Gab1 and anti-Gab2, respectively. Their total phosphorylation levels were determined by subsequent quantitative immunoblotting. Experimental data were scaled to the model predictions by matching the relative phosphorylation level of Akt at 10 min with the prediction curves (indicated by dashed lines). Standard deviations of the measured data were estimated with the standard error model. The experiment was repeated twice with similar results and representative blots are shown.

A

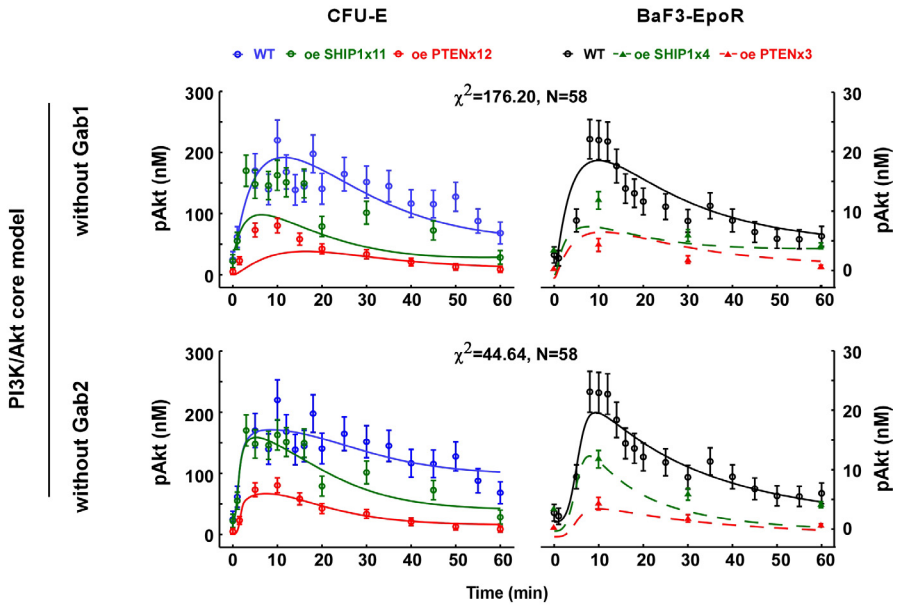

B

$p = pwLRT(\chi^2_1, numPars_1, \chi^2_2, numPars_2)$

pwLRT: the likelihood-ratio test

$\chi^2_{1/2}$: total χ^2 value of model 1 or 2

$numPars_{1/2}$: Number of fitted parameters of model 1 or 2

model 2	fitted parameters	total χ^2 value	p value
PI3K/Akt core model	22	42.56	
model 1			
PI3K/Akt core model without Gab1	18	176.20	0
PI3K/Akt core model without Gab2	18	44.64	0.72

Figure 2.16 Muti-experiment fitting for model reduction and the likelihood-ratio test (LRT). The core PI3K/Akt model was reduced by setting all Gab1 or Gab2 related parameters to 0 and calibrated individually to 4 data sets, performing 5000 fits with random initial parameter guesses. (**A**) Trajectories of the model without Gab1 or without Gab2 are indicated by solid lines and experimental data are represented by circles with the standard error estimation. The model simulations of pAkt in PTEN or SHIP1-overexpressing BaF3-EpoR cells are indicated by dashed lines. Overexpression data in BaF3-EpoR cells is depicted as triangles with experimental error (data refer to Figure 2.13). (**B**) The likelihood-ratio test (LRT). LRT evaluates nested models 1 $\subset$ 2 with numPars1 < numPars2 and determines the probability that the smaller model is sufficient to describe the measurements (Maiwald and Timmer, 2008).

2.5 Distinct cell fate decisions triggered by PI3K/Akt signaling

Akt regulates many processes including cell proliferation and survival, cell growth, glucose metabolism, cell motility and angiogenesis (Bellacosa et al., 2005). This study addressed the following questions: how cellular behavior specifically and quantitatively depends on the signal strength of PI3K/Akt signaling and how distinct cell fate decisions are triggered by PI3K/Akt signaling in different cell types.

2.5.1 Correlation between Akt phosphorylation and cell proliferation

To target Akt-mediated cellular processes, previous studies typically have utilized the PI3K inhibitors LY294002 and wortmannin. However, these inhibitors are not entirely specific for PI3K (Davies et al., 2000; Rajkumar et al., 2005). In this study, the suppression of Akt activation by PTEN and SHIP1 enabled us to specifically assess and target PI3K/Akt-mediated cellular processes. To monitor cell proliferation, DNA content was measured by ^{3}H-Thymidine incorporation assay in CFU-E and BaF3-EpoR cells transduced either with PTEN, SHIP1 or empty vector and stimulated with different doses of Epo from 0.001 to 50 U/ml, which represents the normal Epo concentration range in plasma of healthy persons (Jelkmann, 2004) (Figure 2.17 A). Thymidine incorporation was determined after 14 hours Epo stimulation in CFU-E cells and after 38 hours Epo stimulation in BaF3-EpoR cells. The experimental data showed that PTEN and SHIP1 overexpression in both cell types suppressed cell proliferation in a dose dependent manner, with PTEN having a stronger effect. The dose-response curves exhibited the typical signmoid curve and reach a maximum after 10 U/ml Epo in both cell types. Remarkably, in CFU-E cells both PTEN and SHIP1 overexpression reduced basal proliferation rates at low-dose Epo. However, a reduced pAkt basal level was only observed under PTEN overexpression.

Next, the correlation between the extent of Akt activation and cell proliferation was explored. The extent of signal was determined by the integrated area below the activation curve, which has been linked to DNA synthesis (Asthagiri et al., 2000) and cell proliferation (Schilling et al., 2009). With the established EpoR/PI3K/Akt model, the integral pAkt responses were calculated for elevated concentration of PTEN or SHIP1 and for different doses of Epo in a range from 0.001 to 50 U/ml. For the PI3K/Akt core model calibration, Epo concentrations of 2.5 U/ml in CFU-E cells and 5 U/ml in BaF3-EpoR cells were used. To predict the integrated pAkt signal, the calibrated model was applied to simulate the dose–response curve for the amplitude of Akt phosphorylation (Figure 2.17 B). Model predictions showed good agreement with experiment data, indicating a high accuracy of the model prediction. The χ^2-values were calculated to determine the agreement between measured proliferation data and the integral of pAkt (see Material and methods 4.5.4). The different integration times were examined and the best time window with the lowest χ^2-value was identified at 12 min in CFU-E cells and 16 min in BaF3-EpoR cells. The correlation between the integral of pAkt and cell proliferation was stronger in CFU-E cells than in BaF3-EpoR cells (Figure 2.17 C). Although a correlation was found between the calculated integral of pAkt and the proliferation of wild type and PTEN-overexpressing CFU-E cells, the model failed to describe the reduced basal proliferation of SHIP1-overexpressing CFU-E cells. In BaF3-EpoR cells, the suppression of cell proliferation by PTEN and SHIP1 was less profound than the reduction of pAkt levels.

Taken together, experimental data revealed that PTEN and SHIP1 suppress Akt-mediated cell proliferation in both CFU-E and BaF3-EpoR cells and further indicated that the signal propagation in PI3K/Akt downstream could be different and cell type-specific. The results demonstrate that Akt activation is necessary but not sufficient to predict cell proliferation in both cells. To explore possible mechanisms underlying the PTEN and SHIP1 triggered suppression of cell proliferation, more detailed analyses of the dynamics of Akt downstream targets were performed.

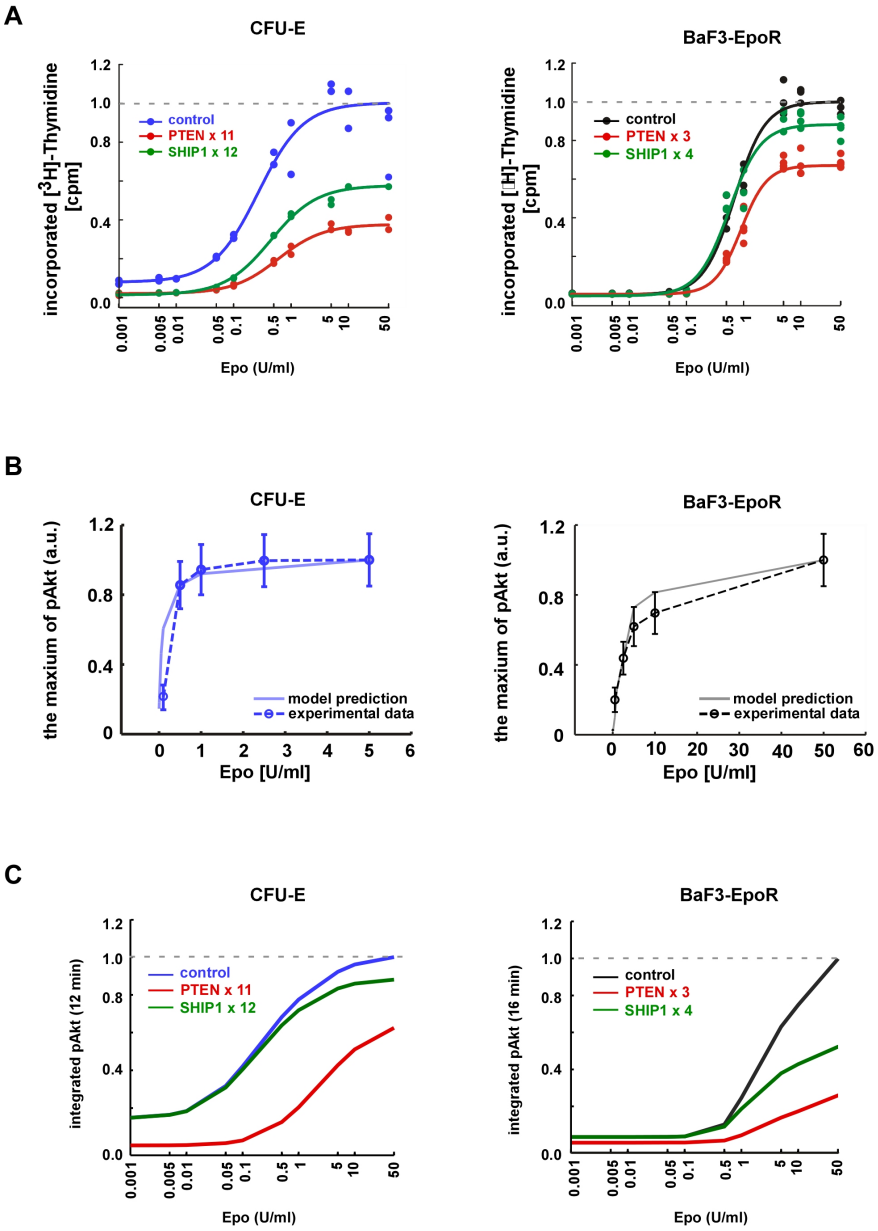

Figure 2.17 Correlation of integrated pAkt signal and cell proliferation. (**A**) Retrovirally transduced CFU-E and BaF3-EpoR cells were incubated with increasing Epo concentrations for 14 h or 38 h, respectively, and DNA content was measured by [^{3}H]-Thymidine incorporation. Experimental data are depicted as dots. Lines represent sigmoidal regression curves. (**B**) Model predicted and experimentally mesured maximum phosphorylation levels of Akt in CFU-E and BaF3-EpoR cells. Standard deviations of the measured data were estimated with the standard error model. (**C**) For different Epo concentrations, integrated responses of pAkt were calculated with the original models and the models with elevated PTEN or SHIP1 levels in CFU-E and BaF3-EpoR cells.

2.5.2 Context-dependent information processing through the Akt/GSK3 and Akt/mTOR pathways

Cell growth and cell cycle progression are generally tightly coupled, allowing cells to proliferate continuously while maintaining their size. As well-known Akt downstream targets, GSK3 and mTOR, which regulate cell survival, protein synthesis and cell cycle progression (Fingar et al., 2004; Liu et al., 2008), were further investigated in CFU-E and BaF3-EpoR cells.

To assess GSK3 and mTOR activities, the phosphorylation levels of GSK3 and S6, a downstream target of mTOR, were analyzed in PTEN-overexpressing cells compared to control CFU-E and BaF3-EpoR cells, respectively. Findings form these experiments can be summarized as: in CFU-E cells (Figure 2.18), (i) the phosphorylation of GSK3 strictly followed Akt phosphorylation, showing a linear response between Akt and its direct target. (ii) In contrast, the phosphorylation of S6 was gradually accumulating over time and reached a plateau from 60 min to the end of the observation period (180 min). (iii) PTEN mediated reduction of pAkt was sufficient to lower the phosphorylation of GSK3 and S6, indicating an absolute control of their activities by pAkt in CFU-E cells. In BaF3-EpoR cells (Figure 2.19), (iv) GSK3 was phosphorylated in response to Epo stimulation but its phosphorylation level was surprisingly not affected by PTEN overexpression, indicating a decoupling of signal transduction from pAkt to pGSK3 in BaF3-EpoR cells. (v) In contrast to the accumulating response in CFU-E cells, the phosphorylation of S6 showed a different kinetic in BaF3-EpoR cells, which decayed over time, but not as rapidly as the pAkt signal. Moreover, PTEN overexpression in BaF3-EpoR cells reduced the peak amplitude of pAkt around 70%, but the peak amplitude of pS6 in PTEN-overexpressing cells was only 30% lower than in control cells. As expected, SHIP1 overexpression exhibited a consistent but relative moderate effects on the reduction of Akt, GSK3 and S6 phosphorylation compared to PTEN overexpression.

To further dissect the underlying mechanism of the decoupling of signal transduction from Akt to GSK3 in BaF3-EpoR cells, the ratio of total and phosphorylated Akt and GSK3 between CFU-E and BaF3-EpoR cells was determined (Figure 2.20). As described before, Akt phosphorylation in BaF3-EpoR cells is much weaker than in CFU-E cells. However, a comparable phosphorylation level of GSK3 was detected in both cell types. By applying the PI3K inhibitor LY294002, Akt phosphorylation was abolished in BaF3-EpoR cells (Figure 2.21 A). The results showed that the exposure to 10μM LY294002 completely blocked Akt phosphorylation, while the phosphorylation level of GSK3 was only slightly reduced. In a preliminary experiment, Akt overexpression dramatically increased the pAkt level around 10-fold after 10 min Epo stimulation, while the pGSK3 level was only slightly elevated (Figure 2.21 B). These findings suggested that the low activation level of Akt may below a threshold

required to activate GSK3 efficiently and instead of Akt, another Epo-induced kinase may phosphorylate GSK3 in BaF3-EpoR cells.

Taken together, the observations revealed that in primary CFU-E cells, Akt phosphorylation is the key player in regulating GSK3 and S6 phosphorylation, while in BaF3-EpoR cells, Akt phosphorylation leads to an inefficient phosphorylation of GSK3 and only partially actives S6, demonstrating a context-dependent Akt downstream signal propagation in different hematopoietic cell types.

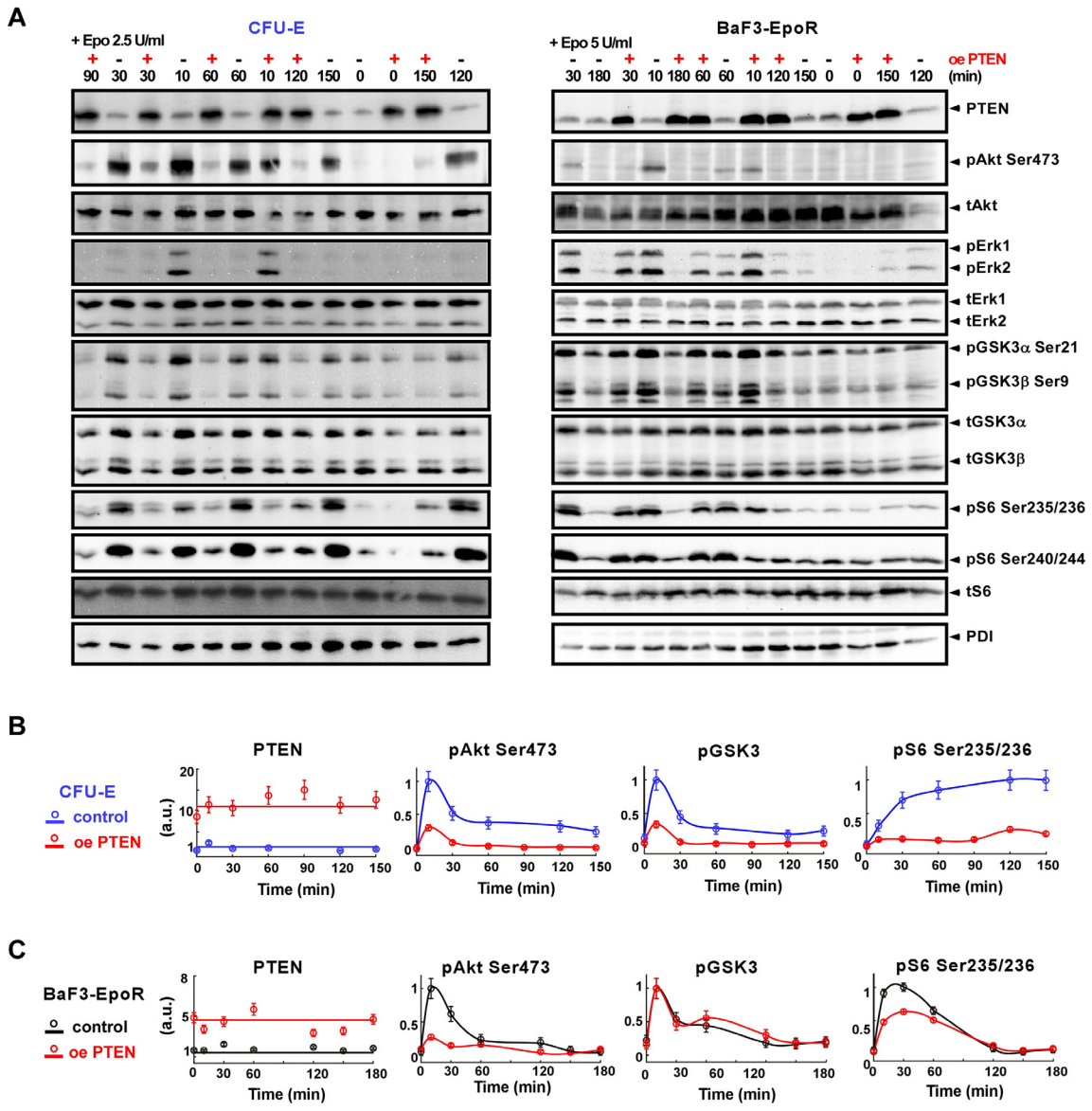

Figure 2.18 Analysis of the dynamics of Akt downstream targets by quantitative immunoblotting. (A) CFU-E and BaF3-EpoR cells retrovirally transduced with PTEN or vector control were stimulated with 2.5 U/ml or 5 U/ml Epo, respectively, for the indicated times and subjected to quantitative immunoblotting. Total PTEN, pAkt Ser473, pGSK3 (the sum of pGSK3α Ser21 and pGSK3β Ser9) and pS6 Ser235/236 levels in (B) CFU-E and (C) BaF3-EpoR cells were quantified. For phosphorylation signals, each time course was normalized setting the maximum signal in control cells to 1. Standard deviations of the measured data were estimated with the standard error model. The sold line represents the smooth spline. PTEN Overexpression in CFU-E cells was repeated two times, while PTEN overexpression in BaF3-EpoR cells was repeated three times with similar results and representative blots are shown.

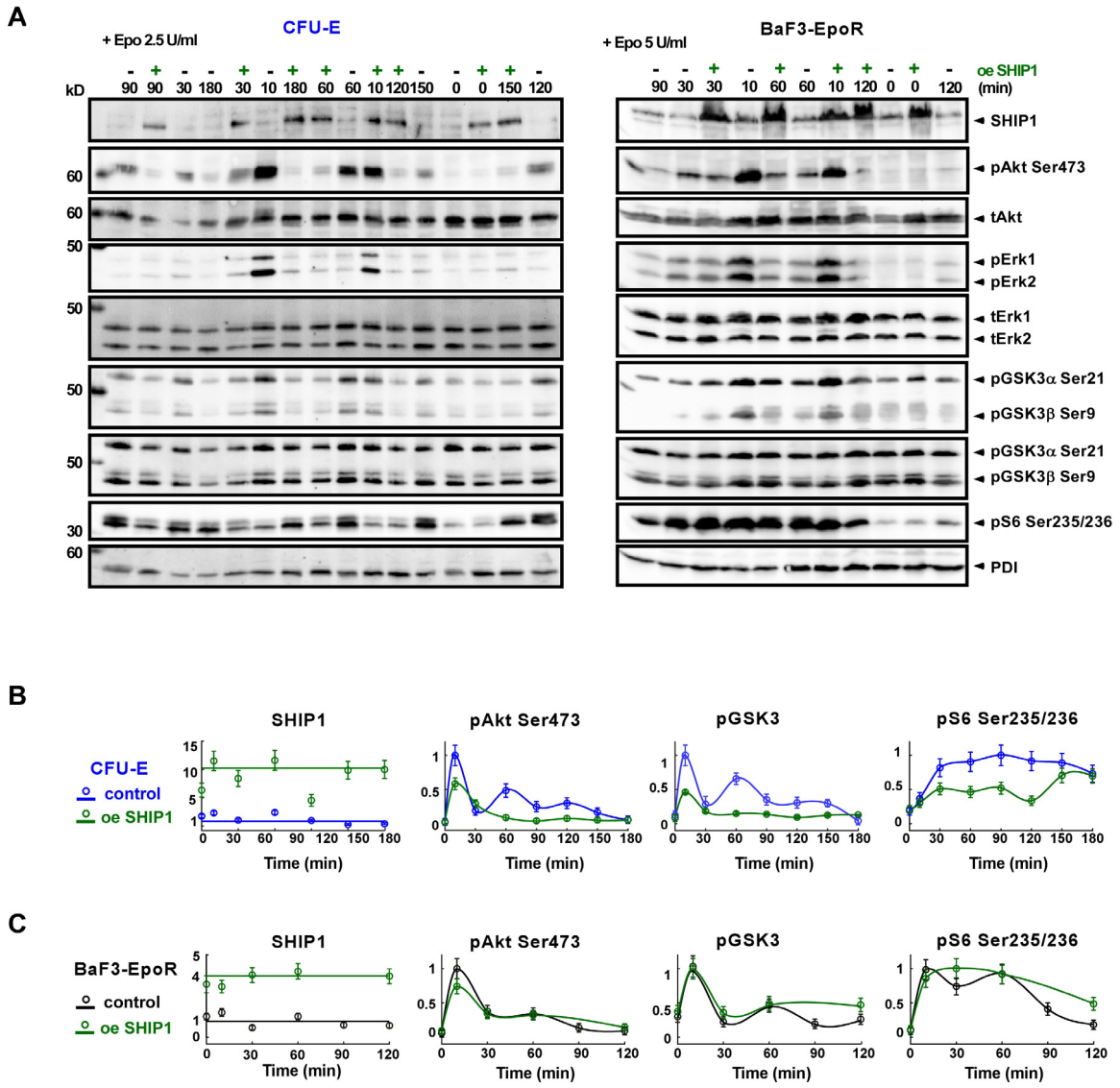

Figure 2.19 Analysis of the dynamics of Akt downstream targets by quantitative immunoblotting. (**A**) CFU-E and BaF3-EpoR cells retrovirally transduced with SHIP1 or vector control were stimulated with 2.5 U/ml or 5 U/ml Epo, respectively, for the indicated times and subjected to quantitative immunoblotting. Total SHIP1, pAkt Ser473, pGSK3 and pS6 Ser235/236 levels in (**B**) CFU-E and (**C**) BaF3-EpoR cells were quantified. For phosphorylation signals, each time-course was normalized setting the maximum signal in control cells to 1. Standard deviations of the measured data were estimated with the standard error model. The sold line represents the smooth spline. SHIP1 Overexpression in CFU-E cells was a preliminary experiment, while SHIP1 overexpression in BaF3-EpoR cells was repeated two times with similar results and representative blots are shown.

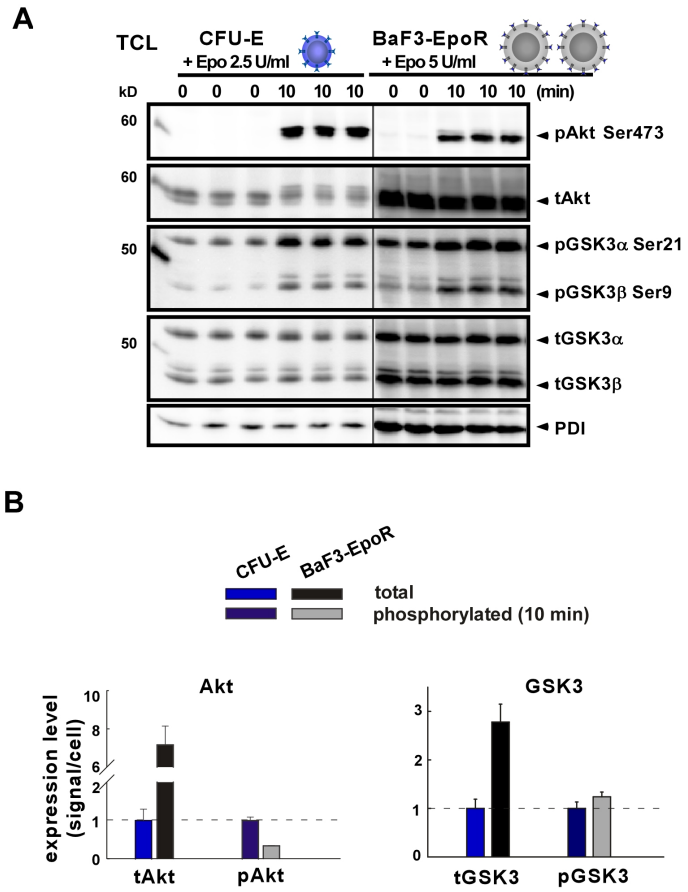

Figure 2.20 Comparison of total and phosphorylated Akt and GSK3 levels between CFU-E and BaF3-EpoR cells. Growth factor-depleted CFU-E cells ($2x10^7$ cells/ml) and BaF3-EpoR cells ($4x10^7$ cells/ml) were stimulated for 10 min with 2.5 or 5 U/ml Epo, respectively. (**A**) TCL (20 µl) were loaded and analyzed by immunoblotting. Blots are part of the same gel, allowing a direct comparison of signals between samples. (**B**)The ratio of total and phosphorylated Akt, GSK3 were depicted as bar charts with standard deviation.

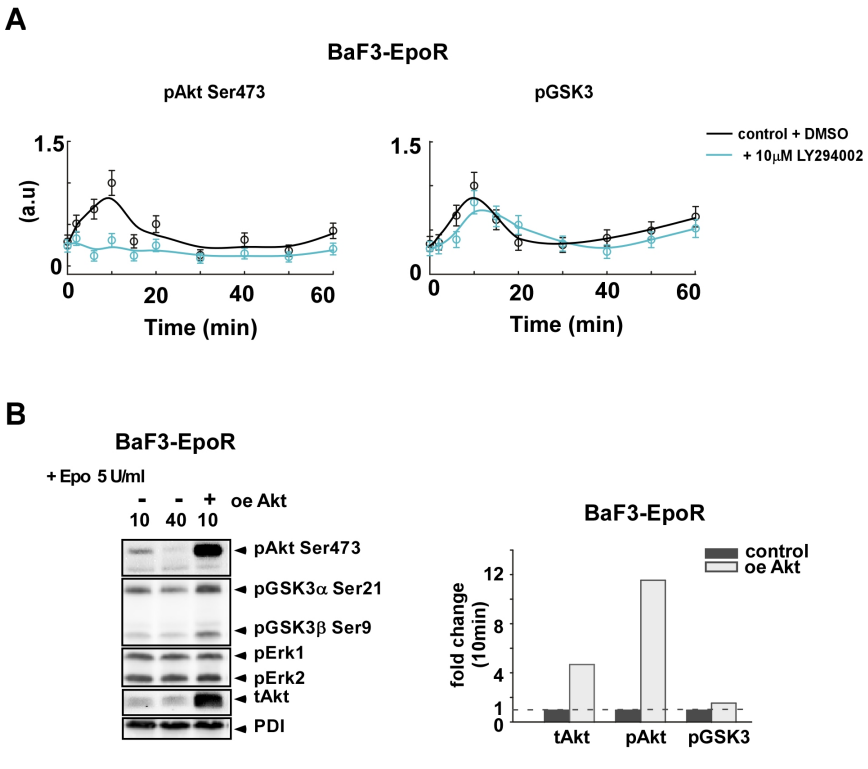

Figure 2.21 Effect of LY294002 and Akt overexpression on the phosphorylation of Akt and GSK3 in BaF3-EpoR cells. (**A**) Effect of LY294002 on the phosphorylation pattern of Akt and GSK3. BaF3-EpoR cells were pre-incubated with 10 µM LY294002 or DMSO as control for 30 min and then stimulated with 5 U/ml Epo for the indicated times. pAkt Ser473 and pGSK3 signals were detected by immunoblotting of the TCL. Experimental data are represented by circles and the smooth splines are indicated by solid lines. (**B**) Effect of Akt overexpression on Akt and GSK3 phosphorylation. Akt was retrovirally transduced in BaF3-EpoR cells. pAkt Ser473, pGSK3, pErk1/2, tAkt and PDI signals were detected in Akt-overexpressing cells compared to control BaF3-EpoR cells. The fold changes of tAkt, pAkt and pGSK3 after 10 min Epo stimulation were depicted as bar charts.

2.5.3 Cell-cycle arrest induced by PTEN overexpression only in CFU-E cells

To provide insight into the roles of Epo and Akt as modulators of cell cycle, genome-wide expression profiling was performed in collaboration with Maria Saile (University Hospital of Heidelberg at Mannheim) and Jie Bao (University of Freiburg). Time-resolved genome wide expression profiling was performed in both CFU-E and BaF3-EpoR cells. CFU-E cells isolated from murine fetal livers were stimulated with 0.5 U/ml Epo and total RNA was extracted at time points 0, 1, 2, 3, 4, 5, 6, 7, 8, 14, 19, 24 h (performed by Julie Bachmann). Control cells were left unstimulated and RNA was isolated every hour between 0 and 7 h. Beyond 7 h without Epo stimulation CFU-E cells undergo apoptosis. Next, to directly target the transcriptional regulation mediated by the PI3K/Akt signaling, Akt activation was specifically suppressed by PTEN overexpression in BaF3-EpoR cells. BaF3-EpoR cells were retroviral transduced either with PTEN or empty vector as control and pre-incubated with 0.5 U/ml Epo for 16 h. Subsequently, transduced cells were selected by MACS and seeded in fresh serum-free medium in a concentration of 20 x 10^4 cells/ml. After 5 h starvation, cells were stimulated with 1 U/ml Epo and total RNA was extracted at time points 0, 1, 2, 3, 4, 5, 7, 18.5 h. For hybridization, the GeneChip Mouse Genome 430 2.0 Array (Affymetrix) was used that comprises 45,100 probe sets representing 20,700 genes. Data analysis was performed by calculating the logarithmic fold change with respect to gene expression at 0 h.

To get a systematic overview of cell cycle regulation, the gene expression profile of all the cyclins (*Ccn*), cyclin-dependent kinases (*Cdk*) and Cdk inhibitors (*Cdkn*) was analyzed. The fold expressions (log2) was plotted as a heat map over time. The profile of CFU-E cells showed that the withdrawal of Epo (Figure 2.22, left) induced a significant decrease of cyclins, such as *Ccnd1*, *Ccnd2*, *Ccng1*, *Ccnh*, *Ccnl2*, while an increase of *Ccng2*, which is up-regulated as cells undergo cell cycle arrest. Epo withdrawal also strongly increased the expression of Cdk inhibitors, such as *Cdkn1a*, *Cdkn1b*, *Cdkn2aip*, *Cdkn2C* and moderately affected Cdks. Compared to Epo withdrawal, during the first 8 h, Epo efficiently suppressed the decrease of cyclins, such as *Ccnd2*, *Ccng1*, *Ccnl2* and also the increase of *Ccng2* and Cdk inhibitors, such as *Cdkn1b*, *Cdkn2aip*, *Cdkn2C*. However, during 14 h to 24 h observation period, the cells with Epo showed a similar gene expression profile than the cells without Epo during the first 7 h Epo (Figure 2.22, right). This might imply that Epo induces an

early transient proliferation phase within a time window of roughly 8 h and afterwards drives cell differentiation by promoting cell cycle exit. In line with the previous study of Fang et al., they showed that Epo promoted the proliferation of erythroblaste at early stage than at later stage (Fang et al., 2007). In BaF3-EpoR cells (Figure 2.23), Epo promoted sustainable up-regulation of *Ccnbilp, Ccnd2* and down-regulation of *Ccng2*, *Cdkn1b.* Several additional genes were also transiently modulated by Epo, including *Cdk18*, *Cdk5r1*, *Cdk7*, *Cdkn1a*, and *Cdkn3*. Surprisingly, their expression profile was not affected by PTEN overexpression, suggesting an Akt-independent cell cycle regulation in BaF3-EpoR cells.

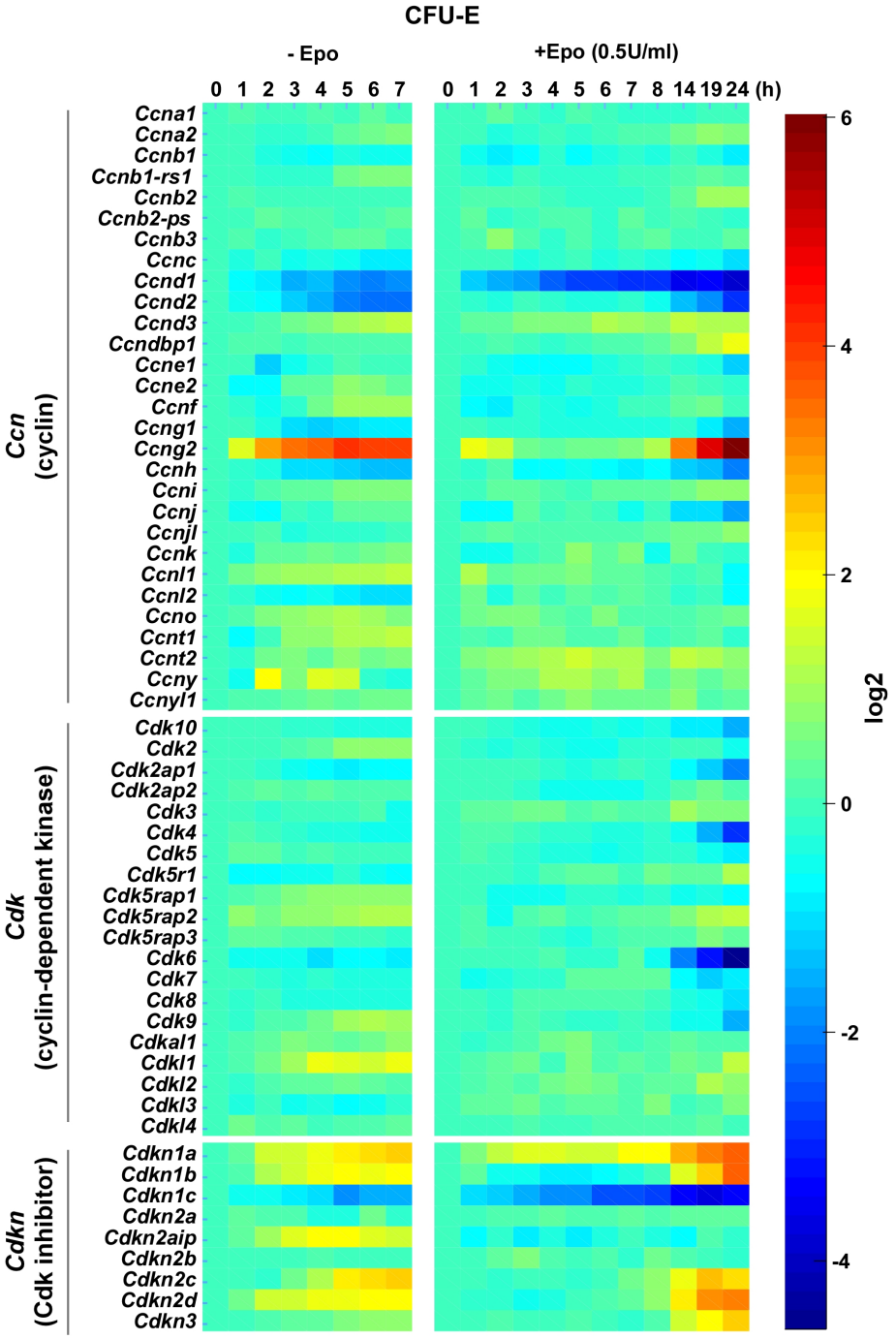

Figure 2.22 Analysis of the expression profile of cell-cycle regulated genes in CFU-E cells. Time-resolved expression profiling was performed in CFU-E cells with or without Epo stimulation. The fold expressions (log2) of all the *Ccn* (cyclin), *Cdk* (cyclin-dependent kinase) and *Cdkn* (Cdk inhibitor) were plotted as a heat map over time.

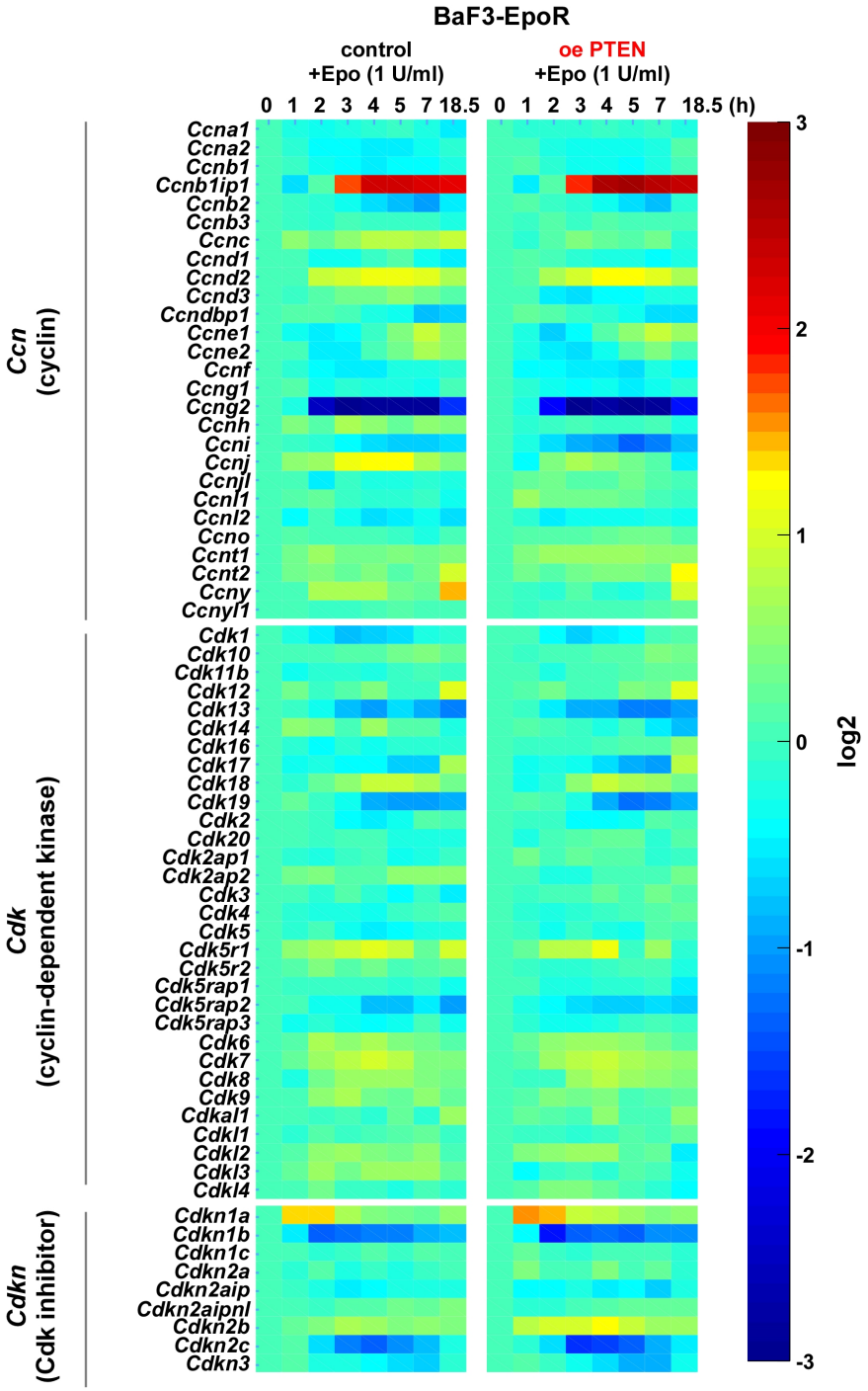

Figure 2.23 Analysis of the expression profile of cell-cycle regulated genes in BaF3-EpoR cells. Time-resolved expression profiling was performed in BaF3-EpoR control and PTEN-overexpressing cells stimulated with 1 U/ml Epo. The fold expressions (log2) of all the *Ccn* (cyclin), *Cdk* (cyclin-dependent kinase) and *Cdkn* (Cdk inhibitor) were plotted as a heat map over time.

PTEN-induced G1-phase cell cycle arrest has been reported in various tumor cells, by which PTEN could manifest its tumor suppressor activity (Radu et al., 2003; Zhu et al., 2001). In concordance with the gene profiling analysis shown above, the mechanism was associated with the reduced levels of cyclin D2 (Huang et al., 2007) and the increased levels of $p27^{KIP1}$ (Seminario et al., 2003) and cyclin G2 expression (Martinez-Gac et al., 2004). Therefore, the expression kinetics of *Ccnd2, Cdkn1b* and *Ccng2* were validated by

quantitative RT-PCR in control cells and PTEN-overexpressing CFU-E and BaF3-EpoR cells. Additionally, it was examined whether PTEN-mediated cell cycle arrest can be mimicked by the PI3K inhibitor LY294002. The quantitative RT-PCR data in Figure 2.24 A showed that in CFU-E cells, Epo addition maintained the mRNA levels of *Cdkn1b* and *Ccng2* at constant initial levels. Overexpression of PTEN (20-fold increased on mRNA level) significantly elevated the basal levels of *Cdkn1b* and *Ccng2* (approximately 2-fold). Consistently, the exposure to 10μM LY294002 also increased the transcription levels of *Cdkn1b* and *Ccng2* and maintained them at high levels. Unexpectedly, the *Ccnd2* level was increased in LY294002 treated CFU-E cells, but not in PTEN-overexpressing cells. The results were confirmed by independent measurements (Figure 2.24 B).

In BaF3-EpoR cells, the application of LY294002 efficiently inhibited the decreases of *Cdkn1b* and *Ccng2* induced by Epo, while it only slightly reduced the overall level of *Ccnd2* without changing its dynamic. Surprisingly, the mRNA levels of all three genes were comparable between control and PTEN-overexpressing cells during the 7h observation period (Figure 2.24 A). The results were confirmed by independent measurements (Figure 2.24 B).

Next, cell-cycle distribution of control cells and PTEN-overexpressing CFU-E and BaF3-EpoR cells were analyzed using propidium iodide (PI) staining by flow cytometry. Growth factor-depletion cells were cultured in the presence of Epo at 1 U/ml. The bar charts showing percentage (%) distribution of cells in SubG1 (or < 2N), G0/G1, S or G2/M phases of the cell cycle are depicted in Figure 2.24 C. In CFU-E cells, Epo addition interestingly decreased S phase fractions after 10 h Epo treatment. This finding is consistent with the Epo-promoted cell cycle exit at late stages indicated by the microarray analysis. Importantly, it was observed that almost 10% more PTEN-overexpressing cells were arrested in G0/G1phase at 0h and 12% more after 10h Epo addition compared to control CFU-E cells. This shows in a good alignment with the gene-expression data that PTEN significantly elevated the mRNA levels of the cell cycle inhibitors $p27^{kip1}$ and cyclinG2, which induced cell cycle arrest at G0/G1 in PTEN expressing CFU-E cells. Additionally, Epo promoted cells into G2/M phase (from 15% to 21%) in control CFU-E cells, which may be blocked by PTEN overexpression (remained at 17%). In line with the gene-expression analysis, the cell cycle distribution of BaF3-EpoR cells did not appreciably differ between control and PTEN-overexpressing cells at 0h, 16h and 40h (Figure 2.22 C).

Collectively, the results showed that cell cycle progression was mainly regulated by PI3K/Akt signaling in CFU-E cells, but not in BaF3-EpoR cells and that PTEN overexpression blocks CFU-E cell cycle progression in the G1 phase, correlating with a significant increase of the mRNA levels of cell cycle inhibitors $p27^{kip1}$ and cyclinG2. Gene expression analysis in SHIP1-overexpressing cells further confirmed the Akt-mediated cell type-specific cell cycle

regulation in CFU-E and BaF3-EpoR cells (Figure 6. 1-3). Additionally, increased basal mRNA levels of $p27^{kip1}$ and cyclinG2 were also observed in SHIP1-overexpressing CFU-E cells. This is again in line with the reduced basal proliferation of SHIP1-overexpressing CFU-E cells, which could not be explained by the change on Akt phosphorylation as well as its downstream proteins in these cells. Discrepancies regarding cell cycle regulation between PTEN-overexpressing and LY294002 treated BaF3-EpoR cells revealed a non-specific, indiscriminate inhibition of the PI3K pathway in this cell type by LY294002.

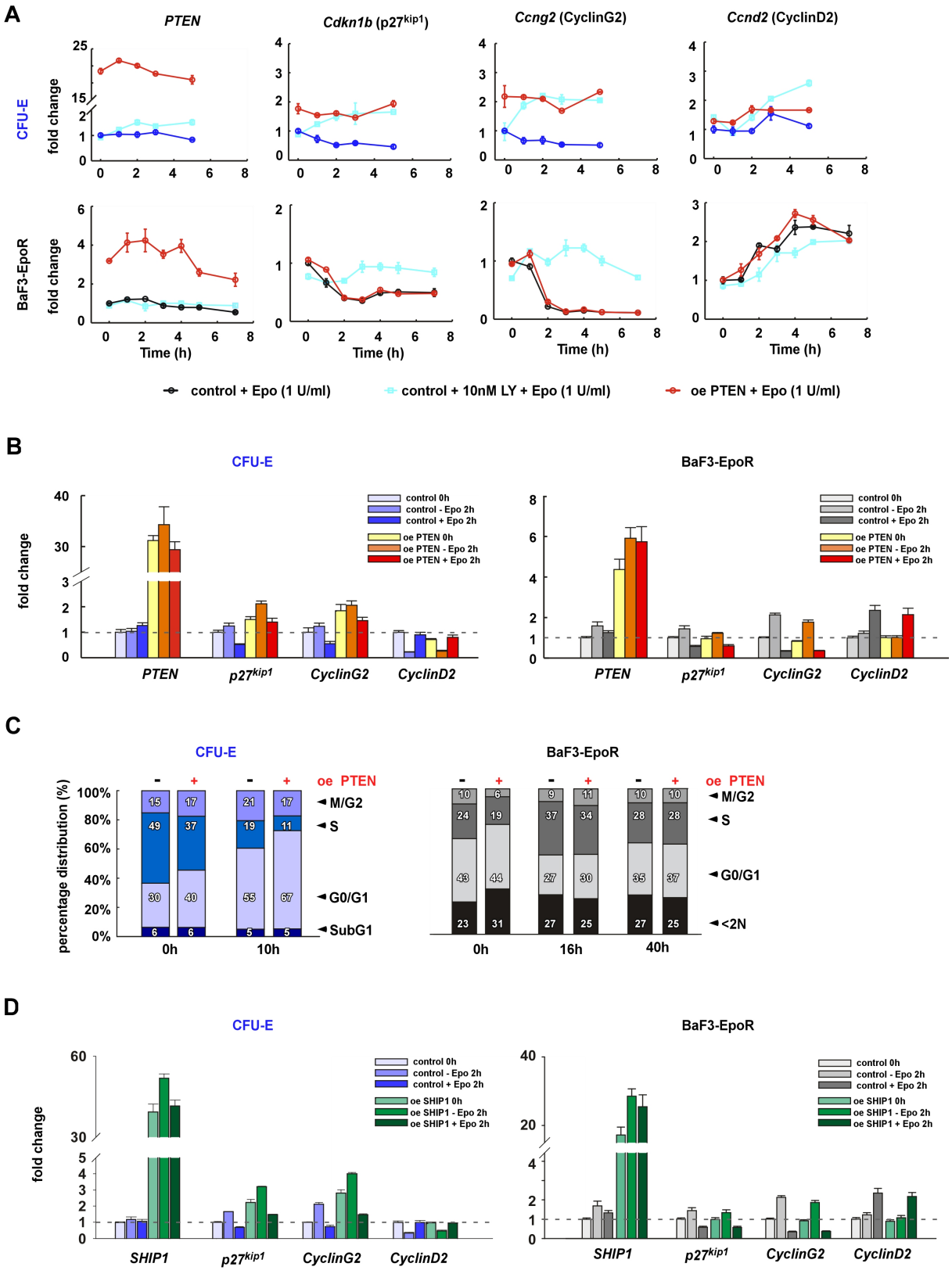

Figure 2. 24 PTEN induced G1 cell cycle arrest only in CFU-E cells. (**A**) CFU-E and BaF3-EpoR cells retrovirally transduced with PTEN or vector control were stimulated with 1 U/ml Epo for the indicated times and subjected to quantitative RT-PCR. Error bars represent standard deviations of technical duplicates. (**B**) PTEN-overexpressing and control CFU-E and BaF3-EpoR cells were stimulated with 1 U/ml Epo for 2 h or left untreated and subjected to quantitative RT-PCR. Error bars represent standard deviations of two to three biological replicates. (**C**) Cell cycle distribution of CFU-E and BaF3-EpoR cells transduced with PTEN or vector control. Cells were stimulated with 1 U/ml Epo or left untreated for the indicated times, stained with propidium iodide, and then subjected to cell cycle

analysis by fluorescence-activated cell sorting (refer to Figure 6.5-7). Percentages of cells in different cell cycle phases are shown. The experiment was repeated three times with similar results and representative data are shown. (**D**) SHIP1-overexpressing and control CFU-E and BaF3-EpoR cells were stimulated with 1 U/ml Epo for 2 h or left untreated and subjected to quantitative RT-PCR. Error bars represent standard deviations of two to three biological replicates.

3 Discussion

3.1 Signal initiation: cell type-specific receptor activation

Primary CFU-E cells endogenously express Epo receptors on their surface and are the most Epo-sensitive cells. BaF3-EpoR cells that exogenously express the EpoR are a well established system to study Epo-dependent signaling. However, by systematically comparing Epo-induced signal initiation through EpoR in primary CFU-E and the cell line BaF3-EpoR, a number of striking differences were observed. Previously, an approximately 10-fold higher EpoR cell surface expression in BaF3-EpoR cells was determined (Becker et al., 2010) compared to primary cells (D'Andrea and Zon, 1990). Additionally, Epo depletion in the medium of BaF3-EpoR cells mediated by receptor endocytosis is more efficient than in CFU-E cells due to the high density of receptors on the cell surface (Becker et al., 2010). In line with this study, here a quantitative analysis of the receptor activation revealed that the maximal activation of pEpoR measured in BaF3-EpoR cells was approximately 10-fold higher compared to in CFU-E cells. Moreover, the duration of receptor activation was more sustained in BaF3-EpoR cells. The mathematical modeling approach helped to elucidate further discrepancies regarding the attenuation of EpoR signaling between these two cell types. As mechanisms for attenuating EpoR signaling, ligand degradation, activation of the phosphatase SHP1 and the Epo-inducible kinase inhibitor SOCS3 were incorporated in the receptor models, which demonstrated good accuracy on describing the experimental data in both CFU-E and BaF3-EpoR cells. However, initially tested model versions, lacking the Epo-inducible kinase inhibitor SOCS3, were already sufficient to capture the receptor activation dynamic in CFU-E cells but poorly reflected the experimental data in BaF3-EpoR cells. Hence, in BaF3-EpoR cells, besides activation of the phosphatase SHP1, rapid Epo degradation in the medium and activation of the additional ligand-inducible signaling suppressor SOCS is essential to attenuate EpoR signaling, whereas in CFU-E cells, these mechanisms are not necessary .

3.2 Epo-induced signal transduction via the PI3K/Akt pathway

3.2.1 Stoichiometry is the major cause for cell type-specific Akt activation

Time-resolved dynamic data of EpoR and Akt activation revealed that despite weaker and shorter EpoR activation, Akt activation is stronger and more sustained in CFU-E cells than in BaF3-EpoR cells. The apparent discrepancies on Akt kinetics in these two cell types provided an efficient model to study the regulatory mechanisms that determine cell type-specific PI3K/Akt signal transduction in response to Epo. To consider the cell context-dependent concentrations of pathway components, the absolute amount of important pathway components were determined based on serial dilutions of recombinant calibrator proteins. This revealed strong alterations in the stoichiometries between primary CFU-E and

BaF3-EpoR cells. In particular, both PTEN and SHIP1 as essential negative regulators of the PI3K/Akt pathway were detected with much higher concentrations in BaF3-EpoR cells than in CFU-E cells. In addition, Gab1 was expressed and phosphorylated in response to Epo in primary CFU-E cells, while Gab2 was the dominant isoform expressed in BaF3-EpoR cells. Other pathway components including PI3K, Akt and PDK1 were detected to be present in comparable concentrations in CFU-E and BaF3-EpoR cells.

The mathematical model was constrained by the initial concentrations of signaling components and calibrated by various Akt dynamics under different conditions. With this modeling approach, the different stoichiometries of components were identified as the major cause for cell type-specific Akt activation. In CFU-E cells, the low levels of PTEN and SHIP1 together with the highly efficient activation of PI3K by Gab1 lead to strong and sustained Akt activation. In contrast, despite high activation level of the receptor, Akt activation was weak and transient in BaF3-EpoR cells due to the high levels of PTEN and SHIP1 and the dominant isoform Gab2, which is inefficient in activation of PI3K.

3.2.2 Role of the specific Gab1/2 isoforms in PI3K/Akt signaling

Epo stimulation induces activation of PI3K through the direct PI3K-binding to the EpoR (Damen et al., 1995) or through the recruitment by Gab isoforms (Bouscary et al., 2003). The adaptor protein Gab coordinates the assembly of the PI3K complex and thereby recruits and enhances the enzymatic activity of PI3K. Gab1 and Gab2 are differentially expressed in various cell lines, but in primary hematopoietic progenitors only Gab1 is expressed (Bouscary et al., 2001; Wickrema et al., 1999). Here, upon Epo stimulation Gab1 and Gab2 were phosphorylated and associated with EpoR, SHP2, p85 and Grb2 while Gab2 in primary CFU-E cells and BaF3-EpoR cells, respectively (Figure 6.12). It would be important to determine whether the PI3K activation mediated by distinct Gab isoforms is redundant and contributes to cell type-specific Akt signaling in these two cell types. To address this point, first, the PI3K/Akt core model was established with isoform-specific parameters for Gab1 and Gab2. The model was sufficient in describing wild type and PTEN- and SHIP1-overexpression data in both cell types. Furthermore, a model reduction was performed by setting all Gab1 or Gab2. This approach related parameters to 0 and revealed a vital role for Gab1 in CFU-E cells but a negligible role for Gab2 in BaF3-EpoR cells. Thus, these findings indicated that in CFU-E cells both Gab-dependent and Gab-independent pathways contribute to PI3K activation. In contrast, in BaF3-EpoR cells PI3K is activated mainly through the Gab-independent direct binding to EpoR.

Both Gab1 and Gab2 were phosphorylated in response to Epo stimulation. However, the Gab-mediated PI3K activation is a two-step activation including the phosphorylation and association of Gab with the receptor and the activation of PI3K by the pGab-pEpoR complex.

Therefore, the phosphorylation status of Gab isoforms may not directly indicate the Gab-mediated PI3K activation. Further model analysis explored the dynamics of the two-step PI3K activation mediated by distinct Gab isoforms, which are beyond experimental observations. The model analysis showed that in the first step, the phosphorylation of Gab1 and Gab2 followed the receptor activation in both cell types. In the second step, PI3K could be activated by pGab1-pEpoR complex with greater efficiency than by pGab2-pEpoR, indicating an isoform-specific activation of PI3K. Recent studies shed light on the underlying mechanisms of the non-redundant Gab1 and Gab2 functions. The recruitment of Gab1 to PIP3 by its PH domain is regarded as a positive feedback loop for activation of Gab1 (Rodrigues et al., 2000), whereas Gab2, but not Gab1 has been shown to be negatively regulated by serine phosphorylation by Akt (Cronshaw et al., 2004). Moreover, in BaF3-c-Kit cells the activation of PI3K by c-Kit has been shown to be both Gab2-dependent and Gab2-independent (Sun et al., 2008). However, since Gab1 and Gab2 have 15 conserved tyrosines, distinct phosphorylation patterns of Gab isoforms evoked by different ligands and receptors might be the molecular basis for signaling selectivity (Brummer et al., 2008; Gual et al., 2000; Lehr et al., 1999).

3.2.3 Overlapping but non-redundant roles of PTEN and SHIP1 in PI3K/Akt signaling

In the hematopoietic system, the termination of PI3K signaling by dephosporylation of PI(3,4,5)P3 involves PTEN, which transforms PI(3,4,5)P3 to PI(4,5)P2, and SHIP1, which generates PI(3,4)P2 from PI(3,4,5)P3 (Vivanco and Sawyers, 2002). Knock out mutations in *Pten* (Alimov et al., 1999, Celebi et al., 2000), but not *Ship1* (Helgason et al., 2000), give a strong cancer phenotype in mice, suggesting their different biological functions. PTEN and SHIP1 appear to be not redundant probably due to distinct products and different activation dynamics. A high binding affinity of Akt to PI(3,4)P2 has been reported *in vitro*, but the activation of Akt by PI(3,4)P2 *in vivo* is still under debate (Isakoff et al., 1998; Lemmon and Ferguson, 2001). Previous studies have indicated that in the majority of cell types PTEN is constitutively active, thereby influencing basal PI(3,4,5)P3 levels, maintaining it below a critical signaling threshold (Stambolic et al., 1998; Sun et al., 1999). In contrast, SHIP1 gets activated upon membrane recruitment mediated by binding to the phosphorylated EpoR (Mason et al., 2000). Here, in our model Akt was solely activated by PIP(3,4,5)P3. The model focused on the investigation of the kinetic properties of PTEN and SHIP1 as well as their roles in regulating Akt activation. Overexpression of either of the phosphatases in CFU-E and BaF3-EpoR cells provided a tool for exploring their molecular regulatory mechanisms. Optimal parameter estimation by multi-experiment fitting and experimental model validation confirmed the initial model assumptions. The results revealed that constitutively active PTEN strongly controls both pAkt amplitude and duration, while SHIP1 has an effect only on the

signal duration, due to its pEpoR dependent activation. Model analysis on how PTEN and SHIP1 affect the integral Akt activation suggested that PTEN maintains basal/low receptor-stimulated levels of PIP3, whereas SHIP1 primarily controls receptor-activated levels of PIP3. This finding is consistent with previous studies that demonstrated that PTEN acts as a 'sentinel' while SHIP1 as a 'gatekeeper', of the Akt signaling cascade (Harris et al., 2008). Importantly, this cooperative action of PTEN and SHIP1 could be of physiological significance as Epo plasma levels can vary between 1.5 x 10^{-3} to 10 U/ml in healthy persons (Jelkmann, 2004), thereby ensuring appropriate cellular responses over a broad range of stimuli in the hematopoietic system.

PTEN acts as a tumor suppressor by negatively regulating PI3K/Akt signaling pathway and has been shown to play a pivotal role in cell apoptosis and cell cycle arrest, preventing cells from growing and dividing too rapidly (Ward, 2004). In certain cells, SHIP1 can also downregulate Akt activation (Kulp et al., 2004) and thereby suppress cell proliferation and survival (Curnock et al., 2004). Here, the ^{3}H-thymidine incorporation assay further demonstrated the proliferation-suppressive effects of PTEN and SHIP1 in line with their crucial role as tumor suppressors. In contrast to PTEN, which strongly suppressed cell proliferation, SHIP1 exhibited a moderate effect on regulating PIP3 levels and Akt-mediated cellular processes. The underlying mechanisms of the PTEN and SHIP1 suppressed cell proliferation in CFU-E and BaF3-EpoR cells were further investigated (see 3.3).

PTEN acts as an antagonist of PI3K. SHIP1 generates PI(3,4)P2, which can interact with an array of protein effectors, as an second messenger (Lemmon and Ferguson, 2000). In addition, SHIP1 contains multiple structural domains, such as SH2-domains, C2 domains and NPXY motifs that allow SHIP1 to function as a scaffolding protein facilitating protein-protein interactions (Rohrschneider et al., 2000; Sly et al., 2007). Hence, SHIP1 may alter the activities of a subset of PIP3 effectors, potentially redirect signaling rather than stop it (Harris et al., 2008).

3.3 Distinct cell fate decisions triggered by cell type-specific PI3K/Akt signaling

3.3.1 Akt activation is not indicative for cell proliferation

A potential correlation between Akt activation and cell proliferation was examined. Cell proliferation was measured in both CFU-E and BaF3-EpoR cells with elevated PTEN or SHIP1 concentration. Then, the correlation between the integral of pAkt signal and the proliferation data was evaluated. The experimental data showed that PTEN and SHIP1 overexpression in both cell types suppressed cell proliferation in a dose dependent manner. In CFU-E cells, a high correlation was found between the integral of pAkt and the proliferation of wild type and PTEN-overexpressing cells. However, the integral of pAkt failed to describe the reduced basal proliferation of SHIP1-overexpressing cells. This indicated that

in this cell type cell proliferation is more sensitive to SHIP1 overexpression than Akt phosphorylation. In BaF3-EpoR cells, the suppression of cell proliferation by PTEN and SHIP1 was less profound than the reduction of pAkt. No effect was detected on survival in response to PTEN and SHIP1 overexpression in both cell types (Figure 6.9, 6.10). In CFU-E and BaF3-EpoR cells, Epo triggers, besides Akt pathway, other pathways such as the JAK2-STAT5 and Ras/Erk pathways. These pathways also influence cell survival, apoptosis and cell proliferation. While activation of JAK2-STAT5 signaling has been primarily associated with survival signaling (Yoon and Watowich, 2003), an essential role of PI3K/Akt and MARK pathway for differentiation and proliferation responses has been shown (Ghaffari et al., 2006; Zhang and Lodish, 2007). Indeed, the proliferation of CFU-E cells has been shown to correlate with overexpression of ERK1 and ERK2 in a dose dependent manner (Schilling et al., 2009). However, in our study, PTEN and SHIP1 mediated inhibition of Akt phosphorylation led to suppression of cell proliferation in CFU-E and BaF3-EpoR cells. The correlation between the integral of pAkt and cell proliferation was stronger in CFU-E cells than in BaF3-EpoR cells. It speculated that the signal propagation in PI3K/Akt downstream could be different and cell type-specific. The quantitative link of the cellular Akt response to cell proliferation revealed that Akt activation is necessary but not sufficient to predict cell proliferation in both cells.

3.3.2 Akt/GSK3 and Akt/mTOR, context-dependent activation

GSK3 and mTOR pathways have been intensively studied in the context of cell growth and proliferation (Fingar et al., 2004; Hahn-Windgassen et al., 2005; Liu et al., 2008). In this study, context-dependent information processing through the Akt/GSK3 and Akt/mTOR pathways was detected in CFU-E and BaF3-EpoR cells. The observations revealed that Akt is the key player in regulating GSK3 and S6 phosphorylation in primary CFU-E cells, while S6 phosphorylation is only partially Akt-dependent and GSK3 phosphorylation is Akt-independent in BaF3-EpoR cells. Further experimental analysis indicated that the low activation level of Akt may be below the threshold required to activate GSK3 efficiently. Instead of Akt, another Epo-induced kinase may phosphorylate GSK3 and partially regulate S6 in BaF3-EpoR cells. A functional overlap has been reported for the serine-threonine kinases Pim and Akt in control of hematopoietic cell growth and survival (Hammerman et al., 2005). In parental BaF3 cells, Pim-1 mRNA expression has been reported to be strictly dependent on IL-3 (Adam et al., 2006). Consistent with this study, an Epo-induced Pim-1 mRNA expression was detected in BaF3-EpoR cells and with relative lower level in CFU-E cells (Figure 6.4).

In line with the proliferation data, PTEN- and SHIP1- mediated signal attenuation was damped in BaF3-EpoR cells due to the decoupling of signal transduction from pAkt to

pGSK3. A model extension is required for studying the mechanisms by which pAkt regulates GSK3 and mTOR in a context-dependent manner. Applying this extended mathematical model, it is possible to quantitatively correlate GSK3 and mTOR activation with the cell proliferation, and to find adequate indicators for distinct cellular outcomes triggered by PI3K/Akt signaling.

3.3.3 Cell cycle regulation is Akt-dependent in CFU-E while Akt-independent in BaF3-EpoR cells

PI3K/Akt signaling promotes cell cycle progression by regulating synthesis, stability or subcellular localization of the transcription factor FoxO and cell cycle regulators cyclinD, $p21^{CIP1}$, cyclinG2, $p27^{KIP1}$ (Chang et al., 2003; Radu et al., 2003; Zhu et al., 2001). PTEN-induced G1 phase cell cycle arrest has been reported in various tumor cells (Radu et al., 2003; Zhu et al., 2001). Our observations showed that cell cycle progression is mainly regulated by the PI3K/Akt signaling in CFU-E cells. PTEN overexpression induced CFU-E cell cycle arrest in the G1 phase, correlating with the increasd basal mRNA levels of cell cycle inhibitors $p27^{kip1}$ and cyclinG2. Moreover, the increased basal mRNA levels of $p27^{kip1}$ and cyclinG2 were also detected in SHIP1-overexpressing CFU-E cells. This is again in line with the reduced basal proliferation of SHIP1-overexpressing CFU-E cells, which could not be explained by the phosphorylation level of Akt as well as its downstream proteins. In contrast to CFU-E cells, cell cycle regulation is Akt-independent in BaF3-EpoR cells. Overexpression of PTEN had no effect either on the gene expression profile of cell cycle regulators, or on cell cycle distribution.

During the preincubation period, in the presence of Epo, SHIP1 similar to PTEN efficiently reduced the pAkt level in CFU-E cells and resulted in increased mRNA levels of cell cycle inhibitors. Subsequently, during the experimental period, Epo addition maintained the mRNA levels of cell cycle regulators at constant initial levels in CFU-E cells. Cellular transformation events, such as cell cycle arrest (Ferrell and Machleder, 1998), initiation of programmed cell death (Eissing et al., 2004) and cellular proliferation (Chickarmane et al., 2009) have previously been modeled with a bistable switch character. Our findings suggested that the long-term preincubation rather than transient Epo stimulation is sufficient to induce changes in the switch's state for cell cycle progression in CFU-E cells and that the basal levels of cell cycle inhibitor $p27^{kip1}$ and cyclinG2 could function as indicator for cell cycle arrest in CFU-E cells.

In contrast to CFU-E cells, Epo significantly upregulated the cell cycle activator cyclinD2 and downregulated the cell cycle inhibitors $p27^{kip1}$ and cyclinG2. Transcription factors FoxO played a central role in regulating cell cycle genes, such as cyclinD2 (Glauser and Schlegel, 2009), $p27^{kip1}$ (Dehan and Pagano, 2005) and cyclinG2 (Martinez-Gac et al., 2004).

Phosphorylation by Akt inhibits FoxO activity by promoting its nuclear export and proteasome-mediated degradation (Burgering and Kops, 2002). Our study showed that cell cycle progression in BaF3-EpoR cells is Epo-dependent, but Akt-independent. Consistent with the observation on GSK3 and S6 activation, the findings indicated that another serine/threonine kinase may share the common substrates with Akt in regulating overlapping cellular responses in BaF3-EpoR cells.

3.4 Conclusion and future perspectives

By a data-based mathematical modeling approach, the stoichiometry of molecular components was identified as a major cause for the cell type-specific behaviors of Akt in CFU-E and BaF3-EpoR cells. Particularly, model analyses delineated the differential role of negative regulators PTEN and SHIP1 as well as distinct isoforms of the scaffold protein Gab in shaping the Akt signal. Next, further exploration of the correlation between PI3K/Akt signaling and cell proliferation revealed how disntinct cell fate decisions are triggered by cell context-dependent signaling in different cell systems.

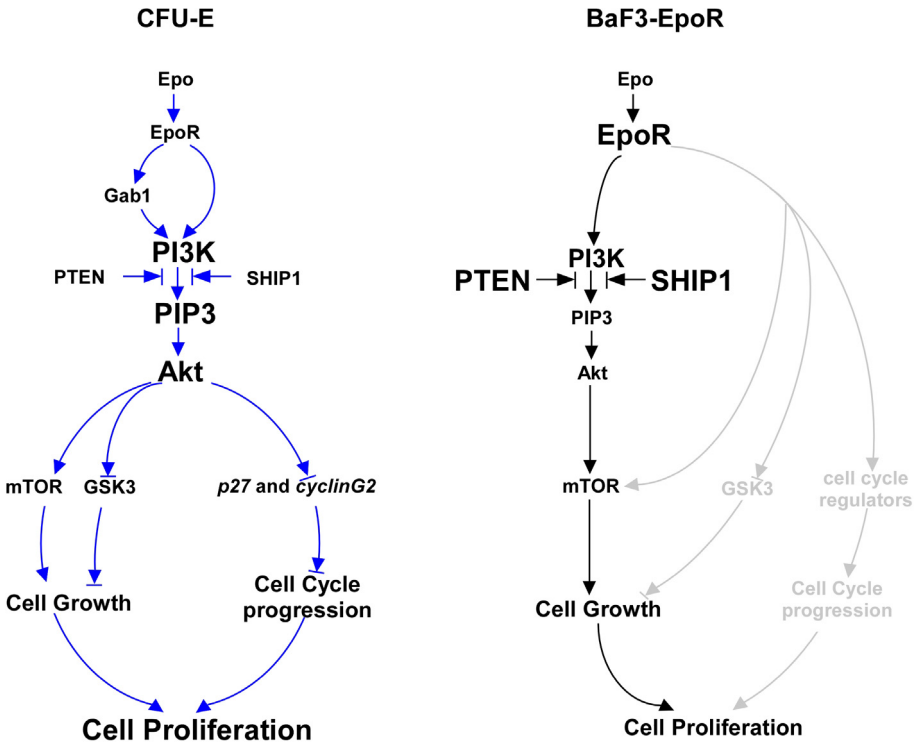

Figure 3.1 Dinstinct cell fate decisions triggered by cell type-specific PI3K/Akt signaling in CFU-E and BaF3-EpoR cells. In CFU-E cells, the low level of PTEN and SHIP1 together with the additional Gab1-mediated PI3K activation leads to strong and sustained Akt activation, which strongly promotes cell proliferation, coordinating cell growth and cell cycle progression. In contrast, in BaF3-EpoR cells, despite high activation of the receptor, Akt activation is weak and transient due to the high levels of PTEN and SHIP1. In BaF3-EpoR cells, only mTOR mediated cell growth is partially regulated by Akt, while the regulation of GSK3 and cell cycle progression is Akt-independent.

As illustrated in Figure 3.1, the abundance of negative regulators PTEN and SHIP1 together with the isoform-specific Gab-mediated PI3K activation led to cell type-specific Akt activation in CFU-E and BaF3-EpoR cells. In CFU-E cells, strong and sustained Akt

activation strongly promoted cell proliferation, coordinating cell growth and cell cycle progression. In contrast, in BaF3-EpoR cells, only cell growth is partially regulated by Akt, while cell cycle progression was Akt-independent. Further model extensions are required to integrate these three pathways and quantitatively correlate the context-dependent PI3K/Akt signaling with cell proliferation. It aims to find adequate indicators for distinct cellular outcomes triggered by PI3K/Akt signaling.

The established mathematical models provide important tools to quantitatively predict the behaviors of pathway components upon alteration of one or more compoents. As a future perspective, sensitivity analysis will be applied to identify the crucial mechanisms that control PI3K/Akt pathway activation and determine cell type-specific signaling in the cell line and primary cells.

To date, a number of the components of the PI3K/Akt pathway have been found mutated or altered in abundance in a wide variety of human cancers highlighting the key role of this pathway in cellular transformation. This mathematical model will provide guidance for the rational design of effective therapeutic molecules and facilitate accurate predictions of the effect of existing drugs.

4. Materials and methods

If not stated otherwise, chemicals were purchased from Sigma and mammalian cell culture media and supplements were obtained from Gibco.

4.1 Molecular biology techniques

4.1.1 Preparation of competent E. coli cells

For high-efficiency transformation of plasmid DNA, the *E. coli* strain DH5α **dam+ (Stratagene)** was used. To prepare chemically competent bacteria, DH5α cells were cultured in a volume of 500 ml LB medium up to an optical density of 0.6-0.8 as measured at 600 nm. After incubation on ice for 10 min, cells were sedimented with 4,100 g for 5 min at 4°C and resuspended in 150 ml TFBI (100 mM RbCl, 50 mM $MnCl_2$, 10 mM $CaCl_2$, 30 mM potassium acetate, 15% glycerol, pH 5.3). Following 20 min of incubation on ice, cells were centrifuged for 5 min at 1,400 g and 4°C, resuspended in 10-15 ml TFBII (10 mM RbCl, 75 mM $CaCl_2$, 10 mM MOPS pH 7.0, 15% glycerol), and aliquots were stored at -80°C.

4.1.2 Purification of plasmid DNA

Plasmid DNA was amplified in *E. coli* cultures either in small analytic or large preparative scale. To isolate plasmid DNA in small scale, *E. coli* cells were cultured o/n at 37°C in 1ml LB medium supplemented with 100 μg/ml ampicillin. After sedimentation, cells were resuspended in 100 μl of remaining medium and lysed by alkaline lysis in 300 μl TENS buffer (10 mM Tris pH 8.0, 1 mM EDTA pH 8.0, 100 mM NaOH, 0.5% SDS). Proteins were precipitated by adding 150 μl sodium acetate (3 M, pH 5.2). After centrifugation for 2 min at 15,700 g, the supernatant was transferred to a new tube and DNA was precipitated using two volumes of ice-cold ethanol. The DNA was washed with 70% ethanol and resuspended in 50 μl TE (10 mM Tris pH 8.0, 1 mM EDTA pH 8.0) supplemented with 40 μg/ml RNaseA (Roche Diagnostics). For sequencing grade, the QIAprep® Spin Miniprep Kit (Qiagen) was used according to the manufacturer's instructions.

To prepare plasmid DNA in large scale, a single colony or 50 μl of an *E. coli* culture were cultured in 100 or 200ml LB medium supplemented with ampicillin for 16-18 h at 37°C. For purification, the JETSTAR 2.0 Maxi Kit (Genomed) was used according to the manufacturer's instructions.

4.1.3 Quantification of plasmid DNA

The concentration of DNA was determined by measuring the absorbance of diluted 1:50 in ddH_2O at 260 nm (Ultrospec 3100 pro, GE Healthcare).

All DNA sequences were verified by sequencing service of MWG Biotech AG, Martinsried, Germany. 1 μg of DNA of plasmid preparations were provide for sequencing.

4.1.4 Molecular cloning of DNA fragments

To generate specific DNA sequences, plasmid DNA was digested using a 3-5 fold excess of the corresponding restriction enzyme (New England Biolabs). For sequential digestion, DNA fragments were purified with the QIAquick® PCR Purification Kit (Qiagen). The resulting DNA fragments were separated on a 1-2% agarose gel (Invitrogen) supplemented with 100 ng/ml ethidiumbromide and excised from the gel using a scalpel. After elution and purification of the DNA fragments with the QIAEX®II Gel Extraction Kit (Qiagen), vector and an excess of insert DNA were ligated for 10-20 min at RT using 1 μl of Quick T4 DNA Ligase (New England Biolabs) and subsequently transformed into competent *E. coli* DH5α cells. For transformation, 40 μl competent DH5α dam+ cells were thawed on ice and mixed with 0.5 μg of plasmid and 5 μl of ligation reaction. After incubation on ice for 20 min, cells were subjected to a heat shock for 5 min at 37°C under shaking (270 rpm) followed by incubation for 10 min on ice. Subsequently, cells were diluted in 1 ml LB medium and incubated at 37°C under shaking for 30min. For transformation of plasmid, 100 μl of cells suspension were plated on LB agar plates supplemented with 100 μg/ml ampicillin. For transformation of ligation reaction, total cells were plate in a volume of 100 μl on TB agar plates (Fluka). The plates were incubated at 37°C o/n and single colonies were picked for further cultivation in LB medium supplemented with 100 μg/ml ampicillin.

4.1.5 Amplification of DNA fragments

To manipulate DNA by site-directed mutagenesis or by introducing restriction sites or linker sequences, DNA was amplified by PCR in a PTC-200 Thermo Cycler (MJ Research). The number and duration of cycles as well as the annealing temperatures were optimized for the expected product length and the corresponding primers. The annealing temperature of the PCR was generally chosen to be 4-8°C lower than the

melting temperature T_M of the primers calculated by the formula T_M in °C = Σ (2x(A+T) + 4x(G+C)). In general, PCR amplification was performed in a 50 µl reaction volume containing 50 ng plasmid template DNA, 100 µM of each dNTP, 1 µM of forward and reverse primer, 10% of DMSO, 2.5 U Cloned *Pfu* DNA Polymerase (Stratagene) and buffer according to the manufacturer's manual.

4.1.6 Generation of plasmids

Retroviral expression vectors were pMOWS-puro-MCS/M2 (pMOWS). For stable transfection of BaF3 with EpoR, pMOWS-Kz-HA-EpoR was generated in our laboratory by Verena Becker (Becker et al., 2008). The murine SHIP1 and human PTEN cDNAs were cloned into pMOWS (by Christian Schröter) and its derivative pMOWSnr-MCS/M2, in which the puromycin resistance gene was replaced by the LNGFR cDNA (Miltenyi Biotech) that allows magnetic bead selection of transduced cells (Ketteler et al., 2002). The murine Gab1 cDNA were amplified by PCR using pCMV-SPORT6-GAB1 as template, introducing restriction sites Pac1 at 5', BamH1 at 3' and cloned into pMOWSnr-M2 (Table 4.1).

Mutagenesis of PTEN and SHIP1 were performed by overlap extension polymerase chain reaction (or OE-PCR) using pMOWS-PTEN and pMOWS-(KZ)HA-SHIP1 as templates, respectively (Figure 4.1). The mutation G to R at the 129-residue of PTEN (PTEN-G129R) abrogates both lipid and protein phosphatase activities, while PTEN-G129E lacks lipid phosphatase activity yet retains protein phosphatase activity (Sharrard and Maitland, 2000). ΔIP-SHIP1 is a 5'-phosphatase-defective SHIP1 (Sasaoka et al., 2004).

Recombinant protein expression plasmids: The pGEX2T system (GE Healthcare) was used to generate N-terminally GST-tagged constructs and the derived pSBPEX system (Keefe et al., 2001) to generate N-terminally SBP-tagged constructs. SBP-PTEN is full length recombinant protein, while GST-Gab1, GST-p110δ and GST-SHIP1 are truncated proteins (Table 4.2). The PCR primers using for the fragments generation are listed in Table 4.3.

Vector	Insert Fragment (Original Vector)		Target Vector	
Name	Name	Restriction sties (5', 3')	Name	Restriction sties (5', 3')
pMOWSnr-(KZ)HA-SHIP1	pMOWS-(KZ)HA-SHIP1	Bgl II, EcoR1	pMOWSnr-MCS	BamH1, EcoR1
pMOWSnr-PTEN	pMOWS-PTEN	EcoR1, BamH1	pMOWSnr-M2	EcoR1, BamH1
pMOWSnr-Gab1	PCR*	Pac1, BamH1	pMOWSnr-M2	EcoR1, BamH1
pMOWS-(KZ)HA-ΔIP-SHIP1	OE-PCR**	Mfel, Ndel	pMOWS-(KZ)HA-SHIP1	Mfel, Ndel
pMOWS-PTEN-G129R	OE-PCR**	EcoR1, BamH1	pMOWS-PTEN	EcoR1, BamH1
pMOWS -PTEN-G129E	OE-PCR**	EcoR1, BamH1	pMOWS-PTEN	EcoR1, BamH1
pMOWS-(KZ)HA-EpoR-F7-479Y	pBa-EpoR-F7-479Y	PmI1, EcoR1	pMOWS-(KZ)HA-EpoR	PmI1, EcoR1

Table 4.1 Retroviral expression vectors. *The oligonucleotides used for construction of pMOWSnr-Gab1 were listed in Table. ** The oligonucleotides used in overlap extension PCR were listed in Figure B

Vector	Insert Fragment (Original Vector)		Target Vector	
Name (kD)	Name	Restriction sties (5', 3')	Name	Restriction sties (5', 3')
pSBP-PTEN (64)	pMOWS-PTEN	EcoR1, BamH1	pSBPEX	EcoR1, BamH1
pGST-Gab1 (110)	PCR*	BamH1, EcoR1I	pGEX2T	BamH1, EcoR1
pGST-p110δ (100)	PCR*	BglII, XmaI	pGEX2T	BamH1, EcoR1
pGST-SHIP1 (120)	PCR*	BglII, EcoR1	pGEX2T	BamH1, EcoR1

Table 4. 2 Recombinant protein expression plasmids. *The oligonucleotides used for construction of recombinant proteins were listed in Table

Name	Use	Sequence (restriction site)
Gab1-EcoR1-for	Ret	cgccgcGAATTCtcacttcacattcttggtgggtgtctcggactc
Gab1-BamH1-rev	Ret	cgccgcGGATCCatgagcggcggcgaagtggtttgctcg
p110-Pac1-for	Ret	cgccgcTTAATTAAactactgtcggttatccttggacacattgtgcgc
p110-BglII-rev	Ret	cgccgcAGATCTatgccccctggggtggactgccccatg
Gab1-EcoR1-for	Cal	cgccgcGAATTCtcacttcacattcttggtgggtgtctcggactc
Gab1-BamH1-rev1724	Cal	cgccgcGGATCCgaagatcctgtgaagccgctgactggctcc
p110-XmaI-for2151	Cal	cgccgcCCCCGGGaacatatgcatcatctccttggtttgggg
p110-BglII-rev	Cal	cgccgcAGATCTatgccccctggggtggactgccccatg
SHIP1-BglII-for	Cal	cgcAGATCTccagagcctgacatgatcacc
SHIP1-EcoR1-rev3060	Cal	gacGAATTCcttagggaaggaactcacggatcc

Table 4.3 Oligonucleotides. The oligonucleotides were used for construction of retroviral expression vectors (Ret), calibrator proteins (Cal). The using restriction enzymes are given in the primer names and their matching oligonucleotides are capitalized.

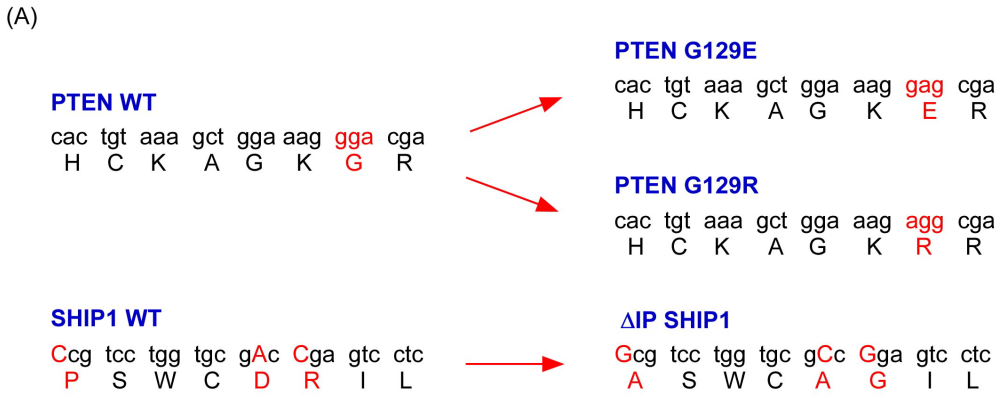

(B) **Primers for OE-PCR**

PTEN G129E
a: 5‘ cgc ***GAA TTC*** atg aca gcc atc atc aaa gag 3’
b: 5‘ tgc aca tat cat tac acc agt **tcg CTC ctt tcc agc ttt aca gtg** aat 3‘
c: 5‘ att **cac tgt aaa gct gga aag GAG cga** act ggt gta atg ata tgt gca 3‘
d: 5‘ cgc ***GGA TCC*** tca gac ttt tgt aat ttg tgt atg 3’

PTEN G129R
a: 5‘ cgc ***GAA TTC*** atg aca gcc atc atc aaa gag 3’
b: 5‘ tgc aca tat cat tac acc agt **tcg CCT ctt tcc agc ttt aca gtg** aat 3‘
c: 5‘ att **cac tgt aaa gct gga aag AGG cga** act ggt gta atg ata tgt gca 3‘
d: 5‘ cgc ***GGA TCC*** tca gac ttt tgt aat ttg tgt atg 3’

ΔIP SHIP1
a: 5‘ ctc agc ***CAA TTG*** aca agt ctg ctg tct tcc 3’
b: 5‘ **ctt cca gag gac tcC gGc gca cca gga cgC caa gtt gta ctt** cat ccc 3‘
c: 5‘ **aag tac aac ttg Gcg tcc tgg tgc gCc Gga gtc ctc tgg aag** tct tac 3‘
d: 5‘ cgc ***CAT ATG*** tca ctg cat ggc agt cct gcc 3’

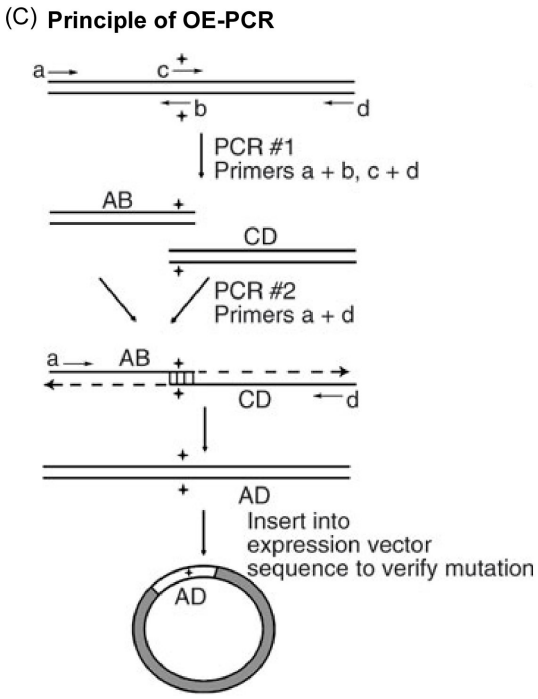

Figure 4.1 Site-directed mutagenesis of PTEN and SHIP1 by OE-PCR. (**A**) Site-directed mutagenesis of PTEN and SHIP1. Letters in red indicate the positions of mutagenesis. (**B**) Primers for OE-PCR. Italic capital letters represent the sequences of the induced restriction enzymes; the black highlights indicate the overlapping sequences containing the site-directed mutations. (**C**) Principle of OE-PCR. Site-directed mutagenesis is accomplished by using mutagenic primers (b and c) and flanking primers (a and d) to generate intermediate PCR products AB and CD that are overlapping fragments of the entire product AD. Products AB and CD are denatured when used as template DNA for the second PCR; strands of each product hybridize at their overlapping, complementary regions that also contain the desired mutation (indicated by the cross). Amplification of product AD in PCR #2 is driven by primers a and d. Final product AD can be inserted into an expression vector (gray circle) to generate larger quantities of DNA, which should also be sequenced to ensure the presence of the desired mutation. (adapted from (Heckman and Pease, 2007)

4.2 Cell culture techniques

4.2.1 Cultivation of mammalian cell lines

The packaging cell line Phoenix eco was cultured in DMEM medium supplemented with 10% FCS and 1% antibiotics (10,000 U/ml penicillin and 10,000 μg/ml streptomycin sulfate). For selection of Phoenix eco cells stably expressing Gag-Pol-Env, cells were treated with 2 μg/ml Diphtheria toxin (Calbiochem) and 200 μg/ml Hygromycin B (Roche Diagnostics). Phoenix eco cells were subcultured by treatment with 0.5 mg/ml Trypsin and 0.2 mg/ml EDTA and never cultured for longer than 2 weeks prior to transfection.

The IL-3 dependent murine pro B cell line BaF3 was cultured in RPMI 1640 medium including 10% WEHI as a source of IL-3 and supplemented with 10% FCS and 1% antibiotics. Cells were subcultured after reaching a density of 5-8 x 10^5 cells/ml.

The murine fibroblast cell line NIH3T3 was cultured in DMEM medium supplemented with 10% calf serum and 1% antibiotics. Cells were grown to 85% confluency and subcultured by treatment with 0.5 mg/ml Trypsin and 0.2 mg/ml EDTA.

In general, cells were stored in liquid nitrogen in 90% serum and 10% DMSO at a density of 5 x 10^6 for Phoenix eco and BaF3 cells or 1 x 10^6 for NIH3T3 cells.

4.2.2 Preparation of WEHI-conditioned medium

To prepare IL-3 containing medium, WEHI-3B cells were cultured in RPMI 1640(Ralph and Nakoinz, 1977; Warner et al., 1969) supplemented with 10% FCS and antibiotics until confluency. After expansion of the cells in a total volume of 50 ml, WEHI-conditioned medium was harvested every 5 days by centrifugation and subsequent filtration through a 0.2 μm filter in order to remove cell debris. The remaining adherent cells as well as the sedimented cells were further supplied with 50 ml of fresh medium and adherent cells were subcultured after 4-6 weeks.

4.2.3 Preparation of murine fetal liver cells

Fetal liver cells (FLC) of Balb/c mice were isolated at d13.5 from the uterus of sacrificed female. Fetal livers of embryos were dissected and resuspended in 500µl ice-cold PBS supplemented with 0.3% BSA. After passing through a 40 μm cell strainer (BD Biosciences), cells were treated with 9 ml Red Blood Cell Lysing Buffer (Sigma-Aldrich) to remove erythrocytes. For negative depletion, FLC of 40 livers were incubated with 10 µl rat antibodies against the following surface markers: GR1, CD41, CD11b, CD14, CD45, CD45R/B220, CD4, CD8, Ter119 (30µl) (all purchased from BD Pharmingen), and with the rat monoclonal antibody YBM/42 (gift from Suzanne M. Watt, University of Oxford, Oxford, UK) for 30 min at 4°C. Cells were washed 3 times in PBS/ 0.3%BSA and were incubated for 30 min at 4°C with anti-rat antibody-coupled magnetic beads and negative sorted with MACS columns according to the manufacturer's instructions (Miltenyi Biotech). Sorted CFU-E cells were cultivated for 14 h in Pancerin 401 (PAN Biotech) and 50 µM β-mercaptoethanol supplemented with 0.5 U/ml Epo (Cilag-Jansen).

4.2.4 Transient transfection of Phoenix eco cells

Transient transfection of Phoenix eco cells was performed by calcium-phosphate precipitation either in small scale (6-well plate) or large scale (25 cm^2 dish).

For small scale transfection, cells were seeded at a density of 8 x 10^5 cells in 6-well plates 16-18 h prior to transfection. A mix of 10 μg of plasmid DNA and 12.5 μl $CaCl_2$ (2.5 M) was precipitated together with 125 μl of 2x HBS (280 mM NaCl, 50 mM HEPES, 1.5 mM Na_2HPO_4, pH 7.05). For large scale transfection cell were seeded at a density of 12x10^6 in 25 cm^2 dishes and 1875 μl of 2x HBS was dropwise added to a mixture of 150 μg plasmid DNA and 187.5 μl $CaCl_2$ (2.5 M) while vortexing. The suspension was dropwise transferred to the cells. To ensure an efficient uptake of DNA, cells were incubated for 6-8 h in DMEM

medium supplemented with 25 μM chloroquine. Subsequently, the medium was replaced by IMDM supplemented with 30% FCS, 1% antibiotics, and 50 μM β-mercaptoethanol. The retrovirus-containing supernatant was harvested after 16-18 h of incubation and filtered through a 0.45 μm filter (Millipore). Supernatants were either directly used or stored at -80°C for up to 3 months. Transfection efficiency was determined by measuring GFP expression in the FL-1 channel of a FACSCalibur (Becton Dickinson), in general yielding a GFP-positive population of 75-90%.

4.2.5 Retroviral transduction of cells

To stably transduced BaF3 cells, 250 μl retroviral supernatants of pMOWS-Kz-HA-EpoR generated with Phoenix eco cells were adjusted to 8 μg/ml polybrene, mixed with 1 x 10^5 BaF3 cells and centrifuged for 2 h at 340 g and 37°C in a round bottom 2-ml microcentrifuge tubes. After centrifugation, cells were cultured for 48 h in standard medium, subsequently selected and further cultured with 1.5 μg/ml puromycin. Transduction efficiency was determined by measuring GFP expression in the FL-1 channel of a FACSCalibur (Becton Dickinson), in general yielding a GFP-positive population of 35-45%.

To transduce BaF3-EpoR and CFU-E cells in large scale, 4.5 ml retroviral supernatants supplemented with 8 μg/ml polybrene were mixed with 5 x 10^6 cells in a 6-well plate and centrifuged at 37 °C for 3h in a Heraeus centrifuge 2200 or 2500 r.p.m., respectively. Following spin-infection cells were cultivated for 12-14 h in the standard mediums.

Successfully transduced cells were isolated using the MACSelect LNGFR selection kit (Miltenyi Biotech) according to the manufacturer's instructions. Briefly, 6x10^7 washed cells were resuspended in 1ml PBS/ 0.3% BSA and incubated with 150 µl MACS beads on ice for 15 min to magnetically label positively transduced cells. LS columns were placed in the magnetic field of a MACS Separator and rinsed with 1 ml PBS/ 0.3% BSA. Cells were applied onto the column in 8 ml PBS/ 0.3% BSA and the flow through was collected as negative unlabeled cell fraction. The column was washed four times with 3 ml PBS/ 0.3% BSA. To elute the positive fraction, the column was removed from the magnetic field and transduced cells were flushed out with 5 ml PBS/ 0.3% BSA by firmly applying the plunger.

Standardized procedures for PTEN or SHIP1 overexpression in CFU-E and BaF3-EpoR cells are depicted in Figure 4.2.

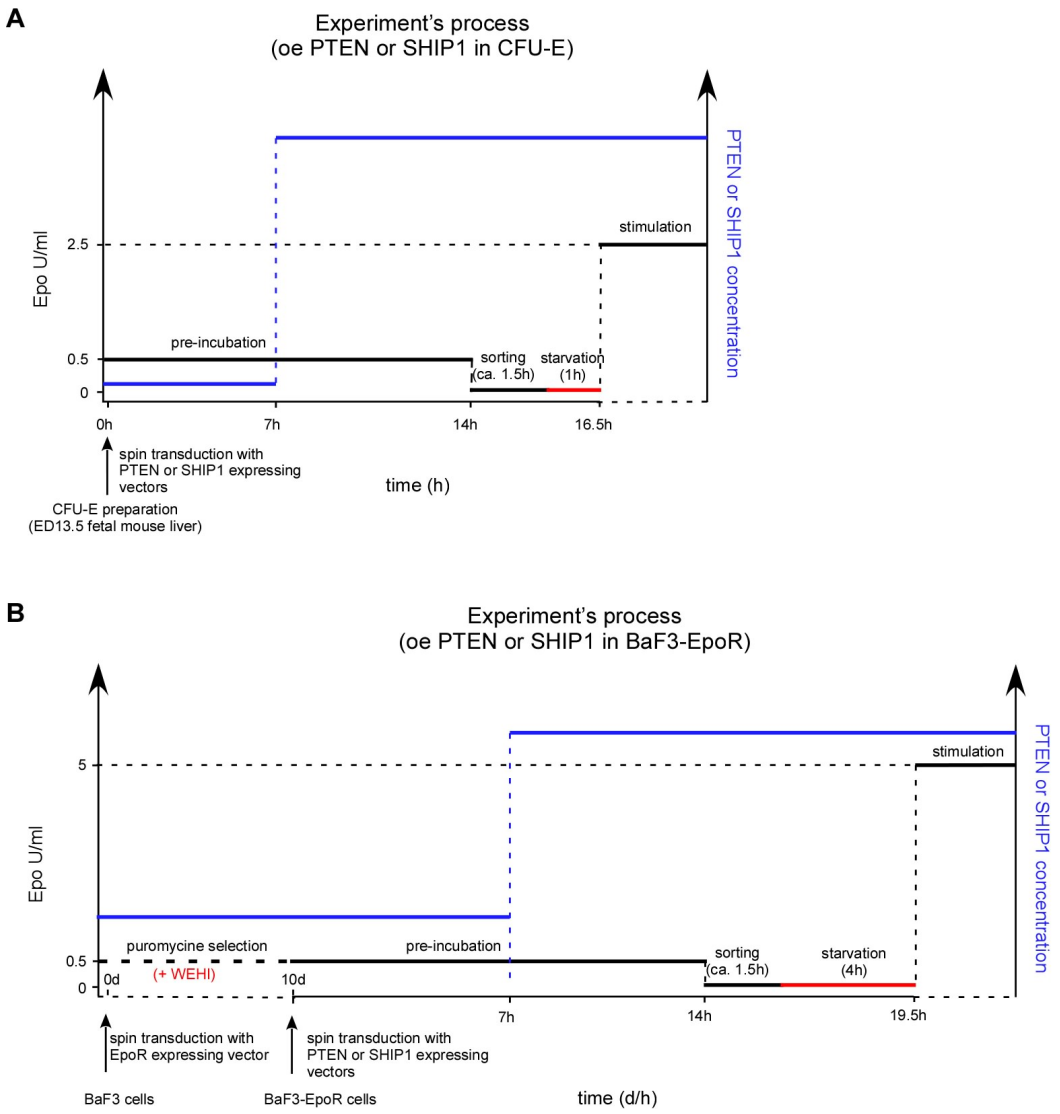

Figure 4.2 Standardized procedures for overexpression PTEN or SHIP1 in CFU-E and BaF3-EpoR cells.

4.2.6 TUNEL assay

For detection and quantification of apoptosis at single cell level, the *In Situ* Cell Death Detection Kit (Roche Diagnostics, Mannheim) was used. The TUNEL (Terminal deoxynucleotidyl Transferase-mediated dUTP nick end labelling) assay relies on the detection of single- and double-stranded DNA breaks that occur during the early stages of apoptosis. Apoptotic cells are identified by using TdT to transfer fluorescein-dUTP to these strand breaks of cleaved DNA. Briefly, 2 x 10^6 cells were fixed in freshly prepared 2% paraformaldehyde and permeabilised with 0.1% Triton X-100, 0.1% sodium citrate for 2 min. The positive control was treated with digestion buffer (DNaseI recombinant, DNaseI buffer, Roche Diagnostics, Mannheim) for 10 min. After washing with PBS/ 0.3% BSA, cells were resuspended in TUNEL reaction mixture (TdT, fluorescein-dUTP, reaction buffer) to label

free 3'-OH groups of single- and double-stranded DNA. Fluorescein-dUTP incorporated in nucleotide polymers is detected and quantified by flow cytometry using the FL-2 channel of a FACSCalibur (Becton Dickinson). For statistical evaluation a two-sided, unpaired Student's *t*-test was performed with $P<0.05$ considered significant.

4.2.7 Cell cycle distribution (PI staining)

For detection and quantification of cell cycle distribution at single cell level, Propidium Iodide staining for DNA content was performed. Propidium iodide (PI) binds to DNA by intercalating between the bases with little or no sequence preference. The intensity of the PI signal, then, is directly proportional to DNA content. Briefly, $2x10^6$ cells were added into 1 ml 'fridge cold' 70% ethanol while vortexing. After at least 30 min incubation at 4 °C, samples may be kept at -20°C for up to 2 weeks. For FACS analysis, cells were washed with PBS/0.3% BSA and incubated with ribonuclease reaction mixture at room temperature for 5 min. After washing with PBS/0.3% BSA, cells were resuspended in propidium iodide solution to label the DNA. The fluorescence emission is detected and quantified by flow cytometry using the FL-2 channel of a FACSCalibur (Becton Dickinson). The histograms were plotted by the MultiCycle (Phoenix Flow Systems) program and the program provided the estimate of percentage of cells in major phases of the cell cycle with fractional DNA content.

4.2.8 Proliferation assay

For proliferation assay, Coulter Counter and ^{3}H-Thymidine incorporation assay were performed to determine the number of cells that were growing in the absence or presence of Epo.

Coulter Counter assay: BaF3-EpoR cells wild type and-overexpressing PTEN or SHIP1 were washing three times with RPML 1640 and plate at densities of 5×10^4 cells/ well in 24-well plates in the absence or presence of Epo (Janssen-Cliag) concentrations range from 0.01 to 5 U/ml in RPMI 1640. After 4 days, cells numbers were determined using a Coulter Counter Z2 (Beckman, particle size 4.00-17.35 μm) and expressed as the percentage of growth obtained in a parallel well containing 5% WEHI-conditioned medium as a source for IL-3.

[^{3}H] -Thymidine incorporation assay: To obtain pure population of CFU-E cells for [^{3}H]-Thymidine incorporation, BFU-E and CFU-E cells were isolated from fetal liver cells (FLC) by negative depletion with MACS as described above without antibody against CD41. Subsequently, retroviral transduction was performed as described above. Transduced cells were seeded in IMDM/sct, which was prepared by supplementing IMDM (Invitrogen) with 15% fetal calf serum, 1% BSA (Sigma-Aldrich), 200 mg/ml hHolo-Transferrin, 10 mg/ml insulin, 50 ng/ml rmSCF, 10 ng/ml rmIL-3, 10 ng/ml rhIL-6 (all from R&D), and 10 U/ml Epo

(Cilag-Jansen). After 14h cultivation, CFU-E cells were sorted by MACS negative selection again. Transduced BaF3-EpoR cells were prepared as describe above. To measure cellular proliferation, [^{3}H]-Thymidine incorporation assay was performed to determine the DNA content of cells that were growing in the absence or presence of Epo. After washing with serum free medium, BaF3-EpoR cells were plated at densities of 10 x 10^4 cells / well in 96-well plates in the absence or presence of Epo (Janssen-Cliag) concentrations range from 0.001 to 10 U/ml in RPMI 1640, while CFU-E cells were plated at densities of 20 x 10^4cells / well in 96-well plates in the absent or present of Epo in Pancerin 401. After 4h incubation, 1 µCi/well ^{3}H-Thymidine was added and cells were cultivated for 38h for BaF3-EpoR cells and 14 h for CFU-E cells. Cells were collected and the incorporated radioactivity was measured using a scintillation counter. To quantify the proliferation assay, regression lines are calculated with a four-parameter Hill regression ($y=y_0+(ax^b/c^b+x^b)$). As the logarithmic transformation is a monotonic transformation, the sigmoidality of the curve is also true for a linear axis (Schilling et al., 2009).

4.3 Biochemical and immunological protein analysis

4.3.1 Time-course experiments in BaF3-EpoR and CFU-E cells

BaF3-EpoR cells were washed three times with RPMI 1640 and starved for 4-5 h at 37°C in RPMI 1640 supplemented with 1 mg/ml BSA. CFU-E cells were washed three times and starved in Panserin 401 supplemented with 50 µM β-mercaptoethanol for 1-2h. For time-course experiments 4 x 10^7 BaF3-EpoR or 2 x 10^7 CFU-E cells/ml were pre-incubated for 5 min at 37°C and subsequently stimulated with 0.5-50 U/ml Epo (Janssen-Cilag) at 37°C. For each time point, 1 x 10^7 BaF3-EpoR or 0.5 x 10^7 CFU-E cells were taken from the pool of cells and lysed by adding 2 x Nonidet P-40 (NP40) lysis buffer, thereby terminating the reaction.

4.3.2 Preparation of cellular lysates

Detergent lysates of cells were prepared with 2 x 1% NP40 buffer (1 x buffer: 1% NP40, 150 mM NaCl, 20 mM Tris pH 7.4, 10 mM NaF, 1 mM EDTA pH 8.0, 1 mM $ZnCl_2$ pH 4.0, 1 mM $MgCl_2$, 1 mM Na_3VO_4, 10% Glycerol) supplemented with 2 µg/ml aprotinin and 200 µg/ml AEBSF. After 30 min of incubation at 4°C with overhead rotation, the lysate was centrifuged for 10 min at 20,000 g and 4°C. The supernatant was either used directly, processed further by immunoprecipitation or total cellular lysates were stored at -80°C.

4.3.3 Immunoprecipitation

Immunoprecipitation was performed with an equivalent of 1 x 10^7 BaF3-EpoR or 0.5 x 10^7 CFU-E cells by adding the target-specific antibody and 25 µl of Protein A/G sepharose (GE

Healthcare) to the lysate for 2-8 h or o/n at 4°C. The immunoprecipitates were washed twice with 1 x 1% NP40 lysis buffer and once with TNE buffer (10 mM Tris pH 7.4, 100 mM NaCl, 1 mM EDTA, pH 8.0, 100 µM Na_3VO_4) and were resuspended in 25 µl 2 x SDS sample buffer (1 x buffer: 2% SDS, 50 mM Tris pH 7.4, 10% glycerol, 5% β-mercaptoethanol, 100 mM DTT, 0.01% bromphenolblue). Immunoprecipitates were immediately subjected to protein gel electrophoresis or stored at -20°C.

Samples for time-course analysis of EpoR, JAK2, p85, SHIP1 or Gab1 were prepared prior to immunoprecipitation by adding adequate mount of calibrator protein to the lysates.

4.3.4 SDS-PAGE and immunoblot analysis

Proteins were separated according to their electrophoretic mobility in a denaturing SDS-PAGE (Laemmli, 1970). Protein samples were boiled at 95 °C for 2 min in SDS sample buffer. Protein samples were separated by 10% or 15% SDS-PAGE with low bis-acrylamide (GE Healthcare) (Table 4.4) and separated in an electric field in running buffer (192 mM glycine, 25 mM Tris, 0.1% SDS). Immunoprecipitates were centrifuged for 2 min at 15,700 g before loading. For total cellular lysates, an amount of 50-100 µg protein resuspended in 2 / 4 x SDS sample buffer were separated by SDS-PAGE. Sample loading on SDS-PAGE was randomized to avoid correlated blotting errors (Schilling et al., 2005b)

	Stacking gel (10 ml)	Separating gel 10% (20 ml)	Separating gel 15% (20 ml)
40% acrylamide	1 ml	5 ml	7.5 ml
2% w/v methylenebisacrylamide	0.5 ml	1.3 ml	0.88 ml
1M Tris-HCl, pH 6.8	1.25 ml	-	-
1.5M Tris-HCl, pH 8.8	-	5 ml	5 ml
10% SDS	0.1 ml	0.2 ml	0.2 ml
ddH_2O	7.15 ml	8.5 ml	6.42 ml
APS (10 %)	100 µl	200 µl	200 µl
Temed	10 µl	20 µl	20 µl

Table 4.4. SDS-Page for 10% and 15% polyacrylamide gels.

Immunoblotting was performed in semi-dry chambers (GE Healthcare) on nitrocellulose membranes with a pore size of 0.2 µm (What man) or PVDF membrane (Millipore)

Blotting was performed in transfer buffer (192 mM glycine, 25 mM Tris, 0.075% SDS, 0.5 mM Na3VO4, 15% methanol) for 1 h at approximately 1.3 mA/cm2. Proteins were reversibly stained immobilized with Ponceau Red. After blocking unspecific antibody binding with 2-5% BSA diluted in TBS-T (10 mM Tris pH 7.4, 150 mM NaCl, 0.2% Tween-20), membranes were incubated with the appropriate first and secondary antibodies and proteins were visualized with the ECL or ECL Advance Western Blotting Detection Reagents (GE Healthcare) and subsequently detected on a Lumi-Imager F1™ (Roche Diagnostics, Mannheim).

Quantification was performed using the LumiAnalyst 3.1 software (Roche Diagnostics, Mannheim). To evaluate total protein levels, membranes were incubated in stripping buffer (62.5 mM Tris pH 6.8, 2% SDS, 100 mM β-mercaptoethanol) for 20-25 min at 65°C, blocked with 2-5 % BSA diluted in TBS-T, and reprobed with the appropriate first and secondary antibody.

4.3.5 Coomassie staining

For Coomassie staining, gels were incubated in *Staining Solution* (0.25% Coomassie Brilliant Blue, 50% methanol, 12.5% acetic acid) for 10 min at room temperature. Subsequently, gels were incubated in *Destaining Solution 1* (45% methanol, 10% acetic acid) for 10 min and in *Destaining Solution 2* (5% methanol, 5% acetic acid) o/n at room temperature.

4.3.6 Expression and purification of recombinant proteins in *E.coli*

For high-efficiency expression of calibrator constructs, expression plasmids were transformed into competent *E. coli* BL21 (DE3) CodonPlusRIL cells (Stratagene) as described for DH5α cells. A single positive colony was cultured in 25 ml LB medium supplemented with 100 μg/ml ampicillin and 50 μg chloramphenicol at 37°C o/n. This o/n culture was then added to 225 ml fresh LB medium supplemented with ampicillin and chloramphenicol and cultured at 37°C for 90 min. After IPTG was added at a final concentration of 0.2 mM to induce protein expression, cells were cultured for another 3 h at 37°C. Cells were sedimented, washed with cold PBS and stored at -20°C o/n.

Upon thawing the cell pellet was resuspended in 15 ml bacterial lysis buffer (10 mM Tris pH 8.0, 100 mM NaCl, 1 mM EDTA) supplemented with 70 μl lysozyme solution (50 mg/ml) and 75 μl 1 M DTT, and lysed on ice for 20 min. After adding 2.25 ml 10% N-lauroylsarcosine the suspension was vortexed for 1 min and sonicated (Sonopuls, Bandelin) three times for 1 min on ice. The bacterial lysate was then centrifuged at 15,000 g for 15 min at 4°C to remove cell debris. The supernatant was carefully transferred to a fresh tube and 350 μl Triton X-100 were added. To bind GST- or SBP-tagged recombinant proteins, the supernatant was incubated with 500 μl glutathione sepharose beads or 500 μl streptavidin sepharose beads, respectively, and rotated for 1 h at 4°C. Subsequently, beads were washed four times with cold 9% PBS, 1% NP40 supplemented with 5 mM DTT and once with cold PBS supplemented with 5 mM DTT. Beads were subsequently transferred to a 0,45 μm filter unit (Millipore) and recombinant proteins were eluted in fractions of 500 μl elution buffer (75 mM Tris pH 8.0, 150 mM NaCl, 0.1% SDS, 5 mM DTT) supplemented with 20 mM reduced glutathione or 2 mM biotin for GST- or SBP-tagged proteins, respectively. Protein aliquots were stored at -80°C.

4.3.7 Quantification of proteins

To determine protein concentrations of cellular lysates the BCA Protein Assay Kit (Pierce) was used according to the manufacturer's instructions.

For quantification of recombinant calibrator proteins, a dilution series of the respective recombinant calibrator protein and a BSA standard series were separated by SDS-PAGE. The gel was Coomassie stained and band intensities were quantified using a Lumi-Imager F1 (Roche Diagnostics, Mannheim) and the LumiAnalyst 3.1 software (Roche Diagnostics, Mannheim).

4.3.8 Antibodies

The following antibodies were used for immunoprecipitation (IP) and immunoblot analysis (IB) (Table 4.5 and 4.6).

primary antibodies	use	specification	company
mouse anti-phosphoTyr	IB (1:10000)	monoclonal, 4G10	UBI
rabbit anti-EpoR	IP (3 μl) IB (1:10000)	polyclonal, M-20	Santa Cruz
mouse anti-SHIP1	IB (1:5000)	monoclonal, P1C1	Santa Cruz
rabbit anti-PI3 kinase p110β	IP (5 μl) IB (1:2000)	monoclonal	Upstate
rabbit anti-PI3 kinase p110δ	IP (5 μl) IB (1:2000)	polyclonal, H-219	Santa Cruz
rabbit anti-PI3 kinase p85 N-SH2 domain	IP (5 μl) IB (1:10000)	polyclonal, serum	Upstate
rabbit anti-Gab1	IP (5 µl) IB (1:2000)	polyclonal	Upstate
rabbit anti-Gab2	IP (5 µl) IB (1:2000)	polyclonal	Upstate
rabbit anti-Akt	IB (10ul) IB (1:2000)	polyclonal	Cell signaling
rabbit anti-Akt Ser473	IB (1:2000)	monoclonal,193H12	Cell signaling
rabbit anti- Akt Thr308	IB (1:2000)	monoclonal, 244F9	Cell signaling
rabbit anti-PDI	IB (1:5000)	polyclonal	Sressgen
rabbit anti-PTEN	IB (1:2000)	polyclonal	Cell signaling
rabbit anti-Grb2	IB (1:2000)	polyclonal	Cell signaling
rabbit anti-Shc	IB (1:2000)	polyclonal	Cell signaling
mouse anti-GSK-3α/β	IB (1:2000)	monoclonal, 0011-A	Santa Cruz
rabbit anti-p GSK-3α/β (Ser21/9)	IB (1:2000)	polyclonal	Cell signaling
mouse anti-S6	IB (1:2000)	monoclonal, 54D2	Cell signaling
rabbit anti-pS6 (Ser240/244)	IB (1:2000)	polyclonal	Cell signaling
rabbit anti-pS6(Ser235/236)	IB (1:2000)	polyclonal	Cell signaling
rabbit anti-p44/p42 MAPK	IB (1:2000)	polyclonal	Cell signaling
rabbit anti-phospho-p44/p42 MAPK (Thr202/Tyr204)	IB (1:2000)	polyclonal	Cell signaling
mouse anti-14-3-3 β	IP (10 μl) IB (1:2000)	monoclonal, H-8	Santa Cruz
mouse anti-p21	IB (1:1000)	monoclonal	BD Pharmingen
mouse anti-p27	IB (1:1000)	monoclonal	BD Pharmingen

Table 4.5. Primary antibodies.

conjugates	use	specification	company
donkey anti-rabbit IgG HRP	IB (1:10000)	polyclonal	GE Healthcare
sheep anti-mouse IgG HRP	IB (1:10000)	polyclonal	GE Healthcare
Protein A HRP	IB (1:10000)	-	GE Healthcare
donkey anti-goat IgG HRP	IB (1:10000)	ploYclonal	Santa Cruz

Table 4. 6. Secondary antibody conjugates used for immunoblot analysis.

4.4 RNA analysis

4.4.1 Extraction of total RNA

Per time point total RNA from1.5 to 3 x 10^6 BaF3-EpoR and CFU-E cells was isolated using the RNeasy Mini Plus Kit (Qiagen). RNA was extracted according to the manufacturer's instructions for suspension cells. To eliminate traces of DNA, on-column digests using the RNAse-free DNAse Set (Qiagen) were performed. RNA was stored at -80°C or directly used for quantification and reverse transcription.

4.4.2 Quantification of RNA

The concentration of total RNA samples was determined by measuring the absorbance of diluted 1:50 in TRIS buffer pH 7.4 at 260 nm (Ultrospec 3100 pro, GE Healthcare).

4.4.3 Quantitative two-step RT-PCR

To generate cDNA, 2 µg of total RNA was transcribed with the QuantiTect Reverse Transcription Kit (Qiagen) according to the manufacturer's instructions (Table 4.7). Quantitative PCR (qPCR) was performed using a LightCycler 480 (Roche Diagnostics, Mannheim) in combination with the hydrolysis-based Universal ProbeLibrary (UPL) platform (Roche Diagnostics, Mannheim). For the detection and quantification of pre-rRNA, qPCR was performed using a LightCycler480 in combination with SYBR Green (Roche Diagnostics, Mannheim). In general, qPCR amplifications were performed in 96-well format in a 20 µl reaction volume containing 5 µl of 1:5 or 1:25 diluted template cDNA, 0.2 µM of forward and reverse primer, 0.2 µl of the appropriate UPL probe and 10 µl LightCycler 480 Probes Master solution (Roche Diagnostics, Mannheim) or with 10ul SYBR Green Master mix I according to the manufacturer's manual. Primer pairs were generated using the automated UPL Assay Design Center (www.roche-applied-science.com) (Table 4.8).

Crossing point (CP) values were calculated using the Second Derivative Maximum method of the LightCycler 480 Basic Software (Roche Diagnostics, Mannheim). PCR efficiency correction was performed for each PCR setup individually based on a dilution series of template cDNA. Relative concentrations were normalized using HPRT or RPL32 as reference genes.

PCR step		Temperature	Time
initial denaturation		95°C	5 min
50 cycles	melting	95°C	10 s
	primer annealing	60°C	30 s
	DNA synthesis and data acquisition	72°C	1 s
cooling		40°C	2 min

Table 4.7. PCR program for quantitative PCR.

Target gen	Sequence	
name	Left	Right
Foxo1_11	cttcaaggataagggcgaca	gacagattgtggcgaattga
Foxo3a_64	gctaagcaggcctcatctca	ttccgtcagtttgagggtct
Ccnd2_45	ctgtgcatttacaccgacaac	cactaccagttcccactccag
Ccng2_12	ccacgcgattgtattttgtc	agctgcgcttcgagtttatc
Cdkn1a_16	aacatctcagggccgaaa	tgcgcttggagtgatagaaa
Cdkn1b_62	gagcagtgtccagggatgag	tctgttctgttggccctttt
PTEN_102	gtggcggaacttgcaatc	ctactttgatatcaccacacacagg
SHIP1_76	cctctgtcgccaaagaagtt	agcttccacctttcccagat
Pim-1_93	cagtctacacggactttgatgg	cgcagaccatgtcatagagc
Junb_3	ccacggagggagagaaaatc	agttggcagctgtgcgtaa

Table 4.8 q RT-PCR primers. UPL probe numbers are given in the primer names.

4.4.4 Microarray analysis

Microarray analysis I: Epo stimulated or non-stimulated CFU-E cells (performed by Julie Bachman) (Figure

Primary CFU-E cells were isolated from mice fetal livers (E13.5) and starved 1 h. Cells were resuspended in Panserin 401/ 50 µM beta-Mercaptoethanol and stimulated with 0.5 U/ml Epo (Jansen-Cilag). Stimulated samples were taken after 0, 1, 2, 3, 4, 5, 6, 7, 8, 14, 19, 24 h, while non-stimulated samples could only collected after 0, 1, 2, 3, 4, 5, 6, 8 h.

Microarray analysis II: Epo promoted BaF3-EpoR cells survival and proliferation

BaF3-EpoR cells were cultured overnight (22h) under pro-starvation condition, namely RPMI supplemented with 0.05U/ml Epo. On the next day, cells were diluted to 50 x 10^4 cells/ml with fresh pro-starvation medium and cultured for 3h. Then, cells were stimulated with 0.5U/ml Epo or remain unstimulated. After 0, 1, 2, 3, 4, 5, 6, 7, 8, 20, 24 h, stimulated and non-stimulated samples were taken.

Microarray analysis III: Epo stimulated PTEN-overexpressing or control BaF3-EpoR cells

PTEN or empty vector as control transduced BaF3-EpoR cells were prepared as described above. After washing with serum free medium, BaF3-EpoR cells were starved for 5 h and resuspend at densities of 20 x 10^4 cells / ml in RPMI medium by supplementing with 0.5 U/ml Epo. Stimulated and non-stimulated samples were taken after 0, 1, 2, 3, 4, 5, 7, 18h.

Per time point total RNA from 2-4 x 10^6 CFU-E or BaF3-EpoR cells was isolated using the RNeasy Mini Plus Kit (Qiagen). RNA was extracted according to the manufacturer's instructions for suspension cells. The quality of total RNA samples was assessed with the Bioanalyzer 2100 (Agilent) to ensure that 28S/18S rRNA ratios were in the range of 1.5 to 2.0 and concentrations were comparable between samples. Mouse Genome 430 2.0 Arrays (Affymetrix) were applied (performed by Maria Saile, Mannheim).

Raw microarray data were processed using the R environment (www.r-project.org) together with the Bioconductor toolbox (www.bioconductor.org). Normalization was performed using the variance stabilization algorithm (vsn) available in Bioconductor (Huber et al., 2002). Quality of the results has been assessed using made4, an R package for multivariate analysis of gene expression data (Culhane et al., 2005). Subsequent probe annotation was handled with the Bioconductor package annaffy. The logarithmic gene fold expression was calculated with respect to the gene expression at 0 hours. The gene expression kinetic from each experiment was ranked according to the absolute value of the combined mean and peak fold expression (performed by Jie Bao, Freiburg).

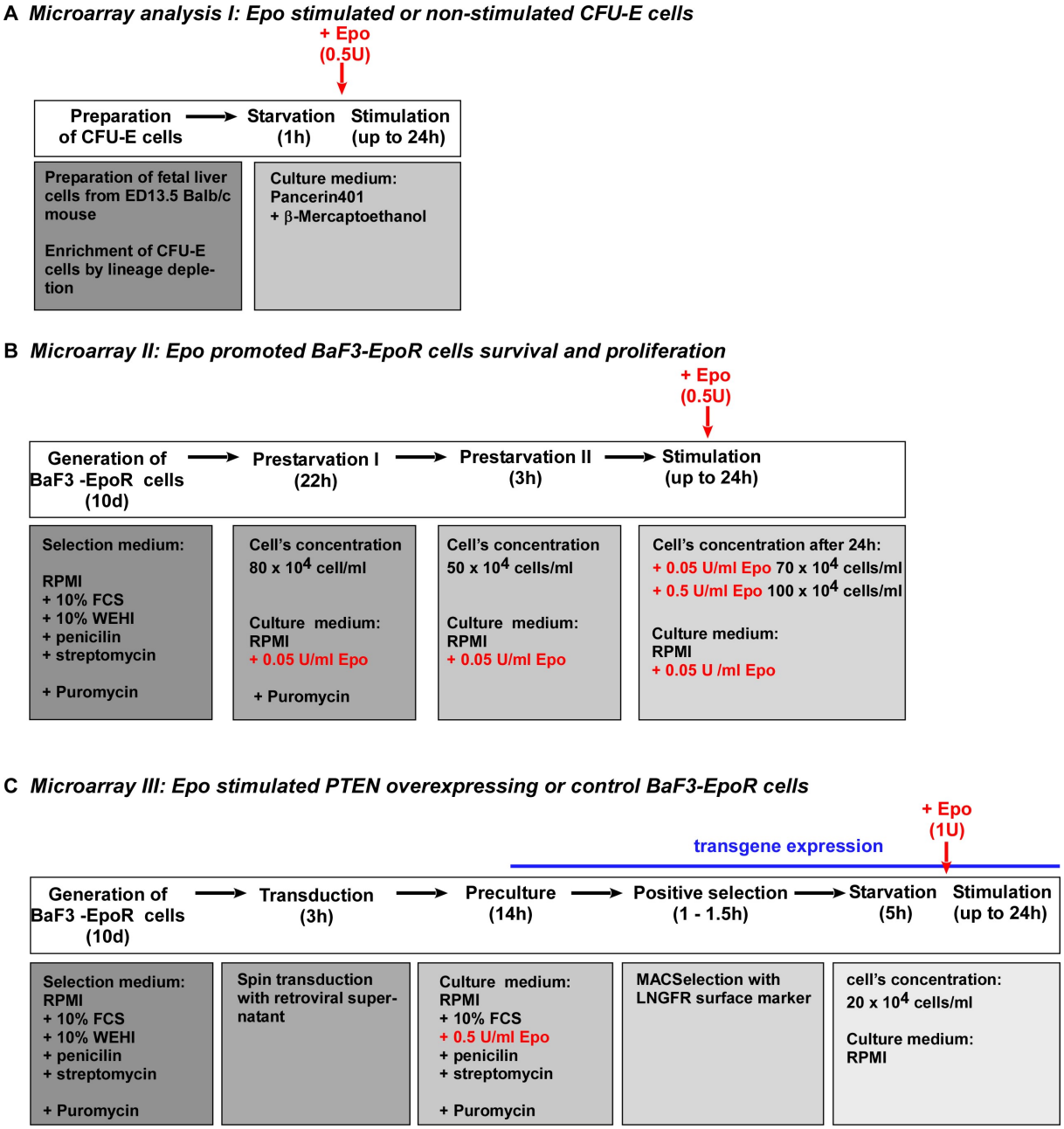

Figure 4.3 The procedures of microarray sample collection.

4.5 Modeling Approaches

4.5.1 Computational data processing

Randomized quantitative immunoblotting data was processed using GelInspector software (Schilling et al., 2005a) to suppress correlated blotting errors. The addition of calibrators allowed for quality control and normalization of the raw data. The following calibrators were applied: GST-EpoR for pEpoR and tEpoR. PDI and β-actin were applied as normalizer for signals from total cell lysate. For first estimates, cubic smoothing splines were determined (MATLAB csaps function with smoothness parameter 0.3) and used for criteria-mediated error reduction.

4.5.2 Scaling factors and error estimation

Immunoblotting measurements typically yield relative concentrations, while the model is formulated in absolute concentrations. To define the absolute receptor phosphorylation level, it was assumed that the receptors on the CFU-E cell surface are maximally 75% phosphorylated (Figure 2.8 C, at 5 min stimulated with 10 U/ml Epo). In addition, a receptor phosphorylation level of 50% or 90% was also tested *in silico*, but this had no significant influence on the model behavior. To define the absolute amount of phosphorylated Akt, a quantitative protein array was applied that combines in-spot normalization and binding model-based calibration. The maximal phosphorylation degree of Akt was determined to be 54% in CFU-E cells stimulated with 2.5 U/ml Epo. Based on such information, experimental data was transferred into absolute concentration in nM.

As the quality of a mathematical model is determined by its deviation from the data relative to the measurement error, the variability of the data had to be estimated. All stimulation experiments were performed at least twice with reproducible results. To estimate the error of the immunoblot results, the standard deviations of experimental data were estimated with an error model, considering contribution of 10 % relative error and a 5 % absolute error. This error estimation confirms the approximately 20 % error of the immunoblotting technique determined in previous studies (Schilling et al., 2005a). To estimate the error of the proliferation data, the standard deviations of experimental data were estimated with 10 % relative error.

4.5.3 Optimization of parameters

Multi-experiment fitting was accomplished by the Matlab toolbox PottersWheel (Maiwald and Timmer, 2008). After rescaling the data from wild-type and overexpression experiments in two cell types, the four datasets were fitted simultaneously. Kinetic parameters starting from random initial values, which were uniformly distributed in a logarithmic space, were optimized by minimizing the sum of the squares of the muti-experiment data from the model simulation. In this process, we constrained the parameters in CFU-E and BaF3-EpoR cells to hold the same values. Local minima in the parameter space were avoided by repeating this process 5000 times. For further analysis of the model we used the best 1% of 5000 optimized parameter sets.

4.5.4 Statistical analysis

The χ^2-values were calculated to determine the agreement between measured proliferation data and the integral of pAkt. The different integration times were examined.The χ^2-values were calculated separately for control cells and PTEN and SHIP1 overexpression in each cell type. The total χ^2-values constituted the sum of χ^2-values. The best time window with the

lowest total χ^2-value was identified at 12 min in CFU-E cells and 16 min in BaF3-EpoR cells. In CFU-E cells, the integral of pAkt failed to describe the reduced basal proliferation of SHIP1-overexpressing cells, resulting in much higher χ^2-values compared to control and PTEN overexpression. Therefore, the SHIP1 overexpression data was excluded for the total χ^2 calcualtion in CFU-E cells.

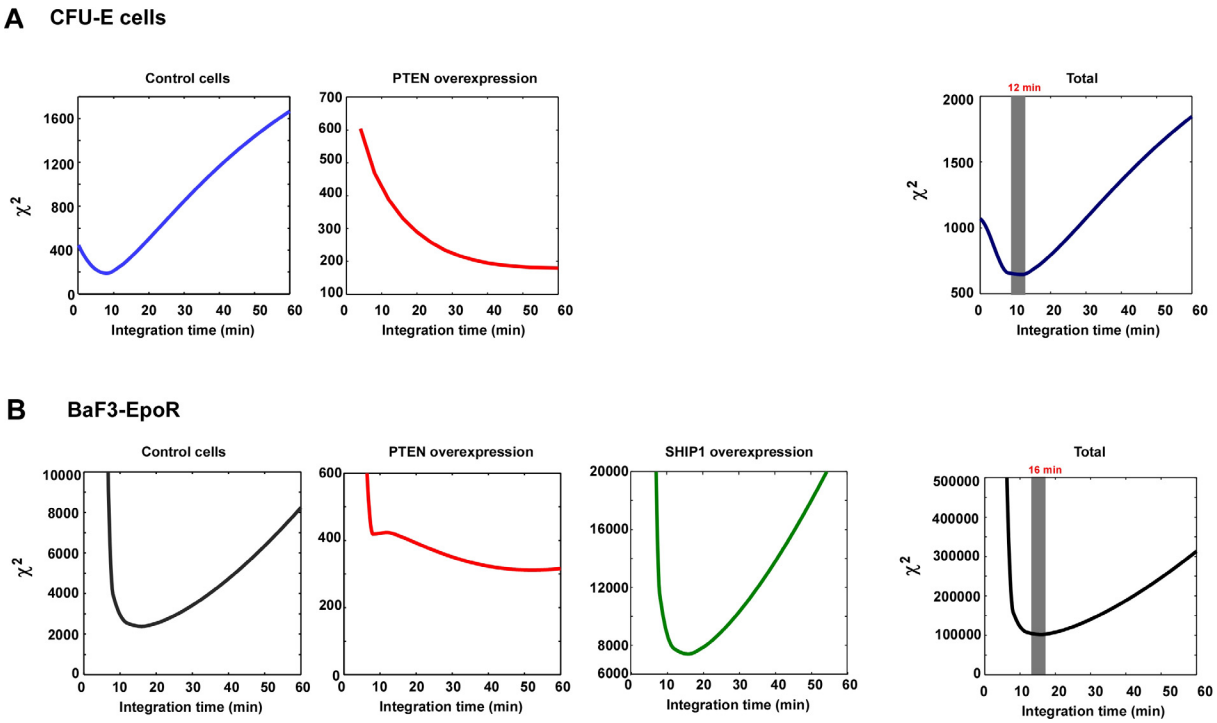

Figure 4.4 Determination of the agreement between measured proliferation data and the integral of pAkt. The different integration times were examined.The χ^2-values were calculated separately for control and PTEN and SHIP1 overexpression data in each cell type. The total χ^2-values constituted the sum of χ^2-values.

5. References

Adam, M., Pogacic, V., Bendit, M., Chappuis, R., Nawijn, M.C., Duyster, J., Fox, C.J., Thompson, C.B., Cools, J., and Schwaller, J. (2006). Targeting PIM kinases impairs survival of hematopoietic cells transformed by kinase inhibitor-sensitive and kinase inhibitor-resistant forms of Fms-like tyrosine kinase 3 and BCR/ABL. Cancer Res *66*, 3828-3835.

Al-Khouri, A.M., Ma, Y., Togo, S.H., Williams, S., and Mustelin, T. (2005). Cooperative phosphorylation of the tumor suppressor phosphatase and tensin homologue (PTEN) by casein kinases and glycogen synthase kinase 3beta. J Biol Chem *280*, 35195-35202.

Alessi, D.R., Deak, M., Casamayor, A., Caudwell, F.B., Morrice, N., Norman, D.G., Gaffney, P., Reese, C.B., MacDougall, C.N., Harbison, D.*, et al.* (1997). 3-Phosphoinositide-dependent protein kinase-1 (PDK1): structural and functional homology with the Drosophila DSTPK61 kinase. Curr Biol *7*, 776-789.

Andrews, S.S., and Arkin, A.P. (2006). Simulating cell biology. Curr Biol *16*, R523-527.

Arcasoy, M.O., and Karayal, A.F. (2005). Erythropoietin hypersensitivity in primary familial and congenital polycythemia: role of tyrosines Y285 and Y344 in erythropoietin receptor cytoplasmic domain. Biochim Biophys Acta *1740*, 17-28.

Asthagiri, A.R., Reinhart, C.A., Horwitz, A.F., and Lauffenburger, D.A. (2000). The role of transient ERK2 signals in fibronectin- and insulin-mediated DNA synthesis. J Cell Sci *113 Pt 24*, 4499-4510.

Backer, J.M. (2005). Substrate specificity: PI(3)Kgamma has it both ways. Nat Cell Biol *7*, 773-774.

Backer, J.M., Myers, M.G., Jr., Shoelson, S.E., Chin, D.J., Sun, X.J., Miralpeix, M., Hu, P., Margolis, B., Skolnik, E.Y., Schlessinger, J.*, et al.* (1992). Phosphatidylinositol 3'-kinase is activated by association with IRS-1 during insulin stimulation. EMBO J *11*, 3469-3479.

Bader, A.G., Kang, S., Zhao, L., and Vogt, P.K. (2005). Oncogenic PI3K deregulates transcription and translation. Nat Rev Cancer *5*, 921-929.

Basu, S., Totty, N.F., Irwin, M.S., Sudol, M., and Downward, J. (2003). Akt phosphorylates the Yes-associated protein, YAP, to induce interaction with 14-3-3 and attenuation of p73-mediated apoptosis. Mol Cell *11*, 11-23.

Batty, I.H., and Downes, C.P. (1996). Thrombin receptors modulate insulin-stimulated phosphatidylinositol 3,4,5-trisphosphate accumulation in 1321N1 astrocytoma cells. Biochemical Journal *317*, 347-351.

Bazan, J.F. (1990). Structural design and molecular evolution of a cytokine receptor superfamily. Proc Natl Acad Sci U S A *87*, 6934-6938.

Becker, V. (2007). Signaling through the Erythropoietin Receptor is Promoted by Dense Packing of the Transmembrane Domain and Regulated by Rapid Receptor Internalization. In Systems biology of signal transduction, german cancer research center (heidelberg, the Ruperto-Carola University of Heidelberg), pp. 100.

Becker, V. (2008). In Combined Faculties for the Natural Sciences and for Mathematics (Heidelberg the Ruperto-Carola University of Heidelberg).

Becker, V., Schilling, M., Bachmann, J., Baumann, U., Raue, A., Maiwald, T., Timmer, J., and Klingmuller, U. (2010). Covering a broad dynamic range: information processing at the erythropoietin receptor. Science *328*, 1404-1408.

Becker, V., Sengupta, D., Ketteler, R., Ullmann, G.M., Smith, J.C., and Klingmuller, U. (2008). Packing density of the erythropoietin receptor transmembrane domain correlates with amplification of biological responses. Biochemistry *47*, 11771-11782.

Bellacosa, A., Kumar, C.C., Di Cristofano, A., and Testa, J.R. (2005). Activation of AKT kinases in cancer: implications for therapeutic targeting. Adv Cancer Res *94*, 29-86.

Bilancio, A., Okkenhaug, K., Camps, M., Emery, J.L., Ruckle, T., Rommel, C., and Vanhaesebroeck, B. (2006). Key role of the p110delta isoform of PI3K in B-cell antigen and IL-4 receptor signaling: comparative analysis of genetic and pharmacologic interference with p110delta function in B cells. Blood *107*, 642-650.

Blanco-Aparicio, C., Renner, O., Leal, J.F., and Carnero, A. (2007). PTEN, more than the AKT pathway. Carcinogenesis *28*, 1379-1386.

Blero, D., Payrastre, B., Schurmans, S., and Erneux, C. (2007). Phosphoinositide phosphatases in a network of signalling reactions. Pflugers Arch *455*, 31-44.

Borisov, N., Aksamitiene, E., Kiyatkin, A., Legewie, S., Berkhout, J., Maiwald, T., Kaimachnikov, N.P., Timmer, J., Hoek, J.B., and Kholodenko, B.N. (2009). Systems-level interactions between insulin-EGF networks amplify mitogenic signaling. Mol Syst Biol *5*, 256.

Bouchard, C., Lee, S., Paulus-Hock, V., Loddenkemper, C., Eilers, M., and Schmitt, C.A. (2007). FoxO transcription factors suppress Myc-driven lymphomagenesis via direct activation of Arf. Genes Dev *21*, 2775-2787.

Bouscary, D., Lecoq-Lafon, C., Chretien, S., Zompi, S., Fichelson, S., Muller, O., Porteu, F., Dusanter-Fourt, I., Gisselbrecht, S., Mayeux, P.*, et al.* (2001). Role of Gab proteins in phosphatidylinositol 3-kinase activation by thrombopoietin (Tpo). Oncogene *20*, 2197-2204.

Bouscary, D., Pene, F., Claessens, Y.E., Muller, O., Chretien, S., Fontenay-Roupie, M., Gisselbrecht, S., Mayeux, P., and Lacombe, C. (2003). Critical role for PI 3-kinase in the control of erythropoietin-induced erythroid progenitor proliferation. Blood *101*, 3436-3443.

Broudy, V.C., Lin, N., Brice, M., Nakamoto, B., and Papayannopoulou, T. (1991). Erythropoietin receptor characteristics on primary human erythroid cells. Blood *77*, 2583-2590.

Brummer, T., Larance, M., Herrera Abreu, M.T., Lyons, R.J., Timpson, P., Emmerich, C.H., Fleuren, E.D., Lehrbach, G.M., Schramek, D., Guilhaus, M.*, et al.* (2008). Phosphorylation-dependent binding of 14-3-3 terminates signalling by the Gab2 docking protein. EMBO J *27*, 2305-2316.

Bunn, H.F., and Poyton, R.O. (1996). Oxygen sensing and molecular adaptation to hypoxia. Physiol Rev *76*, 839-885.

Burgering, B.M., and Kops, G.J. (2002). Cell cycle and death control: long live Forkheads. Trends Biochem Sci *27*, 352-360.

C, V.S., Babar, S.M., Song, E.J., Oh, E., and Yoo, Y.S. (2008). Kinetic analysis of the MAPK and PI3K/Akt signaling pathways. Mol Cells *25*, 397-406.

Cantley, L.C. (2002). The phosphoinositide 3-kinase pathway. Science *296*, 1655-1657.

Castaneda, C.A., Cortes-Funes, H., Gomez, H.L., and Ciruelos, E.M. (2010). The phosphatidyl inositol 3-kinase/AKT signaling pathway in breast cancer. Cancer Metastasis Rev *29*, 751-759.

Chamberlain, M.D., Chan, T., Oberg, J.C., Hawrysh, A.D., James, K.M., Saxena, A., Xiang, J., and Anderson, D.H. (2008). Disrupted RabGAP function of the p85 subunit of phosphatidylinositol 3-kinase results in cell transformation. J Biol Chem *283*, 15861-15868.

Chan, T.O., and Tsichlis, P.N. (2001). PDK2: a complex tail in one Akt. Sci STKE *2001*, pe1.

Chang, F., Lee, J.T., Navolanic, P.M., Steelman, L.S., Shelton, J.G., Blalock, W.L., Franklin, R.A., and McCubrey, J.A. (2003). Involvement of PI3K/Akt pathway in cell cycle progression, apoptosis, and neoplastic transformation: a target for cancer chemotherapy. Leukemia *17*, 590-603.

Chantry, D., Vojtek, A., Kashishian, A., Holtzman, D.A., Wood, C., Gray, P.W., Cooper, J.A., and Hoekstra, M.F. (1997). p110delta, a novel phosphatidylinositol 3-kinase catalytic subunit that associates with p85 and is expressed predominantly in leukocytes. J Biol Chem *272*, 19236-19241.

Chattopadhyay, S., Tracy, E., Liang, P., Robledo, O., Rose-John, S., and Baumann, H. (2007). Interleukin-31 and oncostatin-M mediate distinct signaling reactions and response patterns in lung epithelial cells. J Biol Chem *282*, 3014-3026.

Cheng, J.Q., Godwin, A.K., Bellacosa, A., Taguchi, T., Franke, T.F., Hamilton, T.C., Tsichlis, P.N., and Testa, J.R. (1992). AKT2, a putative oncogene encoding a member of a subfamily of protein-serine/threonine kinases, is amplified in human ovarian carcinomas. Proc Natl Acad Sci U S A *89*, 9267-9271.

Cheng, J.Q., Ruggeri, B., Klein, W.M., Sonoda, G., Altomare, D.A., Watson, D.K., and Testa, J.R. (1996). Amplification of AKT2 in human pancreatic cells and inhibition of AKT2 expression and tumorigenicity by antisense RNA. Proc Natl Acad Sci U S A *93*, 3636-3641.

Chickarmane, V., Enver, T., and Peterson, C. (2009). Computational modeling of the hematopoietic erythroid-myeloid switch reveals insights into cooperativity, priming, and irreversibility. PLoS Comput Biol *5*, e1000268.

Cho, S.H., Lee, C.H., Ahn, Y., Kim, H., Ahn, C.Y., Yang, K.S., and Lee, S.R. (2004). Redox regulation of PTEN and protein tyrosine phosphatases in H(2)O(2) mediated cell signaling. FEBS Lett *560*, 7-13.

Conrad, K.P., Benyo, D.F., Westerhausen-Larsen, A., and Miles, T.M. (1996). Expression of erythropoietin by the human placenta. FASEB J *10*, 760-768.

Constantinescu, S.N., Ghaffari, S., and Lodish, H.F. (1999). The Erythropoietin Receptor: Structure, Activation and Intracellular Signal Transduction. Trends Endocrinol Metab *10*, 18-23.

Creagh, E.M., and Martin, S.J. (2001). Caspases: cellular demolition experts. Biochem Soc Trans *29*, 696-702.

Cronshaw, D.G., Owen, C., Brown, Z., and Ward, S.G. (2004). Activation of phosphoinositide 3-kinases by the CCR4 ligand macrophage-derived chemokine is a dispensable signal for T lymphocyte chemotaxis. J Immunol *172*, 7761-7770.

Csete, M.E., and Doyle, J.C. (2002). Reverse engineering of biological complexity. Science *295*, 1664-1669.

Culhane, A.C., Thioulouse, J., Perriere, G., and Higgins, D.G. (2005). MADE4: an R package for multivariate analysis of gene expression data. Bioinformatics *21*, 2789-2790.

Cully, M., You, H., Levine, A.J., and Mak, T.W. (2006). Beyond PTEN mutations: the PI3K pathway as an integrator of multiple inputs during tumorigenesis. Nat Rev Cancer *6*, 184-192.

Curnock, A.P., Sotsios, Y., and Ward, S.G. (2004). Assessing the role of multiple phosphoinositide 3-kinases in chemokine signaling: use of dominant negative mutants controlled by a tetracycline-regulated gene expression system. Methods Mol Biol *239*, 211-222.

D'Andrea, A.D., Fasman, G.D., and Lodish, H.F. (1990). A new hematopoietic growth factor receptor superfamily: structural features and implications for signal transduction. Curr Opin Cell Biol *2*, 648-651.

D'Andrea, A.D., Lodish, H.F., and Wong, G.G. (1989). Expression cloning of the murine erythropoietin receptor. Cell *57*, 277-285.

D'Andrea, A.D., and Zon, L.I. (1990). Erythropoietin receptor. Subunit structure and activation. J Clin Invest *86*, 681-687.

Damen, J.E., Cutler, R.L., Jiao, H., Yi, T., and Krystal, G. (1995). Phosphorylation of tyrosine 503 in the erythropoietin receptor (EpR) is essential for binding the P85 subunit of phosphatidylinositol (PI) 3-kinase and for EpR-associated PI 3-kinase activity. J Biol Chem *270*, 23402-23408.

Das, S., Dixon, J.E., and Cho, W. (2003). Membrane-binding and activation mechanism of PTEN. Proc Natl Acad Sci U S A *100*, 7491-7496.

Datta, S.R., Brunet, A., and Greenberg, M.E. (1999). Cellular survival: a play in three Akts. Genes Dev *13*, 2905-2927.

Davies, S.P., Reddy, H., Caivano, M., and Cohen, P. (2000). Specificity and mechanism of action of some commonly used protein kinase inhibitors. Biochem J *351*, 95-105.

de la Chapelle, A., Traskelin, A.L., and Juvonen, E. (1993). Truncated erythropoietin receptor causes dominantly inherited benign human erythrocytosis. Proc Natl Acad Sci U S A *90*, 4495-4499.

Dehan, E., and Pagano, M. (2005). Skp2, the FoxO1 hunter. Cancer Cell *7*, 209-210.

Di Cristofano, A., and Pandolfi, P.P. (2000). The multiple roles of PTEN in tumor suppression. Cell *100*, 387-390.

Diehl, J.A., Cheng, M., Roussel, M.F., and Sherr, C.J. (1998). Glycogen synthase kinase-3beta regulates cyclin D1 proteolysis and subcellular localization. Genes Dev *12*, 3499-3511.

Doane, B.D., Fried, W., and Schwartz, F. (1975). Response of uremic patients to nandrolone decanoate. Arch Intern Med *135*, 972-975.

Downes, C.P., Ross, S., Maccario, H., Perera, N., Davidson, L., and Leslie, N.R. (2007). Stimulation of PI 3-kinase signaling via inhibition of the tumor suppressor phosphatase, PTEN. Adv Enzyme Regul *47*, 184-194.

Edmead, C.E., Fox, B.C., Stace, C., Ktistakis, N., and Welham, M.J. (2006). The pleckstrin homology domain of Gab-2 is required for optimal interleukin-3 signalsome-mediated responses. Cell Signal *18*, 1147-1155.

Eissing, T., Conzelmann, H., Gilles, E.D., Allgower, F., Bullinger, E., and Scheurich, P. (2004). Bistability analyses of a caspase activation model for receptor-induced apoptosis. J Biol Chem *279*, 36892-36897.

Erslev, A.J., Caro, J., Kansu, E., and Silver, R. (1980). Renal and extrarenal erythropoietin production in anaemic rats. Br J Haematol *45*, 65-72.

Eulenfeld, R., and Schaper, F. (2009). A new mechanism for the regulation of Gab1 recruitment to the plasma membrane. J Cell Sci *122*, 55-64.

Fang, J., Menon, M., Kapelle, W., Bogacheva, O., Bogachev, O., Houde, E., Browne, S., Sathyanarayana, P., and Wojchowski, D.M. (2007). EPO modulation of cell-cycle regulatory genes, and cell division, in primary bone marrow erythroblasts. Blood *110*, 2361-2370.

Feng, J., Witthuhn, B.A., Matsuda, T., Kohlhuber, F., Kerr, I.M., and Ihle, J.N. (1997). Activation of Jak2 catalytic activity requires phosphorylation of Y1007 in the kinase activation loop. Mol Cell Biol *17*, 2497-2501.

Ferrell, J.E., Jr., and Machleder, E.M. (1998). The biochemical basis of an all-or-none cell fate switch in Xenopus oocytes. Science *280*, 895-898.

Fingar, D.C., Richardson, C.J., Tee, A.R., Cheatham, L., Tsou, C., and Blenis, J. (2004). mTOR controls cell cycle progression through its cell growth effectors S6K1 and 4E-BP1/eukaryotic translation initiation factor 4E. Mol Cell Biol *24*, 200-216.

Friboulet, A., and Thomas, D. (2005). Systems Biology-an interdisciplinary approach. Biosens Bioelectron *20*, 2404-2407.

Geering, B., Cutillas, P.R., Nock, G., Gharbi, S.I., and Vanhaesebroeck, B. (2007). Class IA phosphoinositide 3-kinases are obligate p85-p110 heterodimers. Proc Natl Acad Sci U S A *104*, 7809-7814.

Ghaffari, S., Kitidis, C., Zhao, W., Marinkovic, D., Fleming, M.D., Luo, B., Marszalek, J., and Lodish, H.F. (2006). AKT induces erythroid-cell maturation of JAK2-deficient fetal liver progenitor cells and is required for Epo regulation of erythroid-cell differentiation. Blood *107*, 1888-1891.

Gingras, A.C., and Sonenberg, N. (1997). Adenovirus infection inactivates the translational inhibitors 4E-BP1 and 4E-BP2. Virology *237*, 182-186.

Glauser, D.A., and Schlegel, W. (2009). The FoxO/Bcl-6/cyclin D2 pathway mediates metabolic and growth factor stimulation of proliferation in Min6 pancreatic beta-cells. J Recept Signal Transduct Res.

Gobert, S., Porteu, F., Pallu, S., Muller, O., Sabbah, M., Dusanter-Fourt, I., Courtois, G., Lacombe, C., Gisselbrecht, S., and Mayeux, P. (1995). Tyrosine phosphorylation of the erythropoietin receptor: role for differentiation and mitogenic signal transduction. Blood *86*, 598-606.

Goldwasser, E., Jacobson, L.O., Fried, W., and Plzak, L. (1957). Mechanism of the erythropoietic effect of cobalt. Science *125*, 1085-1086.

Gu, H., Maeda, H., Moon, J.J., Lord, J.D., Yoakim, M., Nelson, B.H., and Neel, B.G. (2000). New role for Shc in activation of the phosphatidylinositol 3-kinase/Akt pathway. Mol Cell Biol *20*, 7109-7120.

Gu, H., and Neel, B.G. (2003). The "Gab" in signal transduction. Trends Cell Biol *13*, 122-130.

Gu, H., Pratt, J.C., Burakoff, S.J., and Neel, B.G. (1998). Cloning of p97/Gab2, the major SHP2-binding protein in hematopoietic cells, reveals a novel pathway for cytokine-induced gene activation. Mol Cell *2*, 729-740.

Gual, P., Giordano, S., Williams, T.A., Rocchi, S., Van Obberghen, E., and Comoglio, P.M. (2000). Sustained recruitment of phospholipase C-gamma to Gab1 is required for HGF-induced branching tubulogenesis. Oncogene *19*, 1509-1518.

Hahn-Windgassen, A., Nogueira, V., Chen, C.C., Skeen, J.E., Sonenberg, N., and Hay, N. (2005). Akt activates the mammalian target of rapamycin by regulating cellular ATP level and AMPK activity. J Biol Chem *280*, 32081-32089.

Hammerman, P.S., Fox, C.J., Birnbaum, M.J., and Thompson, C.B. (2005). Pim and Akt oncogenes are independent regulators of hematopoietic cell growth and survival. Blood *105*, 4477-4483.

Harris, S.J., Parry, R.V., Westwick, J., and Ward, S.G. (2008). Phosphoinositide lipid phosphatases: natural regulators of phosphoinositide 3-kinase signaling in T lymphocytes. J Biol Chem *283*, 2465-2469.

Heckman, K.L., and Pease, L.R. (2007). Gene splicing and mutagenesis by PCR-driven overlap extension. Nat Protoc *2*, 924-932.

Helgason, C.D., Damen, J.E., Rosten, P., Grewal, R., Sorensen, P., Chappel, S.M., Borowski, A., Jirik, F., Krystal, G., and Humphries, R.K. (1998). Targeted disruption of SHIP leads to hemopoietic perturbations, lung pathology, and a shortened life span. Genes Dev *12*, 1610-1620.

Helgason, C.D., Kalberer, C.P., Damen, J.E., Chappel, S.M., Pineault, N., Krystal, G., and Humphries, R.K. (2000). A dual role for Src homology 2 domain-containing inositol-5-phosphatase (SHIP) in immunity: aberrant development and enhanced function of b lymphocytes in ship -/- mice. J Exp Med *191*, 781-794.

Hengl, S., Kreutz, C., Timmer, J., and Maiwald, T. (2007). Data-based identifiability analysis of non-linear dynamical models. Bioinformatics *23*, 2612-2618.

Hlobilkova, A., Knillova, J., Bartek, J., Lukas, J., and Kolar, Z. (2003). The mechanism of action of the tumour suppressor gene PTEN. Biomed Pap Med Fac Univ Palacky Olomouc Czech Repub *147*, 19-25.

Holgado-Madruga, M., Emlet, D.R., Moscatello, D.K., Godwin, A.K., and Wong, A.J. (1996). A Grb2-associated docking protein in EGF- and insulin-receptor signalling. Nature *379*, 560-564.

Huang, L.E., Ho, V., Arany, Z., Krainc, D., Galson, D., Tendler, D., Livingston, D.M., and Bunn, H.F. (1997). Erythropoietin gene regulation depends on heme-dependent oxygen sensing and assembly of interacting transcription factors. Kidney Int *51*, 548-552.

Huang, L.J., Constantinescu, S.N., and Lodish, H.F. (2001). The N-terminal domain of Janus kinase 2 is required for Golgi processing and cell surface expression of erythropoietin receptor. Mol Cell *8*, 1327-1338.

Huang, W., Chang, H.Y., Fei, T., Wu, H., and Chen, Y.G. (2007). GSK3 beta mediates suppression of cyclin D2 expression by tumor suppressor PTEN. Oncogene *26*, 2471-2482.

Huber, W., von Heydebreck, A., Sultmann, H., Poustka, A., and Vingron, M. (2002). Variance stabilization applied to microarray data calibration and to the quantification of differential expression. Bioinformatics *18 Suppl 1*, S96-104.

Isakoff, S.J., Cardozo, T., Andreev, J., Li, Z., Ferguson, K.M., Abagyan, R., Lemmon, M.A., Aronheim, A., and Skolnik, E.Y. (1998). Identification and analysis of PH domain-containing targets of phosphatidylinositol 3-kinase using a novel in vivo assay in yeast. EMBO J *17*, 5374-5387.

Itoh, M., Yoshida, Y., Nishida, K., Narimatsu, M., Hibi, M., and Hirano, T. (2000). Role of Gab1 in heart, placenta, and skin development and growth factor- and cytokine-induced extracellular signal-regulated kinase mitogen-activated protein kinase activation. Mol Cell Biol *20*, 3695-3704.

Jacobson, L.O., Goldwasser, E., Fried, W., and Plzak, L. (1957). Role of the kidney in erythropoiesis. Nature *179*, 633-634.

Jelkmann, W. (2004). Molecular biology of erythropoietin. Intern Med *43*, 649-659.

Jia, S.D., Liu, Z.N., Zhang, S., Liu, P.X., Zhang, L., Lee, S.H., Zhang, J., Signoretti, S., Loda, M., Roberts, T.M.*, et al.* (2008). Essential roles of PI(3)K-p110 beta in cell growth, metabolism and tumorigenesis. Nature *454*, 776-U102.

Kalesnikoff, J., Sly, L.M., Hughes, M.R., Buchse, T., Rauh, M.J., Cao, L.P., Lam, V., Mui, A., Huber, M., and Krystal, G. (2003). The role of SHIP in cytokine-induced signaling. Rev Physiol Biochem Pharmacol *149*, 87-103.

Karathanassis, D., Stahelin, R.V., Bravo, J., Perisic, O., Pacold, C.M., Cho, W., and Williams, R.L. (2002). Binding of the PX domain of p47(phox) to phosphatidylinositol 3,4-bisphosphate and phosphatidic acid is masked by an intramolecular interaction. EMBO J *21*, 5057-5068.

Katso, R., Okkenhaug, K., Ahmadi, K., White, S., Timms, J., and Waterfield, M.D. (2001). Cellular function of phosphoinositide 3-kinases: implications for development, homeostasis, and cancer. Annu Rev Cell Dev Biol *17*, 615-675.

Keefe, A.D., Wilson, D.S., Seelig, B., and Szostak, J.W. (2001). One-step purification of recombinant proteins using a nanomolar-affinity streptavidin-binding peptide, the SBP-Tag. Protein Expr Purif *23*, 440-446.

Ketteler, R., Glaser, S., Sandra, O., Martens, U.M., and Klingmuller, U. (2002). Enhanced transgene expression in primitive hematopoietic progenitor cells and embryonic stem cells efficiently transduced by optimized retroviral hybrid vectors. Gene Ther *9*, 477-487.

Ketteler, R., Moghraby, C.S., Hsiao, J.G., Sandra, O., Lodish, H.F., and Klingmuller, U. (2003). The cytokine-inducible Scr homology domain-containing protein negatively regulates signaling by promoting apoptosis in erythroid progenitor cells. J Biol Chem *278*, 2654-2660.

Kihara, A., Noda, T., Ishihara, N., and Ohsumi, Y. (2001). Two distinct Vps34 phosphatidylinositol 3-kinase complexes function in autophagy and carboxypeptidase Y sorting in Saccharomyces cerevisiae. J Cell Biol *152*, 519-530.

Kim, A.H., Khursigara, G., Sun, X., Franke, T.F., and Chao, M.V. (2001). Akt phosphorylates and negatively regulates apoptosis signal-regulating kinase 1. Mol Cell Biol *21*, 893-901.

Kim, D.H., and Sabatini, D.M. (2004). Raptor and mTOR: subunits of a nutrient-sensitive complex. Curr Top Microbiol Immunol *279*, 259-270.

Kitano, H. (2002). Systems biology: a brief overview. Science *295*, 1662-1664.

Klingmuller, U., Bergelson, S., Hsiao, J.G., and Lodish, H.F. (1996). Multiple tyrosine residues in the cytosolic domain of the erythropoietin receptor promote activation of STAT5. Proc Natl Acad Sci U S A *93*, 8324-8328.

Klingmuller, U., Lorenz, U., Cantley, L.C., Neel, B.G., and Lodish, H.F. (1995). Specific recruitment of SH-PTP1 to the erythropoietin receptor causes inactivation of JAK2 and termination of proliferative signals. Cell *80*, 729-738.

Klingmuller, U., Wu, H., Hsiao, J.G., Toker, A., Duckworth, B.C., Cantley, L.C., and Lodish, H.F. (1997). Identification of a novel pathway important for proliferation and differentiation of primary erythroid progenitors. Proc Natl Acad Sci U S A *94*, 3016-3021.

Klipp, E., and Liebermeister, W. (2006). Mathematical modeling of intracellular signaling pathways. BMC Neurosci *7 Suppl 1*, S10.

Knighton, D.R., Zheng, J.H., Ten Eyck, L.F., Ashford, V.A., Xuong, N.H., Taylor, S.S., and Sowadski, J.M. (1991). Crystal structure of the catalytic subunit of cyclic adenosine monophosphate-dependent protein kinase. Science *253*, 407-414.

Kok, K., Geering, B., and Vanhaesebroeck, B. (2009). Regulation of phosphoinositide 3-kinase expression in health and disease. Trends Biochem Sci *34*, 115-127.

Kolch, W., Calder, M., and Gilbert, D. (2005). When kinases meet mathematics: the systems biology of MAPK signalling. FEBS Lett *579*, 1891-1895.

Krantz, S.B. (1991). Erythropoietin. Blood *77*, 419-434.

Krantz, S.B., and Goldwasser, E. (1984). Specific binding of erythropoietin to spleen cells infected with the anemia strain of Friend virus. Proc Natl Acad Sci U S A *81*, 7574-7578.

Kulp, S.K., Yang, Y.T., Hung, C.C., Chen, K.F., Lai, J.P., Tseng, P.H., Fowble, J.W., Ward, P.J., and Chen, C.S. (2004). 3-phosphoinositide-dependent protein kinase-1/Akt signaling represents a major cyclooxygenase-2-independent target for celecoxib in prostate cancer cells. Cancer Res *64*, 1444-1451.

Kumar, C.C., and Madison, V. (2005). AKT crystal structure and AKT-specific inhibitors. Oncogene *24*, 7493-7501.

Kummer, U., Olsen, L.F., Dixon, C.J., Green, A.K., Bornberg-Bauer, E., and Baier, G. (2000). Switching from simple to complex oscillations in calcium signaling. Biophys J *79*, 1188-1195.

Laemmli, U.K. (1970). Cleavage of structural proteins during the assembly of the head of bacteriophage T4. Nature *227*, 680-685.

Laubenbacher, R., Hower, V., Jarrah, A., Torti, S.V., Shulaev, V., Mendes, P., Torti, F.M., and Akman, S. (2009). A systems biology view of cancer. Biochim Biophys Acta *1796*, 129-139.

Lee, K.S., Lee, H.K., Hayflick, J.S., Lee, Y.C., and Puri, K.D. (2006). Inhibition of phosphoinositide 3-kinase delta attenuates allergic airway inflammation and hyperresponsiveness in murine asthma model. FASEB J *20*, 455-465.

Leevers, S.J., Vanhaesebroeck, B., and Waterfield, M.D. (1999). Signalling through phosphoinositide 3-kinases: the lipids take centre stage. Curr Opin Cell Biol *11*, 219-225.

Lehr, S., Kotzka, J., Herkner, A., Klein, E., Siethoff, C., Knebel, B., Noelle, V., Bruning, J.C., Klein, H.W., Meyer, H.E.*, et al.* (1999). Identification of tyrosine phosphorylation sites in human Gab-1 protein by EGF receptor kinase in vitro. Biochemistry *38*, 151-159.

Lemmon, M.A., and Ferguson, K.M. (2000). Signal-dependent membrane targeting by pleckstrin homology (PH) domains. Biochem J *350 Pt 1*, 1-18.

Lemmon, M.A., and Ferguson, K.M. (2001). Molecular determinants in pleckstrin homology domains that allow specific recognition of phosphoinositides. Biochem Soc Trans *29*, 377-384.

Leslie, N.R., Bennett, D., Lindsay, Y.E., Stewart, H., Gray, A., and Downes, C.P. (2003). Redox regulation of PI 3-kinase signalling via inactivation of PTEN. EMBO J *22*, 5501-5510.

Li, P.F., Li, J., Muller, E.C., Otto, A., Dietz, R., and von Harsdorf, R. (2002). Phosphorylation by protein kinase CK2: a signaling switch for the caspase-inhibiting protein ARC. Mol Cell *10*, 247-258.

Liu, Q.R., Sasaki, T., Kozieradzki, I., Wakeham, A., Itie, A., Dumont, D.J., and Penninger, J.M. (1999). SHIP is a negative regulator of growth factor receptor-mediated PKB/Akt activation and myeloid cell survival. Genes & Development *13*, 786-791.

Liu, R., Wang, L., Chen, C., Liu, Y., Zhou, P., Wang, Y., Wang, X., Turnbull, J., Minassian, B.A., and Zheng, P. (2008). Laforin negatively regulates cell cycle progression through glycogen synthase kinase 3beta-dependent mechanisms. Mol Cell Biol *28*, 7236-7244.

Livnah, O., Stura, E.A., Johnson, D.L., Middleton, S.A., Mulcahy, L.S., Wrighton, N.C., Dower, W.J., Jolliffe, L.K., and Wilson, I.A. (1996). Functional mimicry of a protein hormone by a peptide agonist: the EPO receptor complex at 2.8 A. Science *273*, 464-471.

Luo, J., and Cantley, L.C. (2005). The negative regulation of phosphoinositide 3-kinase signaling by p85 and it's implication in cancer. Cell Cycle *4*, 1309-1312.

Maiwald, T., Kreutz, C., Pfeifer, A.C., Bohl, S., Klingmuller, U., and Timmer, J. (2007). Dynamic pathway modeling: feasibility analysis and optimal experimental design. Ann N Y Acad Sci *1115*, 212-220.

Maiwald, T., and Timmer, J. (2008). Dynamical modeling and multi-experiment fitting with PottersWheel. Bioinformatics *24*, 2037-2043.

Marine, J.C., McKay, C., Wang, D., Topham, D.J., Parganas, E., Nakajima, H., Pendeville, H., Yasukawa, H., Sasaki, A., Yoshimura, A.*, et al.* (1999). SOCS3 is essential in the regulation of fetal liver erythropoiesis. Cell *98*, 617-627.

Martinez-Gac, L., Marques, M., Garcia, Z., Campanero, M.R., and Carrera, A.C. (2004). Control of cyclin G2 mRNA expression by forkhead transcription factors: novel mechanism for cell cycle control by phosphoinositide 3-kinase and forkhead. Mol Cell Biol *24*, 2181-2189.

Mason, J.M., Beattie, B.K., Liu, Q., Dumont, D.J., and Barber, D.L. (2000). The SH2 inositol 5-phosphatase Ship1 is recruited in an SH2-dependent manner to the erythropoietin receptor. J Biol Chem *275*, 4398-4406.

Masuda, S., Okano, M., Yamagishi, K., Nagao, M., Ueda, M., and Sasaki, R. (1994). A novel site of erythropoietin production. Oxygen-dependent production in cultured rat astrocytes. J Biol Chem *269*, 19488-19493.

Medema, R.H., Kops, G.J., Bos, J.L., and Burgering, B.M. (2000). AFX-like Forkhead transcription factors mediate cell-cycle regulation by Ras and PKB through p27kip1. Nature *404*, 782-787.

Mehenni, H., Lin-Marq, N., Buchet-Poyau, K., Reymond, A., Collart, M.A., Picard, D., and Antonarakis, S.E. (2005). LKB1 interacts with and phosphorylates PTEN: a functional link between two proteins involved in cancer predisposing syndromes. Hum Mol Genet *14*, 2209-2219.

Meyer, T., and Vinkemeier, U. (2004). Nucleocytoplasmic shuttling of STAT transcription factors. Eur J Biochem *271*, 4606-4612.

Mirand, E.A., Weintraub, A.H., Gordon, A.S., Prentice, T.C., and Grace, J.T., Jr. (1965). Erythropoietic Activity of Untreated and Deproteinized Normal Human Plasma. Proc Soc Exp Biol Med *118*, 823-826.

Miura, O., Cleveland, J.L., and Ihle, J.N. (1993). Inactivation of erythropoietin receptor function by point mutations in a region having homology with other cytokine receptors. Mol Cell Biol *13*, 1788-1795.

Miura, O., Nakamura, N., Ihle, J.N., and Aoki, N. (1994). Erythropoietin-dependent association of phosphatidylinositol 3-kinase with tyrosine-phosphorylated erythropoietin receptor. J Biol Chem *269*, 614-620.

Miwa, W., Yasuda, J., Murakami, Y., Yashima, K., Sugano, K., Sekine, T., Kono, A., Egawa, S., Yamaguchi, K., Hayashizaki, Y.*, et al.* (1996). Isolation of DNA sequences amplified at chromosome 19q13.1-q13.2 including the AKT2 locus in human pancreatic cancer. Biochem Biophys Res Commun *225*, 968-974.

Miyakawa, Y., Rojnuckarin, P., Habib, T., and Kaushansky, K. (2001). Thrombopoietin induces phosphoinositol 3-kinase activation through SHP2, Gab, and insulin receptor substrate proteins in BAF3 cells and primary murine megakaryocytes. J Biol Chem *276*, 2494-2502.

Moritz, K.M., Lim, G.B., and Wintour, E.M. (1997). Developmental regulation of erythropoietin and erythropoiesis. Am J Physiol *273*, R1829-1844.

Muise-Helmericks, R.C., Grimes, H.L., Bellacosa, A., Malstrom, S.E., Tsichlis, P.N., and Rosen, N. (1998). Cyclin D expression is controlled post-transcriptionally via a phosphatidylinositol 3-kinase/Akt-dependent pathway. J Biol Chem *273*, 29864-29872.

Musacchio, A., Gibson, T., Rice, P., Thompson, J., and Saraste, M. (1993). The PH domain: a common piece in the structural patchwork of signalling proteins. Trends Biochem Sci *18*, 343-348.

Naka, T., Narazaki, M., Hirata, M., Matsumoto, T., Minamoto, S., Aono, A., Nishimoto, N., Kajita, T., Taga, T., Yoshizaki, K.*, et al.* (1997). Structure and function of a new STAT-induced STAT inhibitor. Nature *387*, 924-929.

Nakatani, K., Thompson, D.A., Barthel, A., Sakaue, H., Liu, W., Weigel, R.J., and Roth, R.A. (1999). Up-regulation of Akt3 in estrogen receptor-deficient breast cancers and androgen-independent prostate cancer lines. J Biol Chem *274*, 21528-21532.

Neubauer, H., Cumano, A., Muller, M., Wu, H., Huffstadt, U., and Pfeffer, K. (1998). Jak2 deficiency defines an essential developmental checkpoint in definitive hematopoiesis. Cell *93*, 397-409.

Nishida, K., and Hirano, T. (2003). The role of Gab family scaffolding adapter proteins in the signal transduction of cytokine and growth factor receptors. Cancer Sci *94*, 1029-1033.

Nishida, K., Wang, L., Morii, E., Park, S.J., Narimatsu, M., Itoh, S., Yamasaki, S., Fujishima, M., Ishihara, K., Hibi, M.*, et al.* (2002). Requirement of Gab2 for mast cell development and KitL/c-Kit signaling. Blood *99*, 1866-1869.

Nishida, K., Yoshida, Y., Itoh, M., Fukada, T., Ohtani, T., Shirogane, T., Atsumi, T., Takahashi-Tezuka, M., Ishihara, K., Hibi, M.*, et al.* (1999). Gab-family adapter proteins act downstream of cytokine and growth factor receptors and T- and B-cell antigen receptors. Blood *93*, 1809-1816.

Noble, D. (2006). the music of life: biology beyond the genome (Oxford University press).

Ouyang, W., Li, J., Ma, Q., and Huang, C. (2006). Essential roles of PI-3K/Akt/IKKbeta/NFkappaB pathway in cyclin D1 induction by arsenite in JB6 Cl41 cells. Carcinogenesis *27*, 864-873.

Panayotou, G., Bax, B., Gout, I., Federwisch, M., Wroblowski, B., Dhand, R., Fry, M.J., Blundell, T.L., Wollmer, A., and Waterfield, M.D. (1992). Interaction of the p85 subunit of PI 3-kinase and its N-terminal SH2 domain with a PDGF receptor phosphorylation site: structural features and analysis of conformational changes. EMBO J *11*, 4261-4272.

Papakonstanti, E.A., Zwaenepoel, O., Bilancio, A., Burns, E., Nock, G.E., Houseman, B., Shokat, K., Ridley, A.J., and Vanhaesebroeck, B. (2008). Distinct roles of class IA PI3K isoforms in primary and immortalised macrophages. J Cell Sci *121*, 4124-4133.

Parganas, E., Wang, D., Stravopodis, D., Topham, D.J., Marine, J.C., Teglund, S., Vanin, E.F., Bodner, S., Colamonici, O.R., van Deursen, J.M.*, et al.* (1998). Jak2 is essential for signaling through a variety of cytokine receptors. Cell *93*, 385-395.

Parsons, D.W., Wang, T.L., Samuels, Y., Bardelli, A., Cummins, J.M., DeLong, L., Silliman, N., Ptak, J., Szabo, S., Willson, J.K.*, et al.* (2005). Colorectal cancer: mutations in a signalling pathway. Nature *436*, 792.

Pelletier, S., Gingras, S., Funakoshi-Tago, M., Howell, S., and Ihle, J.N. (2006). Two domains of the erythropoietin receptor are sufficient for Jak2 binding/activation and function. Mol Cell Biol *26*, 8527-8538.

Pesesse, X., Backers, K., Moreau, C., Zhang, J., Blero, D., Paternotte, N., and Erneux, C. (2006). SHIP1/2 interaction with tyrosine phosphorylated peptides mimicking an immunoreceptor signalling motif. Adv Enzyme Regul *46*, 142-153.

Philp, A.J., Campbell, I.G., Leet, C., Vincan, E., Rockman, S.P., Whitehead, R.H., Thomas, R.J., and Phillips, W.A. (2001). The phosphatidylinositol 3'-kinase p85alpha gene is an oncogene in human ovarian and colon tumors. Cancer Res *61*, 7426-7429.

Qiu, D., Mao, L., Kikuchi, S., and Tomita, M. (2004). Sustained MAPK activation is dependent on continual NGF receptor regeneration. Dev Growth Differ *46*, 393-403.

Radu, A., Neubauer, V., Akagi, T., Hanafusa, H., and Georgescu, M.M. (2003). PTEN induces cell cycle arrest by decreasing the level and nuclear localization of cyclin D1. Mol Cell Biol *23*, 6139-6149.

Rajkumar, S.V., Richardson, P.G., Hideshima, T., and Anderson, K.C. (2005). Proteasome inhibition as a novel therapeutic target in human cancer. J Clin Oncol *23*, 630-639.

Ralph, P., and Nakoinz, I. (1977). Antibody-dependent killing of erythrocyte and tumor targets by macrophage-related cell lines: enhancement by PPD and LPS. J Immunol *119*, 950-954.

Raman, M., Chen, W., and Cobb, M.H. (2007). Differential regulation and properties of MAPKs. Oncogene *26*, 3100-3112.

Richmond, T.D., Chohan, M., and Barber, D.L. (2005). Turning cells red: signal transduction mediated by erythropoietin. Trends Cell Biol *15*, 146-155.

Rives, S., Pahl, H.L., Florensa, L., Bellosillo, B., Neususess, A., Estella, J., Debatin, K.M., Kohne, E., Schwarz, K., and Cario, H. (2007). Molecular genetic analyses in familial and sporadic congenital primary erythrocytosis. Haematologica *92*, 674-677.

Rodrigues, G.A., Falasca, M., Zhang, Z., Ong, S.H., and Schlessinger, J. (2000). A novel positive feedback loop mediated by the docking protein Gab1 and phosphatidylinositol 3-kinase in epidermal growth factor receptor signaling. Mol Cell Biol *20*, 1448-1459.

Rohrschneider, L.R., Fuller, J.F., Wolf, I., Liu, Y., and Lucas, D.M. (2000). Structure, function, and biology of SHIP proteins. Genes Dev *14*, 505-520.

Rottapel, R., Turck, C.W., Casteran, N., Liu, X., Birnbaum, D., Pawson, T., and Dubreuil, P. (1994). Substrate specificities and identification of a putative binding site for PI3K in the carboxy tail of the murine Flt3 receptor tyrosine kinase. Oncogene *9*, 1755-1765.

Ruggero, D., Montanaro, L., Ma, L., Xu, W., Londei, P., Cordon-Cardo, C., and Pandolfi, P.P. (2004). The translation factor eIF-4E promotes tumor formation and cooperates with c-Myc in lymphomagenesis. Nat Med *10*, 484-486.

Samuels, Y., Wang, Z., Bardelli, A., Silliman, N., Ptak, J., Szabo, S., Yan, H., Gazdar, A., Powell, S.M., Riggins, G.J.*, et al.* (2004). High frequency of mutations of the PIK3CA gene in human cancers. Science *304*, 554.

Sansal, I., and Sellers, W.R. (2004). The biology and clinical relevance of the PTEN tumor suppressor pathway. J Clin Oncol *22*, 2954-2963.

Sasagawa, S., Ozaki, Y., Fujita, K., and Kuroda, S. (2005). Prediction and validation of the distinct dynamics of transient and sustained ERK activation. Nat Cell Biol *7*, 365-373.

Sasaoka, T., Wada, T., Fukui, K., Murakami, S., Ishihara, H., Suzuki, R., Tobe, K., Kadowaki, T., and Kobayashi, M. (2004). SH2-containing inositol phosphatase 2 predominantly regulates Akt2, and not Akt1, phosphorylation at the plasma membrane in response to insulin in 3T3-L1 adipocytes. J Biol Chem *279*, 14835-14843.

Sattler, M., Verma, S., Byrne, C.H., Shrikhande, G., Winkler, T., Algate, P.A., Rohrschneider, L.R., and Griffin, J.D. (1999). BCR/ABL directly inhibits expression of SHIP, an SH2-containing polyinositol-5-phosphatase involved in the regulation of hematopoiesis. Mol Cell Biol *19*, 7473-7480.

Sawyer, S.T., and Hankins, W.D. (1993). The functional form of the erythropoietin receptor is a 78-kDa protein: correlation with cell surface expression, endocytosis, and phosphorylation. Proc Natl Acad Sci U S A *90*, 6849-6853.

Scheid, M.P., and Duronio, V. (1996). Phosphatidylinositol 3-OH kinase activity is not required for activation of mitogen-activated protein kinase by cytokines. J Biol Chem *271*, 18134-18139.

Schilling, M., Maiwald, T., Bohl, S., Kollmann, M., Kreutz, C., Timmer, J., and Klingmuller, U. (2005a). Computational processing and error reduction strategies for standardized quantitative data in biological networks. FEBS J *272*, 6400-6411.

Schilling, M., Maiwald, T., Bohl, S., Kollmann, M., Kreutz, C., Timmer, J., and Klingmuller, U. (2005b). Quantitative data generation for systems biology: the impact of randomisation, calibrators and normalisers. Syst Biol (Stevenage) *152*, 193-200.

Schilling, M., Maiwald, T., Hengl, S., Winter, D., Kreutz, C., Kolch, W., Lehmann, W.D., Timmer, J., and Klingmuller, U. (2009). Theoretical and experimental analysis links isoform-specific ERK signalling to cell fate decisions. Mol Syst Biol *5*, 334.

Schlegel, J., Piontek, G., and Mennel, H.D. (2002). Activation of the anti-apoptotic Akt/protein kinase B pathway in human malignant gliomas in vivo. Anticancer Res *22*, 2837-2840.

Schoeberl, B., Eichler-Jonsson, C., Gilles, E.D., and Muller, G. (2002). Computational modeling of the dynamics of the MAP kinase cascade activated by surface and internalized EGF receptors. Nat Biotechnol *20*, 370-375.

Schu, P.V., Takegawa, K., Fry, M.J., Stack, J.H., Waterfield, M.D., and Emr, S.D. (1993). Phosphatidylinositol 3-kinase encoded by yeast VPS34 gene essential for protein sorting. Science *260*, 88-91.

Schubbert, S., Shannon, K., and Bollag, G. (2007). Hyperactive Ras in developmental disorders and cancer. Nat Rev Cancer *7*, 295-308.

Seminario, M.C., Precht, P., Wersto, R.P., Gorospe, M., and Wange, R.L. (2003). PTEN expression in PTEN-null leukaemic T cell lines leads to reduced proliferation via slowed cell cycle progression. Oncogene *22*, 8195-8204.

Sharlow, E.R., Pacifici, R., Crouse, J., Batac, J., Todokoro, K., and Wojchowski, D.M. (1997). Hematopoietic cell phosphatase negatively regulates erythropoietin-induced hemoglobinization in erythroleukemic SKT6 cells. Blood *90*, 2175-2187.

Sharrard, R.M., and Maitland, N.J. (2000). Phenotypic effects of overexpression of the MMAC1 gene in prostate epithelial cells. Br J Cancer *83*, 1102-1109.

Shayesteh, L., Lu, Y., Kuo, W.L., Baldocchi, R., Godfrey, T., Collins, C., Pinkel, D., Powell, B., Mills, G.B., and Gray, J.W. (1999). PIK3CA is implicated as an oncogene in ovarian cancer. Nat Genet *21*, 99-102.

Shiota, C., Woo, J.T., Lindner, J., Shelton, K.D., and Magnuson, M.A. (2006). Multiallelic disruption of the rictor gene in mice reveals that mTOR complex 2 is essential for fetal growth and viability. Dev Cell *11*, 583-589.

Sly, L.M., Ho, V., Antignano, F., Ruschmann, J., Hamilton, M., Lam, V., Rauh, M.J., and Krystal, G. (2007). The role of SHIP in macrophages. Front Biosci *12*, 2836-2848.

Stambolic, V., Suzuki, A., de la Pompa, J.L., Brothers, G.M., Mirtsos, C., Sasaki, T., Ruland, J., Penninger, J.M., Siderovski, D.P., and Mak, T.W. (1998). Negative regulation of PKB/Akt-dependent cell survival by the tumor suppressor PTEN. Cell *95*, 29-39.

Steck, P.A., Pershouse, M.A., Jasser, S.A., Yung, W.K., Lin, H., Ligon, A.H., Langford, L.A., Baumgard, M.L., Hattier, T., Davis, T.*, et al.* (1997). Identification of a candidate tumour suppressor gene, MMAC1, at chromosome 10q23.3 that is mutated in multiple advanced cancers. Nat Genet *15*, 356-362.

Stokoe, D., Stephens, L.R., Copeland, T., Gaffney, P.R., Reese, C.B., Painter, G.F., Holmes, A.B., McCormick, F., and Hawkins, P.T. (1997). Dual role of phosphatidylinositol-3,4,5-trisphosphate in the activation of protein kinase B. Science *277*, 567-570.

Sun, H., Lesche, R., Li, D.M., Liliental, J., Zhang, H., Gao, J., Gavrilova, N., Mueller, B., Liu, X., and Wu, H. (1999). PTEN modulates cell cycle progression and cell survival by regulating phosphatidylinositol 3,4,5,-trisphosphate and Akt/protein kinase B signaling pathway. Proc Natl Acad Sci U S A *96*, 6199-6204.

Sun, J., Pedersen, M., and Ronnstrand, L. (2008). Gab2 is involved in differential phosphoinositide 3-kinase signaling by two splice forms of c-Kit. J Biol Chem *283*, 27444-27451.

Sun, M., Wang, G., Paciga, J.E., Feldman, R.I., Yuan, Z.Q., Ma, X.L., Shelley, S.A., Jove, R., Tsichlis, P.N., Nicosia, S.V.*, et al.* (2001). AKT1/PKBalpha kinase is frequently elevated in human cancers and its constitutive activation is required for oncogenic transformation in NIH3T3 cells. Am J Pathol *159*, 431-437.

Swameye, I., Muller, T.G., Timmer, J., Sandra, O., and Klingmuller, U. (2003). Identification of nucleocytoplasmic cycling as a remote sensor in cellular signaling by databased modeling. Proc Natl Acad Sci U S A *100*, 1028-1033.

Takahashi-Tezuka, M., Yoshida, Y., Fukada, T., Ohtani, T., Yamanaka, Y., Nishida, K., Nakajima, K., Hibi, M., and Hirano, T. (1998). Gab1 acts as an adapter molecule linking the cytokine receptor gp130 to ERK mitogen-activated protein kinase. Mol Cell Biol *18*, 4109-4117.

Tan, C.C., Eckardt, K.U., Firth, J.D., and Ratcliffe, P.J. (1992). Feedback modulation of renal and hepatic erythropoietin mRNA in response to graded anemia and hypoxia. Am J Physiol *263*, F474-481.

Testa, J.R., and Bellacosa, A. (2001). AKT plays a central role in tumorigenesis. Proc Natl Acad Sci U S A *98*, 10983-10985.

Thomas, C.C., Deak, M., Alessi, D.R., and van Aalten, D.M. (2002). High-resolution structure of the pleckstrin homology domain of protein kinase b/akt bound to phosphatidylinositol (3,4,5)-trisphosphate. Curr Biol *12*, 1256-1262.

Tolkacheva, T., Boddapati, M., Sanfiz, A., Tsuchida, K., Kimmelman, A.C., and Chan, A.M. (2001). Regulation of PTEN binding to MAGI-2 by two putative phosphorylation sites at threonine 382 and 383. Cancer Res *61*, 4985-4989.

Trencia, A., Perfetti, A., Cassese, A., Vigliotta, G., Miele, C., Oriente, F., Santopietro, S., Giacco, F., Condorelli, G., Formisano, P.*, et al.* (2003). Protein kinase B/Akt binds and phosphorylates PED/PEA-15, stabilizing its antiapoptotic action. Mol Cell Biol *23*, 4511-4521.

Ueki, K., Fruman, D.A., Yballe, C.M., Fasshauer, M., Klein, J., Asano, T., Cantley, L.C., and Kahn, C.R. (2003). Positive and negative roles of p85 alpha and p85 beta regulatory subunits of phosphoinositide 3-kinase in insulin signaling. J Biol Chem *278*, 48453-48466.

Ungureanu, D., Saharinen, P., Junttila, I., Hilton, D.J., and Silvennoinen, O. (2002). Regulation of Jak2 through the ubiquitin-proteasome pathway involves phosphorylation of Jak2 on Y1007 and interaction with SOCS-1. Mol Cell Biol *22*, 3316-3326.

Valiente, M., Andres-Pons, A., Gomar, B., Torres, J., Gil, A., Tapparel, C., Antonarakis, S.E., and Pulido, R. (2005). Binding of PTEN to specific PDZ domains contributes to PTEN protein stability and phosphorylation by microtubule-associated serine/threonine kinases. J Biol Chem *280*, 28936-28943.

Vanhaesebroeck, B., and Alessi, D.R. (2000). The PI3K-PDK1 connection: more than just a road to PKB. Biochem J *346 Pt 3*, 561-576.

Vanhaesebroeck, B., Guillermet-Guibert, J., Graupera, M., and Bilanges, B. (2010). The emerging mechanisms of isoform-specific PI3K signalling. Nat Rev Mol Cell Biol *11*, 329-341.

Vanhaesebroeck, B., Leevers, S.J., Ahmadi, K., Timms, J., Katso, R., Driscoll, P.C., Woscholski, R., Parker, P.J., and Waterfield, M.D. (2001). Synthesis and function of 3-phosphorylated inositol lipids. Annu Rev Biochem *70*, 535-602.

Vanhaesebroeck, B., Leevers, S.J., Panayotou, G., and Waterfield, M.D. (1997). Phosphoinositide 3-kinases: a conserved family of signal transducers. Trends Biochem Sci *22*, 267-272.

Vivanco, I., and Sawyers, C.L. (2002). The phosphatidylinositol 3-Kinase AKT pathway in human cancer. Nat Rev Cancer *2*, 489-501.

Volinia, S., Dhand, R., Vanhaesebroeck, B., MacDougall, L.K., Stein, R., Zvelebil, M.J., Domin, J., Panaretou, C., and Waterfield, M.D. (1995). A human phosphatidylinositol 3-kinase complex related to the yeast Vps34p-Vps15p protein sorting system. EMBO J *14*, 3339-3348.

Walrafen, P., Verdier, F., Kadri, Z., Chretien, S., Lacombe, C., and Mayeux, P. (2005). Both proteasomes and lysosomes degrade the activated erythropoietin receptor. Blood *105*, 600-608.

Wang, C.C., Cirit, M., and Haugh, J.M. (2009). PI3K-dependent cross-talk interactions converge with Ras as quantifiable inputs integrated by Erk. Mol Syst Biol *5*, 246.

Wang, D.S., and Shaw, G. (1995). The association of the C-terminal region of beta I sigma II spectrin to brain membranes is mediated by a PH domain, does not require membrane proteins, and coincides with a inositol-1,4,5 triphosphate binding site. Biochem Biophys Res Commun *217*, 608-615.

Wang, G.L., and Semenza, G.L. (1993). General involvement of hypoxia-inducible factor 1 in transcriptional response to hypoxia. Proc Natl Acad Sci U S A *90*, 4304-4308.

Wang, J., Auger, K.R., Jarvis, L., Shi, Y., and Roberts, T.M. (1995). Direct association of Grb2 with the p85 subunit of phosphatidylinositol 3-kinase. J Biol Chem *270*, 12774-12780.

Ward, S.G. (2004). Do phosphoinositide 3-kinases direct lymphocyte navigation? Trends Immunol *25*, 67-74.

Warner, N.L., Moore, M.A., and Metcalf, D. (1969). A transplantable myelomonocytic leukemia in BALB-c mice: cytology, karyotype, and muramidase content. J Natl Cancer Inst *43*, 963-982.

Watowich, S.S., Hilton, D.J., and Lodish, H.F. (1994). Activation and inhibition of erythropoietin receptor function: role of receptor dimerization. Mol Cell Biol *14*, 3535-3549.

Wendel, H.G., De Stanchina, E., Fridman, J.S., Malina, A., Ray, S., Kogan, S., Cordon-Cardo, C., Pelletier, J., and Lowe, S.W. (2004). Survival signalling by Akt and eIF4E in oncogenesis and cancer therapy. Nature *428*, 332-337.

Wickrema, A., Uddin, S., Sharma, A., Chen, F., Alsayed, Y., Ahmad, S., Sawyer, S.T., Krystal, G., Yi, T., Nishada, K.*, et al.* (1999). Engagement of Gab1 and Gab2 in erythropoietin signaling. J Biol Chem *274*, 24469-24474.

Wiley, H.S., Shvartsman, S.Y., and Lauffenburger, D.A. (2003). Computational modeling of the EGF-receptor system: a paradigm for systems biology. Trends Cell Biol *13*, 43-50.

Witthuhn, B.A., Quelle, F.W., Silvennoinen, O., Yi, T., Tang, B., Miura, O., and Ihle, J.N. (1993). JAK2 associates with the erythropoietin receptor and is tyrosine phosphorylated and activated following stimulation with erythropoietin. Cell *74*, 227-236.

Wohrle, F.U., Daly, R.J., and Brummer, T. (2009). Function, regulation and pathological roles of the Gab/DOS docking proteins. Cell Commun Signal *7*, 22.

Wojchowski, D.M., Gregory, R.C., Miller, C.P., Pandit, A.K., and Pircher, T.J. (1999). Signal transduction in the erythropoietin receptor system. Exp Cell Res *253*, 143-156.

Wolf, I., Jenkins, B.J., Liu, Y., Seiffert, M., Custodio, J.M., Young, P., and Rohrschneider, L.R. (2002). Gab3, a new DOS/Gab family member, facilitates macrophage differentiation. Mol Cell Biol *22*, 231-244.

Wu, H., Liu, X., Jaenisch, R., and Lodish, H.F. (1995). Generation of committed erythroid BFU-E and CFU-E progenitors does not require erythropoietin or the erythropoietin receptor. Cell *83*, 59-67.

Wymann, M.P., and Marone, R. (2005). Phosphoinositide 3-kinase in disease: timing, location, and scaffolding. Curr Opin Cell Biol *17*, 141-149.

Wymann, M.P., Zvelebil, M., and Laffargue, M. (2003). Phosphoinositide 3-kinase signalling--which way to target? Trends Pharmacol Sci *24*, 366-376.

Xu, X., Sakon, M., Nagano, H., Hiraoka, N., Yamamoto, H., Hayashi, N., Dono, K., Nakamori, S., Umeshita, K., Ito, Y.*, et al.* (2004). Akt2 expression correlates with prognosis of human hepatocellular carcinoma. Oncol Rep *11*, 25-32.

Yamada, S., Shiono, S., Joo, A., and Yoshimura, A. (2003). Control mechanism of JAK/STAT signal transduction pathway. FEBS Lett *534*, 190-196.

Yoon, D., and Watowich, S.S. (2003). Hematopoietic cell survival signals are elicited through non-tyrosine-containing sequences in the membrane-proximal region of the erythropoietin receptor (EPOR) by a Stat5-dependent pathway. Exp Hematol *31*, 1310-1316.

Yoon, S., and Seger, R. (2006). The extracellular signal-regulated kinase: multiple substrates regulate diverse cellular functions. Growth Factors *24*, 21-44.

Yoshimura, A., D'Andrea, A.D., and Lodish, H.F. (1990). Friend spleen focus-forming virus glycoprotein gp55 interacts with the erythropoietin receptor in the endoplasmic reticulum and affects receptor metabolism. Proc Natl Acad Sci U S A *87*, 4139-4143.

Yoshimura, A., Zimmers, T., Neumann, D., Longmore, G., Yoshimura, Y., and Lodish, H.F. (1992). Mutations in the Trp-Ser-X-Trp-Ser motif of the erythropoietin receptor abolish processing, ligand binding, and activation of the receptor. J Biol Chem *267*, 11619-11625.

Zarich, N., Oliva, J.L., Martinez, N., Jorge, R., Ballester, A., Gutierrez-Eisman, S., Garcia-Vargas, S., and Rojas, J.M. (2006). Grb2 is a negative modulator of the intrinsic Ras-GEF activity of hSos1. Mol Biol Cell *17*, 3591-3597.

Zeng, R., Aoki, Y., Yoshida, M., Arai, K., and Watanabe, S. (2002). Stat5B shuttles between cytoplasm and nucleus in a cytokine-dependent and -independent manner. J Immunol *168*, 4567-4575.

Zhang, J., and Lodish, H.F. (2007). Endogenous K-ras signaling in erythroid differentiation. Cell Cycle *6*, 1970-1973.

Zhou, B.P., and Hung, M.C. (2003). Dysregulation of cellular signaling by HER2/neu in breast cancer. Semin Oncol *30*, 38-48.

Zhu, X., Kwon, C.H., Schlosshauer, P.W., Ellenson, L.H., and Baker, S.J. (2001). PTEN induces G(1) cell cycle arrest and decreases cyclin D3 levels in endometrial carcinoma cells. Cancer Res *61*, 4569-4575.

Zi, Z., Cho, K.H., Sung, M.H., Xia, X., Zheng, J., and Sun, Z. (2005). In silico identification of the key components and steps in IFN-gamma induced JAK-STAT signaling pathway. FEBS Lett *579*, 1101-1108.

6 Appendix

6.1 Observables and data sets

CFU-E time course stimulated with 2.5U Epo						
# MCode	drivingFunctions(1).name = 'CFUE-Epo';					
# MCode	drivingFunctions(1).stimuli(1) = pwGetDrivingFunction('steps',[-60 0],[0 1]);					
		pEpoR		pAkt		
Time-min	Stimulus	blu/cell	nM/cell	blu/cell	nM/cell	
0	1	0.41	0.02	5.28	24.50	
1	1	10.30	0.45	13.27	61.58	
5	1	35.60	1.56	36.63	170.02	
8	1	33.20	1.45	30.09	139.68	
10	1	27.60	1.21	47.40	220.00	
12	1	27.20	1.19	36.25	168.24	
14	1	25.40	1.11	29.90	138.78	
16	1	26.10	1.14	31.15	144.58	
18	1	21.10	0.92	42.59	197.69	
20	1	18.00	0.79	30.29	140.57	
25	1	16.90	0.74	35.48	164.67	
30	1	15.20	0.67	32.69	151.72	
35	1	12.00	0.53	31.25	145.03	
40	1	8.21	0.36	25.09	116.47	
45	1	8.94	0.39	24.90	115.58	
50	1	8.28	0.36	27.50	127.63	
55	1	7.03	0.31	18.94	87.91	
60	1	4.62	0.20	14.71	68.28	

Table 6. 1 1h time course of EpoR and Akt phosphorylation in CFU-E cells stimulated with 2.5U Epo.

BaF3-EpoR time course stimulated with 5U Epo					
# MCode	drivingFunctions(1).name = 'BaF3-Epo';				
# MCode	drivingFunctions(1).stimuli(1) = pwGetDrivingFunction('steps',[-60 0],[0 1]);				
		pEpoR		pAkt	
Time-min	Stimulus	blu/cell	nM/cell	blu/cell	nM/cell
0	1	70.13	0.87	1.89	2.50
1	1	89.29	1.11	1.48	1.95
5	1	269.30	3.35	6.25	8.28
8	1	288.02	3.59	16.57	21.95
10	1	290.90	3.62	16.46	21.80
12	1	316.83	3.95	16.29	21.58
14	1	308.91	3.85	13.17	17.44
16	1	324.03	4.03	10.31	13.66
18	1	290.18	3.61	9.71	12.86
20	1	340.59	4.24	8.67	11.48
25	1	234.74	2.92	8.01	10.61
30	1	265.70	3.31	6.20	8.21
35	1	213.14	2.65	8.12	10.75
40	1	207.38	2.58	6.25	8.28
45	1	226.10	2.82	4.79	6.35
50	1	186.50	2.32	3.94	5.22
55	1	169.21	2.11	3.87	5.13
60	1	131.77	1.64	4.25	5.63

Table 6. 2 1h time course of EpoR and Akt phosphorylation in BaF3-EpoR stimulated with 5U Epo.

Dose response						
CFU-E receptor phosphorylation (20081020)						
tEpoR	1000 molecules/cell	Volum 399	4.16 nM			
	10U (5min) 75% phosphorlyated :		3.12 nM			
Time-min	0.1	0.5	1.0	2.5	5.0	10.0 U/ml Epo
0	0.05	0.05	0.05	0.05	0.05	0.05
5	0.19	0.98	1.31	1.56	2.31	3.12
10	0.25	0.93	1.60	1.41	2.53	2.04
20	0.19	0.64	0.92	1.87	1.20	1.69
60	0.14	0.30	0.30	0.27	0.34	0.40
120	0.12	0.27	0.28	0.34	0.42	0.44
BaF3-EpoR receptor phosphorylation (20110215)						
Time-min	0.5	5	50	U/ml Epo		
0	0.53	0.53	0.53			
5	0.94	2.80	5.09			
10	0.91	3.60	5.96			
30	0.55	1.23	2.72			
60	0.26	1.24	2.53			
120	0.17	0.55	1.61			
180	0.17	0.31	0.94			

Table 6. 3 Dose response of EpoR phosphorylation in CFU-E and BaF3-EpoR cells

Dose response						
Akt phosphorylation (nM) in CFU-E cells (20081022)						
Time (min)	0.1	0.5	1	2.5	5	U/ml Epo
0	4.29	4.29	4.29	4.29	4.29	
5	13.57	123.93	162.00	183.51	185.34	
10	49.92	202.82	223.90	220.00	237.17	
20	44.32	124.49	201.76	236.14	215.99	
60	26.21	70.72	87.71	54.41	74.59	
120	10.73	39.92	38.20	86.66	91.27	
Dose response						
Akt phosphorylation (nM) in BaF3-EpoR cells						
Time (min)	2.5	5	5	10	50	U/ml Epo
0	3.37	3.37	3.91	3.91	3.37	
5	15.10	25.77	27.56	31.02	44.52	
10	19.50	20.87	22.73	30.20	38.07	
20	7.72	7.18	9.52	9.68	18.91	
60	10.21	5.64	5.86	8.53	16.18	
120	7.72	2.68	5.67	5.84	5.77	
180.0	8.65	2.83	5.72	5.80	7.28	

Table 6. 4 Dose response of Akt phosphorylation in CFU-E and BaF3-EpoR cells

CFU-E oe PTEN x 12 fold					
# MCode	drivingFunctions(1).name = 'CFUE-Epo';				
# MCode	drivingFunctions(1).stimuli(1) = pwGetDrivingFunction('steps',[-60 0],[0 1]);				
# xCol-Time-min	parCol-Stimulus	nM/cell			
0	1	4.93			
1.5	1	23.15			
5	1	73.21			
10	1	80.40			
15	1	58.27			
20	1	42.42			
30	1	33.64			
40	1	20.87			
50	1	12.77			
60	1	8.80			
CFU-E oe SHIP1 x 11 fold					
# MCode	drivingFunctions(1).name = 'CFUE-Epo';				
# MCode	drivingFunctions(1).stimuli(1) = pwGetDrivingFunction('steps',[-60 0],[0 1]);				
# xCol-Time-min	parCol-Stimulus	nM/cell			
0	1	22.28			
1	1	55.27			
3	1	170.14			
5	1	148.12			
8	1	145.96			
10	1	162.80			
12	1	151.14			
16	1	149.41			
20	1	79.02			
30	1	101.48			
45	1	72.55			
60	1	28.28			

Table 6. 5 Effect of PTEN or SHIP1 overexpression on Akt phosphorylation in CFU-E cells

BaF3-EpoR	oe PTEN x 3 fold				
	oe SHIP1 x 4 fold				
#Time-min	Cells	Blot	pAkt nM 21.8	Middel Value	Standard Deviation
0	control	1	0.53	2.99	3.49
0	control	2	5.46		
10	control	1	21.80	21.80	1.25
10	control	2	23.05		
10	control	2	20.55		
30	control	1	11.54	12.09	2.34
30	control	1	14.57		
30	control	2	13.14		
30	control	2	9.13		
60	control	1	6.08	6.42	0.91
60	control	1	7.41		
60	control	2	5.33		
60	control	2	6.87		
0	oe PTEN	1	0.43	0.43	
10	oe PTEN	1	3.29	4.11	1.15

10	oe PTEN	1	4.92		
30	oe PTEN	1	1.37	1.79	0.59
30	oe PTEN	1	2.20		
60	oe PTEN	1	0.51	0.73	0.30
60	oe PTEN	1	0.94		
0	oe SHIP1	2	3.73	3.73	
10	oe SHIP1	2	13.02	12.03	1.40
10	oe SHIP1	2	11.04		
30	oe SHIP1	2	5.39	6.05	0.94
30	oe SHIP1	2	6.71		
60	oe SHIP1	2	5.05	4.72	0.46
60	oe SHIP1	2	4.40		

Table 6. 6 Effect of PTEN or SHIP1 overexpression on Akt phosphorylation in BaF3-EpoR cells

PTEN x 11 fold-overexpressing cells and control CFU-E cells stimulated with 2.5 U/ml Epo						
20100927						
Time (min)	Cells	PTEN	pAkt	pGSK3	pS6	pErk
0	control	0.63	0.01	0.13	0.04	0.04
10	control	2.39	1.00	1.00	0.32	1.00
30	control	1.07	0.52	0.45	0.70	0.08
60	control	1.19	0.38	0.27	0.85	0.07
120	control	0.57	0.33	0.18	1.00	0.04
150	control	0.93	0.25	0.24	1.00	0.06
0	oe PTEN	8.65	0.00	0.06	0.01	0.04
10	oe PTEN	11.51	0.31	0.34	0.12	0.85
30	oe PTEN	10.70	0.09	0.08	0.12	0.07
60	oe PTEN	13.71	0.04	0.05	0.10	0.04
90	oe PTEN	15.05	0.02	0.04	0.11	0.03
120	oe PTEN	11.40	0.02	0.05	0.26	0.05
150	oe PTEN	12.70	0.01	0.05	0.20	0.03
PTEN x 4.2 fold-overexpressing and control BaF3-EpoR cells stimulated with 5U/ml Epo						
20100309						
Time (min)	Cells	PTEN	pAkt	pGSK3	pS6	pErk
0	control	0.806	0.06	0.23	0.06	0.01
10	control	0.786	1.00	1.00	0.91	1.00
30	control	1.539	0.62	0.54	1.00	0.67
60	control	0.872	0.24	0.44	0.65	0.16
120	control	1.195	0.20	0.19	0.09	0.10
150	control	0.744	0.08	0.17	0.04	0.03
180	control	1.059	0.06	0.21	0.08	0.02
0	oe PTEN	4.840	0.09	0.16	0.04	0.01
10	oe PTEN	3.417	0.49	1.00	0.48	0.91
30	oe PTEN	4.363	0.13	0.47	0.64	0.50
60	oe PTEN	5.876	0.14	0.56	0.51	0.27
120	oe PTEN	2.956	0.12	0.30	0.13	0.07
150	oe PTEN	3.206	0.07	0.19	0.06	0.03
180	oe PTEN	4.633	0.10	0.19	0.09	0.02

Table 6. 7 Effect of PTEN on the phosphorylation patterns of GSK3 and mTOR in CFU-E and BaF3-EpoR cells.

SHIP1x 10 fold-overexpressing and control CFU-E cells stimulated with 2.5 U/ml Epo					
20101108					
Time (min)	SHIP1	pAkt	pGSK3	pS6 Ser235/236	pErk
0	1.76	0.02	0.12	0.19	0.05
10	2.32	1.00	1.00	0.37	1.00
30	1.03	0.19	0.28	0.82	0.08
60	2.40	0.48	0.66	0.90	0.11
90	0.97	0.25	0.35	1.00	0.04
120	0.27	0.30	0.31	0.92	0.06
150	0.40	0.16	0.30	0.89	0.11
180	0.97	0.06	0.04	0.73	0.05
0	6.36	0.02	0.08	0.21	0.07
10	11.57	0.58	0.46	0.30	0.45
30	8.45	0.29	0.18	0.51	0.14
60	11.67	0.09	0.15	0.46	0.11
90	4.55	0.04	0.14	0.52	0.06
120	9.91	0.07	0.09	0.33	0.09
150	10.05	0.05	0.13	0.70	0.10
180	14.46	0.05	0.13	0.70	0.13
SHIP1x 4 fold-overexpressing and control BaF3-EpoR cells stimulated with 5U/ml Epo					
20101108					
Time (min)	SHIP1	pAkt	pGSK3	pS6 Ser235/236	pErk
0	1.26	0.06	0.30	0.10	0.03
10	1.50	1.00	1.00	0.99	1.00
30	0.58	0.38	0.22	0.74	0.27
60	1.27	0.34	0.46	0.92	0.29
90	0.74	0.14	0.19	0.41	0.08
120	0.72	0.09	0.26	0.18	0.07
0	3.22	0.09	0.37	0.11	0.03
10	3.08	0.74	1.03	0.86	1.12
30	3.78	0.34	0.36	1.00	0.31
60	4.00	0.32	0.49	0.91	0.23
120	3.71	0.14	0.47	0.49	0.18

Table 6. 8 Effect of SHIP1 on the phosphorylation patterns of GSK3 and mTOR in CFU-E and BaF3-EpoR cells.

Hill function	BaF3-EpoR 20080811					Hill function	CFU-E 20080805			
f=y0+a*x^b/(c^b+x^b)		M2	PTEN	SHIP1		f=y0+a*x^b/(c^b+x^b)		M2	PTEN	SHIP1
	a	1.00	0.67	0.89			a	0.92	0.36	0.56
	b	1.62	1.90	1.57			b	1.10	1.10	1.08
	c	0.69	0.90	0.56			c	0.27	0.60	0.45
	y0	0.00	0.00	0.00			y0	0.08	0.02	0.01
	Epo	M2	PTEN	SHIP1			Epo	PTEN	SHIP1	M2
	100	1.07	0.68	0.76			50	0.35	0.57	0.96

	100	0.88	0.60	0.86			50	0.41	0.62	0.93
	100	0.89	0.62	0.82			10	0.34	0.57	1.06
	100		0.57	0.87			10	0.34	0.57	0.87
	50	0.94	0.68	0.88			5	0.35	0.48	1.10
	50	0.97	0.73	0.80			5	0.38	0.50	1.06
	50	1.01	0.69	0.87			1	0.22	0.42	0.90
	50		0.66	0.92			1	0.26	0.43	0.63
	10	1.06	0.63	0.90			0.5	0.18	0.32	0.68
	10	0.99	0.76	0.86			0.5	0.19	0.32	0.75
	10	1.05	0.63	0.94			0.1	0.06	0.10	0.32
	10		0.67	0.95			0.1	0.07	0.10	0.30
	5	0.94	0.68	0.85			0.05	0.04	0.05	0.21
	5	0.99	0.65	0.95			0.05	0.05	0.05	0.20
	5	1.11	0.72	0.96			0.01	0.03	0.03	0.10
	5		0.67	0.91			0.01	0.02	0.03	0.10
	1	0.54	0.27	0.45			0.005	0.03	0.02	0.10
	1	0.57	0.35	0.65			0.005	0.02	0.02	0.09
	1	0.68	0.46	0.53			0.001	0.01	0.02	0.09
	1		0.33	0.65			0.001	0.02	0.02	0.07
	0.5	0.40	0.17							
	0.5	0.34	0.19	0.44						
	0.5	0.52	0.21	0.45						
	0.5		0.18	0.52						
	0.1	0.01	0.01	0.01						
	0.1	0.01	0.01	0.01						
	0.1	0.02	0.01	0.02						
	0.1		0.01	0.03						
	0.05	0.01	0.01	0.01						
	0.05	0.01	0.01	0.01						
	0.05	0.02	0.01	0.01						
	0.05		0.01							
	0.01	0.01	0.01	0.01						
	0.01	0.01	0.01	0.01						
	0.01	0.01	0.01	0.01						
	0.01		0.01							
	0.005	0.01	0.00	0.01						
	0.005	0.01	0.00	0.01						
	0.005	0.01	0.01	0.01						
	0.001	0.01	0.01	0.01						
	0.001	0.01	0.00	0.01						
	0.001	0.01	0.00	0.01						
	0	0.01	0.00	0.01						
	0		0.00	0.01						
	0	0.01	0.01	0.01						

Table 6. 9 Effect of PTEN and SHIP1 overexpression on cell proliferation (^{3}H-Thymidine incorporation assay) in CFU-E and BaF3-EpoR cells

6.2 Initial amount of molecules in the receptor and PI3K/Akt core models

Parameter	Symbol	Value	Unit
Concentrations or densities			
CFU-E cells			
Cytoplam volume		399	μm^3
Cell surface area		372	μm^2
EpoR		4.16	nM
		2.7	molecules/μm^2
EpoR phosphatase		41.5	nM
Gab1		21.2	nM
PI3K		12.45	nM
PI(4,5)P2		1.0e4	nM
SHIP1		15.4	nM
PTEN		10.4	nM
Akt		406.5	nM
PDK1		41.5	nM
BaF3-EpoR			
Cytoplam volume		1400	μm^3
Cell surface area		729	μm^2
EpoR		18.64	nM
		21.5	molecules/μm^2
EpoR phosphatase		41.5	nM
Gab2		35.6	nM
PI3K		12.5	nM
PI(4,5)P2		1.0e4	nM
SHIP1		84.2	nM
PTEN		107.3	nM
Akt		509.94	nM
PDK1		41.5	nM

Table 6. 10 Initial amount of molecules in the receptor and PI3K/Akt core models.

6.3 Ordinary differential equations of receptor and core PI3K/Akt models

Ordinary differential equations

Receptor model

Epo (*CFU-E*) : $\dot{x}_1 = 0$

Epo (*BaF3-EpoR*) : $\dot{x}_1 = -k_0 * x_1$

EpoR : $\dot{x}_2 = 0$

Phosphatase : $\dot{x}_3 = 0$

pEpoR : $\dot{x}_4 = + (((k_1 / (1 + (x_5 / k_7))) * (x_2 - x_4) * x_1 - (k_4 * x_4 * x_6)$

$Kinase_{inhibitor}$: $\dot{x}_5 = + (k_5 * x_4\text{^}k_8 / (k_9\text{^}k_8 + x_4\text{^}k_8)) - (k_6 * x_5)$

actPhosphatase : $\dot{x}_6 = + k_2 * (x_3 - x_6) * x_4 - (k_3 * x_6)$

Core-model

SHIP1t : $\dot{x}_7 = 0$

Gab1t (*CFU-E*) : $\dot{x}_8 = 0$

Gab2t (*BaF3-EpoR*) : $\dot{x}_8 = 0$

PI3Kt : $\dot{x}_9 = 0$

PI45P2 : $\dot{x}_{10} = 0$

PTEN : $\dot{x}_{11} = 0$

PDK1t : $\dot{x}_{12} = 0$

Aktt : $\dot{x}_{13} = 0$

pEpoR_PI3K : $\dot{x}_{14} = + k11 * (x9 - x14 - x15) * (x4 - x14) - k12 * x14$

pEpoR_Gab2_PI3K : $\dot{x}_{15} = + k15 * x16 * (x9 - x14 - x15) - (k16 * x15)$

pEpoR_Gab2 : $\dot{x}_{16} = + k13 * (x8 - x16 - x15) * (x4 - x16 - x15) - (k14 * x16) - (k15 * x16 * (x9 - x14 - x15)) + k16 * x15$

pEpoR_SHIP1 : $\dot{x}_{17} = + k17 * (x7 - x17) * (x4 - x17) - (k18 * x17)$

PIP3 : $\dot{x}_{18} = + k19 * x10 * (x14 + x15) - (k20 * x18 * x11) - (k21 * x18 * x17 - k22 * x18 * (x12 - x19) + k23 * x19- (k24 * x18 * (x10 - x20 - x21)) + k25 * x20 + (k26 * x20 * x19) + k28 * x10 * (x9 - x14 - x15)$

PIP3_PDK1 : $\dot{x}_{19} = + k22 * x18 * (x12 - x19) - (k23 * x19)$

PIP3_Akt : $\dot{x}_{20} = + k24 * x18 * (x13 - x20 - x21) - (k25 * x20) - (k26 * x20 * x19)$

pAkt : $\dot{x}_{21} = + k26 * x20 * x19 - (k27 * x21)$

Parameters

Epo degradation	k_0
EpoR activation by Epo	k_1
Phosphatase activation by pEpoR	k_2
Phosphatase deactivation	k_3
pEpoR deactivation by phosphatase	k_4
$Kinase_{inhibitor}$ induced by pEpoR	k_5
$Kinase_{inhibitor}$ deactivation	k_6
Inhibition of EpoR activation by $Kinase_{inhibitor}$	k_7
n (Hill coefficient)	k_8
Ji (EpoR occupying half of the binding sites)	k_9
PI3K activation	k_{11}
PI3K deactivation	k_{12}
Gab1/ 2 activation	k_{13}
Gab1/ 2 deactivation	k_{14}
Gab1/ 2_PI3K assocoation	k_{15}
Gab1/ 2_PI3K dissociation	k_{16}
SHIP1 activation by pEpoR	k_{17}
SHIP1 deactivation	k_{18}
PIP3 generation by PI3K	k_{19}
PI45P2 generation by SHIP1	k_{20}
PI34P2 generation by P	k_{21}
PDK1_PIP3 association	k_{22}
PDK1_PIP3 dissociation	k_{23}
Akt_PIP3 association	k_{24}
Akt_PIP3 dissociation	k_{25}
Akt phosphorylation by PDK_PIP3	k_{26}
Akt dephosphorylation	k_{27}
PIP3_basal generation by free PI	k_{28}

Constraints

$pEpoR_{CFU\text{-}E\_10UEpo\_5min} / tEpoR_{CFU\text{-}E} = 0.75$

$pAkt_{CFU\text{-}E\_2.5UEpo\_10min} / tAkt_{CFU\text{-}E} = 0.54$

Observables

pEpoR : $y_1 = x_4$

pAkt : $y_2 = x_{21}$

6.4 Estimated kinetic parameters

parameters			parameters estimated	parameters (best
CFU-E:receptor activation model				
k_0		Epo degradation	0 (fix)	0
k_1		EpoR activation by Epo	0.236 ±2.0e-4 (0%)	0.2358
k_2		Phosphatase activation by pEpoR	0.0257 ±3.0e-4 (0%)	0.0260
k_3		Phosphatase deactivation	0.0317 ±7.7e-5 (0%)	0.0316
k_4		pEpoR deactivation by phosphatase	0.0054 ±5.1e-5 (1%)	0.0053
k_5		$Kinase_{inhibitor}$ induced by pEpoR	0.3297 ±0.77 (234%)	0.1308
k_6		$Kinase_{inhibitor}$ deactivation	0.0042 ±2.6e-6 (1%)	0.0042
k_7		Ki (Inhibition of EpoR activation by $Kinase_{inhibitor}$)	0.0801 ±0.188 (235%)	0.0313
k_8		n (Hill coefficient)	1 ±1.2e-6 (0%)	1
k_9		Ji (EpoR occupying half of the binding sites)	2.517 ±0.038 (11%)	2.5661
BaF3-EpoR:receptor activation model				
k_0		Epo degradation: 0.05 U/ml	0.173287 (fix)	0.173287
		5 U/ml	0.0173287 (fix)	0.0173287
		50 U/ml	0.00173287 (fix)	0.0017328
k_1		EpoR activation by Epo	0.0457 ±8.4e-6 (0%)	0.0457
k_2		Phosphatase activation by pEpoR	0.5331 ±1.1e-4 (0%)	0.5341
k_3		Phosphatase deactivation	0.0959 ±1.7e-4 (0%)	0.0962
k_4		pEpoR deactivation by phosphatase	0.0006 ±2.4e-7 (0%)	0.0006
k_5		$Kinase_{inhibitor}$ induced by pEpoR	9.8500 ±18.43 (187%)	16.8256
k_6		$Kinase_{inhibitor}$ deactivation	0.0013 ±5.9e-6 (0%)	0.0013
k_7		Ki (Inhibition of EpoR activation by $Kinase_{inhibitor}$)	0.0023 ±0.005 (195%)	0.0003
k_8		n (Hill coefficient)	5.8250 ±0.010 (0%)	5.7963
k_9		Ji (EpoR occupying half of the binding sites)	11.85 ±1.274 (11%)	19.2718
PI3K/Akt core model				
k_{11}	kPI3K	PI3K activation	1.7e-5 ±8.3e-6 (50%)	4.3e-8
k_{12}	lPI3K	PI3K deactivation	0.0048 ±0.0471 (982%)	2.3e-5
k_{13}	kGab1	Gab1 activation	44.899 ±45.370 (101%)	0.1071
	kGab2	Gab2 activation	0.0204 ±0.0080 (39%)	0.0051
k_{14}	lGab1	Gab1 deactivation	50.429 ±189.85 (376%)	325.44
	lGab2	Gab2 deactivation	0.1743 ±0.2433 (140%)	0.6303
k_{15}	kGab1PI3K	Gab1_PI3K assocoation	70.900 ±69.052 (97%)	3.4014
	kGab2PI3K	Gab2_PI3K assocoation	0.0057 ±0.0027 (47%)	5.7e-5
k_{16}	lGab1PI3K	Gab1_PI3K dissociation	66.114 ±169.96 (257%)	151.15
	lGab2PI3K	Gab2_PI3K dissociation	0.7392 ±0.0883 (12%)	0.8464
k_{17}	kSHIP1	SHIP1 activation by pEpoR	8.0e-5 ± 5.4e-6 (7%)	8.4e-5
k_{18}	lSHIP1	SHIP1 deactivation	4.1e-6 ± 3.9e-6 (94%)	1.5e-6
k_{19}	vPIP3	PIP3 generation by PI3K	2.3622 ±6.7260 (285%)	23.697
k_{20}	vPI34P2	PI34P2 generation by SHIP1	6.2412 ±2.6429 (42%)	5.9458
k_{21}	vPI45P2	PI45P2 generation by PTEN	0.0536 ±0.0213 (40%)	0.0528
k_{22}	kPDK1	PDK1_PIP3 association	0.0834 ±0.2905 (348%)	0.0408
k_{23}	lPDK1	PDK1_PIP3 dissociation	10.172 ±12.952 (127%)	9.8477
k_{24}	kAkt	Akt_PIP3 association	0.8012 ±0.5015 (63%)	0.6998
k_{25}	lAkt	Akt_PIP3 dissociation	24.685 ±13.584 (55%)	23.492
k_{26}	vpAkt	Akt phosphorylation by PDK_PIP3	0.1607 ±0.1413 (88%)	0.0992
k_{27}	dpAkt	Akt dephosphorylation	7.3371 ±6.4479 (88%)	4.5795
k_{28}	vPIP3_basal	PIP3_basal generation by free PI3K	0.0002 ±2.4e-5 (15%)	0.0002

6.5 Q-PCR analysis of PTEN and SHIP1 mediated mRNA expression

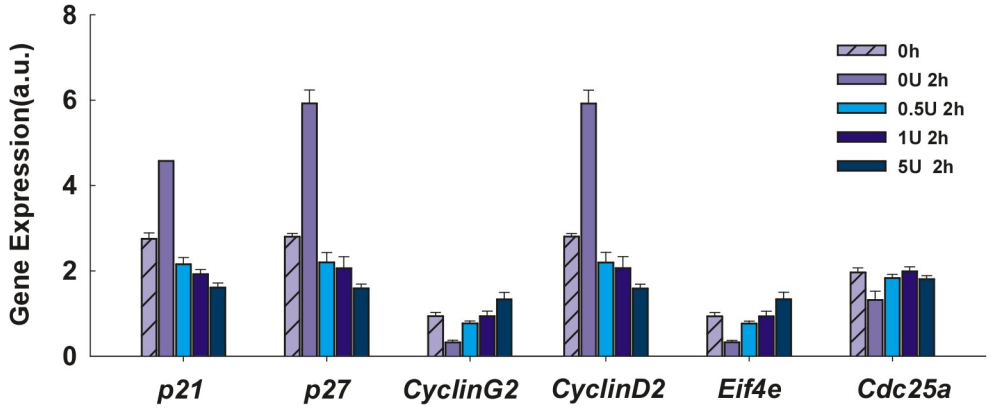

Figure 6.1 Epo regulated mRNA expressions of genes of interest in CFU-E cells. Starved CFU-E cells were stimulated with 0.5, 1 and 5 U/ml Epo or remained non-stimulated for 2h. mRNA levels of the indicated genes were analysed by quantitative RT-PCR. Relative concentrations were normalized with RPL32. Error bars represent standard deviations of three biological replicates.

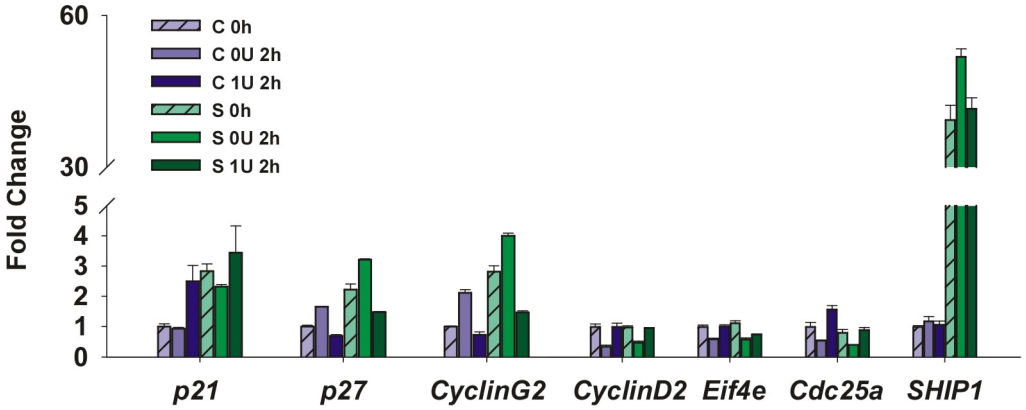

Figure 6.2 Q-PCR analysis of SHIP1 mediated mRNA expressions in CFU-E. CFU-E cells-overexpressing SHIP1 (S) or control vector (C) were starved and stimulated with 1 U/ml Epo or remained non-stimulated for 2h. mRNA levels of the indicated genes were analysed by quantitative RT-PCR. Relative concentrations were normalized with RPL32 and the fold change was calculated with respect to the expression of control cells at 0h. Error bars represent standard deviations of two to three biological replicates.

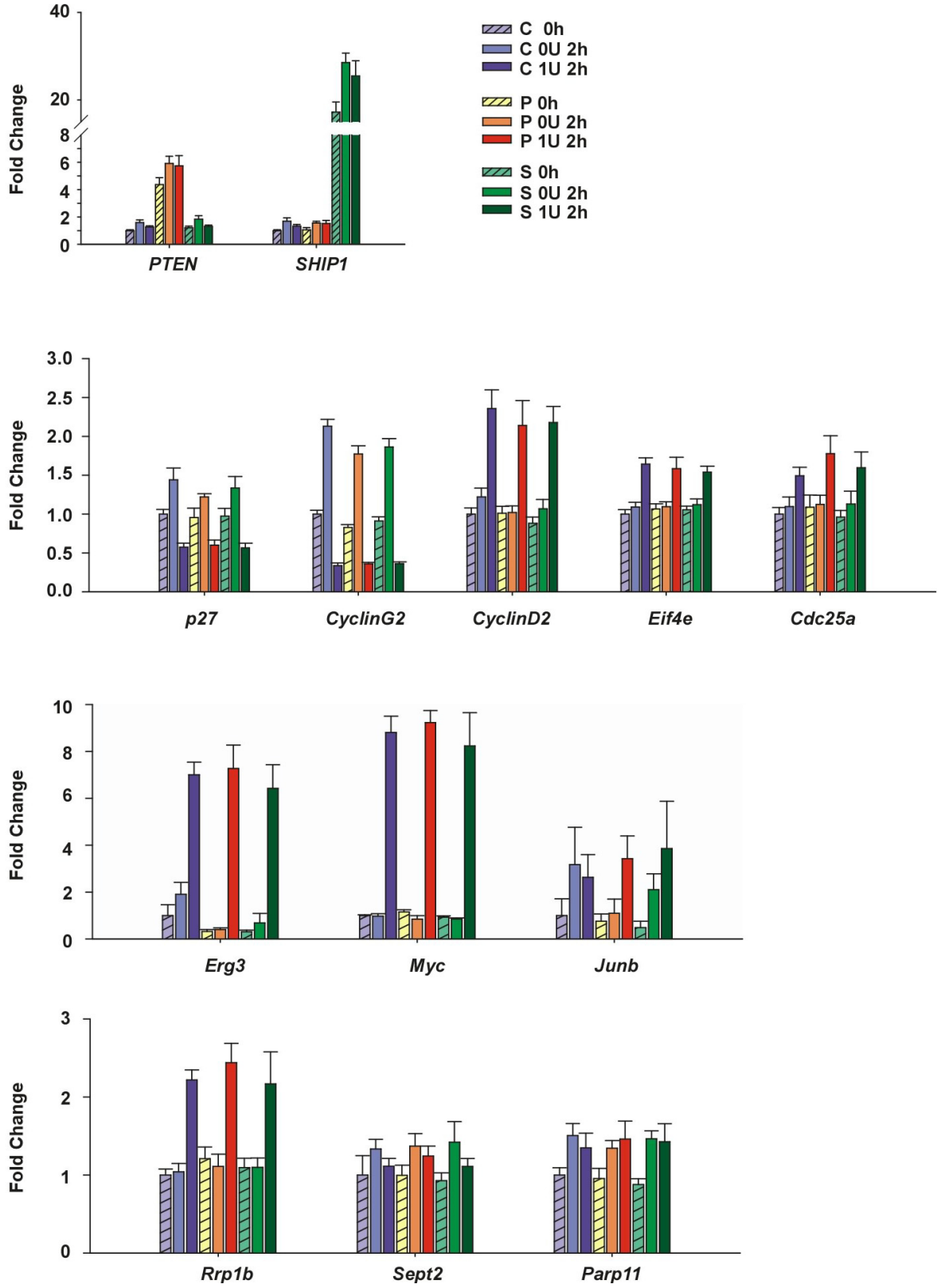

Figure 6.3 Q-PCR analysis of PTEN and SHIP1 mediated mRNA expressions in BaF3-EpoR cells. BaF3-EpoR cells-overexpressing control vector (C), PTEN (P) or SHIP1 (S) were starved and stimulated with 1 U/ml Epo or remained non-stimulated for 2h. mRNA levels of the indicated genes were analysed by quantitative RT-PCR. Relative concentrations were normalized with HPRT and the fold change was calculated with respect to the expression of control cells at 0h. Error bars represent standard deviations of two to three biological replicates.

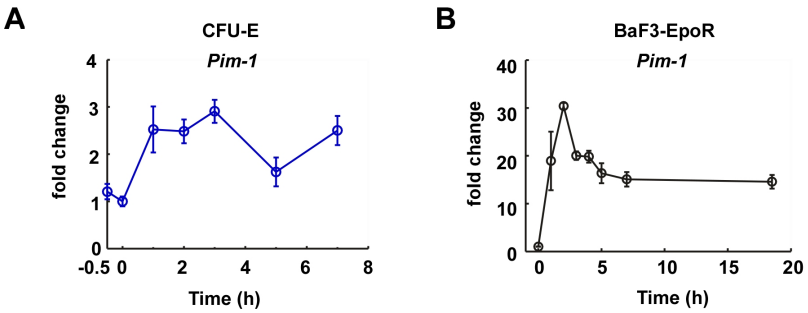

Figure 6.4 Q-PCR analysis of Epo-induced *Pim-1* expression in CFU-E and BaF3-EpoR cells. Growth factor-withdraw (**A**) CFU-E cells and (**B**) BaF3-EpoR cells were stimulated for the indicated times with 1 U/ml Epo. mRNA levels of *Pim-1* were analysed by quantitative RT-PCR. Relative concentrations were normalized with RPL32 in CFU-E cells and with HPRT in BaF3-EpoR cells. The fold change was calculated with respect to the expression of control cells at 0h. Error bars represent standard deviations of two technical replicates.

6.6 PI staining and TUNEL assay data

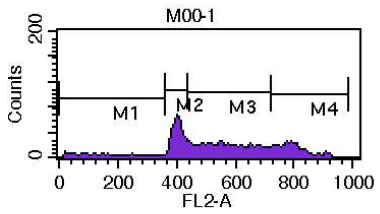

Sample ID: M00-1 Gate: G1
Total Events: 10000

Marker	% Gated	% Total	Geo Mean
All	100.00	79.69	495.16
M1	5.70	4.54	107.58
M2	29.19	23.26	402.75
M3	46.78	37.28	564.74
M4	18.84	15.01	782.99

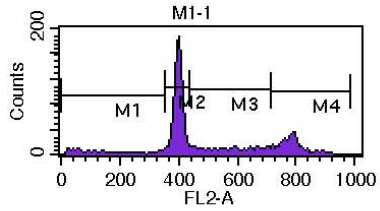

Sample ID: M1-1 Gate: G1
Total Events: 10000

Marker	% Gated	% Total	Geo Mean
All	100.00	79.22	451.61
M1	5.18	4.10	106.11
M2	57.37	45.45	396.59
M3	17.76	14.07	570.19
M4	19.88	15.75	777.91

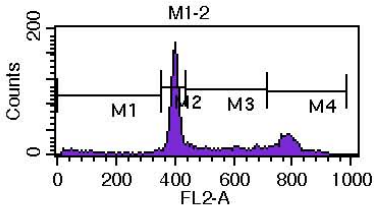

Sample ID: M1-2 Gate: G1
Total Events: 10000

Marker	% Gated	% Total	Geo Mean
All	100.00	78.20	460.15
M1	4.87	3.81	108.18
M2	55.28	43.23	398.44
M3	19.36	15.14	568.13
M4	20.66	16.16	781.57

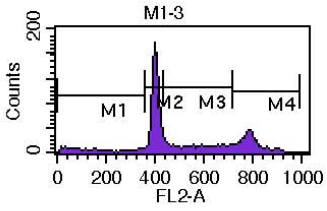

Sample ID: M1-3 Gate:
Total Events: 10000

Marker	% Gated	% Total	Geo Mear
All	100.00	79.36	457.30
M1	5.63	4.47	111.44
M2	53.87	42.75	396.87
M3	19.72	15.65	572.16
M4	21.04	16.70	777.79

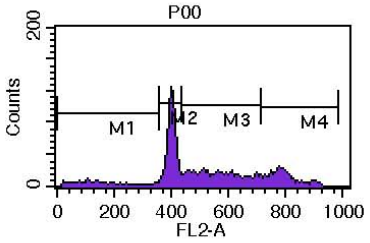

Sample ID: P00 Gate: G1
Total Events: 10000

Marker	% Gated	% Total	Geo Mean
All	100.00	79.47	465.46
M1	6.68	5.31	110.18
M2	39.27	31.21	398.30
M3	36.94	29.36	557.98
M4	17.44	13.86	782.40

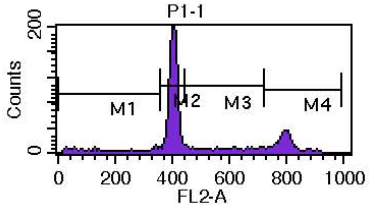

Sample ID: P1-1 Gate: G1
Total Events: 10000

Marker	% Gated	% Total	Geo Mean
All	100.00	86.65	436.02
M1	6.17	5.35	135.58
M2	66.76	57.85	399.97
M3	9.99	8.66	577.49
M4	17.24	14.94	786.89

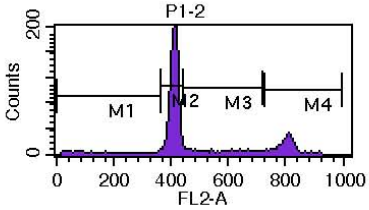

Sample ID: P1-2 Gate: G1
Total Events: 10000

Marker	% Gated	% Total	Geo Mean
All	100.00	84.14	443.75
M1	4.77	4.01	111.62
M2	67.76	57.01	405.26
M3	10.26	8.63	571.01
M4	17.40	14.64	794.58

Figure 6.5 Overexpression of PTEN affects the cell cycle distribution of CFU-E cells. The cell cycle distribution of the control (M) and PTEN-overexpressing (P) CFU-E cells was analyzed by PI staining and FACS. M00-1: control cells at 0 h; M1-1, M1-2, M1-3: biological triplicates of cells 10 h after stimulation with 1 U/ml Epo; P00: PTEN-overexpressing cells at 0h; P1-1, P1-2: biological duplicates of cells 10h after stimulation with 1U/ml Epo. M1: SubG1; M2: G0/G1; M3: S; M4: M/G2.

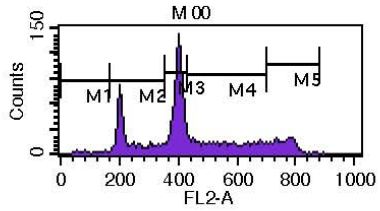

Sample ID: M 00 Gate: G1

Marker	% Gated	% Total	Geo Mean
All	100.00	87.71	405.26
M1	0.75	0.66	96.29
M2	22.11	19.39	231.87
M3	43.16	37.86	398.95
M4	23.68	20.77	557.42
M5	10.66	9.35	753.19

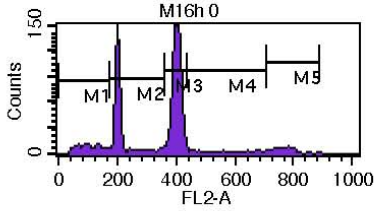

Sample ID: M16h 0 Gate: G1

Marker	% Gated	% Total	Geo Mean
All	100.00	84.92	309.14
M1	7.62	6.47	96.92
M2	28.19	23.94	209.18
M3	58.30	49.51	400.89
M4	2.31	1.96	563.61
M5	3.70	3.14	762.16

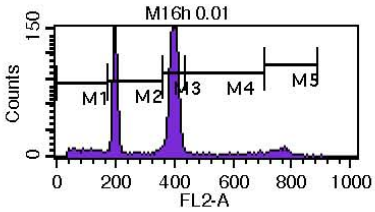

Sample ID: M16h 0.01 Gate: G1

Marker	% Gated	% Total	Geo Mean
All	100.00	86.51	316.72
M1	5.16	4.46	92.60
M2	28.00	24.22	208.19
M3	61.22	52.96	396.78
M4	2.60	2.25	573.40
M5	3.16	2.73	755.74

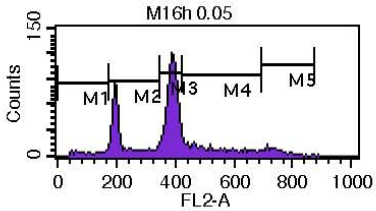

Sample ID: M16h 0.05 Gate: G1

Marker	% Gated	% Total	Geo Mean
All	100.00	80.53	345.44
M1	2.69	2.17	97.52
M2	26.09	21.01	215.04
M3	51.79	41.71	387.92
M4	15.63	12.59	527.44
M5	4.16	3.35	737.26

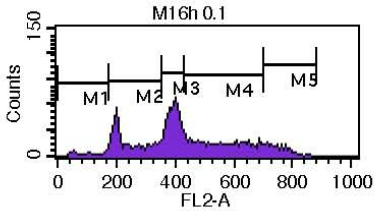

Sample ID: M16h 0.1 Gate: G1

Marker	% Gated	% Total	Geo Mean
All	100.00	84.03	394.17
M1	1.80	1.51	94.87
M2	25.75	21.64	240.62
M3	34.09	28.65	392.71
M4	31.56	26.52	553.44
M5	7.35	6.18	746.24

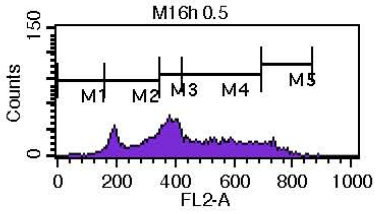

Sample ID: M16h 0.5 Gate: G1

Marker	% Gated	% Total	Geo Mean
All	100.00	81.29	400.49
M1	1.78	1.45	124.75
M2	26.92	21.88	249.06
M3	27.97	22.74	382.18
M4	36.70	29.83	551.03
M5	7.21	5.86	734.50

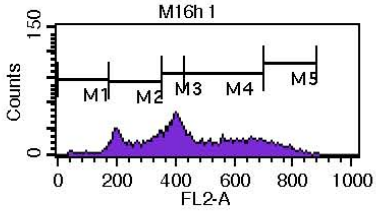

Sample ID: M16h 1 Gate: G1

Marker	% Gated	% Total	Geo Mean
All	100.00	83.88	415.04
M1	1.98	1.66	132.23
M2	26.69	22.39	257.09
M3	26.81	22.49	395.40
M4	35.99	30.19	563.27
M5	8.97	7.52	752.52

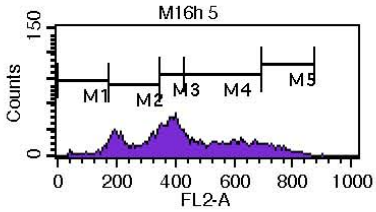

Sample ID: M16h 5 Gate: G1

Marker	% Gated	% Total	Geo Mean
All	100.00	81.91	394.86
M1	2.72	2.23	133.48
M2	27.98	22.92	253.77
M3	28.98	23.74	387.25
M4	34.05	27.89	549.51
M5	7.00	5.73	745.25

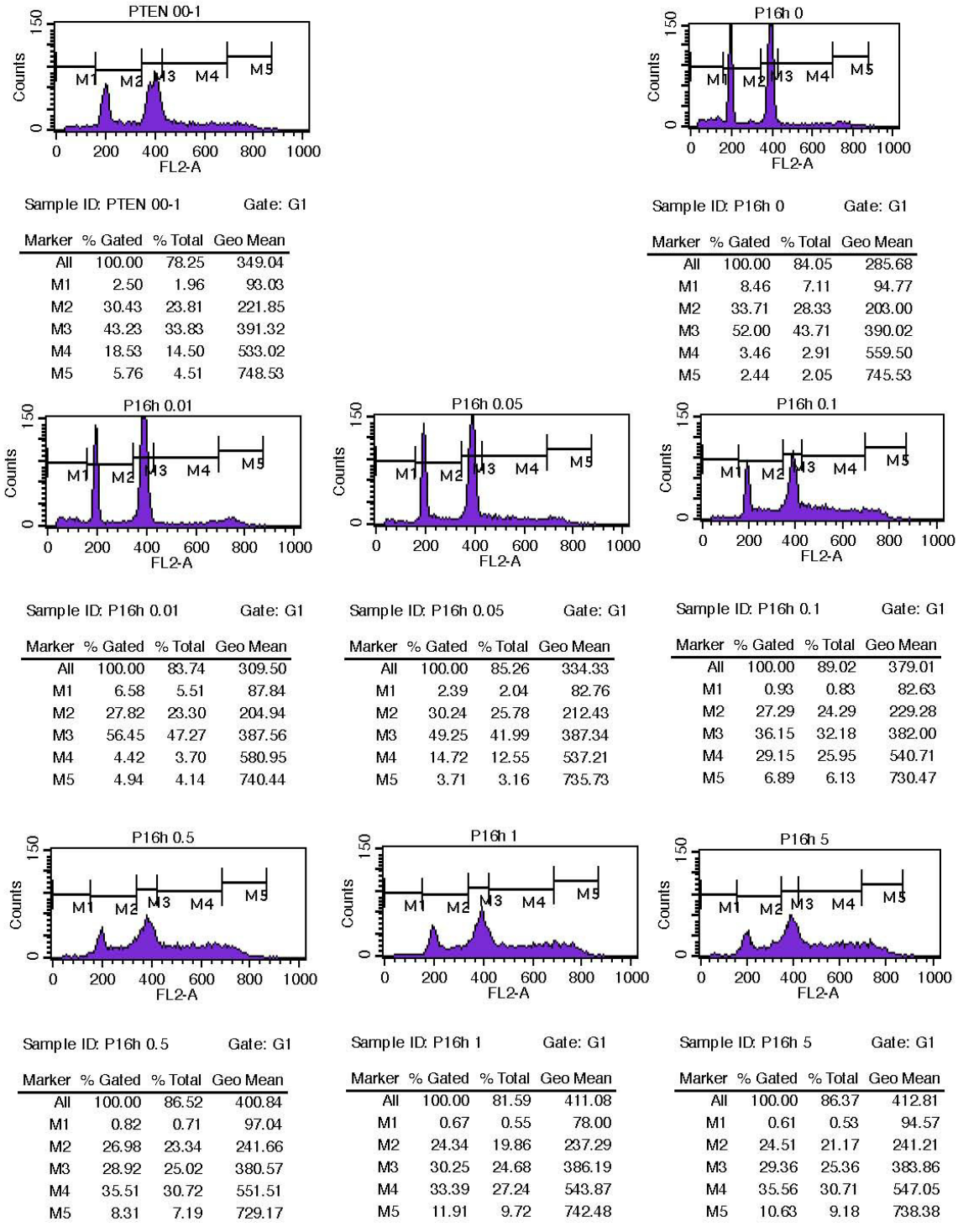

Figure 6.6 Overexpression of PTEN affects the cell cycle distribution of BaF3-EpoR cells (I). The cell cycle distribution of control (M) and PTEN-overexpressing (P) BaF3-EpoR cells was analyzed by PI staining and FACS. Cells at 0h (00) and cells after 16h stimulation with different dose of Epo in the range from 0 to 5 U/ml were analyzed. M1+ M2: <2N; M3: G0/G1; M4: S; M5: M/G2.

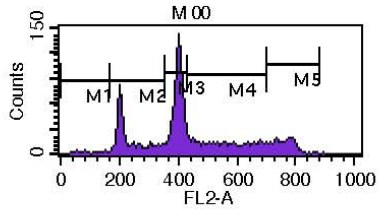

Sample ID: M 00 Gate: G1

Marker	% Gated	% Total	Geo Mean
All	100.00	87.77	404.44
M1	0.83	0.73	87.40
M2	22.09	19.39	231.87
M3	43.14	37.86	398.95
M4	23.66	20.77	557.42
M5	10.64	9.34	753.24

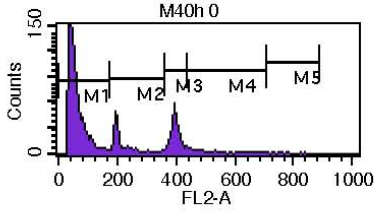

Sample ID: M40h 0 Gate: G1

Marker	% Gated	% Total	Geo Mean
All	100.00	73.69	92.11
M1	70.97	52.30	54.91
M2	10.45	7.70	214.08
M3	15.69	11.56	395.59
M4	2.73	2.01	506.98
M5	0.23	0.17	763.12

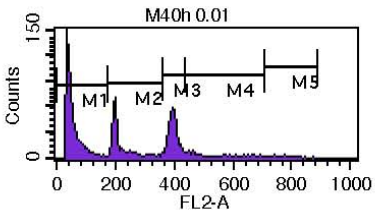

Sample ID: M40h 0.01 Gate: G1

Marker	% Gated	% Total	Geo Mean
All	100.00	60.10	126.90
M1	50.08	30.10	49.37
M2	19.47	11.70	214.24
M3	24.33	14.62	395.71
M4	4.79	2.88	536.38
M5	1.51	0.91	756.42

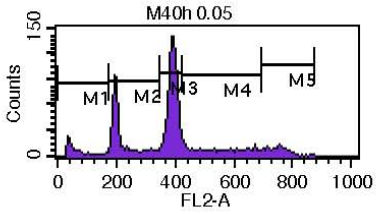

Sample ID: M40h 0.05 Gate: G1

Marker	% Gated	% Total	Geo Mean
All	100.00	80.17	332.64
M1	5.19	4.16	53.38
M2	24.17	19.38	214.18
M3	50.87	40.78	390.59
M4	13.57	10.88	550.39
M5	6.47	5.19	744.15

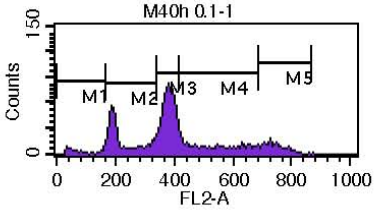

Sample ID: M40h 0.1-1 Gate: G1

Marker	% Gated	% Total	Geo Mean
All	100.00	78.22	361.44
M1	2.21	1.73	70.04
M2	24.83	19.42	221.97
M3	46.28	36.20	379.82
M4	19.64	15.36	542.75
M5	7.68	6.01	733.42

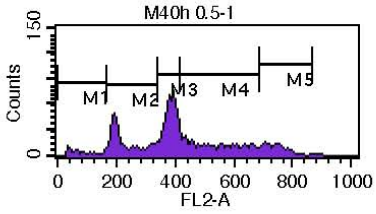

Sample ID: M40h 0.5-1 Gate: G1

Marker	% Gated	% Total	Geo Mean
All	100.00	77.59	375.16
M1	2.90	2.25	68.86
M2	23.93	18.57	227.25
M3	37.40	29.02	383.14
M4	26.59	20.63	537.91
M5	9.64	7.48	737.35

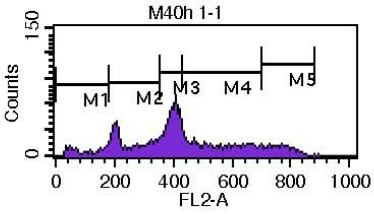

Sample ID: M40h 1-1 Gate: G1

Marker	% Gated	% Total	Geo Mean
All	100.00	75.53	376.74
M1	5.44	4.11	91.98
M2	25.75	19.45	249.13
M3	34.13	25.78	396.61
M4	26.19	19.78	554.28
M5	9.12	6.89	759.34

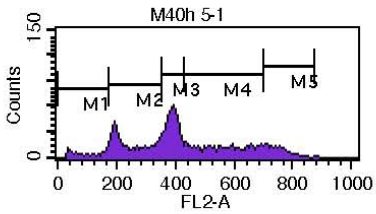

Sample ID: M40h 5-1 Gate: G1

Marker	% Gated	% Total	Geo Mean
All	100.00	75.58	372.85
M1	4.76	3.60	89.02
M2	27.31	20.64	243.21
M3	32.28	24.40	387.99
M4	27.04	20.44	557.15
M5	9.17	6.93	746.26

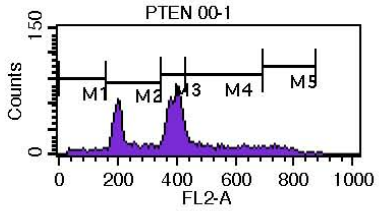

Sample ID: PTEN 00-1 Gate: G1

Marker	% Gated	% Total	Geo Mean
All	100.00	78.42	346.96
M1	2.75	2.16	85.43
M2	30.36	23.81	221.85
M3	43.14	33.83	391.32
M4	18.46	14.48	532.89
M5	5.74	4.50	748.55

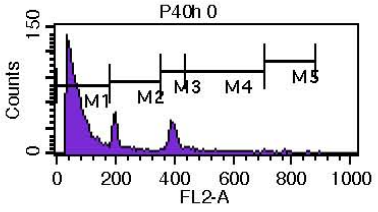

Sample ID: P40h 0 Gate: G1

Marker	% Gated	% Total	Geo Mean
All	100.00	78.51	92.55
M1	76.02	59.68	62.89
M2	10.44	8.20	214.88
M3	10.75	8.44	395.22
M4	2.61	2.05	509.85
M5	0.28	0.22	754.86

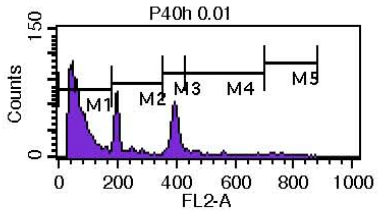

Sample ID: P40h 0.01 Gate: G1

Marker	% Gated	% Total	Geo Mean
All	100.00	79.19	121.40
M1	60.06	47.56	63.03
M2	15.36	12.16	212.14
M3	19.60	15.52	393.65
M4	3.80	3.01	514.06
M5	1.31	1.04	756.66

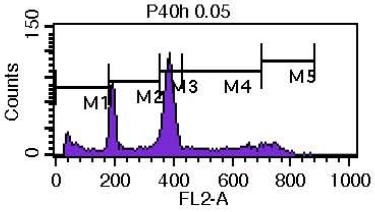

Sample ID: P40h 0.05 Gate: G1

Marker	% Gated	% Total	Geo Mean
All	100.00	83.09	308.89
M1	11.01	9.15	79.72
M2	25.57	21.25	223.81
M3	45.25	37.60	384.58
M4	13.35	11.09	570.57
M5	5.66	4.70	739.61

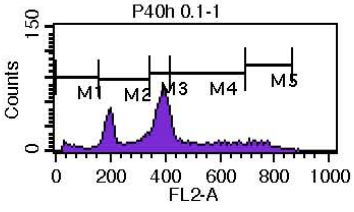

Sample ID: P40h 0.1-1 Gate: G1

Marker	% Gated	% Total	Geo Mean
All	100.00	79.29	347.12
M1	3.28	2.60	64.44
M2	28.60	22.68	226.81
M3	42.10	33.38	384.84
M4	20.24	16.05	533.61
M5	6.23	4.94	741.17

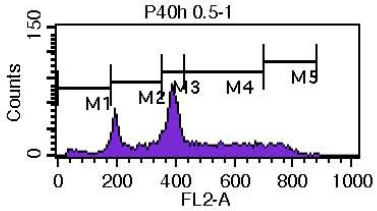

Sample ID: P40h 0.5-1 Gate: G1

Marker	% Gated	% Total	Geo Mean
All	100.00	81.16	384.55
M1	4.98	4.04	114.26
M2	24.53	19.91	248.60
M3	35.66	28.94	389.98
M4	26.68	21.65	562.98
M5	8.90	7.22	746.57

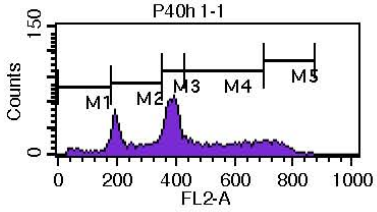

Sample ID: P40h 1-1 Gate: G1

Marker	% Gated	% Total	Geo Mean
All	100.00	79.71	380.78
M1	4.94	3.94	106.03
M2	24.18	19.27	243.46
M3	35.25	28.10	387.03
M4	27.26	21.73	557.55
M5	9.13	7.28	741.20

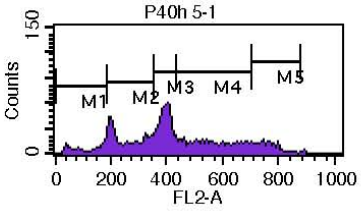

Sample ID: P40h 5-1 Gate: G1

Marker	% Gated	% Total	Geo Mean
All	100.00	78.67	379.04
M1	5.80	4.56	109.82
M2	25.51	20.07	250.30
M3	32.39	25.48	389.11
M4	27.98	22.01	554.23
M5	9.06	7.13	747.90

Figure 6.7 Overexpression of PTEN affects the cell cycle distribution of BaF3-EpoR cells (II). The cell cycle distribution of control (M) and PTEN-overexpressing (P) BaF3-EpoR cells was analyzed by PI staining and FACS. Cells at 0h (00) and cells after 40h stimulation with different dose of Epo in the range from 0 to 5 U/ml were analyzed. M1+ M2: <2N; M3: G0/G1; M4: S; M5: M/G2.

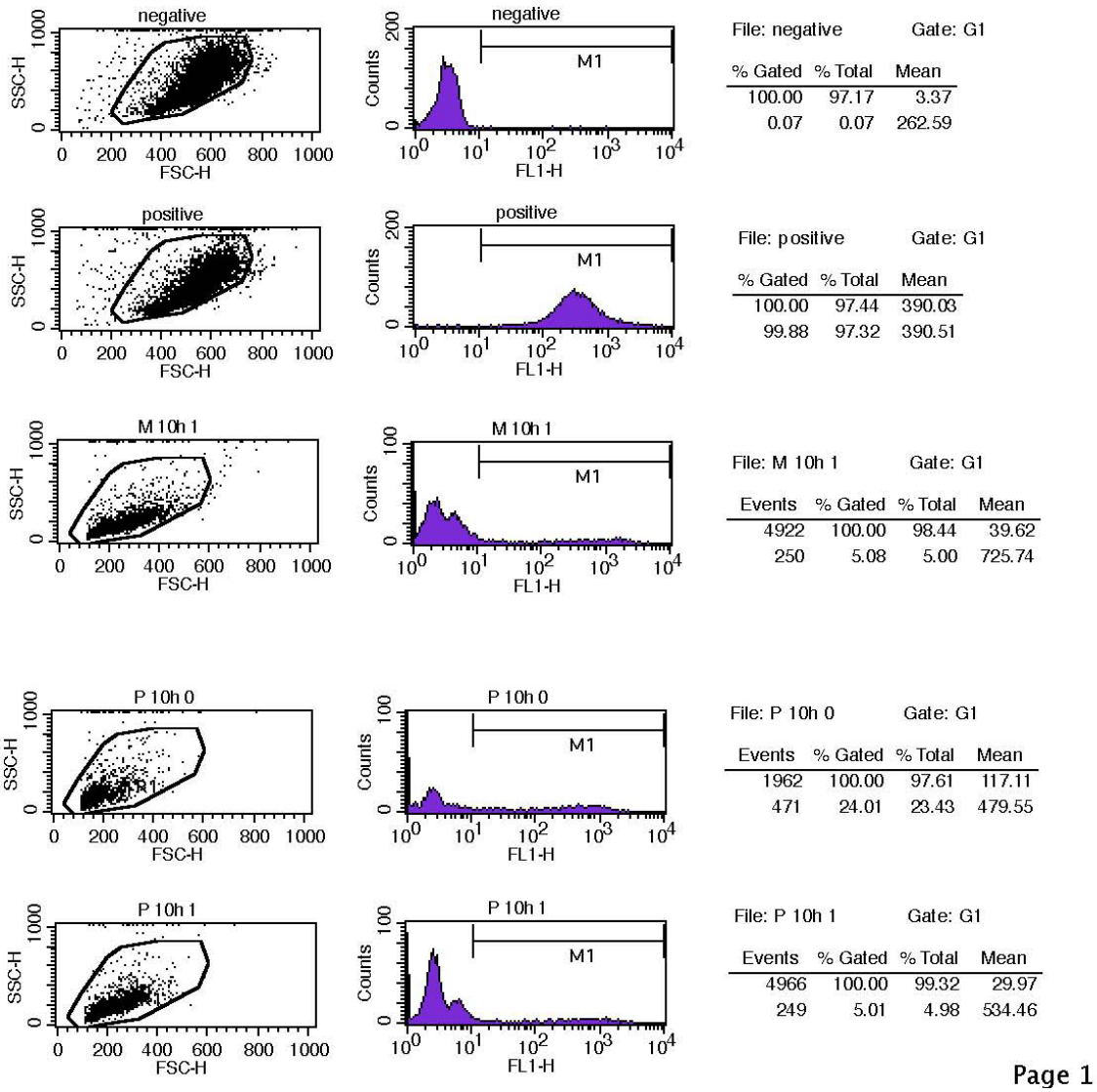

Figure 6.8 Overexpression of PTEN affects the apoptosis of CFU-E cells. The apoptosis of control (M) and PTEN-overexpressing (P) CFU-E cells was analyzed by TUNEL assay and FACS. Cells after 10h treatment with or without 1U/ml Epo were analyzed.

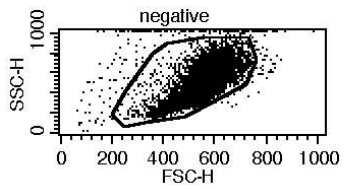

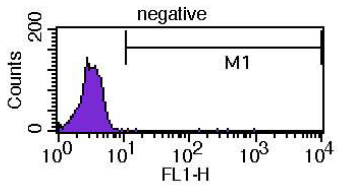

File: negative Gate: G1

% Gated	% Total	Mean
100.00	97.17	3.37
0.07	0.07	262.59

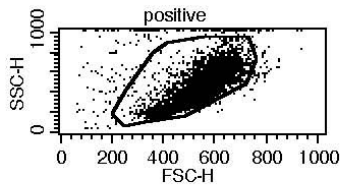

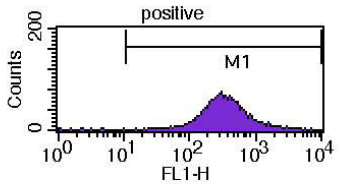

File: positive Gate: G1

% Gated	% Total	Mean
100.00	97.44	390.03
99.88	97.32	390.51

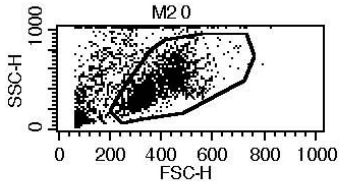

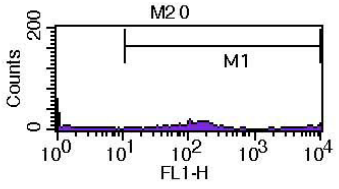

File: M2 0 Gate: G1

% Gated	% Total	Mean
100.00	65.66	711.95
83.15	54.60	855.75

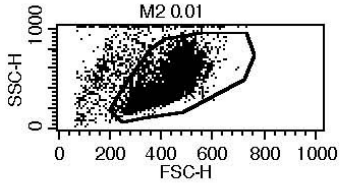

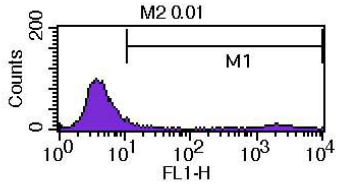

File: M2 0.01 Gate: G1

% Gated	% Total	Mean
100.00	92.66	97.17
8.25	7.64	1130.81

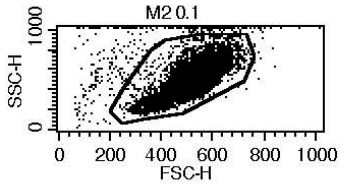

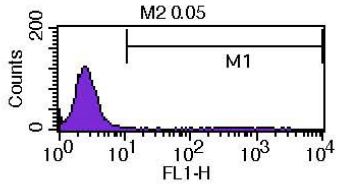

File: M2 0.05 Gate: G1

% Gated	% Total	Mean
100.00	95.99	10.30
1.27	1.22	602.15

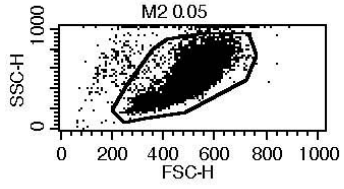

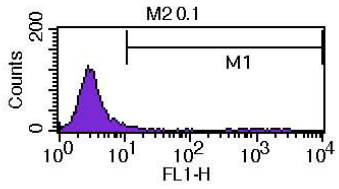

File: M2 0.1 Gate: G1

% Gated	% Total	Mean
100.00	96.54	9.86
1.97	1.90	338.38

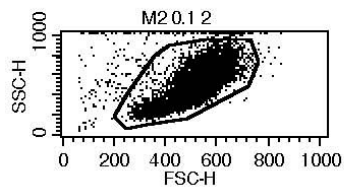

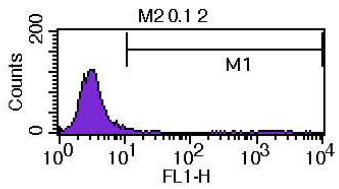

File: M2 0.1 2 Gate: G1

% Gated	% Total	Mean
100.00	97.17	11.29
1.69	1.64	480.21

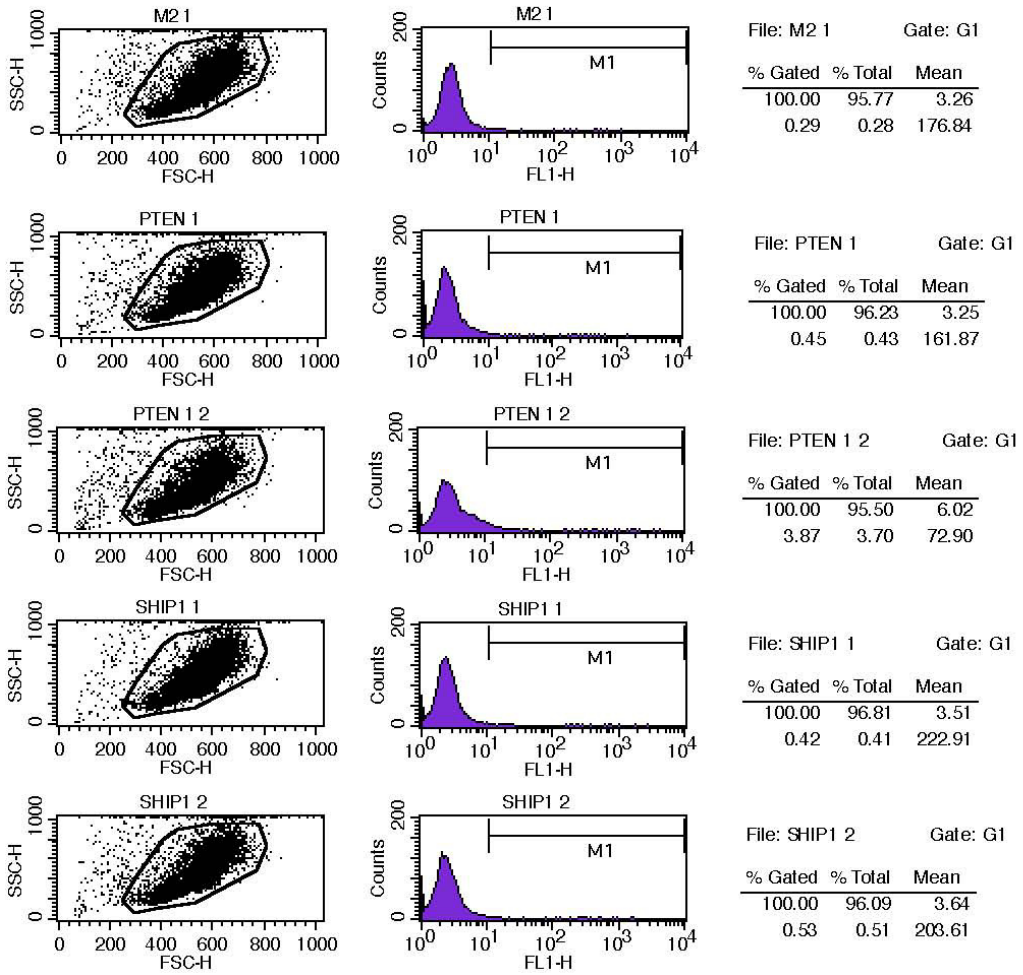

Figure 6.9 Overexpression of PTEN affects the apoptosis of BaF3-EpoR cells. The apoptosis of control (M2) and PTEN-overexpressing (PTEN) as well as SHIP1-overexpressing (SHIP1) CFU-E cells was analyzed by TUNEL assay and FACS. Control Cells after 24h treatment with different dose of Epo in the range from 0 to 1 U/ml Epo were analyzed. PTEN and SHIP1-overexpressing cells after 24h treatment with 1U/ml Epo were analyzed.

6.7 Other appendix data

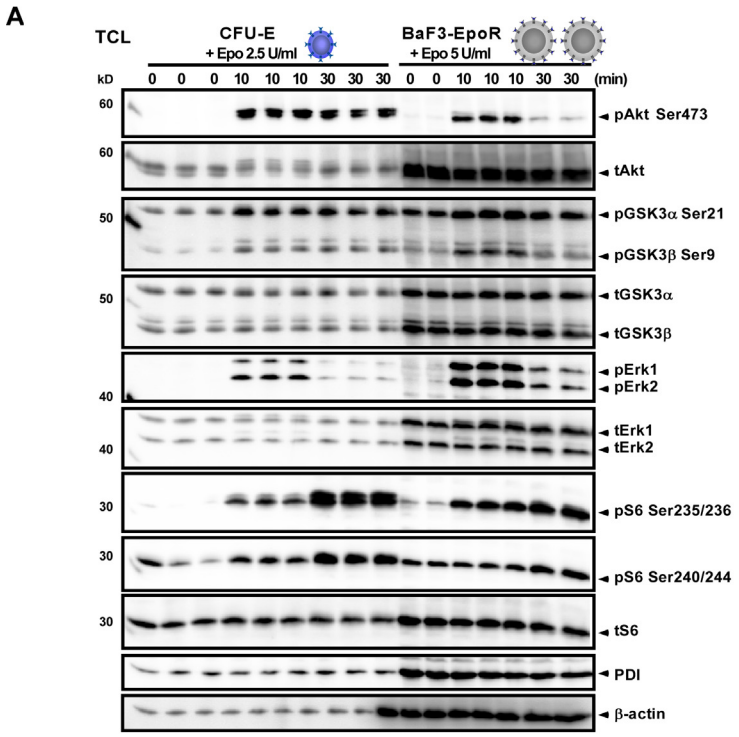

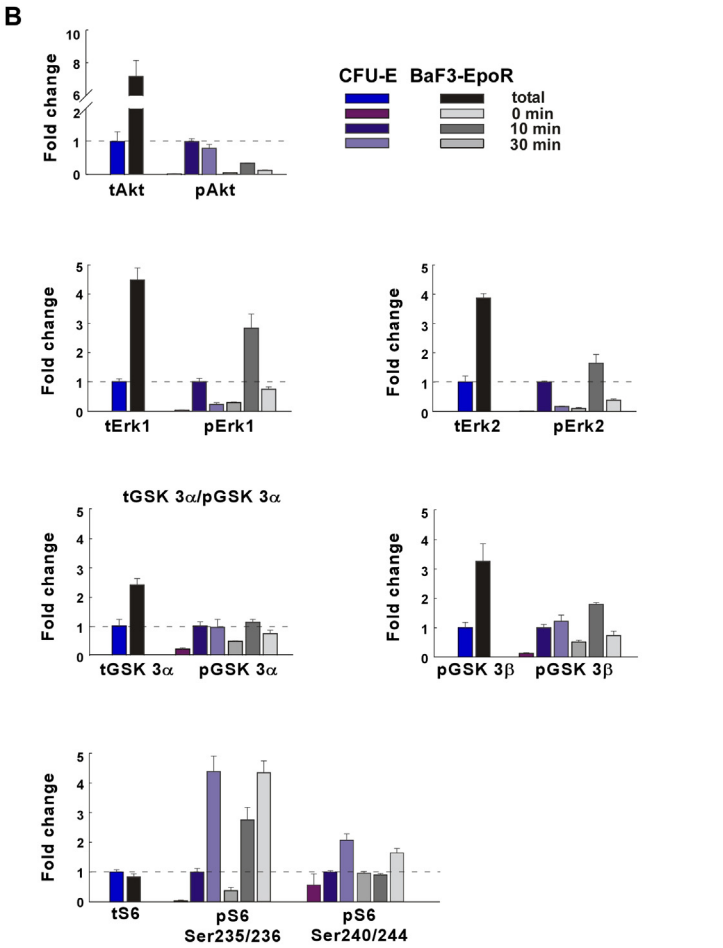

Figure 6.10 Comparison of stoichiometries and Epo-induced activation dynamics of signaling components in CFU-E and BaF3-EpoR cells. Growth factor-depleted CFU-E cells ($2x10^7$ cells/ml) and BaF3-EpoR cells ($4x10^7$ cells/ml) were stimulated for the indicated times with 2.5 or 5 U/ml Epo, respectively. (**A**) TCL (20 μl) were loaded and analyzed by immunoblotting. (**B**)The ratio of total and phosphorylated signaling components between CFU-E and BaF3-EpoR cells were depicted as bar charts with standard deviation.

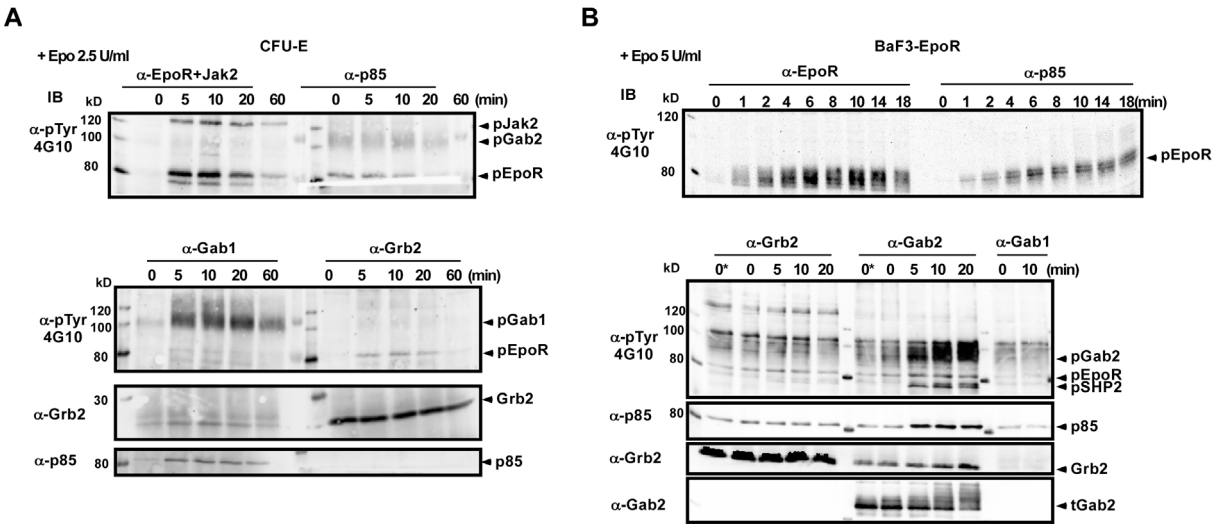

Figure 6.11 Epo-induced activation and association pattern of Gab insoforms in CFU-E and BaF3-EpoR cells. Growth factor-depleted CFU-E cells ($2x10^7$ cells/ml) and BaF3-EpoR cells ($4x10^7$ cells/ml) were stimulated for the indicated times with 2.5 or 5 U/ml Epo, respectively. The lysates were immunoprecipitated (IP) with the indicated antibodies and the immunoprecipitates were subjected to immunoblotting (IB) in (A) CFU-E and (B) BaF3-EpoR cells.

6.8 Abbreviations

4E-BP1	Eukaryotic translation initiation factor 4E (eIF4E) binding protein 1
7-AAD	7-aminoactinomycin D
Akt	thymoma viral proto-oncogene
BFU-E	burst forming unit-erythroid
bp	base pairs
BSA	bovine serum albumin
Ccnd1	cyclin D1
Ccnd2	cyclin D2
Ccnd3	cyclin D3
Ccng2	cyclin G2
CD	cluster of differentiation
cDNA	complementary DNA
CFU-E	colony forming unit-erythroid
CFU-GEMM	colony forming unit-granulocytes, erythrocytes, monocytes, macrophages
CIS	cytokine-inducible SH2 domain-containing protein
d	days postconception
DMEM	Dulbecco's modified eagle medium
DMSO	dimethyl sulfoxide
DNA	deoxyribonucleic acid
dNTP	deoxyribonucleotide triphosphate
Dox	doxycycline
DTT	dithiothreitol
E. coli	Escherichia coli
ECL	enhanced chemiluminescence
EDTA	ethylenediaminetetraacetic acid
EGFR	epidermal growth factor receptor
EGFP	enhanced green fluorescent protein
Epo	erythropoietin
EpoR	erythropoietin receptor
ER	endoplasmic reticulum
FACS	fluorescence activated cell sorter
FCS	fetal calf serum
FLC	fetal liver cells
Foxo1	forkhead box O1
Foxo3	forkhead box O3
g	g force

G418	geneticin
Gab	Grb2-associated binder
G-CSF	granulocyte colony-stimulating factor
GFP	green fluorescent protein
GHR	growth hormone receptor
Grb	growth factor receptor-bound protein
GSK 3	glycogen synthase kinase 3
h	hours
HA	hemagglutinin
HBS	hepes buffered saline
HEPES	4-(2-Hydroxyethyl)piperazine-1-ethanesulfonic acid
HIF	hypoxia-inducible transcription factor
HPRT	hypoxanthine guanine phosphoribosyl transferase
HRP	horseradish peroxidase
HSC	hematopoietic stem cell
IB	immunoblot
Ig	immunglobulin
IL	interleukin
IMDM	Isocove's modified Dulbecco's medium
IP	immunoprecipitation
JAK	Janus kinase
kDa	kilodalton
LB	Luria Bertani broth
M	molarity
MAPK	mitogen-activated protein kinase
min	minutes
ml	milliliter
mTOR	mammalian target of rapamycin
µl	microliter
neo	neomycin resistance gene
nm	nanometer
o/n	over night
ODE	ordinary differential equations
p21	Cdkn1a cyclin-dependent kinase inhibitor 1A
$p27^{kip1}$	Cdkn1b cyclin-dependent kinase inhibitor 1B
p85	phosphatidylinositol 3-kinase 85 kDa regulatory subunit
p110	phosphatidylinositol 3-kinase 110 kDa catalytic subunit

PAGE	polyacrylamide gel electrophoresis
PBS	phosphate buffered saline
PCR	polymerase chain reaction
PDGFR	platelet-derived growth factor receptor
PDK1	3-phosphoinositide-dependent protein kinase 1
PE	phycoerythrin
Pfu	*Pyrococcus furiosus*
PI3K	phosphatidylinositol 3-kinase
PKB	protein kinase B
PKC	protein kinase C
PtdIns(3,4)P2	Phosphatidylinositol (3,4)-bisphosphate
PtdIns(3,4,5)P3	Phosphatidylinositol (3,4,5)-trisphosphate
PtdIns(4,5)P2	Phosphatidylinositol (3,4)-bisphosphate
PTEN	phosphatase and tensin homolog
puro	puromycin
rhEpo	recombinant human erythropoietin
rpm	rounds per minute
RPL	ribosomal protein L32
RT	room temperature
SBP	streptavidin-binding peptide
SCF	stem cell factor
SDS	sodium dodecyl sulfate
SH	Src homology
SHIP1	Phosphatidylinositol-3,4,5-trisphosphate 5-phosphatase 1
SHP	SH2 domain-containing protein tyrosine phosphatase
S6K1	Ribosomal protein S6 kinase beta-1
S6	Ribosomal protein S6
SOCS	suppressor of cytokine signaling
Sos	son of sevenless
STAT	signal transducer and activator of transcription
strep	streptavidin
TAE	Tris-acetate-EDTA
Taq	Thermus aquaticus
TB	Terrific broth
TBS	Tris buffered saline
TBST	Tris buffered saline with Tween-20
TE	Tris-EDTA

Tet	tetracycline
TfR	transferrin receptor
TM	transmembrane
TPO	thrombopoietin
Tris	Tris(hydroxymethyl)-aminomethane
U	unit of enzyme activity
WEHI	Walter and Eliza Hall Institute
w/v	weight per volum

6.9 Erklärung

Ich erkläre hiermit, dass ich die vorgelegte Dissertation selbst verfasst und mich dabei keiner anderen als der von mir ausdrücklich bezeichneten Quellen und Hilfen bedient habe.
Weiterhin erkläre ich hiermit, dass ich an keiner anderen Stelle ein Prüfungsverfahren beantragt bzw. die Dissertation in dieser oder anderer Form bereits anderweitig als Prüfungsarbeit verwendet oder einer anderen Fakultät als Dissertation vorgelegt habe.

Heidelberg, den 21. June 2011

Bin She